Characterising the phosphorylation and SUMOylation of cardiac troponin I in heart failure

Bracy Andrea Fertig

MSc, BSc (Hons)

Thesis submitted in fulfilment of the requirements for the Degree of Doctor of Philosophy (PhD)

Institute of Cardiovascular and Medical Sciences
College of Medical, Veterinary and Life Sciences
University of Glasgow

September 2019

Abstract

Troponin I (TnI) is the inhibitory subunit of the troponin (Tn) complex of the myofilament. TnI's function is regulated by phosphorylation at a number of sites by different kinases. As a result of ß-adrenergic stimulation, protein kinase A (PKA) phosphorylates TnI at Ser23/24, which causes positive lusitropy and inotropy. The PKA-mediated phosphorylation events on cardiac excitation contraction coupling proteins are often controlled by phosphodiesterase (PDE) enzymes which degrade cyclic 3',5'-adenosine monophosphate (cAMP), reducing local activation of PKA. This is accomplished by the integration of PDEs into macromolecular complexes, or signalosomes, containing PKA, PKA substrate proteins, anchoring proteins and often other kinases and phosphatases. Research published in another thesis from the Baillie lab indicated that PDE4D9 binds directly to TnI, thereby regulating the cAMP dynamics at the myofilament and the PKA phosphorylation events. Little is known about other post-translational modifications of TnI, but the identification of other modifications could lead to better understanding of the regulation of TnI function within the myofilament and how this is altered in disease states. SUMOylation is a post-translational modification in which a small ubiquitin-like modifier (SUMO) is covalently attached to a substrate protein by an enzymatic cascade similar to the ubiquitination cascade.

This thesis began with the testing of a disruptor peptide which was designed to interrupt the proposed interaction between PDE4D9 and TnI. It was hypothesised that disruptor peptides would 'unhook' the PDE4D9-TnI complex, allowing enhanced cAMP dynamics at the myofilament and enhanced PKA phosphorylation of TnI. However, using fluorescence resonance energy transfer (FRET) and immunoblotting for phosphorylation levels, it was shown that disruption of the proposed interaction did not significantly affect the outcomes of ß-adrenergic signalling at the myofilament. Subsequent attempts to confirm the existence of the proposed interaction were unsuccessful suggesting that PDE4D9 may not be a TnI binding partner after all. Further study is necessary to determine the mechanisms by which PDEs regulate signalling at the myofilament.

In silico analysis of TnI revealed a high probability SUMOylation site (K177) suggesting that TnI could be a SUMO substrate. This hypothesis was tested in the

second part of this thesis. For the first time, it was shown that TnI can be SUMOylated using a number of biochemical techniques. Furthermore, detection of SUMOylated TnI was facilitated by the successful development of a SUMO-TnI site-specific antibody, the first of its kind to detect a SUMOylated substrate protein. Interestingly, the levels of SUMOylated TnI were significantly enhanced in human heart disease, suggesting a role in the pathophysiology of disease.

Functional analyses of the role of TnI SUMOylation in protein stability and myofilament dynamics were then carried out. Viral overexpression of mutant TnI in which the SUMO acceptor lysine was mutated did not have any effect on TnI stability nor the contractility of neonatal rat ventricular myocytes (NRVM). However, functional differences were discovered when mutant TnI was overexpressed in adult rabbit ventricular myocytes (ARVM) and SUMOylation was globally upregulated. The data suggested that TnI SUMOylation may have a scavenging effect, sequestering SUMO proteins from other myofilament SUMO targets.

The present work provides a major contribution to the field, showing for the first time that TnI can be modified by SUMOylation and that the modified protein alters myofilament function. Understanding the way post-translational modifications affect the function of cardiac excitation-contraction coupling proteins is necessary for a full understanding of pathophysiology, especially when the modification has been shown to be altered in disease states. Further work elucidating the molecular mechanisms by which TnI SUMOylation alters myofilament dynamics may reveal potential therapeutic targets for heart disease.

Table of Contents

List of Tables

List of Figures

Acknowledgment

I would like to express my deepest gratitude to my supervisor, Professor George S. Baillie. I could never have envisaged a more enjoyable and supportive environment than the Baillie Lab. George, you have been the best boss I will probably ever have, and I will never forget all that you have done for me. I truly feel lucky every day that I have had this experience. Del, as my second supervisor, I did not get to spend nearly as much time with you as I would have liked, but you have always been there to help me through any difficult times. For that, I am extremely grateful. Thank you to the British Heart Foundation for the generous funding and opportunities throughout.

I would like to extend a huge thank you to all of the members of the Baillie Lab, past and present. It has been an honour and pleasure to work with you all. Ella, Amy, Tara, Joyce, Connor, Lauren, Alice, Gonzalo, Angie, Jane, Gillian, you have made my PhD much more fun than a PhD probably should have been! There is no way this work could have been completed without the technical (and sometimes emotional) support of every one of you. Thank you to the Freeman lab, Fiona, Galvin, Dilys and Oom, who have been a pleasure to work alongside in Lab 535.

I have been incredibly lucky to benefit from a number of collaborations over the past three years. Thank you to everyone who has hosted me for various projects: Professor Manuela Zaccolo (Oxford University), Professor Don Maurice (Queen's University), Professor Jolanda van der Velden (VU Medical Centre) and Professor Godfrey Smith (University of Glasgow). I learned so much from each of you and you have made my experience so rich.

Finally, thank you to my family and friends, near and far, who have supported me through the last three years. I could never thank my extraordinary parents enough for giving me the chance to live, study and work abroad, and I will never take that for granted. Merlin, thank you for standing beside me always and to all of the beautiful people I have met in Glasgow, thank you.

This work is dedicated to Zander Valente Fertig (5th Nov 1997-21st June 2019). You are so missed.

Author's Declaration

I declare that the work presented in this thesis has been carried out by myself, except where otherwise cited or acknowledged. It is entirely of my own composition and has not, in whole or part, been submitted for any other higher degree.

Bracy Andrea Fertig
September 2019

Definitions/Abbreviations

˚C	degrees celcius
25-mer	25 amino acid peptide
5'-AMP	5'-adenosine monophosphate
5'-GMP	5'-guanosine monophosphate
ß-AR	ß adrenergic receptor
AC	adenylyl cyclase
ACE	angiotensin converting enzyme
AKAP	A-kinase anchoring protein
ALC-1	atrial form of myosin light chain
ANOVA	a one way analysis of variance
ARB	angiotensin receptor blocker
ARVM	adult rabbit ventricular myoctye
ATP	adenosine triphosphate
BSA	bovine serum albumin
C	catalytic subunit
Ca^{2+}	calcium
cAMP	cyclic 3',5' adenosine monophosphate
$CaCl_2$	calcium chloride
CD50	time from 50% contraction to 50% relaxation
CFP	cyan fluorescent protein
CHX	cyclohexamide
cGMP	cyclic 3',5' guanosine monophosphate
Co-IP	co-immunoprecipitate
CO_2	carbon dioxide
cm	centimetre
CNBD	cyclic nucleotide binding domain
CNGC	cyclic nucleotide gated channels
CNP	c-type natriuretic peptide
cpm	counts per minute
CUTie	cAMP universal tag for imaging experiments
D/N	dominant negative
DAG	diacylglycerol
DAPI	4', 6-diamidino-2-phenylindole

ddH_2O	double distilled water
dH_20	distilled water
DMEM	Dulbecco's modified eagle medium
DMSO	dimethyl sulfoxide
DNA	deoxyribonucleic acid
DOWN90	time form peak to 90% relaxation
DP	disruptor peptide
dsDNA	double stranded DNA
E. Coli	*Escherichia coli*
E1	SUMO activating enzyme
E2	SUMO conjugating enzyme, UBC9
E3	SUMO ligase
EC_{50}	half maximal effective concentration
ECL	enhanced chemiluminescence
EDTA	ethylenediaminetetraacetic acid
Epac	exchange proteins directly activated by cAMP
EtOH	ethanol
FBS	foetal bovine serum
F_{max}	maximal force
$F_{passive}$	passive force
FRET	fluorescent resonance energy transfer
FKS	forskolin
g	grams
GAPDH	glyceraldehyde 3-phosphate dehydrogenase
GC	gyanylyl cyclase
GDP	guanosine diphosphate
GFP	green fluorescence protein
GPCR	g-protein coupled receptor
GST	glutathione S-transferase
GTP	guanosine triphosphate
H_2PO_4	dihydrogen phosphate
HA	haemagglutinin
HCl	hydrochloric acid
HEK-239	human embryonic kidney-293 cells
HEPES	4-(2-hydroxyethyl)-1-piperazineethanesulfonic acid

HF	heart failure
HFpEF	heart failure with preserved ejection fraction
HFrEF	heart failure with reduced ejection fraction
HPSC-CM	human pluripotent stem cell-derived cardiac myocytes
HRP	horseradish peroxidase
HS	horse serum
HSCM	hydrophobic cluster-dependent SUMOylation motif
HSP	heat shock protein
I_{Ca2+}	inward Ca_{2+} current
IκBα	nuclear factor of κ light polypeptide gene enhancer in B-cells inhibitor α
IBMX	3-isobutyl-1-methylxanthine
IgG	immunoglobulin G
IK_s	slowly activating delayed rectifier potassium channel
IP	immunoprecipitation
IP_3	inositrol triphosphate
I/R injury	ischaemia/reperfusion injury
Iso	isoprenaline
KCl	potassium chloride
kDa	kilodalton
KO	knock-out
LB	lysogeny broth
LTCC	L-type calcium channel
LSM	laser-scanning confocal microscope
M	molar
M1	NRVM day 1 medium
M199	medium 199
M2	NRVM day 2 medium
MI	myocardiac infarction
mg	milligram
MG-132	carbobenzoxy-Leu-Leu-leucinal
Mg-ATP	magnesium adenosine triphosphate
$MgCl_2$	magnesium chloride
$MgSO_4$	magnesium sulphate
MHC	myosin heavy chain

ml	millilitre
mm	millimetre
mM	millimolar
MOI	multiplicity of infection
MS	mass spectrometry
MyBP-C	myosin binding protein C
N106	4-methoxy – *N*-5-(4-methoxyphenyl)-1,3,4-oxadiazol-2-yl-2 benzothizolamine
Na_2ATP	disodium adenosine triphosphate
Na_3PO_4	trisodium phosphate
NaCl	sodium chloride
NaF	sodium fluoride
NaOH	sodium hydroxide
NCS	neonatal calf serum
NCX	sodium calcium exchanger
NDSM	negatively charged amino acid-dependent SUMOylation motif
NEAA	minimum essential medium non-essential amino acids
NF-κB	κ light chain enhancer of activated B cells
ng	nanogram
nm	nanometre
nM	nanomolar
NO	nitric oxide
NRVM	neonatal rat ventricular myocyte
P/S	penicillin/streptomycin
PBS	phospho-buffered saline
pCa_{2+}	$-\log[Ca_{2+}]$
PCR	polymerase chain reaction
PDE	phosphodiesterase
PDSM	phosphorylation-dependent SUMOylation motif
PFA	paraformaldehyde
PIAS	protein inhibitor of activated STAT
PKA	protein kinase A
PKC	protein kinase C
PKG	protein kinase G
PLB	phospholamban

POPDC	popeye domain-containing proteins
R	regulatory subunit
RFP	red fluorescent protein
Rol	rolipram
RNA	ribonucleic acid
rpm	rotations per minute
RyR	ryanodine receptor
SAT	cAMP-saturating dose of IBMS (100 µM) and FSK (25 µM)
SC	scrambled control
SDS	sodium dodecyl sulphate
SDS-PAGE	sodium dodecyl sulphate polyacrylamide gel electrophoresis
SEM	standard error of the mean
SENP	sentrin-specific protease
SERCA	sarcoplasmic reticulum calcium ATPase
SIM	SUMO interacting motif
siRNA	small interfering ribonucleic acid
SR	sarcoplasmic reticulum
SUMO	small ubiquitin-like modifier
TAC	transverse aortic constriction
TDG	thymine DNA glycosylase
TBS	tris buffered saline
TBS-T	tris buffered saline with Tween-20
Tm	tropomyosin
Tn	troponin
TnC	troponin C
TnI	troponin I
TnI-HA Mut	TnI-HA protein with SUMOylation site mutation (KK177-8RR)
TnI-HA WT	TnI-HA protein wild type
TnT	troponin T
UBC9	SUMO conjugating enzyme, also referred to as E2
UFDS	UBC9 fusion-directed SUMOylation
UP90	time from baseline to 90% contraction
V	volt
VLC-1	ventricular form of myosin light chain
v/v	volume/volume

w/v	weight/volume
WT	wild type
YFP	yellow fluorescent protein
µg	microgram
µm	micrometre
µM	micromolar

Chapter 1 Introduction

1.1 Cardiac Excitation-Contraction Coupling

Cardiac excitation-contraction coupling is the process by which electrical signals in the heart are converted to mechanical contraction of the cardiac muscle. This is achieved by the coordinated activity of calcium handling proteins and myofilament proteins and is stimulated by the cardiac action potential (Figure 1.1) (reviewed in (Bers 2002)).

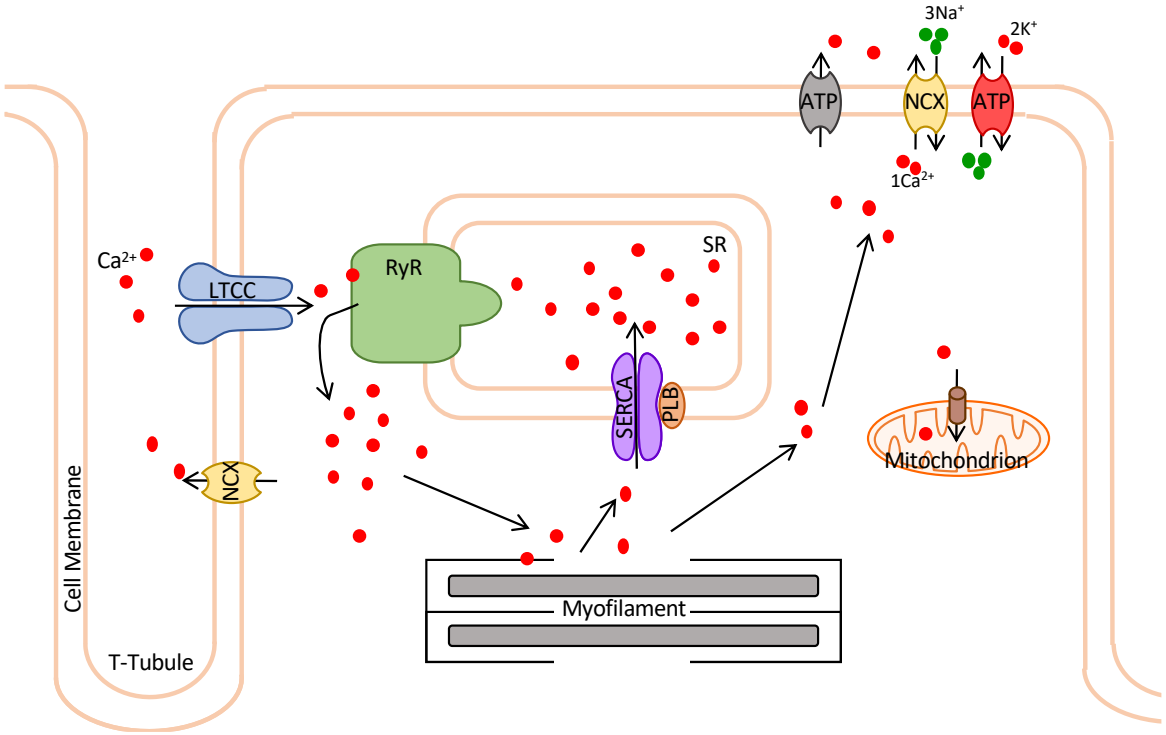

Figure 1.1: Cardiac excitation-contraction coupling. Ca^{2+} enters the cell through LTCC located in cell membrane invaginations called T-tubules. This small amount of Ca^{2+} entry stimulates Ca^{2+}-induced Ca^{2+} release from intracellular stores by RyR. Upon increased [Ca^{2+}], the myofilament contracts. Relaxation is caused by decreasing [Ca^{2+}] to diastolic levels by resequestering in the SR through SERCA and extrusion across the cell membrane. (ATP, ATPase, LTCC, L-type Ca^{2+} channel, NCX, Na^{+}/Ca^{2+} exchanger, PLB, phospholamban, RyR, ryanodine receptor, SERCA, sarco/endoplasmic reticulum Ca^{2+} ATPase) (Adapted from (Bers 2002)).

Depolarisation of the myocyte membrane activates the inward Ca^{2+} current (I_{Ca}) by opening the depolarisation-activated L-type calcium channel (LTCC). This small influx of calcium triggers a process called Ca^{2+}-induced Ca^{2+} release, in which Ca^{2+} is released from the sarcoplasmic reticulum (SR) into the cytosol through the ryanodine receptor (RyR). This causes the cytoplasmic Ca^{2+} concentration ($[Ca^{2+}]_i$) to rise to such an extent that Ca^{2+} binds to the myofilament, stimulating contraction. Relaxation is triggered by a reduction of

$[Ca^{2+}]_i$ to resting levels, leading to dissociation of Ca^{2+} from the myofilament. $[Ca^{2+}]_i$ is reduced through several mechanisms. The largest source of Ca^{2+} efflux from the cytosol is through the SR Ca^{2+}-ATPase (SERCA), which replenishes the intracellular Ca^{2+} stores in the SR. The Na^{+}/Ca^{2+} exchange pump (NCX) and Ca^{2+} ATPase extrude Ca^{2+} across the cell membrane into the extracellular space. Finally, the Ca^{2+} uniport allows Ca^{2+} to enter the mitochondria, creating an additional small intracellular store. Upon the next depolarisation, the process repeats itself (Bers 2002).

1.1.1 Cardiac Myofilament

The cardiac myofilament is made up of a thin and a thick filament. The thin filament is comprised of actin, tropomyosin (Tm) and the troponin (Tn) complex. The Tn complex is a hetero-trimer containing troponin C (TnC), troponin T (TnT) and troponin I (TnI) (de Tombe 2003). The thick filament is comprised of myosin, which is made up of several regions with discrete functions. The interactions between these proteins are altered with the binding of Ca^{2+}, ultimately resulting in myofilament contraction (reviewed in (de Tombe 2003)).

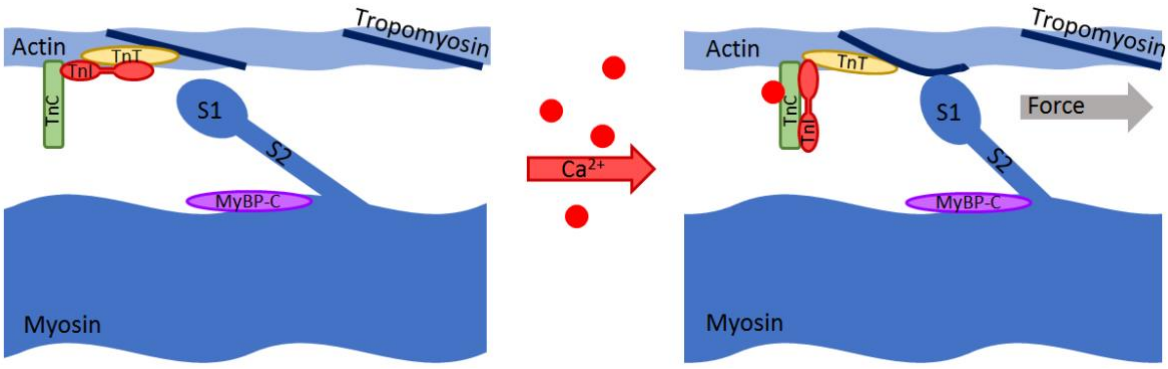

Figure 1.2: Cardiac myofilament in increasing $[Ca^{2+}]$. The components of the Tn complex are arranged such that Ca^{2+} binding to TnC reveals the myosin binding site on tropomyosin. As the S1 domain of myosin binds to this site, ATP is hydrolysed, and the sarcomere contracts. (MyBP-C, myosin binding protein C; TnC, troponin C; TnI, troponin I; TnT, troponin T). (Adapted from (de Tombe 2003)).

When $[Ca^{2+}]_i$ rises, Ca^{2+} binds to TnC, inducing a conformational change in the protein. TnC has two high affinity Ca^{2+} binding sites, which are constantly occupied. It is the binding of Ca^{2+} to TnC's third, low affinity binding site which results in a conformational change (Holroyde, Robertson et al. 1980). This conformational change affects the interactions between the three components

of the Tn complex; the interaction between TnC and TnI is weakened, which releases TnT from the inhibitory influence of TnI. These changes in the conformation of the Tn complex cause a conformational change in Tm, tightening its binding to actin, and allowing binding sites for the globular head portion (S1) of myosin to be revealed (Lehman, Craig et al. 1994, Solaro and Rarick 1998). Thereby, cross-bridging between actin and myosin can occur and the myofilament contracts, utilising ATP, which is hydrolysed by the S1 domain of myosin (Figure 1.2). The simultaneous contraction of all electrically stimulated cardiac myocytes of the ventricle is sufficient to expel blood, propelling it into the circulation. While many of the physiological and pathophysiological alterations in contractile function can be ascribed to changes in Ca^{2+} handling, there is increasing awareness of the role of myofilament properties in the modulation and fine tuning of cardiac contractility (Hamdani, Kooij et al. 2008).

1.2 Cardiac Troponin I

Cardiac TnI (hereby referred to as TnI) is the inhibitory subunit of the heterotrimeric Tn complex of the thin filament. The thin filament is comprised of long actin polymers. Within the grooves of the actin polymer chains, resides the elongated protein, Tm, which spans seven actin proteins. Each Tm is accompanied by a Tn heterotrimer (Gordon, Homsher et al. 2000, Metzger and Westfall 2004). The three Tn subunits each have a discrete function: TnC binds Ca^{2+}, TnI has an inhibitory role and TnT binds Tm. Together, the Tn complex serves as the link between Ca^{2+} binding and cross-bridging/force generation. At low $[Ca^{2+}]_i$ during diastole, TnI inhibits these interactions, thereby inhibiting contraction and holding the myofilament in a relaxed state. However, during systole, when $[Ca^{2+}]_i$ rises, the binding of Ca^{2+} to TnC causes a conformational change, which eliminates TnI's inhibitory influence, allowing the cross-bridging to occur and the myofilament to contract (Metzger and Westfall 2004, Layland, Solaro et al. 2005).

1.2.1 Troponin Structure

A description of the structure and function of TnI is impossible without explanation of the context of the heterotrimeric Tn complex. TnC, TnI and TnT

are three separate polypeptide chains from separate gene products. These three proteins are folded around each other, interacting at numerous sites. The complex is highly flexible, which is integral to its functional dependence upon changes in protein conformation. There are two structurally separate subdomains of the Tn complex: the regulatory head domain and the IT arm. The regulatory head is made up of TnC 3-84 and TnI 150-159, and the IT arm is made up of TnC 93-161, TnI 42-136, and TnT 203-271. The structure of the Ca^{2+}-bound form of the complex has been elucidated using X-ray crystallography, as shown in Figure 1.3 (Takeda, Yamashita et al. 2003).

The N-terminal portion of TnI (residues 1-42) was not well defined by this study (Takeda, Yamashita et al. 2003). Therefore, the crystal structure begins N-terminally with residues 43-79, which form an α-helix in the IT arm (labelled A in Figure 1.3). The N-terminal end of this α-helix interacts with TnC. Upstream of this region, residues 80-89 break the α-helical pattern and extend, forming a binding site with TnT (B). Residues 90-135 form another α-helix which can be considered as a coiled-coil structure with the helical segment of TnT (C). The inhibitory region (137-148) although not defined within the present structure, is thought to be extended and flexible (D). Finally, the C-terminal portion of TnI is comprised of 2 α-helices, one formed of residues 150-159 (E), which interacts weakly with TnC, and one formed of residues 164-188 (F), which protrudes and has not been shown to interact with the rest of the troponin molecule (Takeda, Yamashita et al. 2003, Takeda 2005).

TnC has two similarly sized globular domains connected by a helix (Figure 1.3). Each of these globular domains contains Ca^{2+} binding sites (Herzberg and James 1985, Sundaralingam, Bergstrom et al. 1985). The C-terminal sites are constantly occupied and therefore, do not have a significant functional role. However, the N-terminal site has a lower affinity for Ca^{2+}, and is only occupied during systolic $[Ca^{2+}]_i$.

TnT's structure underpins its function of binding tropomyosin, and anchoring the troponin complex to the thin filament. TnT's structure is comprised primarily of α-helices, one of which, residues 226-276, forms a coiled coil around TnI's residues 90-135 as previously described. The C-terminal domain of TnT (residues 272-288) forms the tropomyosin binding region.

In conditions of diastolic $[Ca^{2+}]_i$, the inhibitory region of TnI is bound to actin, blocking cross-bridging. However, when sarcoplasmic $[Ca^{2+}]_i$ rises to systolic levels, occupation of the N-terminal Ca^{2+} binding site of TnC induces a conformational change in TnC which reveals a hydrophobic binding patch, to which the α-helix directly downstream of TnI's inhibitory region (C) binds (Li, Spyracopoulos et al. 1999). This causes TnI to detach from actin and tropomyosin, and the inhibitory effect is relieved. Determination of the structure of the troponin complex via X-ray crystallography has been integral to understanding the way Ca^{2+} binding to the myofilament triggers contraction (Takeda 2005).

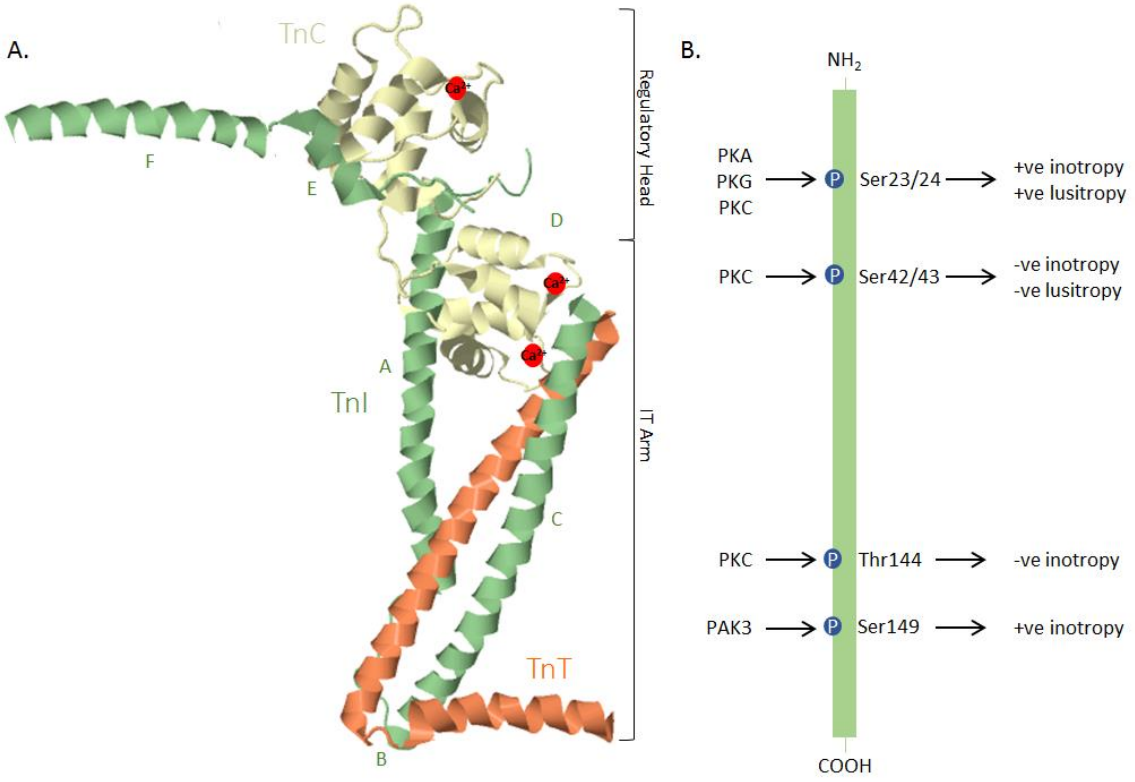

Figure 1.3: Molecular structure and phosphorylation sites of TnI. A. Crystal structure of the troponin molecule. The troponin heterotrimer is made up primarily of α-helices. There are two structurally separate subdomains: the regulatory head domain and the IT arm. The regulatory head is made up of TnC 3-84 and TnI 150-159, and the IT arm is made up of TnC 93-161, TnI 42-136, and TnT 203-271. B. Schematic view of the phosphorylation sites of TnI. Under stimulation via β-adrenergic stimulation, PKA is activated, and can phosphorylate TnI at Ser23/24, leading to an increase in cross-bridge cycling and decreased myofilament Ca^{2+} sensitivity. This site can also be phosphorylated by PKG, which is activated by nitric oxide (NO) or C-type natriuretic peptide (CNP) signalling. PKC phosphorylation can occur at Ser23/24, Ser42/43, and Thr144; PKC can be activated due to AngII, ET-1 or α-adrenergic agonists. PKC phosphorylation at the latter two of these sites results in opposing functional effects to Ser23/24 phosphorylation. Finally, PAK3 can phosphorylate the final site, Ser149. (Adapted from (Takeda, Yamashita et al. 2003, Layland, Solaro et al. 2005). Created using (Rose, Bradley et al. 2018) (PDB ID: 1J1D)).

Post-translational modifications of TnI have been shown to have regulatory effects on cardiac contractile function. In particular, the phosphorylation of specific serine and threonine residues has been widely studied (Figure 1.3B) (reviewed in (Metzger and Westfall 2004, Layland, Solaro et al. 2005)).

Most relevant to the work presented here is the phosphorylation of Ser23/24 by protein kinase A (PKA). Under conditions of increased cardiac demand, ß-adrenergic stimulation triggers production of cAMP which activates PKA, resulting in the phosphorylation a number of substrate proteins. The concomitant phosphorylation of calcium handling and myofilament proteins by PKA results in positive inotropic and lusitropic effects. Studies in rodents have shown that PKA phosphorylation of Ser23 and Ser24 (Ser22/23 in mouse) plays a part in this effect by enhancing the relaxation of the myocyte by altering myofilament properties. When TnI is phosphorylated at this site, the myofilament shows a reduced sensitivity for Ca^{2+} and an increased rate of dissociation of Ca^{2+} (Zhang, Zhao et al. 1995). Studies have also reported increased cross-bridge cycling rate and unloaded shortening velocity. When TnI expression was altered by the replacement of endogenous TnI with either slow skeletal TnI (ssTnI, which lacks 27-33 N-terminal residues including the phosphorylation site) or mutated TnI in which the phosphorylation site has been replaced by non-phosphorylatable alanine residues, the lusitropic response to ß-adrenergic stimulation was attenuated (Fentzke, Buck et al. 1999, Kentish, McCloskey et al. 2001, Pi, Kemnitz et al. 2002, Pi, Zhang et al. 2003). Furthermore, the changes in myofilament Ca^{2+} sensitivity were abolished. On the other hand, overexpression of constitutively “phosphorylated” TnI in which Ser22/23 were replaced with aspartate residues, enhanced the lusitropic effects (Takimoto, Soergel et al. 2004). Together, these studies provide convincing evidence that TnI phosphorylation contributes to the positive lusitropic response observed following ß-adrenergic stimulation. However, it is important to note that these findings are considered rather controversial, as other studies did not record functional changes at the myofilament under similar conditions (Janssen and de Tombe 1997, Johns, Simnett et al. 1997). More recently, these studies have been expanded to determine the role of biphosphorylation and monophosphorylation in human myocardium. Using isolated cells from donor and transplant human myocardium, endogenous TnI was exchanged for either of the

two monophosphorylated mutants (aspartic acid at either Ser23 or Ser24), a biphosphorylated mutant (aspartic acid at both Ser23/24) or a non-phosphorylatable mutant (alanine at Ser23/24) (Wijnker, Foster et al. 2013). The results from this work suggested that phosphorylation at both serine residues was necessary to observe the reduced myofilament sensitivity to Ca^{2+} in both healthy and diseased cardiac myofilaments.

Phosphorylation of TnI by PKC is less well established with numerous conflicting reports in terms of functional effects. In cardiac myocytes, PKC can be activated by several agents, including angiotensin II, endothelin-1 and phenylephrine. PKC isoforms expressed in the heart include PKC_{α}, PKC_{δ} and PKC_{ε}; several of these isoforms are upregulated in disease, such as $PKC_{\beta1/\beta2}$ and PKC_{α} (Metzger and Westfall 2004). PKC has been shown to phosphorylate TnI at three sites, Ser23/24, Ser43/45, and Thr144. Interestingly, the activation of PKC by different physiological agonists has been observed to affect cardiac contractility in different ways (Metzger and Westfall 2004). This is likely due to the widespread myofilament and non-myofilament effects of PKC phosphorylation in the cells. Briefly, studies employing the use of phosphomimetic Ser43/45 TnI have shown that phosphorylation at this site leads to reduced myofilament Ca^{2+} sensitivity, reduced shortening and slowed contraction (Noland, Raynor et al. 1996, Burkart, Sumandea et al. 2003, Liu, Lopez et al. 2014, Lang, Schwank et al. 2015). The role of phosphorylation at Thr144 has been studied in a similar way, by replacing endogenous TnI with phosphomimetic TnI. The functional role of this modification, although shown in some studies to have little influence, likely involves the desensitisation of the myofilament to Ca^{2+} with little effect on other functional parameters (Burkart, Sumandea et al. 2003, Lu, Hinken et al. 2010). Studying the functional effects of phosphorylation at the PKC sites is further complicated by the evidence of extensive crosstalk between the sites. Several research groups have employed the use of multiple site phosphomimetic TnI to determine the additive effects of multiple phosphorylations (Lu, Hinken et al. 2010, Lang, Schwank et al. 2015). It has been shown that that phosphorylation of Ser23/24 enhances the Ser43/45 induced decrease in function while phosphorylation at Thr144 reduces the functional effect of phosphorylation at Ser43/45 (Lang, Schwank et al. 2015).

1.3 Cardiac Troponin I and Heart Disease

1.3.1 Heart Failure

Although heart disease comes in many forms, the present work will focus mainly on heart failure, which was estimated to affect nearly one million people in the UK in 2014 (Conrad, Judge et al. 2018). Put simply, heart failure is a syndrome caused by the inability of the heart to meet the needs of the circulation. Often, this is caused by damage to the heart, such as myocardial infarction (MI) or pressure overload due to high systemic blood pressure, which leads to structural or functional changes in the heart. Symptoms often include breathlessness, fatigue and pulmonary oedema. Such symptoms can display at rest or during activity depending on disease severity. This complex and multifactorial disease is often diagnosed with a number of comorbidities, such as hypertension, and causes increased likelihood for a number of other cardiovascular diseases, such as stroke.

One way of categorising heart failure is on the basis of ejection fraction, which is the fraction of left ventricular blood pumped out of the heart with each contraction. Patients who have impaired cardiac contractility (<40%) are diagnosed with HFrEF (heart failure with reduced ejection fraction, or HF with systolic dysfunction); patients whose ejection fraction is normal or only mildly reduced and who have a normal, undilated left ventricle, but other signs of structural damage of the myocardium, have HFpEF (heart failure with preserved ejection fraction) ((SIGN) 2016).

Heart failure can also be described in terms of the stage of disease (Figure 1.4) (Tham, Bernardo et al. 2015). Following cardiac stress or injury, hypertrophic growth and remodelling of the heart can be compensatory, allowing the cardiac output to meet the demands of the circulation. Although this growth is still considered pathological, it is reversible with lifestyle change and/or treatment. Chronic stress on the heart, however, can lead to dilated, decompensated heart failure, in which the ventricles become dilated and dysfunctional. The ventricles are no longer able to contract sufficiently to produce sufficient cardiac output to meet the circulatory demands, and symptoms, such as exercise intolerance become much more profound.

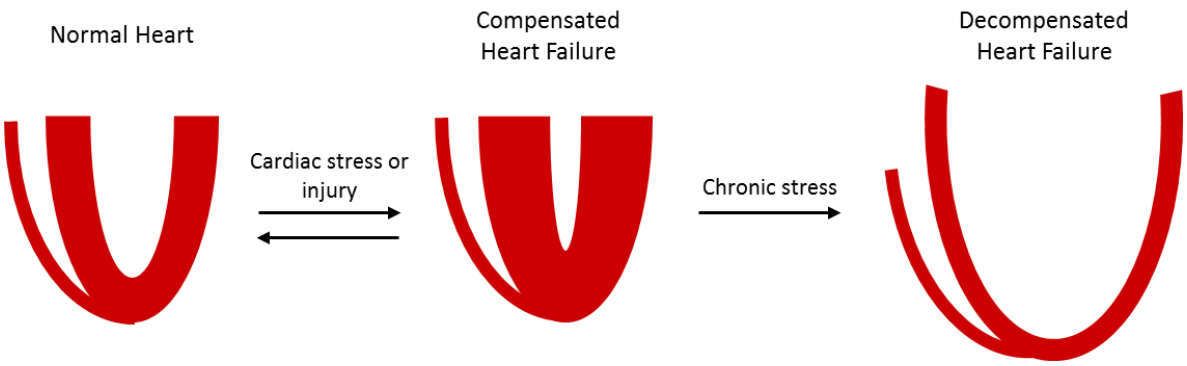

Figure 1.4: Pathological remodelling of the ventricle in heart failure. In reaction to stress or injury, the left ventricle undergoes hypertrophic remodelling. If the stress is sustained, remodelling can result in the onset of decompensated heart failure, in which the ventricle is enlarged and dilated and systolic dysfunction leads to decreased cardiac output. (Adapted from (Tham, Bernardo et al. 2015)).

There are a number of ways in which heart failure is managed, from lifestyle changes to pharmacological therapy and interventional procedures, all of which are outlined by national clinical guidelines ((SIGN) 2016). Although numerous pharmacological agents are used for the management of this syndrome, the most common are ß-adrenergic receptor blockers (ß-blockers), angiotensin-converting enzyme inhibitors (ACE inhibitors) and angiotensin receptor blockers (ARBs) ((SIGN) 2016). ß-blockers function by reversing the detrimental neurohormonal effects of sympathetic nervous system hyperactivation. This hyperactivation is first compensatory by increasing cardiac output, but later becomes detrimental, inducing hypertrophy and impaired function (Bavishi, Chatterjee et al. 2015). ACE inhibitors and ARBs act by reducing systemic vascular resistance through its interaction with the renin-angiotensin system. These drugs reduce fluid retention by attenuating the activity of angiotensin, reducing blood volume, which has a direct effect on the systemic blood pressure (Brown and Vaughan 1998). Other pharmacological agents include mineralocorticoid receptor antagonists, neprilysin inhibitors and various diuretics (which decrease systemic blood pressure), ivabradine (which induces negative chronotropy to normalise sinus rhythm) and digoxin (which induces positive inotropy) (Campbell and MacDonald 2003, Koruth, Lala et al. 2017). Intraventional therapies generally treat the underlying cause of heart failure rather than the symptoms of the syndrome itself. Cardiac resynchronisation therapy and implantable cardioverter defibrillators are used to normalise sinus rhythm and to protect against ventricular fibrillation ((SIGN) 2016). Finally, cardiac transplantation has been

used with good outcomes for patients with advanced heart failure (Anyanwu, Rogers et al. 2002). Most heart failure management plans also involve lifestyle interventions, including a healthy, low sodium diet and exercise.

1.3.2 Troponin I in Heart Failure

In the context of heart disease, Tn is most commonly referred to in the context of Tn level detection for diagnostics. Elevated TnI or TnT levels in the blood indicate damage to the heart as the damaged myocardium releases Tn into the circulation (Mahajan and Jarolim 2011, Shah, Ferry et al. 2017). Current tests detect TnI in the blood with high sensitivity (NICE 2014). However, studying post-translational modifications of TnI has shown that this protein has functional effects in pathophysiological states beyond its diagnostic utility.

For over two decades, it has been known that the phosphorylation of Ser23/24 of TnI is reduced in chronic heart disease, from dilated cardiomyopathy to chronic heart failure (Bodor, Oakeley et al. 1997, Zakhary, Moravec et al. 1999). The cause and effect relationship of this reduction between healthy and pathological states is not well established. However, reduced TnI phosphorylation may be due to the downregulation of the ß-adrenergic signalling pathway which is often characteristic of heart failure (Wolff, Buck et al. 1996, Layland, Solaro et al. 2005). The functional effects of reduced phosphorylation at this site are consistent with the pathophysiology of the disease. Decreased PKA-dependent phosphorylation increases Ca^{2+} sensitivity of the myofilament as well as impairing cross-bridge dynamics, and these effects may contribute to impaired contraction and relaxation of the myocardium in disease states (Layland, Solaro et al. 2005). Interestingly, the functional role of Ser23/24 phosphorylation by PKA has been shown to change in disease states due to the reduced basal phosphorylation during disease. Activation of PKA following ß-adrenergic stimulation in failing myocardium that has reduced phosphorylation and increased basal Ca^{2+} sensitivity, results in a greater reduction in Ca^{2+} sensitivity than in healthy myocardium with normal phosphorylation levels (McConnell, Moravec et al. 1998, van der Velden, Papp et al. 2003, Kooij, Saes et al. 2010). More recent studies have shown that the outcome of TNI phosphorylation by PKA is dependent on disease stage. Simply put, in heart failure caused by pressure overload (e.g. congestive heart failure) the myocardium first compensates for

the increased demand by exhibiting hypertrophy and preserved contractility. In later stages of disease, the ventricle dilates and contractility is impaired. Hence, in early stage, compensated heart failure, TnI phosphorylation increases, while late stage, dilated heart failure is marked by reduced phosphorylation (Walker, Fullerton et al. 2013).

Conversely, the PKC-mediated phosphorylation of Ser43/45 is upregulated in heart failure in conjunction with an increased expression of PKC_{β}, which may contribute to impaired cardiac function and increased myofilament Ca^{2+} sensitivity observed in disease (Layland, Solaro et al. 2005, Christopher, Pizarro et al. 2009, Walker, Walker et al. 2010). Again, these alterations may be dependent on the stage of disease.

In heart failure, although the overall phosphorylation levels of TnI are unchanged, the levels of Ser23/24 and Ser43/45 phosphorylation are increased and decreased respectively compared to healthy myocardium. This observation is consistent with the functional roles of these post-translational modifications and suggests that the changes may have a role in the pathophysiology of heart disease. Often, it is thought that Ca^{2+} handling and altered Ca^{2+} dynamics are the major factor in cardiac myocyte dysfunction in disease, but increasingly, altered myofilament dynamics are thought to have an important role (Hamdani, Kooij et al. 2008).

Noteworthy evidence for a functional role of TnI truncation and degradation in heart disease also exists. In a rodent model of I/R injury, TnI was cleaved at its C-terminal end, leaving truncated TnI_{1-192}. Although replacement of full-length TnI with truncated TnI aid not alter maximal force development, it increased myofilament Ca^{2+} sensitivity significantly (Hamdani, Kooij et al. 2008). Low levels of TnI degradation were also observed in a porcine model of myocardial infarction (van der Velden, Merkus et al. 2004).

1.3.3 Myofilament Dysfunction in Heart Failure

The pathophysiology of heart failure is often attributed to changes in structure of the heart (such as dilation or hypertrophy), cell death or alterations Ca^{2+}-handling. More recently, however, it has become clear that impaired

myofilament function can contribute to decreased inotropy and lusitropy within the failing myocardium. More specifically, development of reduced sarcomeric maximal force attenuates contractility while increased Ca^{2+} sensitivity and passive stiffness contribute to impaired relaxation (Hamdani, Kooij et al. 2008). There are multiple factors which may contribute to these observations, including altered expression of different sarcomere protein isoforms, proteolysis or protein degradation and post-translational modifications, namely phosphorylation.

In the failing myocardium, it has been observed that foetal protein isoform expression is increased. A small shift in expression of the fast α-MHC to the slow ß-MHC has been shown to reduce both energy consumption and the speed of contraction (Barany 1967, Lompre, Schwartz et al. 1979, Mercadier, Bouveret et al. 1983, Miyata, Minobe et al. 2000, Narolska, van Loon et al. 2005). Furthermore, MLC-1 expression was changed in diseased ventricles. In adults, the normally expressed ventricular form (VLC-1) was replaced by the atrial form (ALC-1), which caused increased maximal force (Ritter, Luther et al. 1999). Finally, expression of foetal TnT has been observed, but without a clear indication of a functional effect (Mesnard-Rouiller, Mercadier et al. 1997, Hamdani, Kooij et al. 2008). Importantly, the expression changes were highly variable across different studies, and some were more significant in rodent studies than in humans, casting doubt upon a significant functional role in the pathophysiology of human disease (Lompre, Mercadier et al. 1981). In fact, it has been postulated that these changes do not explain dysfunction, but conversely, represent compensatory changes (Hamdani, Kooij et al. 2008).

Phosphorylation of sarcomeric proteins has been widely shown to have a pathophysiological role in heart failure. Much of the altered protein phosphorylation can be attributed to changes in neurohormonal signalling. In heart failure, desensitisation and down-regulation of ß-adrenergic receptors reduces the activation of PKA, which leads to a reduction in the phosphorylation of several myofilament proteins such as TnI and MyBP-C (Bristow, Ginsburg et al. 1986). As previously mentioned, reduced PKA phosphorylation of TnI leads to increased Ca^{2+} sensitivity, which has been directly observed in permeabilised human myocytes isolated from diseased hearts (Wolff, Buck et al. 1996, Bodor, Oakeley et al. 1997, van der Velden, Papp et al. 2003, Messer, Jacques et al.

2007). Moreover, the increased Ca^{2+} sensitivity of the myofilament can be completely reversed by treatment with PKA catalytic subunit, confirming the role of phosphorylation in this parameter of myofilament dysfunction in disease (van der Velden, Papp et al. 2003). Overall, reduced phosphorylation of TnI contributes to impaired relaxation in the failing myocardium (Hamdani, Kooij et al. 2008).

More recently, it has been shown in both human heart failure and in animal models (dogs with pacing induced end-stage heart failure) that the PKA phosphorylation of MyBP-C is dramatically reduced in diseased myocardium (El-Armouche, Pohlmann et al. 2007, Kooij, Holewinski et al. 2013). MyBP-C is associated with the cardiac thick filament, and functions by maintaining the structure of the sarcomere and regulating crossbridging of actin and myosin (Carrier, Mearini et al. 2015). Phosphorylation by PKA accelerates cross-bridging of actin and myosin by alleviating the inhibitory influence of non-phosphorylated MyBP-C (Gautel, Zuffardi et al. 1995, Shaffer, Kensler et al. 2009, Moss, Fitzsimons et al. 2015, Kensler, Craig et al. 2017). Therefore, reduced phosphorylation restores this inhibitory influence, attenuating cross-bridging and slowing cross-bridge kinetics. The relative contribution of these phosphorylation changes to the pathophysiology of disease requires further investigation.

1.4 Cyclic Nucleotide Signalling

1.4.1 Intracellular Signal Transduction and Second Messengers

Signal transduction is the mechanism by which an extracellular stimulus is converted to an intracellular effect. Generally speaking, this process begins with the interaction of an extracellular ligand, often a hormone or neurotransmitter, with a membrane bound receptor. Upon activation, the receptor initiates an intracellular signalling cascade, which often involves a second messenger. Second messengers provide the link between receptors and cellular effector proteins which convert a signal into a physiological action (Sutherland 1972). Activation of receptors alters the intracellular concentration of the corresponding second messenger, which in turn affects the activity of cellular effector proteins, which orchestrate the appropriate, receptor-specific response. The response is ended when the concentration of second messenger is reduced

to a resting state, which can be accomplished via the efflux of second messenger out of the cell, or the degradation of second messenger by specialised proteins. Some second messengers which are widely employed by cells for signal transduction include Ca^{2+}, inositol triphosphate (IP_3), diacylglycerol (DAG) and the cyclic nucleotides (Berridge 1984). There are two main cyclic nucleotide species, cyclic 3',5'-adenosine monophosphate (cAMP) and cyclic 3',5'-guanosine monophosphate (cGMP), which are each comprised of a nucleotide with a single phosphate which have two single bonds between the sugar and phosphate groups, creating a cyclic structure (Figure 1.5). Less well-known non-canonical cyclic nucleotides, such as cyclic 3',5'-cysteine monophosphate (cCMP) and cyclic 3',5'-uracil monophosphate (cUMP) will not be described in the present work.

1.4.2 cAMP Signalling Pathway

The concept of a second messenger was born out of the discovery of cAMP (Rall and Sutherland 1958).

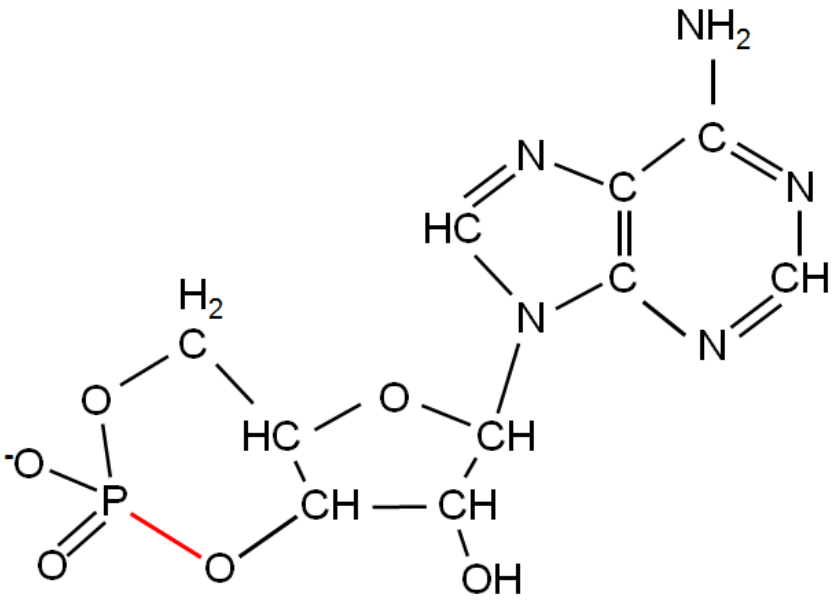

Figure 1.5: Molecular structure of cAMP. The cyclic structure derives from the presence of two single bonds between the sugar within the nucleotide and the phosphate group. One of these phosphodiester bonds, highlighted in red, is hydrolysed by PDEs, yielding the product, 5'-adenosine monophosphate (5'-AMP) (adapted from (Bender and Beavo 2006)).

The cAMP signalling pathway begins with the interaction of a ligand with a G-protein-coupled receptor (GPCR). In humans, approximately 4% of the protein coding genome codes for GPCRs; these receptors are widespread in terms of

expression and physiological actions, from hormonal and neuronal signalling to sensory transduction (Fredriksson, Lagerstrom et al. 2003). The receptors are comprised of an extracellular N-terminal region, seven transmembrane α-helices and an intracellular C-terminal region. Generally, the N-terminal domain contains the ligand binding site while the C-terminal region interacts with heterotrimeric G-proteins, which contain α, ß, and γ subunits (Cherezov, Rosenbaum et al. 2007). Upon activation by ligand binding, the GPCR causes the α-subunit's attached guanosine diphosphate (GDP) to be exchanged for guanosine triphosphate (GTP), causing a conformational change and the dissociation of the Gα. There are three types of Gα subunit with distinct functions: $G\alpha_s$, $G\alpha_i$ and $G\alpha_q$ (Pierce, Premont et al. 2002). $G\alpha_s$ positively interacts with the enzyme, adenylyl cyclase (AC), which catalyses the production of cAMP. Conversely, $G\alpha_i$ negatively interacts with AC, inhibiting its action. Finally, $G\alpha_q$ acts independently of AC and the cAMP pathway, instead activating phospholipase C and signalling through the second messengers IP_3 and DAG. Additionally, the βγ complex of the G protein often mediates alternative signalling pathways. Each subunit is coded by numerous genes (sixteen α, five ß and twelve γ), and the various ways in which these subunits combine add to the functional diversity of GPCR signalling (Pierce, Premont et al. 2002).

As mentioned, the classical signalling pathway of GPCRs involves the activation or inhibition of the membrane bound enzyme AC by $G\alpha_s$ and $G\alpha_i$ respectively. When AC was first cloned in 1989, its complex structure led the researchers to infer a channel or transporter function (Krupinski, Coussen et al. 1989). It is comprised of NH_2 and COOH terminal domains, two transmembrane clusters (TM1 and TM2), and two cytoplasmic loops. The two cytoplasmic loops contain the catalytic regions, C1A and G2A, which are conserved ATP-binding regions. These regions dimerise, forming the catalytic site of the enzyme. Since the initial characterisation, eight more structurally similar AC isoforms have been identified (Krupinski, Lehman et al. 1992, Willoughby and Cooper 2007). Upon activation by the association with $G\alpha_s$, AC is activated and catalyses the production of cAMP from ATP. The structure of the catalytic site is remarkably similar to DNA polymerase, suggesting that it functions by the same phosphoryl transfer mechanism (Tesmer, Sunahara et al. 1997, Zhang, Liu et al. 1997). In fact, the catalytically active site contains two aspartate residues which allow

the binding of two Mg^{2+} molecules. These metal ions facilitate phosphoryl-transfer, promoting the cyclisation of cAMP and the release of the two phosphate groups (Willoughby and Cooper 2007). The activity of AC results in an increase in the intracellular concentration of cAMP.

1.4.3 cAMP Effector Proteins

A rise in the concentration of cAMP above threshold levels activates four main types of effector proteins: protein kinase A (PKA), exchange proteins directly activated by cAMP (Epac), cyclic nucleotide gated ion channels (CNGC) and popeye domain-containing proteins (POPDC) (Figure 1.6).

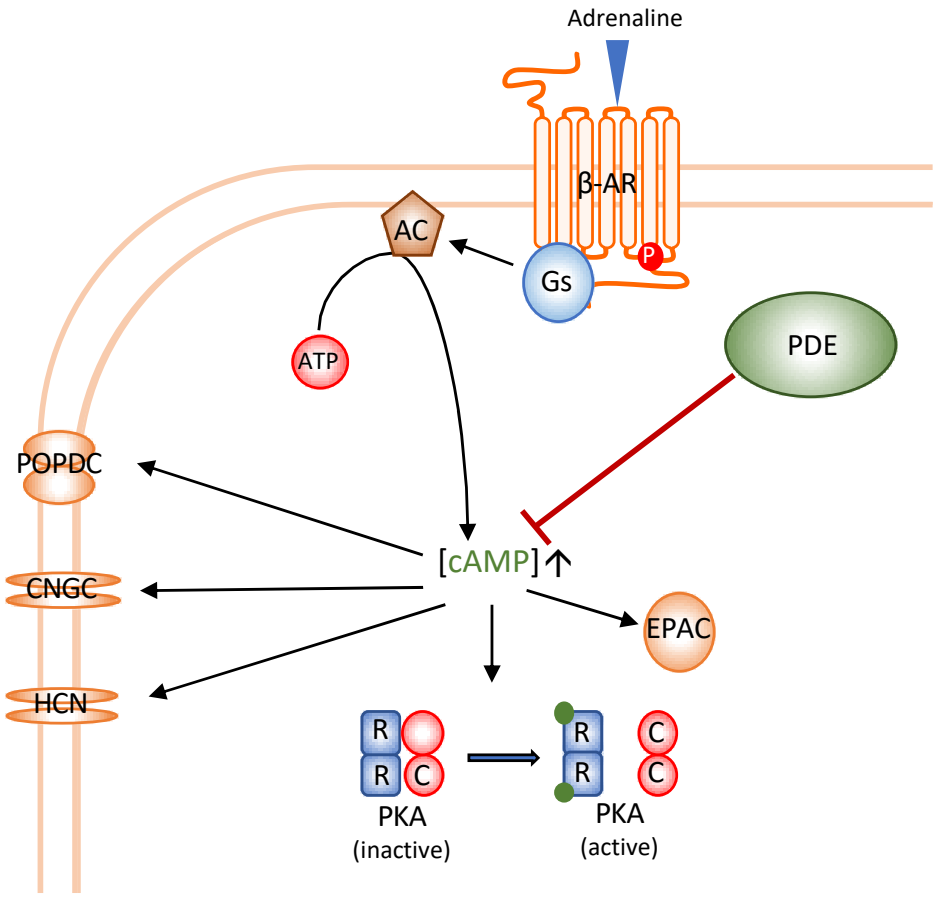

Figure 1.6: β-adrenergic signalling utilising cAMP as a second messenger. Although this figure uses the β-adrenergic receptor as an example, a number of GPCRs utilise similar signalling pathways. Following the activation of the GPCR, the tethered Gs protein is activated, stimulating AC to produce cAMP from ATP. cAMP activates four types of effector proteins: CNGC, PKA, EPAC and POPDC, all of which have varied cellular effects. HCN channels are also gated by cAMP and are important in cardiac cells. PDEs are enzymes which hydrolyse cAMP, having an inhibitory effect on its second messenger activity. (AC, adenylyl cyclase; ATP, adenosine tri-phosphate; β-AR, β-adrenergic receptor; C, catalytic subunit of PKA; CNGC, cyclic nucleotide gated channel; EPAC, exchange protein directly activated by cAMP; Gs, stimulatory G-protein; HCN, hyperpolarisation-activated cyclic nucleotide-gated channel; PDE, phosphodiesterase; PKA, protein kinase A; POPDC, popeye domain containing protein; R, regulatory subunit of PKA).

PKA exists as a tetrameric enzyme with two regulatory subunits (R) and two catalytic subunits (C) (Kemp, Bylund et al. 1975). The regulatory subunits bind cAMP, which causes a conformational change and the dissociation of the catalytic subunits. The dissociation of the regulatory subunits from the catalytic subunits serves to activate the enzyme's catalytic activity. Recently, this classical view of activation via regulatory subunit dissociation has been challenged, with evidence that dissociation was not necessary for activation of catalytic activity (Smith, Esseltine et al. 2017). PKA belongs to a family of serine/threonine kinases; its active site catalyses the transfer of a phosphate group from ATP to threonine or serine residues on its target proteins, which are typically integrated into the motif R-R-Ø-S (Ø in this case is a hydrophobic amino acid) (Skalhegg and Tasken 2000). Phosphorylation of PKA substrate proteins can have a myiad of cellular effects. For example, in cardiomyocytes, PKA is a very influential cAMP effector, phosphorylating and affecting the function of many proteins involved in excitation-contraction coupling (Wolff, Buck et al. 1996, Baryshnikova, Li et al. 2008, Jones, Meng et al. 2008, Barefield and Sadayappan 2010).

Epac was identified more recently as a cAMP effector when it was shown to have a cAMP binding domain similar to that of PKA's regulatory subunits (de Rooij, Zwartkruis et al. 1998, Kawasaki, Springett et al. 1998). This protein functions to activate the Rap1 and Rap 2 proteins, which belong to the Ras family of small GTPases (Cheng, Ji et al. 2008). The two isoforms, Epac1 and Epac2, have different expression patterns, with Epac1 being more widespread and Epac2 having more restricted expression. These proteins have been shown to be involved in many cellular processes including cell adhesion and junction formation as well as the control of neurotransmitter and hormone release (Bos 2006). Many of these processes depend on the integrated activities of PKA and Epac.

First discovered in rod photoreceptors in the eye, cyclic nucleotide-gated ion channels (CNGC) are the third type of cyclic nucleotide effector protein. In the rod photoreceptor cells, these channels are predominantly activated by cyclic guanosine monophosphate (cGMP) (Chen and Yau 1994, Liu, Chen et al. 1994). CNGCs are composed of four subunits which all share similar structures and are organised around a central pore through which cations can flow. The subunits

each contain six transmembrane domains and a C-terminal region with a cyclic nucleotide binding domain (CNBD) (Matulef and Zagotta 2003). Binding of a cyclic nucleotide to this domain results in the opening of the channel and the influx of cations into the cell. Of particular physiological importance in the heart is the hyperpolarisation-activated cyclic nucleotide-gated (HCN) channel (Herrmann, Schnorr et al. 2015). Activated by membrane hyperpolarisaion, these channels are open and permeable to Na^+ and K^+ near the resting membrane potential of cardiac cell, resulting in the I_f current (Benarroch 2013). The I_f current provides the initial depolarisation of the cardiac action potential. Binding of cAMP to the CNBD of these channels activates their current by lowering the threshold potential for channel opening (DeBerg, Brzovic et al. 2016).

Recently, the POPDC family of proteins (POPDC1, POPDC2 and POPDC3) has been identified as a novel class of cAMP effector proteins. These transmembrane proteins are abundant in muscle cells and have been shown to bind cAMP with high affinity, but their functional role and biochemical activity is not well understood (Brand and Schindler 2017). Most of the current understanding of POPDC's function comes from knockout animals. In mice, POPDC1 and 2 are highly expressed in the myocardium and knocking out these genes caused altered cardiac phenotypes. In rodents, myocardium lacking POPDC1 displayed reduced recovery after cardiotoxin injection and ischaemic reperfusion (I/R) injury than wildtypes, suggesting a role for the protein in recovery (Alcalay, Hochhauser et al. 2013, Kliminski, Uziel et al. 2017). Furthermore, POPDC1 and 2 are enriched in the conduction system of the heart, and knockout animals displayed age-dependent dysfunction in pacemaking (Froese, Breher et al. 2012).

1.5 Cyclic Nucleotide Phosphodiesterases

Ending cyclic nucleotide driven responses requires the concentration of the second messenger within the cell to decrease below the activation threshold of cAMP effectors, which occurs via the action of cyclic nucleotide phosphodisterases (PDEs). PDEs are the only known enzymes which can degrade cyclic nucleotides. These enzymes function by hydrolysing the 3',5'-phosphodiester bond of cAMP or cGMP, converting it to 5'-AMP or 5'-GMP respectively.

Although there are three classes of PDEs, all mammalian enzymes fall under Class 1. There are 21 genes in this class, which have been grouped into eleven families. The numerous splice variants that can be expressed in each family result in nearly 100 PDE isoforms (Maurice, Ke et al. 2014). This large family of enzymes has a wide variety of distributions and functions, but the general structure of these enzymes remains fairly consistent. The large C-terminal region comprises cyclic nucleotide binding regions and areas which regulate catalytic activity. The increasingly important localisation information is mostly housed within the N-terminal region of the proteins, although it is becoming clear that other conserved targeting domains are possible. For example, a multifunctional docking domain has been identified within the catalytic domain of PDE4 (Houslay, Christian et al. 2017). Between the C-terminal and isoform-specific N-terminal parts, the conserved catalytic domain is the largest segment that carries out the hydrolysis and degradation of cAMP (Omori and Kotera 2007). It has been shown that the catalytic activity of this domain is inhibited by caffeine, which in turn potentiates cAMP signalling due to the inhibition of its degradation (Sutherland and Rall 1958).

Of the numerous members of the PDE superfamily, only a subset of isoforms has been shown to be active in the heart. These isoforms will be discussed in more detail in later sections of this work.

Considering the widespread role of PDEs in the ubiquitous cyclic nucleotide signalling pathways, it is not surprising that the ablation of their hydrolytic activities have been targeted as a therapeutic strategy by many research labs and pharmaceutical companies. In the early 1960s, the caffeine derivative, theophylline was shown to potentiate cardiac inotropic responses by enhancing adrenergic signalling (Rall and West 1963). Since then, the efforts to target PDEs pharmacologically have continued, and a few drugs, which target PDE families specifically have reached the market.

1.5.1 PDE4 Family

The PDE4 family of enzymes is the most relevant for the present work. The four PDE4 genes (PDE4A, B, C and D) are alternatively spliced into over 20 isoforms (Houslay, Baillie et al. 2007). Generally, PDE4s are comprised of an isoform

specific N-terminal transduction domain (TD), upstream conserved regions 1 and 2 (UCR1 and UCR2), which are linked to each other and to the catalytic region by linker regions 1 and 2 (LR1 and LR2) respectively, and the conserved C-terminal catalytic domain (Houslay, Baillie et al. 2007, Fertig and Baillie 2018). Based on the presence and size of UCR1 and UCR2 in PDE4 splice variants, family members can be further categorised into long, short, super-short or dead-short isoforms (Figure 1.7). The TD has been shown to be important for targeting of PDE4 isoforms to specific subcellular locations; however, it has recently been shown that other regions can direct localisation, including the multifunctional docking site at the C-terminal end of the catalytic domain (Houslay, Christian et al. 2017). UCR1 and UCR2 function by regulating the outcomes of PDE4 phosphorylation by PKA or ERK (Hoffmann, Baillie et al. 1999, MacKenzie, Baillie et al. 2002). Finally, the catalytic domain has been shown to include a deep hydrophobic pocket, which provides the active site for cAMP hydrolysis (Ke and Wang 2007).

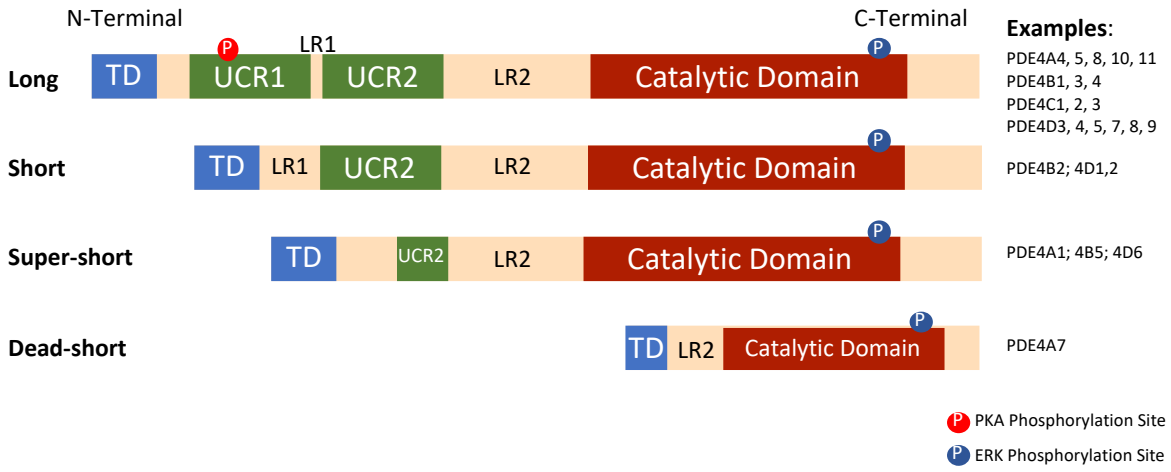

Figure 1.7: PDE4 isoforms. A schematic representation of the domain organisation of PDE4 enzymes and the organisation of the isoforms into long, short, super-short and dead-short. (LR, linker region; TD, transduction domain; UCR, upstream conserved region.) (Adapted from (Fertig and Baillie 2018)).

1.5.2 Compartmentalisation of cAMP Signalling by PDEs

cAMP is a small, highly diffusible molecule. When it is produced by membrane bound AC, it should quickly diffuse throughout the cell, uniformly increasing the cytosolic and nuclear concentration and subsequently activating all available effector proteins. If this were true, however, it would not be possible for cAMP

to cause multiple different, receptor-specific responses within the same cell. The reality is that many cells utilise cAMP signalling in response to many different stimuli to produce discrete, non-overlapping responses. The mechanism behind these receptor-specific responses was first investigated by Brunton and colleagues, who showed that many different GPCRs in cardiac myocytes elevated cAMP concentration to similar levels within the cell, yet resulted in different physiological outcomes (Hayes, Brunton et al. 1980). In conclusion, the researchers proposed the concept of the compartmentalisation of signalling, in which specific cAMP effectors were restricted to specific compartments within the cell, and certain receptors could only activate certain pools of these effectors depending on their proximity to PDEs (Brunton, Hayes et al. 1981, Hayes and Brunton 1982).

Early immunohistochemical staining techniques were able to show localisation and compartmentalisation of cyclic nucleotides (Steiner, Whitely et al. 1975), but advances in the field were slow before the development of genetically encoded optical probes, which could detect cyclic nucleotide dynamics in real time in living cells, using fluorescence resonance energy transfer (FRET) (discussed in more detail later) (Zaccolo, De Giorgi et al. 2000, Nikolaev, Gambaryan et al. 2006, Nikolaev and Lohse 2006). The visualisation of discrete cAMP microdomains in the cardiac myocyte due to different receptor stimulations was one of the first major ground-breaking studies using this technique (Figure 1.8) (Zaccolo and Pozzan 2002). Several pre-existing observations led to this study. It had already been shown that PKA was localised in specific subcellular locations by A-kinase anchoring proteins (AKAPs), and there was evidence for the localisation of PDEs by the same mechanism (Yang, Drazba et al. 1998, Dodge and Scott 2000, Dodge, Khouangsathiene et al. 2001). These observations provided the necessary framework to make the proposed mechanism of cAMP compartmentalisation feasible.

Many studies have now provided direct evidence for the mechanism of cAMP compartmentalisation and receptor-specific responses. Localisation of PDEs in discrete subcellular locations creates a mechanism by which these enzymes can act as local ‘sinks’ which decrease local cAMP concentration and restrict the diffusion of the second messenger (Baillie 2009). This allows subcellular cAMP gradients to be created within the cell, dependent on the specific receptor that

has been stimulated. These gradients were displayed in cardiac myocytes using genetically encoded cAMP reporters (Zaccolo and Pozzan 2002). In this study, when cardiac myocytes were treated with β-adrenergic agonists, there were defined, simultaneous cAMP gradients formed throughout the cell. However, when these cells were treated with the non-specific PDE inhibitor, IBMX, the areas of high cAMP concentration expanded until the whole cell was swamped in a uniformly high cAMP concentration. This observation was key in signifying the importance of localised PDE activity in restricting the free diffusion of cAMP and shaping cAMP gradients in space and time. Therefore, this is a mechanism by which the cAMP concentration can increase in the vicinity of the appropriate effector proteins without ubiquitously activating all effectors in the cell. Of course, this is made possible by the anchoring of the effectors to specific locations, for example, the anchoring of PKA by AKAPs. When a receptor is activated, the concentration of the respective pool of cAMP is elevated enough to swamp the correctly positioned PDEs, and the relevant effector can be activated.

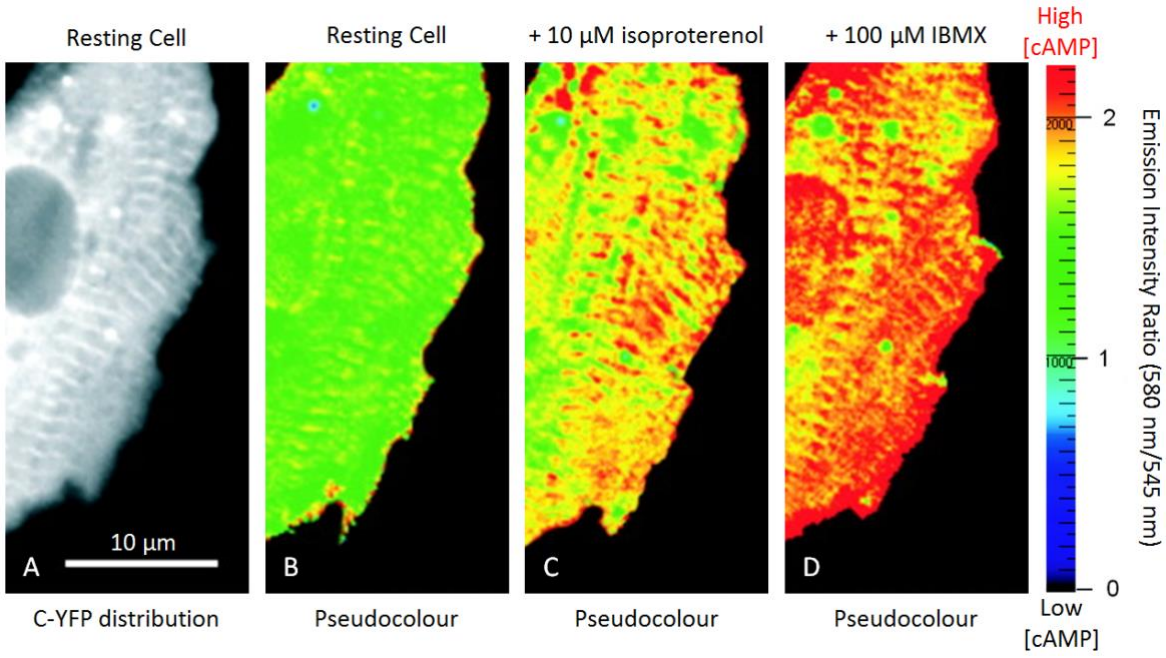

Figure 1.8: The effect of β-adrenergic stimulation and PDE inhibition on cAMP diffusion in a cardiac myocyte. Cells were transfected with cAMP reporters (based on the structure of PKA, RII-CFP and C-YFP), allowing local changes in [cAMP] to be detected. A. The distribution of C-YFP within the cell. When cells were treated with isoproterenol (C) to stimulate β-adrenergic signalling, local increases in cAMP were observed compared to the low basal levels in a resting cell (B). Treatment of the same cell with nonspecific PDE inhibitor, IBMX, resulted in the diffusion of these high [cAMP] areas throughout the cell (D), displaying the role of PDE in the compartmentalisation of signalling (Adapted from (Zaccolo and Pozzan 2002)).

An important concept in the compartmentalisation of cAMP signalling is that of the ‘signalosome’. Compartmentalisation relies on the spatial restriction of the protein machinery involved in the signalling pathway, which is made possible by the formation of macromolecular complexes called ‘signalosomes’. These complexes contain enzymes which produce, degrade, and are activated by cAMP as well as scaffolding, or structural proteins (Maurice, Ke et al. 2014). When coupled with the formation of cAMP gradients in discrete microdomains, this organisation allows the spatial and temporal regulation of signalling, which is key for the promotion of specific physiological outcomes from different receptors.

1.5.3 PDEs in the Cardiovascular System

Cyclic nucleotide signalling in the heart and vessels has been studied widely. In healthy myocardium, cyclic nucleotide signalling is generally beneficial, with acute cAMP elevation regulating excitation-contraction coupling. However, when cAMP is raised chronically in conditions of chronic sympathetic stimulation, this signalling pathway contributes to hypertrophy and heart failure (Bobin, Belacel-Ouari et al. 2016). The role of cyclic nucleotides in the pathophysiology of disease has led researchers to investigate the therapeutic potential of targeting the pathway, often by targeting PDEs. PDE3 and PDE4 subfamilies are the major players in the heart and vessels. However, there is also evidence for the roles of other subfamilies, (PDE1, PDE2, PDE5 and PDE9) in the context of disease (Bobin, Belacel-Ouari et al. 2016). Although PDE family-specific inhibitors have been shown to have widespread utility in pre-clinical studies, their use clinically has been rather limited. PDE3 inhibitors, such as milrinone, increase contractility, but were shown to increase mortality when used for the treatment of chronic heart failure due to cardiac arrhythmia; however, milrinone is still used for in acute decompensated heart failure and to maintain cardiac function following surgery (Packer, Carver et al. 1991, Baillie, Tejeda et al. 2019).

The major pathway for the present work involves ß-adrenergic signalling in the heart. During the ‘fight or flight’ response or other increases in cardiac demand, the sympathetic nervous system is activated, and adrenaline binds to ß-adrenergic receptors. These receptors are Gs-coupled GPCRs, which in turn activate AC, raising intracellular [cAMP]. Due to the compartmentalised nature

of cAMP signalling, this activates specific pools of PKA, which phosphorylate a number of substrate proteins, including LTCC, RyR, PLB, and TnI. The cumulative effect of these phosphorylation events results in the positive inotropic, chronotropic and lusitropic responses characteristic of the ß-adrenergic response. The phosphorylation of these substrates is tightly controlled by PDEs, which are often integrated into signalosomes containing PDEs, PKA holoenzyme, PKA substrate protein and scaffolding proteins (AKAPs) (Figure 1.9).

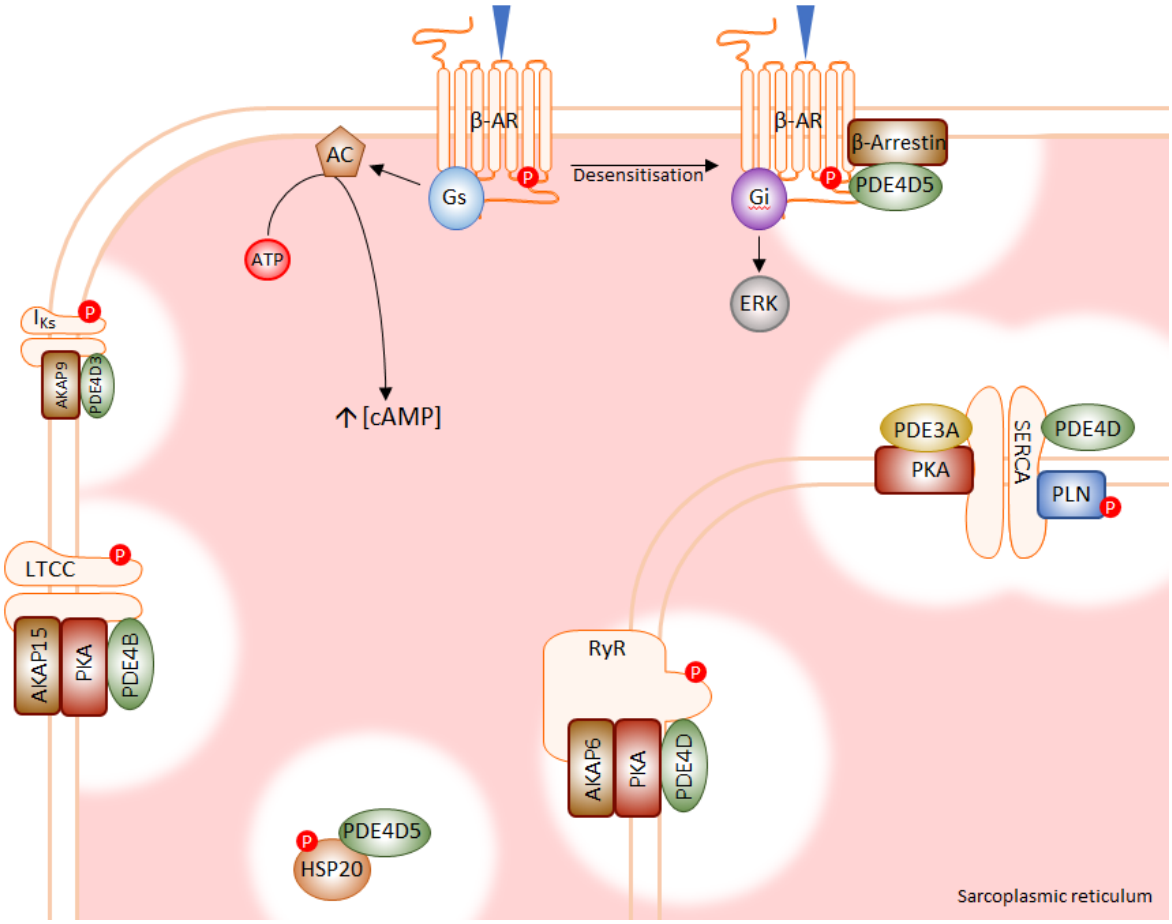

Figure 1.9: Cardiac PDE signalosomes. Many of the protein components of cardiac excitation-contraction coupling have been shown to be PKA phosphorylated in a process which is tightly regulated be members of the PDE3 and PDE4 families. This is made possible by the formation of macromolecular complexes, or signalosomes. β-arrestin forms a complex with PDE4D5, regulating receptor desensitisation (Bolger, McCahill et al. 2003). The cardiac IK_S channel interacts directly with PDE4D3, regulating the channel's regulation by cAMP (Terrenoire, Houslay et al. 2009). LTCC and RyR are regulated by PDE4B and PDE4D respectively, regulating the process of calcium-induced calcium release (Lehnart, Wehrens et al. 2005, Leroy, Richter et al. 2011). SERCA interacts with PDE4D, which regulates reuptake of calcium into the intracellular store (Beca, Helli et al. 2011). Finally, HSP20's cardioprotective effects are mediated by PDE4D5 (Sin, Edwards et al. 2011). (Adapted from (Maurice, Ke et al. 2014, Fertig and Baillie 2018)).

The specific PDE isoforms integrated into several of these signalosomes have been identified using a number of techniques. Firstly, pharmacological inhibition

of PDE families and subsequent analysis of the phosphorylation of the substrate protein was used to identify the family of PDEs involved (Sin, Edwards et al. 2011). To increase the specificity to the subfamily, knockout animals were used to reduce the expression of specific PDE genes, for example, PDE4A, B, C or D (Lehnart, Wehrens et al. 2005). Finally, isoform level specificity was achieved using a dominant negative approach or specially designed siRNA (Maurice, Ke et al. 2014). The theory behind this approach is that the overexpression of dominant-negative catalytically inactive PDE mutants displace the endogenous functional PDEs, allowing the identification of the specific PDE isoform involved in the regulation of substrate phosphorylation. However, this approach can affect more than one functional "pool" of one PDE isoform in more than one cellular location. These approaches have been used in combination with peptide array technology, which allows the identification of binding sites between signalosome members. Data from this technique has been used to design and synthesise disruptor peptides which can "unhook" one PDE isoform from one discrete location (Lee, Maurice et al. 2013). Furthermore, the use of FRET probes which have been tethered to specific substrate proteins have provided additional evidence for the roles of PDE isoforms in the regulation of localised signalling (Sin, Edwards et al. 2011).

1.6 SUMOylation

SUMOylation is a post-translational modification based on the covalent bonding of small ubiquitin-like modifier (SUMO) protein to a substrate. This highly conserved modification has been shown to have a number of functional effects from the regulation of transcription and cell cycle to subcellular localisation and degradation of proteins (Muller, Hoege et al. 2001, Seeler and Dejean 2003, Verger, Perdomo et al. 2003, Hannoun, Greenhough et al. 2010).

Three SUMO homologues are expressed in mammals: SUMO-1, SUMO-2 and SUMO-3. SUMO-2 and -3 have 95% sequence homology but only share 50% sequence homology with SUMO-1. Despite their misleading name, these 11 kDa proteins share less than 20% sequence homology with 8 kDa ubiquitin (Muller, Hoege et al. 2001). SUMO proteins are bound to lysine residues of substrate proteins, which are often contained within a consensus motif, ψKxD/E, where ψ is a large hydrophobic residue, K is a lysine, x is any amino acid and D/E is aspartic

acid/glutamic acid (Hannoun, Greenhough et al. 2010). However, it is worth noting that many proteins have been shown to be SUMOylated at residues that are not contained within a consensus motif (Ulrich 2009, Hannoun, Greenhough et al. 2010). The binding takes the form of an isopeptide bond between the C-terminal carboxyl group of the SUMO protein and the ε-amino group of the lysine residue of the consensus motif of the substrate protein (Hannoun, Greenhough et al. 2010). Additionally, SUMO-2 and -3 can be involved in polySUMOylation due to their N-terminal SUMO consensus motifs. Additional SUMO proteins covalently bind to these consensus motifs in SUMO itself forming a chain. SUMO-1 does not contain this site, and therefore, acts as the end of a chain (Kroetz 2005, Ulrich 2009).

1.6.1 SUMOylation Cascade

The enzymatic cascade for the addition of SUMO to a substrate protein is very similar to the ubiquitination cascade (Figure 1.10). Three enzymes are involved: E1, the activating enzyme, E2, the conjugating enzyme, and E3, the ligase (Takahashi, Toh-e et al. 2001, Hannoun, Greenhough et al. 2010).

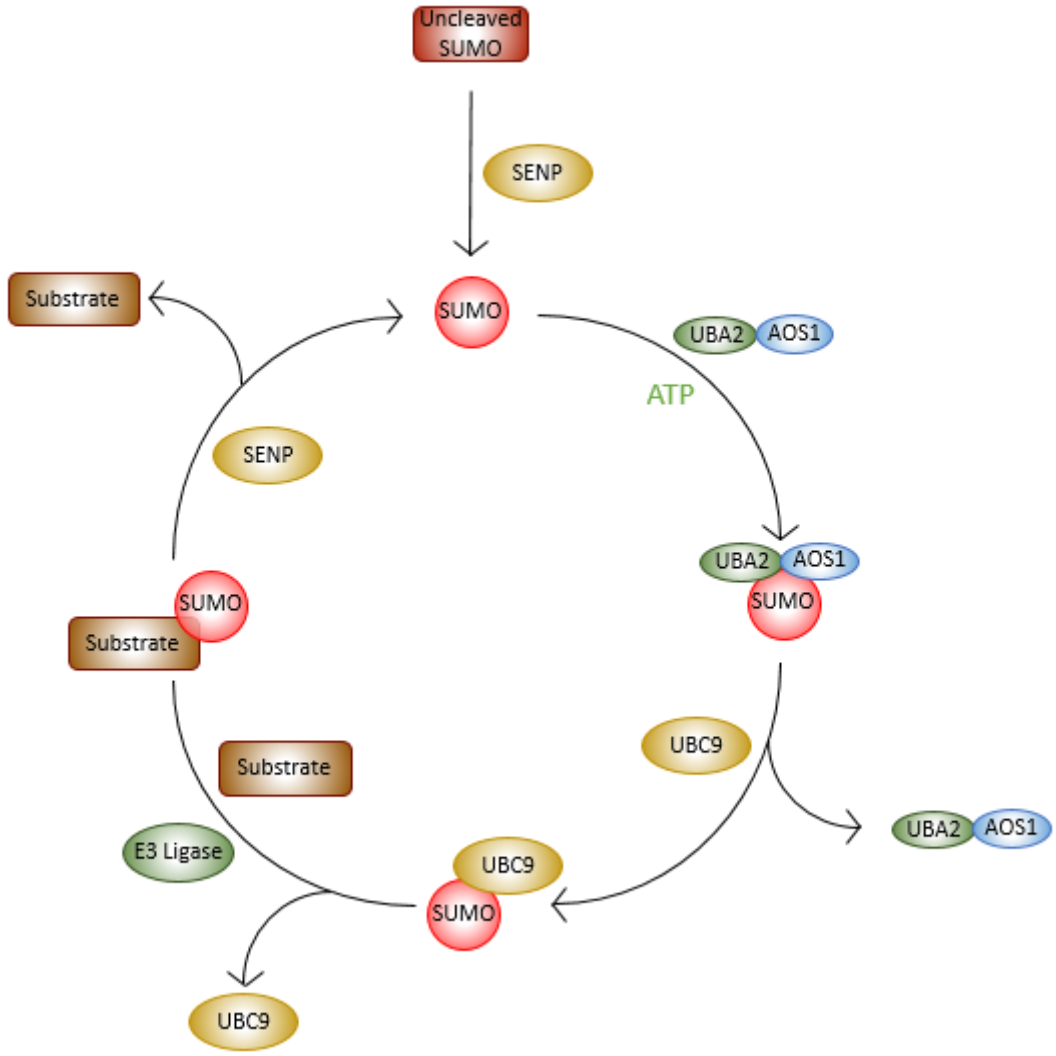

Figure 1.10: SUMOylation Cascade. The SUMOylation cascade begins with the cleavage of the C-terminal portion of the pro-from of SUMO by SENP isopeptidases. The SUMO protein is then bound to the E1 protein, which exists as a heterodimeric complex of UBA2/AOS1, in an ATP-dependent process. SUMO is then transferred to the E2 conjugating enzyme, UBC9, where a reactive bond between the UBC9 and SUMO forms. An E3 ligase then facilitates removal of SUMO from UBC9 and covalent attachment to the SUMOylation motif of the substrate protein. SENPs remove SUMO from substrate proteins in this dynamic process. (Adapted from (Hannoun, Greenhough et al. 2010)).

The SUMOylation cascade begins with the cleavage of precursor SUMO protein to the active species by SENP SUMO deconjugating enzymes, which expose SUMO's carboxy-terminal diglycine motif (Kerscher 2007, Mukhopadhyay and Dasso 2007). Next, the SUMO activating enzyme (E1) interacts with SUMO, forming an energetic thioester bond. The E1 enzyme is comprised of a heterodimer of Aos1 (SAE1) and Uba2 (SAE2). The formation of the high energy thioester bond by this enzyme prepares SUMO for conjugation by the E2 enzyme. There is only one known E2 enzyme, Ubc9. UBC9 includes an active site which binds SUMO via a

cysteine residue, directly binding SUMO to the consensus motif of a target sequence. Ubc9 then facilitates the formation of an isopeptide bond between the ε-amino group of the substrate protein's lysine residue within the consensus motif, which is directly recognised by the enzyme (Ulrich 2009). Unlike the SUMO E2 ligase, numerous SUMO E3 ligases have been identified, each of which has substrate specificity for various SUMO target proteins. Rather than having any catalytic activity which contributes to the transfer of SUMO from Ubc9 to the substrate, the E3 ligases contribute to the cascade by acting as a scaffold, bringing the Ubc9-SUMO complex into close proximity to the substrate (Ulrich 2009). The most prominent E3 ligases belong to the protein inhibitor of activated STAT (PIAS) family, which, in humans, includes 5 proteins from 4 genes, PIAS1, PIAS3, PIASxα, PIASxβ and PIASγ (Palvimo 2007). The PIAS proteins include SP-RING domains, which can bind to Ubc9, and SUMO interacting motifs (SIMs) which bind to SUMO directly, thereby promoting SUMOylation of substrate proteins (Hochstrasser 2001). These proteins have a level of substrate specificity, with specific PIAS proteins influencing the SUMOylation of specific subsets of target proteins, often with little redundancy in the system (Schmidt and Muller 2002, Hannoun, Greenhough et al. 2010).

Finally, like phosphorylation, SUMOylation is reversible; a family of cysteine proteases called sentrin-specific proteases (SENPs) are able to remove SUMO from its substrate in a process known as deSUMOylation. There are six known members of the SENP family which can function in this way, with a degree of specificity for the different SUMO proteins (Lee 2016 – 31). The variety and differential expression of the SUMO proteins and the enzymes involved in the cascade suggest that the process of SUMOylation and deSUMOylation is dynamic, reacting and responding to cellular environment and stressors (Lee 2016).

1.6.2 Functional Effects of SUMOylation

There is no single effect of target protein SUMOylation, as studies investigating the SUMOylation of a myriad of target proteins have concluded that a wide variety of functional effects are possible. However, there are some indications for general functional effects of SUMOylation (reviewed in (Ulrich 2009)). Examples of the functional effect of SUMOylation of specific substrates will be described in later sections.

Firstly, SUMOylation of target proteins can alter a protein's interactions with other proteins (Ulrich 2009, Wang 2011). For example, the conjugation of SUMO can produce an additional binding site, allowing binding partners to interact or the substrate to be targeted to a specific intracellular location. Using a two-hybrid approach, it has been shown that some proteins interact with SUMO covalently via SUMO's C-terminal di-glycine motif, as in target protein/SUMO interactions. However, some proteins also interact with SUMO in a non-covalent manner due to the presence of SIMs. The first reported interaction involving a SIM showed that only SUMOylated p73 (a member of the p53 family of tumour suppressor genes) could interact with certain binding partners (Minty, Dumont et al. 2000). It has now been determined that SIM binding depends on the presence of a hydrophobic core within the SIM, which has a consensus sequence of V/I-X-V/I-V/I, where X is any amino acid (Song, Durrin et al. 2004). The SIM forms a ß-strand which integrates into a ß-sheet on the SUMO protein (Kerscher 2007). It has been shown that numerous downstream effectors contain SIMs and interact with SUMO in this way. Furthermore, several components of the SUMOylation cascade itself, including PIASx and E2 ligase subunit Uba2) have been shown to include SIMs, which are essential for their function (Kerscher 2007). In contrast, SUMOylation can also block interaction sites, preventing protein-protein interactions from forming (Ulrich 2009). Finally, it has been shown that SUMOylation can modify the conformation of substrate proteins, which can also affect the way the substrate interacts with other binding partners (Steinacher and Schar 2005).

SUMOylation has also been shown to regulate other post translational modifications of substrate proteins. For example, SUMOylation can block ubiquitination, which also requires a lysine residue of a substrate protein (Ulrich 2005). SUMO and ubiquitin sometimes compete for the same lysine on a substrate, acting in antagonism to control the properties or the fate of the protein. However, in many cases, the situation is much more complex and SUMO and ubiquitin crosstalk still occurs even when the proteins modify different lysine residues on the same protein (Ulrich 2005). The first example of the former, antagonistic relationship, involves the inhibitor of the transcription factor NF-κB (IκBα) (Desterro, Rodriguez et al. 1998). The ubiquitination of IκBα results in its proteasomal degradation, freeing the NF-κB to regulate

transcriptional activity in the nucleus. However, when one of IκBα's two ubiquitination sites is SUMOylated instead, it appears to be protected from this degradation, inhibiting NF-κB induced transcription. Even this paradigm of the 'simple' antagonistic relationship has since been shown to be more complicated, involving crosstalk between a phospho-site that must be modified for ubiquitination to occur (Karin and Ben-Neriah 2000). On the other hand, in some situations, SUMO and ubiquitin act cooperatively; for example, SUMOylation of a target in the cytosol can promote nuclear localisation, where the protein is then ubiquitinated (Huang, Wuerzberger-Davis et al. 2003, Ulrich 2005). Crosstalk between phosphorylation and SUMOylation has also been reported. Phosphorylation of substrate proteins can both promote and inhibit SUMOylation, and SUMOylation of substrate proteins can also modulate the functional effects of protein phosphorylation (Hietakangas, Ahlskog et al. 2003, Yang, Jaffray et al. 2003, Li, Vadrevu et al. 2010). Some SUMOylation sites may only be occupied if nearby phosphosites are phosphorylated. In fact, a phosphorylation-dependent SUMOylation motif with the sequence, ψKxExxSP, has been identified on numerous transcription factors. This motif contains the classical SUMOylation motif followed by a phosphorylation site, separated by two amino acids (Hietakangas, Anckar et al. 2006). An example in which SUMOylation of a substrate regulates the functional effects of phosphorylation involves cAMP-degrading PDE4D5. The PDE's activity is modified by its phosphorylation by various kinases including activation by PKA and inhibition by ERK MAPKinase. SUMOylation of PDE4D5 locks it in a hyperactive state following PKA phosphorylation and the SUMO modification also prevents inactivation of the PDE by ERK (Li, Vadrevu et al. 2010).

Although many SUMOylated proteins are nuclear and involved in regulation of transcriptional activity, there is an emerging role for SUMOylation of cytosolic proteins with widely varied functional implications. Taken together, SUMOylation can modulate a protein's targeting within the cell, its activity, its interactions with binding partners and its stability (Ulrich 2009). Given the wide variety of SUMO substrates that have been confirmed, the potential substrates that have yet to be identified, and the ubiquitous expression of the SUMO cascade components, the scope of the functional effects of SUMOylation is vast.

1.6.3 SUMOylation in Cardiac Function and Disease

Although the SUMO pathway has been shown to play a part in a number of physiological and pathological states, the present work will focus on the role of SUMOylation in the heart. There is an abundance of evidence for the role of this post-translational modification in cardiac development, function and disease (Lee, Oh et al. 2016).

Firstly, the use of transgenic animals in which different components of the SUMOylation cascade have been knocked out or overexpressed has shown the integral, non-redundant roles of these proteins in cardiac function. Both global and cardiac-specific SUMO1 knockout mice developed severe cardiac phenotypes, including septal defects and progressive dysfunction leading to sudden cardiac death (SCD) (Kho, Lee et al. 2011, Wang, Chen et al. 2011). On the other hand, although SUMO2 knockout led to global developmental defects, no cardiac specific phenotype was observed, suggesting the dominant role of SUMO1 in the cardiac setting (Wang, Wansleeben et al. 2014). Furthermore, alterations in the expression levels of deSUMOylating enzymes, SENP2 and SENP5 had dramatic functional effects on the heart. Knockout of SENP2 was embryonic lethal, with embryonic heart defects observed; to the contrary, overexpression of SENP2 and SENP5, leading to enhanced deSUMOylation, resulted in dilated cardiomyopathy in mice, suggesting the detrimental effects of reducing the levels of SUMOylated proteins in the heart (Kim, Chen et al. 2012, Kim, Zhang et al. 2015). Although studies employing the use of changed expression in murine models are highly informative, they are limited by the potential for species differences between mice and humans. In human heart failure, it has been shown that several of these proteins have altered activity and expression. Compared to healthy hearts, the expression of SUMO1 has been shown to be decreased in failing hearts. SENP1 and SENP5 expression have been shown to be upregulated in failing hearts caused by idiopathic cardiomyopathy (Kho, Lee et al. 2011, Wang, Wansleeben et al. 2014, Kim, Zhang et al. 2015). Taken together, these observations suggest a role for SUMOylation in cardiac function and pathology, making the pathway and the proteins involved attractive therapeutic targets.

1.6.3.1 SERCA2a SUMOylation

Several cardiac proteins have been shown to be targets of SUMOylation, but the most relevant and highly characterised stems from the work of Hajjar and colleagues, showing the role of SERCA2a SUMOylation in heart failure (Kho, Lee et al. 2011). SERCA2a functions to resequester Ca^{2+} into the sarcoplasmic reticulum, resulting in reduced cytoplasmic [Ca^{2+}] and diastole. It has long been implicated in heart failure, which is characterised by reduced expression and function of SERCA2a. Enhancing the expression of SERCA2a using gene therapy was thought to be a potential therapeutic, showing great promise until it failed in stage 2 clinical trials (Greenberg, Butler et al. 2016). The role of SERCA2a in the pathophysiology of disease is undeniable, so researchers looked to post-translational modifications of the protein as a potential target to treat heart failure.

Hajjar and colleagues identified a SUMOylation consensus motifs at lysines 480 and 585 of SERCA2a which were shown to be targets of the post translational modification (Kho, Lee et al. 2011). SUMOylated SERCA2a was shown to have enhanced function and stability compared to SERCA2a which had not been modified in this way. Coupled with the observation that both SUMO1 and SERCA2a expression are reduced in heart failure, it was determined that this modification could be targeted as a therapeutic target. Adenoviral gene transfer of SUMO1 was used effectively to treat heart failure in both murine and porcine models of disease (Kho, Lee et al. 2011, Tilemann, Lee et al. 2013). In mice which had been subjected to transverse aortic constriction (TAC) to induce heart failure, adenoviral mediated overexpression resulted in restoration of SERCA2a function and expression to healthy levels. Cardiac myocytes isolated from these animals showed increased reuptake of Ca^{2+} into the sarcoplasmic reticulum and increase cell shortening, which was mirrored by enhanced contractility of the mice hearts. Overall, cardiac function in animals with heart failure was restored and animal survival significantly improved.

Following the positive results of this approach in mice, a pre-clinical porcine model of I/R induced heart failure was used to test the therapeutic potential of SUMO1 gene transfer (Chapman, Lee et al. 2017). The I/R-induced heart failure was characterised by left ventricular remodelling and dysfunction as well as

reduced expression of SUMO1 and SERCA2a and reduced SUMOylation of SERCA2a. Similarly to the previous study, the adenoviral mediated gene transfer of SUMO1 increased expression levels of SUMO1 and SUMOylated SERCA2a levels back to that of sham-operated animals. Interestingly, the treatment also increased the expression of SERCA2a, consistent with the role of SUMOylation in enhancing the stability of the protein. Cardiac function was significantly improved, and pathological left ventricular remodelling was attenuated.

1.7 Hypothesis & Aims

TnI is a key protein in the process of excitation contraction-coupling in cardiac myocytes. It has been shown previously that post-translational modification of TnI can regulate its function, thereby fine-tuning the regulation of cardiac myocyte Ca^{2+} signalling and contractile dynamics. Post-translational modifications of TnI have also been shown to be relevant in disease, with downregulated phosphorylation of Ser23/24 observed in failing myocardium (Bodor, Oakeley et al. 1997, Zakhary, Moravec et al. 1999).

ß-adrenergic enhancement of contractility relies on the PKA phosphorylation of numerous cardiac excitation-contraction coupling proteins, a process which has been shown to be tightly regulated by integration of PDE isoforms into signalosomes with the protein components. PKA phosphorylation of TnI at Ser23/24 (Ser22/23 in rodents) contributes to the overall enhancement of contractility by increasing crossbridge cycling dynamics and also enhances diastolic relaxation by decreasing myofilament Ca^{2+} sensitivity (Pi, Kemnitz et al. 2002, Pi, Zhang et al. 2003, Takimoto, Soergel et al. 2004). Previous evidence has suggested that a PDE4 isoform interacts with TnI, thereby regulating its phosphorylation (Edwards 2012). To date, the proposed interaction between PDE4 and TnI has not been confirmed, nor has a functional role of the interaction been shown. It was hypothesised that PDE4 regulates the PKA phosphorylation of TnI and that this modulation would be disrupted by a custom designed cell-permeable peptide that specifically uncouples PDE4 and TNI. The peptide disruption of the proposed PDE4-TnI complex was hypothesised to enhance Ser23/24 phosphorylation, thereby enhancing the positive lusitropic effects of this modulation. The aims of this study were as follows:

- To test the efficacy of a peptide disruptor of the proposed TnI-PDE interaction by studying cAMP dynamics at the myofilament and the phosphorylation levels of TnI

- To confirm the proposed interaction using co-immunoprecipitation and peptide array technology

- If PDE4-TnI interaction confirmed, use range of PDE4 inhibiting tools (PDE4 inhibitors, siRNA, dominant negative PDE4 and TnI-PDE4 disruptor peptide) to characterise function of PDE4-TnI complex in healthy and diseased heart

Another post-translational modification, SUMOylation, has also been shown to be relevant in the cardiac setting. It has been shown that cardiac excitation-contraction coupling protein, SERCA2a, is SUMOylated, maintaining its function and protecting it against degradation in pathophysiological states. TnI contains a SUMOylation motif, but it has not yet been shown whether this site can be SUMOylated. It was hypothesised that TnI would be SUMOylated at K177 within the identified SUMOylation motif and that this modification would have physiological and/or pathophysiological relevance in the heart. The aims of this study were as follows:

- To determine whether the C-terminal SUMOylation motif of TnI can be SUMOylated

- To develop and test a custom antibody specific to SUMOylated TnI

- To determine whether SUMOylation of TnI is of functional importance in cardiac myocytes and whether it has a role in the myofilament dysfunction observed in cardiac disease

Chapter 2 Materials and Methods

2.1 General Laboratory Practice

Equipment and reagents were purchased from Sigma-Aldrich (Dorset, UK) unless otherwise stated. Any hazardous reagents or procedures were handled and disposed of according to the relevant Control of Substances Hazardous to Health regulations. Personal protective equipment including laboratory coats and gloves were worn during all procedures.

Glassware was washed using Decon 75 detergent (Decon Laboratories Ltd, East Sussex, UK), rinsed with distilled water and thoroughly dried prior to use. Sterile disposable plastic containers and dispensers were used including microcentrifuge tubes (Grenier Bio-one, Stonehouse, UK), universals (Corning, Birmingham, UK) stripettes (Corning, Birmingham, UK) and pipette tips (Rainin, California, USA). To sterilise reagents, laboratory items and liquids were autoclaved in a Prestige Medical autoclave (Prestige Medical, Blackburn, UK). For the preparation of buffers, solutions and media, solid chemicals were weighed using a Mettler Toledo balance (sensitive to 0.01 g, Ohio, USA) or Sartorius CP124S balance (sensitive to 0.0001 g, Bradford, UK). Solutions were prepared using distilled water unless otherwise stated. The pH of these solutions was measured using a Mettler Toledo Seven Easy digital pH meter (Mettler Toledo, Ohio, USA) and adjusted using HCl or NaOH. Volumes were dispensed using a Gilson battery powered pipetting aid (1-25 ml) and Gilson pipettes (0.5-1000 µl; Gilson Medical Instruments, Staffordshire, UK). Centrifugation was carried out in a temperature controlled Sigma-Aldrich 1-14K rpm table top microcentrifuge (Sigma-Aldrich, Dorset, UK), a ThermoFisher Scientific Cl31 multispeed centrifuge (ThermoFisher Scientific, Paisley, UK), or a Beckman Coulter Optima L-80 XP ultracentrifuge (Beckman Coulter, High Wycombe, UK) depending on the sample container, volume and speed requirements. Temperature sensitive incubations were completed using a Grant OLS200 water bath (Grant Instruments, Cambridgeshire, UK) or a Techne Dri-Block DB2A heat block (Teche, Staffordshire, UK).

2.2 Isolation and Preparation of Plasmid DNA

Plasmid DNA was used throughout this work for the transient expression of proteins in cell lines and primary cells. The following describes the process in which the DNA constructs were isolated.

2.2.1 Transformation of Chemically Competent Cells

Following storage in 10 µl aliquots at -80ºC, chemically competent TOP10 cells (Invitrogen) were thawed slowly on wet ice. 1-2 ng of plasmid DNA was added to the cells and mixed gently. The preparation was incubated on ice for 15 minutes before heat shocking for precisely 1 minute at 42ºC, and then was returned to ice for a further 2 minutes. 200 µl of sterilised SOC medium (Invitrogen) was then added and the preparation was incubated in a 37ºC shaking incubator for 1 hour. Agar plates were prepared using sterilised lysogeny broth (LB) (1% (w/v) bactotryptone, 0.5% (w/v) yeast extract, and 170 mM NaCl, pH 7.5) with 1.5% (w/v) agar. Once cooled to handling temperature, appropriate antibiotic (50 µM) was added and LB agar was poured into 90 mm petri dishes and left to set proximal to a Bunsen flame for sterility. Plates were stored at 4ºC for use within one month. 50 µl of the transformed cells were plated and left to incubate upside down overnight at 37ºC. Successful transformation was determined by the presence of colonies. Sterile pipette tips were used to pick single colonies for inoculation of 5 mls of LB broth. Cultures were incubated overnight at 37ºC in an orbital shaker. These cultures were used in several ways depending on planned experiments.

2.2.2 Preparation of Plasmid DNA

Glycerol stocks for storage were produced by mixing 0.8 ml of overnight culture with 0.2 ml of autoclaved glycerol in a cryovial. Stocks were produced in triplicate and snap frozen on dry ice before being stored at -80ºC for long term use.

2.2.3 Isolation of Plasmid DNA

250 ml of LB with appropriate antibiotic (50 uM) was inoculated with small overnight cultures or scrapings of glycerol stocks and subjected to overnight incubation in a 37ºC orbital shaker. Qiagen Plasmid Maxi Kits were used to isolate large amounts of DNA as per manufacturer's instructions. Sterile nuclease free water was used to resuspend DNA. A NanoDrop 2000 spectrophotometer (ThermoFisher) was used to assess DNA concentration and purity. Absorbance at 260 nm was used for measurement of concentration and the A_{260}/A_{280} ratio was used for assessment of purity. Preparations were stored at -20ºC.

2.3 Site Directed Mutagenesis

Site directed mutagenesis was used for the production of plasmid DNA constructs with point mutations that resulted in changes of amino acids, allowing the determination of the effects of modification of the residues of interest.

QuikChange site-directed mutagenesis kits (Agilent) were used as per manufacturer's instructions. This method employed Pfu Turbo DNA polymerase and a temperature cycling protocol similar to polymerase chain reaction (PCR). The plasmid DNA with the wild-type insert was incubated in the reaction with two oligonucleotide primers, designed to be complimentary to the region of interest, with the exception of the desired mutations. Pfu Turbo DNA polymerase was used as it is able to replicate both DNA strands, leaving the mutant oligonucleotide primers in place – thereby introducing the mutant into the plasmid DNA. Each reaction contained the following: Agilent reaction buffer, dsDNA template, 'sense' oligonucleotide primer, 'antisense' oligonucleotide primer, dNTP mix, and ddH_2O. The thermal cycling protocol began with an initial denaturation step at 95ºC, which was followed by 18 cycles of 95ºC denaturation, 55ºC annealing, and 68ºC extension. The extension time was calculated based on the length of the plasmid.

Following the amplification of the mutant insert-containing plasmids, a restriction endonuclease digestion was carried out to purify the mutated DNA by digesting the template dsDNA plasmids. DpnI is an endonuclease which is specific for methylated DNA; as DNA isolated from E. Coli is methylated, treatment of the amplification reaction with DpnI results in the digestion of wild-type, template dsDNA, leaving the newly produced mutant plasmids intact.

The product of the thermal cycling and DpnI digestion was then used to transform XL1-Blue supercompetent bacterial cells. The plasmid was added to aliquots of cells, and incubated on ice for 30 minutes. The cells were subjected to a 45 second heat shock at 42ºC and placed on ice for 2 minutes. Pre-warmed NZY_+ broth (10% (w/v) NZ amine, 5% (w/v) yeast extract, 5% (w/v) NaCl, 12.5 mM $MgCl_2$, 12.5 mM $MgSO_4$, 20 mM glucose, pH 7.5) was then added and the transformation reactions were incubated at 37ºC for one hour in an orbital shaker at 240 rpm. The transformation reactions were then added to antibiotic

containing agar plates at various volumes (10-250 µl) and incubated overnight at 37ºC.

Single colonies from agar plates were selected and used to inoculate 4 ml cultures of LB broth containing the appropriate antibiotic. These cultures were incubated overnight in 37ºC orbital shakers at 220 rpm. Half of this culture was used for plasmid DNA purification using a Qiagen Spin Miniprep Kit, and the sample was analysed using agarose gel electrophoresis (where the mutant introduced a novel restriction endonuclease recognition site) and Sanger sequencing. Upon a positive result indicating the presence of mutant plasmid, the remaining 2 mls of overnight culture were used to inoculate 250 ml LB broth cultures which were incubated overnight in 37ºC orbital shakers and plasmid DNA was purified in large quantities using Qiagen Maxiprep Kits as previously described.

2.4 Mammalian Cell Culture

Class II flow hoods (ThermoFisher) were used for cell culture procedures. Standard aseptic techniques were used and all solutions and instruments were autoclaved and kept in sterile conditions. Unless otherwise stated, media and reagents were acquired from Gibco (ThermoFisher) while flasks, plates and other consumables were acquired from Corning (Sigma Aldrich). A phase contrast inverted microscope (Leitz Diavert) was used for regular visual examination of cultured cells.

2.4.1 HEK-293 Cell Culture

Human Embryonic Kidney (HEK) 293 cells were used for a variety of experiments due to their robust nature, quick growth and easy transfection. HEK-293 growth medium was comprised of Dulbecco's modified eagle medium (DMEM) supplemented with 10% foetal bovine serum (FBS), 1% penicillin/streptomycin, 1% L-glutamine and 1% non-essential amino acids (NEAA). The cells were cultured in T150 flasks containing growth medium in incubators with humidified air at 37ºC and 5% CO_2.

When the cells reached approximately 90% confluency, they were passaged. To passage cells, medium was removed and flasks were washed twice with sterile phosphate buffered saline (PBS) solution. The washes were then removed and trypsin-EDTA solution was added at a volume of 5 ml per T150 flask and cells were incubated at 37ºC. When cells were seen to detach under light microscopy, 10 mls of growth medium was added to inactivate the trypsin. The cells were transferred to a 50 ml Falcon tube and centrifuged at 150g for 3 minutes to remove trypsin and collect cells. The cells were resuspended in 3-10 ml of growth medium depending on desired concentration. For maintenance of cells, 1 ml of cells was added to a new T150 flask with 25 ml of fresh growth medium and incubated as previously described. For use in experiments, cells were plated at various concentrations in six well plates or 10 cm dishes. For biochemical experiments requiring preparation of whole cell lysates, cells were plated at $3x10^5$ cells per well of a six well plate. For FRET imaging experiments, cells were plated more sparsely, at $1x10^5$ cells per well.

2.4.2 Neonatal Rat Ventricular Myocytes

Neonatal rat ventricular myocytes (NRVM) are a commonly used model to investigate cardiac biochemical processes due to biochemical similarities to adult ventricular myocytes and relative ease of isolation and culture.

2.4.2.1 Isolation of Neonatal Rat Ventricular Myocytes

Hearts were removed from 1-2 day old Sprague-Dawley rats following sacrifice by anaesthesia overdose via intraperitoneal injection of Euthatal. Animals were handled in accordance with the UK Animals (Scientific Procedures) Act of 1986. The hearts were placed directly into a 5 cm dish containing ice-cold ADS buffer (120 mM NaCl, 20 mM HEPES, 1 mM Na_2PO_4, 5 mM glucose, 5.4 mM KCl, 1.8 mM $MgSO_4$, pH 7.4) and dissected to remove atrial and aortic tissue. The hearts were squeezed gently with forceps to remove residual blood in the ventricles and transferred to a new 5 cm dish with fresh ice-cold ADS buffer. The hearts were then minced into $1mm^3$ pieces and transferred to a 50 ml falcon tube. The minced hearts were left to settle and the ADS was removed. Collagenase buffer containing 0.06% (w/v) pancreatin and 0.03% (w/v) collagenase was used for serial enzymatic digestions. The collagenase buffer was added and the hearts

were incubated in a 37ºC shaking water bath. An initial digestion of 5 minutes was used to remove pericardial collagen; after this digestion, the supernatant which contained single cells was removed and discarded. Subsequently, the hearts were subjected to 5 20 minute digestions. After each digestion, the minced hearts were allowed to settle and the supernatant was removed and added to a sterile 15 ml Falcon tube containing 0.5 ml neonatal calf serum (NCS) to end the digestion. These were centrifuged at 1250 rpm for 5 minutes and pellets were resuspended in 2 ml of NCS and incubated at 37ºC until subsequent digestions were completed. After the final digestion, cells were pooled and centrifuged as before and resuspended in 10 ml of Day 1 Medium (M1) (4:1 ratio of DMEM/Medium 199 (M199) supplemented with 10% horse serum (HS), 5% NCS, 1% L-glutamine and 1% penicillin/streptomycin) per 5 hearts. At this stage of the protocol, the cells were a mixed culture comprised mainly of fibroblasts and NRVM. To remove the fibroblasts, a pre-plating step was required. 10 mls of cells in M1 were plated onto 10 cm dishes and incubated at 37ºC for two hours. In this time, the fibroblasts stuck down to the surface of the dish and the NRVM remained suspended in the medium, as the do not adhere to uncoated materials. Following the incubation, the NRVM and medium was removed from the dishes and transferred to a fresh 50 ml falcon tube. An extra 5 ml of M1 was used to wash the dishes; this was also added to the 50 ml falcon tube. The cells were centrifuged as before and the pellet was resuspended in 10 ml of M1. Following counting using a standard haemocytometer to determine the yield (usually 20-30 million cells per average litter of 10-12 rats), the cells were seeded in coated 6 well plates at varying concentrations. For biochemical experiments, plates were coated with 1% (w/v) bovine gelatin, and cells were seeded at $8x10_6$ cells per well. For FRET imaging experiments, coverslips were sterilised in 1:1 ethanol/ether, added to each well, and air dried before coating with 1 μg/cm_2 mouse laminin. Cells were seeded at $4x10_6$ cells per well. Cells were incubated in humidified air at 37ºC with 5% CO_2.

2.4.2.2 Maintenance of Neonatal Rat Ventricular Myocytes

After 18-24 hours of culture in M1, the NRVM were washed twice with ADS and the medium was replaced with Day 2 Medium (M2) (1:4 ratio of DMEM/M199 supplemented with 5% HS, 0.5% NCS, 1% L-glutamine and 1% penicillin/streptomycin). For transient transfection with plasmid DNA, the cells

were left in the incubator for at least two hours following washing and addition of fresh medium before the addition of transfection reactions. The cells were then incubated as before, and the medium changed to fresh M2 as described every other day.

2.4.3 Adult Rabbit Ventricular Myocytes

Adult rabbit ventricular myocytes (ARVM) were isolated as described in (Donahue, Kikkawa et al. 1997). Isolations were carried out by Aileen Rankine. Adult rabbits were intravenously injected with heparin to prevent coagulation and phenobarbital (50 mg/kg). Working quickly, the heart was dissected out of the animal and rinsed twice in ice-cold Krebs buffer (138.2 mM Na^+, 5.4 mM K^+, 1.2 mM Mg^{2+}, 1.0 mM Ca^{2+}, 144.4 mM Cl^-, 1.2 mM SO_4^{2-}, 1.2 mM $H_2PO_4^-$, 20 mM HEPES, 15 mM glucose, saturated with O2, pH 7.4). A cannula was inserted into the aorta and suspended on a Langendorff perfusion rig, in which the perfusion was retrograde through the ascending aorta into the coronary arteries. First, the heart was perfused with Krebs buffer for 2.5 minutes at a rate of 30 ml/min followed by Ca^{2+}-free Krebs buffer for 10 minutes at 10 ml/min. Digestion of the myocardium occurred by perfusion with an enzyme solution (0.025 mM Ca^{2+}, 1 mg/ml collagenase B, 0.1 mg/ml protease, 60 mM taurine, 8 mM glutamic acid, and 2 mM carnitine in Krebs). Following digestion, ventricles were separately excised (left, right and septal) and agitated using a Pasteur pipette. Valve and tendon cells and tissues were excluded from the cells by straining through 200 µm nylon mesh filters. Ca^{2+} was gradually reintroduced by resuspending in Krebs with increasing Ca^{2+} concentrations; this was done in 4 steps with at least 10 minutes equilibration between each step. Finally, the cells were cultured in supplemented M199 (5 mM creatine, 5 mM carnitine, 5 mM taurine, 0.1 mg/ml penicillin/streptomycin) in cell culture dishes coated with 1 µg/cm^2 laminin. Approximately one hour after plating, medium was removed and replaced to reduce the number of dead cells in the culture. Cell counts were measured at this point by counting the cells in 10 high-power fields and multiplying over the surface area of the dish. This was determined to be the most accurate way of determining cell count because many cells did not survive the plating process.

2.5 Transient Transfection

Cells were transiently transfected with plasmid DNA for the expression of proteins which were not endogenously expressed at sufficient levels in cells. Transient transfection was used for the expression of various proteins, such as FRET probes and TnI and SUMO proteins for the detection of modified TnI. The process of transient transfection allows the expression of the desired protein in cells without the incorporation of the DNA into the cell's genome. Lipofectamine LTX Lipid Reagent (Invitrogen) was used to transiently transfect cells as per the manufacturer's instructions. The following describes volumes used for transfections in 6 well plates. Serum free medium was used to prepare transfection reactions (M199 for NRVM and Opti-MEM for HEK-293 cells). Each transfection was prepared in two 1.5 ml Eppendorf tubes. In the first tube, 5 µl of LTX reagent and 2 µl of PLUS reagent were added to 250 µl of medium. In the second, 2 µg of plasmid DNA was added to 250 µl of medium. These were incubated for 5 minutes at room temperature before adding them together, mixing, and incubating for a further 20 minutes. The full contents of the tube were then added dropwise to the cells and incubated for 24-48 hours to allow adequate expression.

2.6 Viral Infection

Cells were transduced with plasmid DNA via adenoviral infection to introduce mutations not endogenously present in cells. Custom E1/E3 deleted adenoviruses expressing wild-type and mutant TnI were acquired from a commercial source (Welgen, Inc). These deletions ensure that the viruses are able to replicate only in HEK-293 cells, but are replication deficient in any other cells or cell lines. Virus titre was provided by the company. Dosage was calculated as multiplicity of infection (MOI) based on the cell counts in the plates being transduced, (eg. MOI 1 = 1 viral particle (vp) to 1 cell). To treat cells with virus, appropriate amount of the virus was added to an appropriate volume of cell culture medium, mixed thoroughly, and used to replace existing cell culture medium in plates. Cells were incubated in virus containing medium for 24-48 hours to allow adequate expression.

2.7 Preparation of Whole Cell Lysates

The preparation of cell lysates was performed with all reagents and tubes on ice to limit protein degradation. Lysates could be analysed by gel electrophoresis and western immunoblotting to identify and quantify proteins of interest. Cells were washed twice with ice-cold PBS before the addition of 120-200 µl of 3T3 lysis buffer (25 mM HEPES, 50 mM NaCl, 50 mM NaF, 30 mM, $Na_4P_2O_7$, 5 mM EDTA, 10% glycerol, 1% triton, pH 7.5 supplemented with protease cocktail inhibitor tablets (Roche)) depending on cell confluency and desired protein concentration. The plates were then incubated on ice on an orbital shaker for 5 minutes. Following incubation, the cells were scraped using an upside down P1000 pipette tip and the lysate was collected. The lysates were rotated at 4ºC for 30 minutes and then centrifuged at 14,000 rpm for 10 minutes at 4ºC. The supernatant was collected, snap frozen, and stored at -20ºC for short term use and -80ºC for long term use.

2.8 Protein Quantification

Quantification of protein concentration of cell lysates and purified recombinant proteins was determined by the Bradford Method (Bradford 1976). This assay employs the use of a colour change for quantification. Assays were prepared in clear 96 well plates. A standard curve was constructed using known bovine serum albumin (BSA) concentrations from 0-5 µg. Each well was composed of 50 µl of 1:50-1:200 dilution of the sample of unknown concentration and 200 µl of Bradford Reagent (BioRad), which had been prepared as a 1:5 dilution. All samples and standards were added in triplicate. Samples and standards were measured for 595 nm absorbance using an Anthos 2010 plate reader fitted with a 595 nm filter, and analysed using ADAP software. Using the BSA standards, a curve was constructed, and concentrations could be derived and adjusted for dilution.

2.9 SDS-PAGE

Following quantification of protein concentration, samples were equalised for concentration using 3T3-lysis buffer and diluted in 5x laemlli protein sample buffer (10 mM Tris-Cl, pH 6.8, 10 % glycerol, 5% ß-mercaptoethanol, 2% SDS, 0.01%

bromophenol blue). Samples were then boiled for 3 minutes at 90ºC to cause protein denaturation; the samples were then ready for use in SDS-PAGE (sodium dodecyl sulphate polyacrylamide gel electrophoresis) or could be stored at -20ºC for future use. SDS-PAGE is commonly used for the separation of proteins within a sample by size. Defined amounts of protein (15-30 µg for cell lysates and much lower amounts for purified protein) were added to wells of precast gels (NuPAGE 4-12% Bis-Tris Gel). 2 µl of molecular weight marker (BioRad) was added to the first well of each gel for a size reference. Gels were immersed in running buffer (MES Running Buffer if proteins of interest were 20-50 kDa or MOPS Running Buffer if proteins of interest were larger) within an Invitrogen XCell SureLock MiniCell system (ThermoFisher Scientific). Gels were run at 150-180V until bromophenol blue dye was seen to run off the bottom of the gel – usually 60-90 minutes; although, gels could be run longer if additional separation of protein size was necessary.

2.10 Western Immunoblotting

Directly following SDS-PAGE, proteins were transferred from the gel to nitrocellulose membranes (ProTran) using an Invitrogen XCell II Blot Module (ThermoFisher) filled with transfer buffer (5% 20x NuPAGE transfer buffer, 20% (v/v) methanol diluted in dH_2O). 30V of current was applied for 90 minutes. Efficiency of the transfer was determined by visualising the prestained molecular weight marker's presence on the nitrocellulose membrane. The membranes, now containing protein, were then blocked in 5% Marvel milk powder, 5% Phosphoblocker or 5% bovine serum albumin (BSA) (Cell Biolabs Inc.) in 1x TBS-T (20 mM Tris-Cl pH 7.6, 150 mM NaCl, 0.1% Tween-20) to prevent non-specific antibody binding. The membranes were then incubated under constant agitation at 4ºC for 4 hours or overnight in a solution of 1% milk, 1% phosphoblocker or 1% BSA containing an appropriate concentration of a primary antibody against the protein of interest (Table 1).

Table 1: Primary Antibodies. (IF, immunofluorescence; IP, immunoprecipitation; PA, peptide array; WB, western blotting).

Primary Antibody	Host Species	Immunogen	Dilution	Supplier; Product Number	Application
phospho-CTnI (Ser23/24)	Rabbit	Synthetic phosphopeptide corresponding to residues surrounding Ser23/24 of human troponin I (cardiac)	1:1000	Cell Signaling Technolgies; 4004	WB
phospho-cTnI	Rabbit polyclonal	Synthetic phosphopeptide derived from mouse cTnI around the phosphorylation site of Ser22,23	1:1000	Abcam; ab58545	WB
cTnI	Rabbit monoclonal	Synthetic peptide within human cardiac Troponin I (N-terminal)	1:500-1:1000	Abcam; ab52862	WB; IP
cTnI	Rabbit polyclonal	Synthetic peptide conjugated to KLH derived from within residues 1-100 of human cardiac troponin I	1:1000	Abcam; ab47003	WB; IP
GAPDH	Mouse	Glyceraldehyde-3-phosphate dehydrogenase (GAPDH) from rabbit muscle	1:5000	Millipore; MAB374	WB
GFP	Rabbit	Recombinant full length protein corresponding to GFP	1:1000	Abcam; ab290	WB
Flag Tag	Rabbit	Synthetic peptide: DYKDDDDKC	1:1000	Thermofisher; PA1-984B	WB
HA Tag	Mouse monoclonal	Synthetic peptide: YPYDVPDYA	1:100-1:1000	Cell Signaling Technologies	WB; IF
Pan-PDE4A	Rabbit serum	Conserved C-terminal region of rat PDE4A isoforms	1:1000	In-house	WB
Pan-PDE4B	Sheep serum	Conserved C-terminal region of rat PDE4B isoforms of all species	1:5000	In-house	WB
Pan-PDE4D	Sheep serum	Conserved C-terminal region of PDE4D isoforms pf all species	1:5000	In-house	WB
PDE4D9	Rabbit	Isoform-specific N-terminal sequence	1:1000	Millipore	WB
PDE3A	Rabbit monoclonal	Recombinant fragment corresponding to residues in Human PDE3A	1:1000	Abcam; ab169534	WB
polyHistidine	Mouse	Recombinant polyHistidine tagged fusion protein	1:3000	Sigma; H1029	PA
phospho-cMyBP-C	Rabbit	Synthetic peptide corresponding to aa 276-288 of cMyBP-C phosphorylated at	1:1000	Enzo; ALX-215-057-R050	WB

		Ser282			
Phospho-(Ser/Thr) PKA Substrate	Rabbit	Synthetic phospho-PKA substrate peptide	1:1000	Cell Signaling Technolgies; 9621	WB
SUMO1 (C-terminal)	Rabbit polyclonal	Synthetic peptide corresponding to aa 72-97 of human SUMO-1	1:1000	Enzo; BML-PW9460-0025	PA; WB; IF
SUMO2/3 (N-terminal)	Rabbit polyclonal	Synthetic peptide corresponding to aa 1-15 of human SUMO-2	1:1000	Enzo; BML-PW9465-0025	PA
SUMO-TnI	Rabbit	SUMOylated TnI peptide: HLKQVKKEDTEK	1:10-1:5000	Custom made with Badrilla	PA
UBC9	Mouse monoclonal	Amino acids 1-81 of UBC9 of human origin	1:1000	Santa Cruz Biotechnology; sc-271057	PA; WB
V5 Tag	Mouse monoclonal	Mice were infected with the paramyxovirus SV5, Simian-Virus 5	1:1000	Abcam; ab27671	PA; WB

Table 2: Secondary Antibodies. (HRP, horse radish peroxidase; IF, immunofluorescence; PA, peptide array; WB, western blotting).

Secondary Antibody	Host Species	Immunogen	Dilution	Supplier; Product Number	Application
Donkey anti-goat	Donkey	IgG	1:5000	Licor; 925-68074	WB
Donkey anti-mouse	Donkey	IgG	1:5000	Licor; 925-68072	WB
Donkey anti-rabbit	Donkey	IgG	1:5000	Licor; 925-68073	WB
Anti-mouse HRP	Sheep	IgG	1:5000	Sigma; NXA931	PA; WB
Anti-rabbit HRP	Goat	IgG	1:5000	Sigma; A6154	PA; WB
Goat anti-mouse 488	Goat	IgG H+L from mouse	1:500	Invitrogen; A21071	IF
Goat anti-rabbit 488	Rabbit	IgG H+L from rabbit	1:500	Invitrogen; A21121	IF

The membranes were then subjected to three 5 minute washes in 1x TBS-T at room temperature under constant agitation. The membrane was then placed in a solution of 1% milk containing a 1:5000 dilution of secondary antibody (Table 2) which reacts with the species in which the primary antibody was raised, and incubated for 60 minutes at room temperature under conditions of constant agitation. In general, two different types of secondary antibodies were used, ones which were conjugated to Alexa-Fluor fluorescent moieties, and ones which were conjugated to HRP. Alexa-Fluor antibodies (Licor) are photo-sensitive, so

were incubated under aluminium foil to preserve their activity. Membranes were washed three times as before directly prior to visualisation.

For membranes incubated with Licor Alexa-Fluor antibodies, a Licor Odyssey Scanner was used for visualisation of bound antibodies. The scanner allows the detection of the secondary antibody. Both 700 nm and 800 nm wavelengths could be visualised, allowing the use of antibodies reacting to different species (i.e. mouse or rabbit) to be visualised. In this manner, proteins of similar molecular weights within the same sample could be distinguished on the same membrane. Digital images were acquired and analysed using Licor Odyssey software.

Membranes incubated with HRP-conjugated secondary antibodies were analysed using the enhanced chemi-luminescence (ECL) method (Amersham BioSciences) to detect bound antibodies. Following the three wash steps, membranes were incubated with ECL solution for 1-3 minutes and exposed to light-sensitive autoradiography film in a dark environment. The films were developed using a Kodak X-Omat 2000 processor.

Quantification of bands detected on membranes required comparison to "housekeeping protein" glyceraldehyde-3-phosphate dehydrogenase (GAPDH), which was used as a loading control. Both fluorescent and ECL images were analysed and quantified using Image J software (NIH).

2.11 *In Vitro* SUMOylation Assay

To determine whether proteins of interest could be SUMOylated, the hypothesised target proteins were SUMOylated *in vitro* using a SUMOylation Kit (Enzo). This kit includes the essential components of the SUMOylation pathway to provide SUMOylated proteins linked by covalent bonds. The assay components include SUMO activating enzyme (E1), UBC9 (SUMO E2), SUMO enzyme solutions (SUMO1, SUMO2, SUMO3), buffer, Mg-ATP, and dH_2O. Following preparation on ice as per manufacturer's instructions, the reaction was incubated at 30ºC for 30 minutes. Although formulated for use on target proteins within overexpressing cell lysates, *in vitro* SUMOylation was also carried out on peptide arrays, which is described in a later section.

2.12 Analysis of Protein-Protein Interactions

The identification and analysis of protein-protein interactions was central to the present work, and required a number of techniques, including co-immunoprecipitation (co-IP) and peptide arrays.

2.12.1 Immunoprecipitation

All steps in the immunoprecipitation (IP) protocol were carried out on ice unless otherwise explained. Cell lysates were equalised to desired concentration in 3T3-lysis buffer or a co-IP buffer (developed by Roland Schindler, Imperial College London) (150 mM NaCl, 1% v/v triton-x100, 2 mM EDTA, 0.35% w/v bovine gelatin, pH 8, supplemented with protease cocktail inhibitor tablets (Roche)). For IPs using endogenous proteins from NRVM, 400 μg of protein was used. 1 μg of primary antibody was then added to the lysate and the IP reactions were rotated at 4˚C overnight. The following day, 30 μl of G-Sepharose beads (GE Healthcare Biosciences) were rinsed four times in 500 μl of TBS (20 mM Tris-Cl pH 7.6, 150 mM NaCl) via centrifugation at 500 rpm for three minutes. The lysate and antibody reactions were added to the beads and rotated at 4˚C for three hours. The reactions were washed four times in 500 μl of TBS. Following the final wash, the beads were resuspended in 20-50 μl of 5x loading buffer and vortexed. They were then microcentrifuged at 14,000 rpm for 30 seconds and heated at 95˚C for five minutes. Finally, the IP samples were microcentrifuged at 14,000 rpm for 1 minute. At this point the samples were ready to be loaded onto a gel and analysed by Western Immunoblotting.

Alternatively, immunoprecipitation experiments were carried out using TrueBlot® IP Ig Agarose beads. These were used as per the manufacturer's instructions. Again, cell lysates were equalised to the desired concentration in 3T3-lysis buffer or Co-IP buffer. Lysates were added to 50 μl of TrueBlot® beads and rotated for 30-60 minutes to preclear. Following a spin to pull down the beads, the lysates were aspirated and added to a fresh tube with 1 μl of primary antibody. These reactions were rotated for 60 minutes at 4˚C. 50 μl of fresh, washed beads were then added to these reactions and rotated for 60 minutes at 4˚C. The beads were then washed and prepared for analysis by Western Immunoblotting as previously described.

2.12.2 Solid phase peptide array

2.12.2.1 Solid phase peptide array synthesis

Peptide arrays were used to identify interacting proteins and to determine the amino acids involved in the interactions. Solid phase peptide arrays were produced by direct synthesis onto Whatman cellulose membranes or glass slides using Autospot Robot ASS 222 (Intavis, Koln, Germany) as described previously (Frank, 2002). The robot functions by delivering specific volumes of solvents to small droplets on membranes or slides which contain the synthesis reaction. The peptides were synthesised and spotted in house. Briefly, this technique is based on Fmoc (9-fluorenylmethoxycarbonyl) chemistry, which involves the synthesis of proteins by coupling the carboxyl group on one amino acid to the amino group on the next (Fields and Nobel, 1990). Fmoc is used to protect the functional side chains of preceding amino acids to prevent them from interacting with free carboxyl or amino groups. This allows the isolation of the carboxyl group for interaction and the synthesis of amino acid chains. This process is shown in detail in Figure 2.1. Peptide arrays were comprised of overlapping 25-mer peptides sequentially shifted by 5 amino acids, unless otherwise specified. Following synthesis, the arrays were stored at 4ºC until they were used for a variety of experiments including the identification of protein-protein interactions, the identification of SUMOylation sites and the testing of custom antibodies.

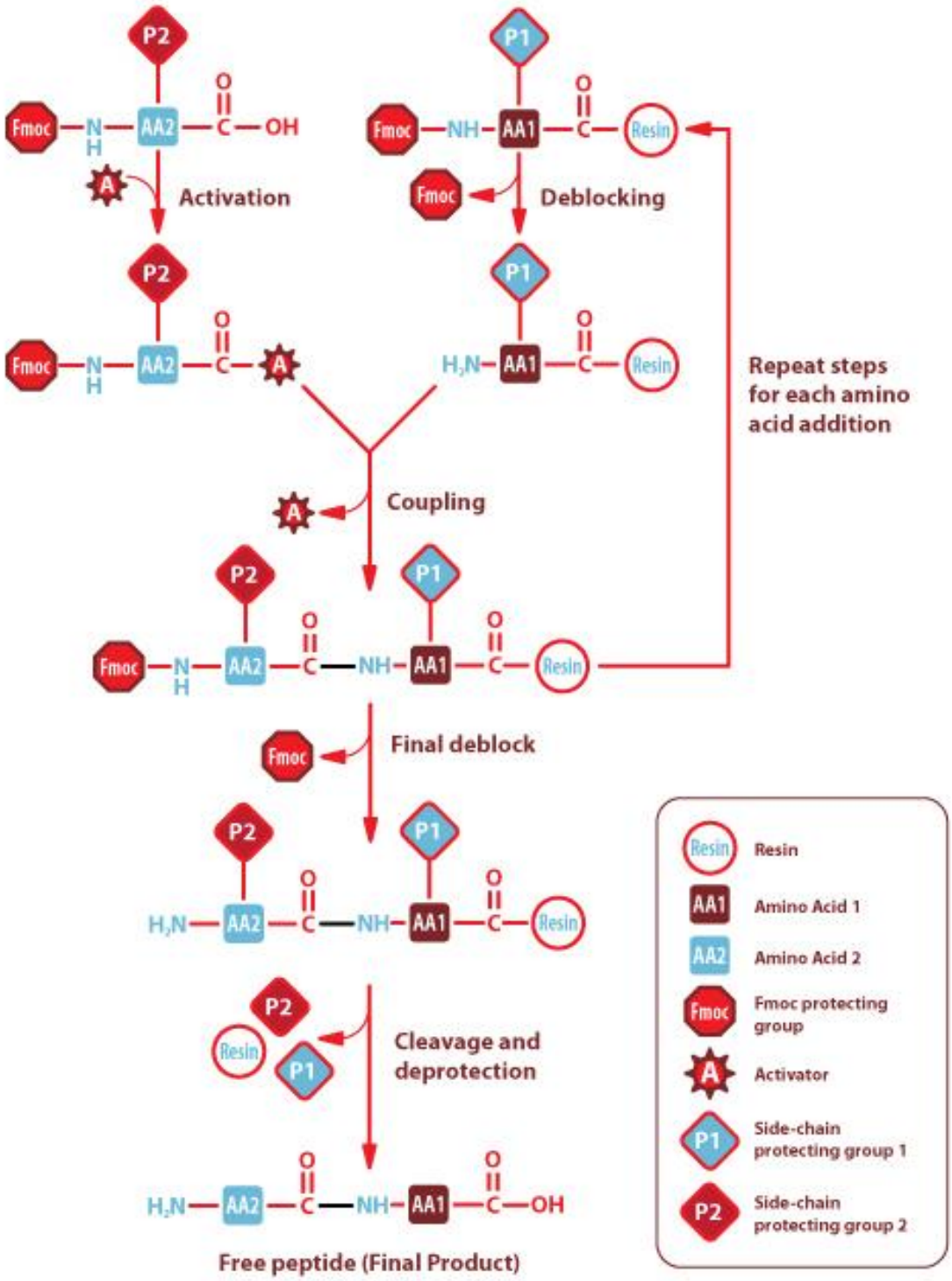

Figure 2.1: Solid phase peptide synthesis for the coupling of two amino acids. The first amino acid of the 25-mer chain was coupled to a solid support by its carboxyl group, and its amino group was protected by Fmoc. The addition of the second amino acid began with the activation of its carboxyl group, which its amino group remained protected by Fmoc. The Fmoc was also removed from the amino group of the first amino acid in the deblocking step. The active carboxyl group of the second amino acid could then interact with the amino group of the first amino acid. These steps were repeated until the chain reached the desired length. When all amino acids had been added, additional protective groups were removed and the peptide could be cleaved from the resin if necessary (Aldrich 2019).

2.12.2.2 Peptide array overlay

Proteins of interest were overlaid on peptide arrays using the following steps. All incubation steps were carried out under gentle agitation. Arrays were bathed in 100% ethanol and washed in TBS-T for 10 minutes at room temperature. The arrays were then blocked to remove non-specific binding for 2 hours in blocking buffer (5% (w/v) BSA or Marvel milk powder in TBS-T) and again washed using TBS-T. The protein of interest was then overlaid on the arrays. The protein could be purified or in the form of cell lysate overexpressing the protein of interest. If purified protein was used, an antibody only control was included for comparison; if overexpressing lysate was used, antibody only and non-transfected lysate controls were included. Proteins were added to the arrays at a concentration of 0.4-1 µg/ml in probing buffer (1% (w/v) BSA or milk in TBS-T) and incubated for 1-4 hours at 4ºC under gentle agitation. The arrays were then subjected to three TBS-T washes before the addition of a primary antibody in probing buffer to be incubated for 2-16 hours at 4ºC with gentle agitation. Again, the arrays were washed in TBS-T before the addition of a HRP conjugated secondary antibody in probing buffer for 1 hour at room temperature. Finally, the arrays were washed again in TBS-T and developed by exposing them to ECL and film.

Peptide arrays on membranes could be stripped for reuse. Stripping buffer (20 mM DTT, 70 mM SDS, 60 mM Tris-HCl, pH 6.8) was heated to 70ºC before being poured onto arrays and incubated for 30 minutes under gentle agitation. The arrays were subsequently washed twice for 10 minutes in TBS-T and air dried. It was necessary to develop the arrays as previously described to ensure that the stripping was successful.

2.12.2.3 SUMOylation of peptide arrays

In vitro SUMOylation of peptide arrays was used to confirm SUMOylation at consensus motifs. Peptide arrays containing the proposed SUMOylation sites of target proteins were produced and subjected to *in vitro* SUMOylation assays (SUMOylation Kit, Enzo) as described previously. Membrane or glass slide peptide arrays were bathed in ethanol, washed in TBS-T and blocked in 5% BSA for two hours at room temperature. SUMOylation kit components sufficient for 20 reactions (the contents of one entire kit) were combined and further diluted to a

final volume of 1 ml. Arrays were incubated in the SUMOylation reaction mixture for 1 hour at room temperature. The reaction mixture could then be reused by transferring it onto another membrane. Following incubation, the arrays were washed in TBS-T and incubated overnight in polyHistidine primary antibody. Again, the arrays were washed and incubated with appropriate HRP-conjugated secondary antibodies before development using ECL and film. Antibody only control assays were used to ensure a lack of non-specific antibody reactivity.

2.13 Functional Assays

2.13.1 Phosphodiesterase Activity Assay

A two-step radioactive assay was used to measure PDE activity associated with TnI, which has previously been described (Marchmont and Houslay 1980). In the first step of the assay, the samples were incubated with radiolabelled 8-[$_3$H]-cAMP substrate, and the PDEs in the sample hydrolysed the 8-[$_3$H]-cAMP to [3H]-5'-AMP. In the second hydrolysis step, snake venom was added to the samples, which caused the hydrolysis of the [3H]-5'-AMP to [3H]-adenosine. Finally, ion exchange resin was added, which binds the negatively charged, unhydrolysed cAMP, leaving the [3H]-adenosine to be measured by scintillation counting. This measurement was used to calculate the rate of cAMP hydrolysis.

Unless otherwise specified, all steps were performed on ice. Samples to be assayed were diluted to a final volume of 50 µl in Buffer A (20 mM Tris-CL, pH 7.4). If necessary, these samples included appropriate concentrations of PDE inhibitors. cAMP substrate mix, containing 2 µl of 1 mM cAMP (unlabelled) and 3 µl of radiolabelled 8-[$_3$H]-cAMP (final cAMP concentration 100 µM), was then added to the samples and incubated for 10-30 minutes at 30˚C. Reactions were boiled for 2 minutes to end the hydrolysis reaction and then chilled on ice for 15 minutes. Snake venom (*Ophiophagus hannah*) was then added to a final concentration of 0.2 mg/ml and samples were incubated for 10 minutes at 30˚C. 400 µl of Dowex anion exchange resin slurry (resin:H_2O:ethanol 1:1:1) was added to each sample. Samples were vortexed and incubated on ice for at least 15 minutes. Following the incubation, the tubes were vortexed and centrifuged at 13,000 rpm for 3 minutes. 150 ml of the supernatant from each sample was then added to 1 ml of Opti Flow SAFE 1 scintillant and samples were mixed by

vortexing. An additional sample containing 50 µl of cAMP substrate solution and 1 ml of scintillant was also prepared to assess the total counts per minute. All samples were counted on a Tri-Carb 2900TR Liquid Scintillation Analyser (Packard BioScience, Connecticut, USA) to determine the amount of radiolabelled 8-[^{3}H]-cAMP substrate.

The PDE activity of each sample in pmol cAMP hydrolysed/min/mg protein was determined using the following formula:

$$PDE\ activity = 2.61 \times \frac{count\ of\ sample - count\ of\ blank}{average\ total} \times 10^{-11} \times 10^{12} \times \frac{1000}{ug\ protein}$$

where 2.61 corrects for the fraction of supernatant used from the anion exchange phase, 10^{-11} corrects for the time in which the hydrolysis occurred and the moles of cAMP used, 10^{12} corrects to pmoles, and (1000/µg protein) corrects for the protein concentration.

2.14 Microscopic Imaging

2.14.1 Fluorescence Resonance Energy Transfer

Fluorescence Resonance Energy Transfer (FRET) was used to monitor cAMP dynamics in live cells (Nikolaev and Lohse 2006). FRET describes the transfer of energy from a donor to an acceptor fluorophore. When the donor is excited by a particular wavelength, it emits fluorescence at a characteristic wavelength. However, when the donor and acceptor fluorophores are in close proximity, their emission spectra overlap, and the characteristic emission of the acceptor can be detected.

2.14.1.1 FRET Probes

The sensors used within the present study were called CUTie (cAMP Universal Tag for imaging experiments) sensors (Surdo, Berrera et al. 2017). These sensors contain two fluorescent moieties, a donor, CFP, and an acceptor, YFP. In conditions of low cAMP concentration, these fluorophores are in close proximity, so energy transfer from donor to acceptor can occur, and YFP's characteristic emission is detected. However, when the concentration of cAMP is increased,

the binding of cAMP to the sensor causes a conformational change, which increases the distance between the donor and acceptor, and the transfer of energy stops; now, the donor, CFP's characteristic emission is detected. FRET imaging records the ratio of donor to acceptor emission to monitor changes in the cAMP concentration over the course of the experiment and in response to stimuli, such as drug additions.

CUTie sensors were developed by the Zaccolo group to overcome various limitations of previously used sensors, such as EPAC1-cAMPs (Surdo, Berrera et al. 2017).

2.14.1.2 FRET Imaging

Cells were plated onto sterilised 24 mm coverslips (VWR) at low density so that single cells and clear background regions were available. 24 hours prior to imaging, the cells were transiently transfected with FRET sensors as previously described.

The coverslip was carefully removed from a six-well plate with watchmaker's forceps, inserted into a metal ring bath and secured carefully. The coverslip was then washed three times with FRET saline (125 mM NaCl, 5 mM KCl, 1 mM Na_3PO_4, 1 mM $MgSO_4$, 20 mM HEPES, 5.5 mM glucose, 1 mM $CaCl_2$, pH 7.4) before applying 1 ml to the bath. The cells were then viewed on an Olympus IX71 Inverted Microscope under 40x or 60x oil immersion lenses (Zeiss).

Image acquisition was commenced, and the FRET ratio was monitored in real time. Cells were left to reach a stable baseline FRET ratio or to reach a plateau before stimulation with various drugs, including 0.5 nM isoprenaline (non-specific ß-adrenergic receptor agonist), 10 uM rolipram (PDE4 inhibitor) and 10 uM cilostamide (PDE3 inhibitor). All experiments were ended following treatment with a saturating dose of 100 µM IBMX (non-specific PDE inhibitor) + 25 µM forskolin (AC activator), which was included to ensure the proper functioning of the probe.

Images were acquired with a 5 second time-lapse, which reduced effects of photobleaching. A beam splitter separated CFP and YFP images so that the

images could be used to obtain a ratio of CFP to YFP in defined regions which had been drawn around cells. The images were converted to mean intensity values for each image and ratios were calculated. The ratios were used to determine mean FRET change over the course of the experiment and as a result of treatment with various compounds.

2.14.2 Immunofluorescence

To confirm the viral overexpression of proteins of interest and the correct targeting of these proteins, immunofluorescent staining and microscopy was used. Cells were plated on glass coverslips at low densities to ensure adequate background. Medium was removed and coverslips were washed with PBS. Cells were fixed onto coverslips by incubation in 4% paraformaldehyde (PFA) for one hour on an orbital shaker at room temperature. The fixed coverslips were washed with PBS 3 times for 10 minutes to remove residual PFA. Coverslips were then incubated in blocking buffer (0.2% Triton-X, 0.5% BSA in PBS) for 1 hour to reduce non-specific binding. Cells were then incubated overnight in appropriate primary antibodies (diluted 1:500 in blocking buffer) in a humidity chamber at 4˚C. Following the overnight incubation, coverslips were washed 3 times for 10 minutes in PBS. Appropriate Alexa Fluor® secondary antibodies were prepared at a concentration of 1:500 and coverslips were incubated in the secondary antibody solutions for 2 hours at room temperature in a humidity chamber, protected from light. The coverslips were then washed in PBS 3 times for 10 minutes. Finally, the coverslips were mounted onto microscope slides using one drop of ProLong™ Gold antifade reagent with DAPI and left to dry overnight in the dark at room temperature. If necessary, the slides were stored long term at 4˚C. A Zeiss Pascal laser-scanning confocal microscope (LSM) 510 Meta and an Axiovert 100 microscope with water immersion objective were used to image slides. Images were acquired with Zeiss LSM Image examiner and analysed on Image J.

2.15 Proteomics

Proteomic experiments and analyses were carried out by Glasgow Polyomics, Uniersity of Glasgow, UK. Specifically, this approach was used to identify proteins which interacted with TnI.

2.15.1 Sample Preparation

Proteomics analysis was carried out on gel slices, which were sent to Glasgow Polyomics at room temperature. All steps were carried out in a laminar flow hood to avoid keratin contamination. Bands were destained using Farmer's reducing agent (1:1 20% sodium thiosulphate:1% potassium ferricyanide). Gel pieces were then washed in 100 mM ammonium bicarbonate and then in 50% acetonitrile/100 mM ammonium bicarbonate. The gels were reduced by incubating with 100 mM ammonium bicarbonate supplemented with 45 mM DTT at 60˚C. Gel pieces were cooled to room temperature before alkylation using 100 mM iodoacetamide. Reduced, alkylated gel slices were washed in 50% acetonitrile/100 mM ammonium bicarbonate. The pieces were shrunken by adding acetonitrile. The pieces were thoroughly dried in a vacuum centrifuge. Trypsin resuspended in 25 mM ammonium bicarbonate was used to rehydrate the gel pieces and the protein was digested overnight at 27˚C. The next day, the samples were centrifuged to pellet the gel pieces. Supernatant was transferred to a 96 well plate. 5% formic acid was added to the gel pieces prior to the addition of acetonitrile. These were briefly centrifuged to pellet the gel pieces and the supernatant was added to the 96 well plate, pooling the supernatant from each sample together. These were then dried in a vacuum centrifuge and stored at -20˚C until being analysed by mass spectrometry (MS).

2.15.2 Mass Spectrometry

MS allows the identification of proteins based on a peptide's mass-to-charge ratio. Proteins within the sample were digested into peptides by enzymatic digestion with trypsin and Lys C, which increases solubility and sensitivity (Glish and Vachet 2003). More specifically, trypsin cleaves polypeptides C-terminally to each arginine and lysine residue while Lys C cleaves polypeptides C-terminally to each lysine residue. Samples were then ionised by passing electrical potential through a needle in a process known as electrospray ionisation. The peptides were then subjected to electrical fields within a vacuum chamber. The differential responses of the peptides to the electrical fields allowed their mass-to-charge ratio to be detected by Orbitrap Elite MS (ThermoFisher Scientific). This allowed the generation of a spectrum specific to each sample. The spectrums were analysed to determine the theoretical amino acid sequences of

each peptide, which were then identified using the Mascot search engine (v2.6.2, Matrix Science Inc) and compared against the NCBI Genbank database (https://www.ncbi.nlm.nih.gov/protein) (Steen and Mann 2004).

In the present study, TnI immunoprecipitates were run on SDS-PAGE gels and gel slices containing proteins between the weights of 50-150 kDa were analysed by MS.

2.16 Statistical Analysis

All values are presented as mean ± SEM from at least three experimental replicates unless otherwise stated. Level of statistical significance was determined by p-values calculated using paired or unpaired *t*-tests or one way analysis of variance (ANOVA) depending on the conditions with which the data were collected. A p-value of <0.05 (*) was considered significant, p-value <0.01 (**) considered highly significant and p-value <0.001 (***) extremely significant, p-value >0.05 (NS) considered non-significant.

Chapter 3 Investigating the TnI-PDE4D9 Interaction

3.1 Introduction

PDEs have been shown to integrate into signalosomes containing cardiac excitation-contraction coupling proteins in cardiac myocytes. This allows fine tuning of ß-adrenergic induced PKA phosphorylation of these proteins. Although the components of many of these complexes have been determined, until recently, there was no evidence for the interaction of a PDE isoform with TnI at the myofilament for the regulation cAMP dynamics and PKA phosphorylation (Edwards 2012). This signalling paradigm is likely to be functionally relevant considering the functional effects of PKA phosphorylation and the disease relevance of this modification. Under conditions of ß-adrenergic stimulation, phosphorylation of Ser23/24 of TnI changes the functional properties of the protein such that the myofilament's sensitivity for Ca^{2+} is reduced. This has been shown to contribute to the positive lusitropic response observed under these conditions (Zhang, Zhao et al. 1995, Layland, Solaro et al. 2005). Furthermore, numerous studies have reported that the phosphorylation levels of TnI is reduced in chronic heart disease, likely contributing to impaired relaxation of the cardiac muscle (Wolff, Buck et al. 1996, McConnell, Moravec et al. 1998, Zakhary, Moravec et al. 1999, Mahajan and Jarolim 2011, Shah, Ferry et al. 2017).

3.1.1 Evidence for TnI-PDE4D9 Interaction

Previous studies from the Baillie lab at the University of Glasgow found evidence that TnI interacts with PDE4D9, a cAMP hydrolysing member of the PDE4 family (Edwards 2012). First, pharmacological studies employed the use of family-specific inhibitors of PDEs in combination with targeted FRET sensors to study the cAMP dynamics at the myofilament, in the direct vicinity of TnI. Following submaximal ß-adrenergic stimulation, the effects of PDE4 inhibition with rolipram and PDE3 inhibition with cilostamide on cAMP dynamics in the cytosol and myofilament were compared in NRVM. Treatment of cells with rolipram caused a significantly larger increase in FRET ratio as measured by TnI-tethered sensors compared to cytosolic sensors (Figure 3.1). This indicates that PDE4 has a dominant effect in the regulation of cAMP levels around TnI at the myofilament. The opposite was observed when cells were treated with cilostamide, suggesting that PDE3 has a more dominant effect in the cytosol (Edwards 2012).

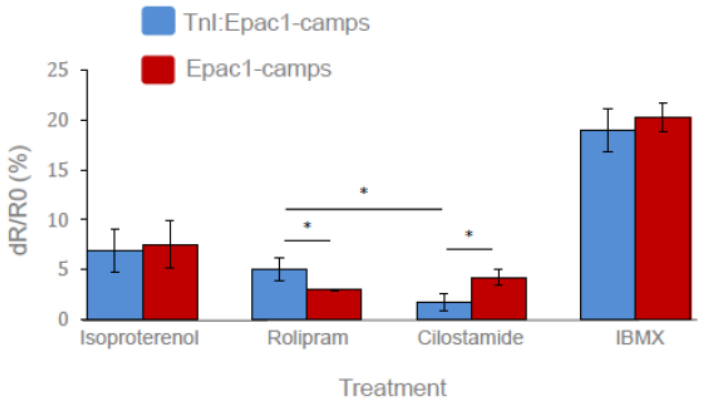

Figure 3.1: Change in FRET ratio at the myofilament and in the cytosol in response to PDE4 or PDE3 inhibition. NRVM were treated sequentially with isoproterenol (1 nM), rolipram (10 μM) or cilostamide (10 μM), and a saturating dose of IBMX (100 μM). Changes in FRET ratio were measured and compared between a cyctosolic Epac1-camps sensor and a TnI-tethered TnI-Epac1-camps sensor, which would measure cAMP dynamics at the myofilament. The cAMP response at TnI following rolipram treatment was significantly larger than the response to cilostamide. There were no significant differences between the change in FRET ratios of the different probes in response to isoproterenol or IBMX in these experiments (Edwards 2012).

This observation was consistent with increased levels of phosphorylated TnI in response to treatment with rolipram with and without ß-adrenergic stimulation. These findings led to the hypothesis that a PDE4 isoform interacted with TnI and that inhibition of this PDE with rolipram led to increased cAMP at the myofilament, allowing increased activation of PKA and increased phosphorylation of TnI.

The next step was to identify the specific isoform of PDE4 which was involved in this paradigm. Numerous co-immunoprecipitation studies were performed using NRVM cell lysates (Edwards 2012). TnI immunoprecipitates were probed for PDE4 subfamilies, and it was found that PDE4D co-immunoprecipitated with TnI. Similar immunoprecipitations were then probed using isoform specific antibodies. It was shown that PDE4D9 co-immunoprecipitated with TnI (Figure 3.2A). It is important to note that in these studies, the immunoprecipitation of TnI was not confirmed as its molecular weight was too similar to the light chain of IgG and could not be visualised on the western blots. Consistent with this evidence, confocal microscopy showed that there was significant colocalisation between TnI and PDE4D9 (Figure 3.2B) (Edwards 2012).

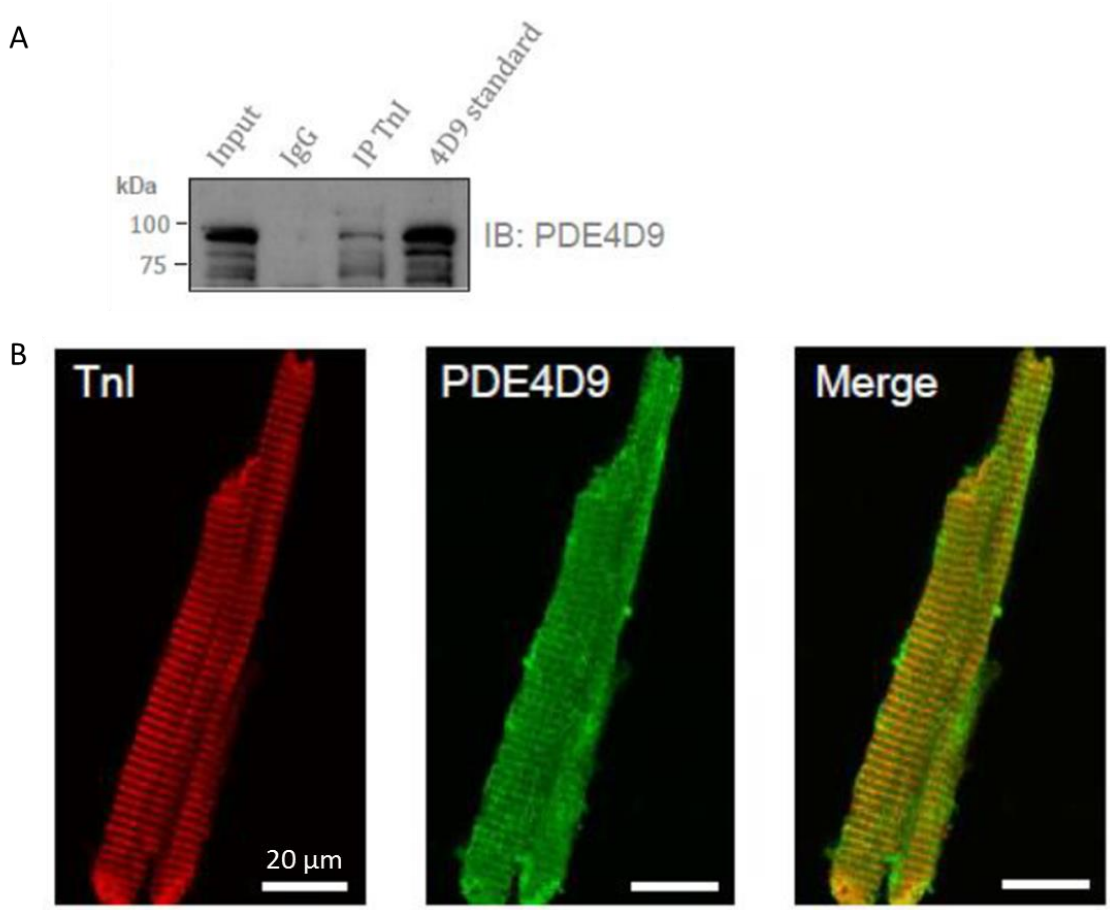

Figure 3.2: PDE4D9 interacts with TnI in ARVM. A. Immunoblotting TnI immunoprecipitations with a PDE4D9 specific antibody revealed that PDE4D9 immunoprecipitated with TnI. The specificity of the antibody was confirmed by the inclusion of a PDE4D9 standard protein sample. Other PDE4D isoforms did not immunoprecipitate with TnI (data not shown). B. PDE4D9 and TnI were shown to colocalise in confocal images with a clear striated pattern, consistent that the proteins are in close enough proximity for a direct interaction to be plausible (Edwards 2012).

Finally, peptide array technology was used to identify the binding site on TnI to which PDE4D9 interacts (Edwards 2012). GST-tagged PDE4D9 protein was overlaid onto a full length TnI peptide array, and positive spots indicated binding of PDE4D9 to the flexible C-terminal region of TnI. Alanine scans were used to determine which amino acids in this region were necessary for binding, and it was determined that the dual lysine residues (KK177-8) in the C-terminal region of the protein were necessary for binding (Edwards 2012). When these amino acids were mutated to alanine, binding of GST-PDE4D9 to the peptide array was reduced. Other spots with different, sequential alanine mutations did not affect the binding. Based on this evidence, a short disruptor peptide including this binding sequence was developed. The theory behind the use of the disruptor peptide was that it would bind PDE4D9 in cells, thereby competing with TnI for

this interaction. This would ‘unhinge’ the PDE from the myofilament, thereby removing the local regulation of cAMP dynamics.

3.1.2 Advances in FRET sensor technology

FRET is a live cell imaging technique allowing the measurement of changes in cAMP concentrations in real time. This technique employs the use of FRET sensors which are comprised of a cyclic nucleotide binding domain (CNBD), and donor and acceptor fluorophores, often cyan fluorescent protein (CFP) and yellow fluorescent protein (YFP) respectively. During imaging, the donor fluorophore is excited at a specific wavelength and emits fluorescence at another specific wavelength, which can be detected. However, if the donor and acceptor fluorophores are in close proximity and the emission spectrum of the donor overlaps with the excitation spectrum of the acceptor, this will result in the transfer of energy from the donor to acceptor fluorophore, or FRET, and the acceptor’s emission can be detected. If the fluorophores are not in close proximity, however, FRET cannot occur and only the donor’s emission is detected (Nikolaev, Bunemann et al. 2004).

Until recently, the most commonly used cAMP FRET probes (Epac1-camps) were based on the structure of EPAC (Nikolaev, Bunemann et al. 2004). Binding of cAMP to the CNBD results in a conformational change which increases the distance between the donor and acceptor fluorophores, reducing FRET; this is known as a ‘loss of FRET’ sensor. To measure the cAMP dynamics in specific cellular microdomains, Epac1-camps was tethered to various cellular proteins, for example TnI, causing them to target to specific intracellular locations (Gesellchen, Stangherlin et al. 2011). Although these sensors have been used in numerous studies, there were several important limitations. Importantly, targeted Epac1-camp sensors have been shown to have variable maximal FRET changes, making comparisons between targeted and cytosolic sensors technically challenging (Surdo, Berrera et al. 2017).

To overcome this limitation, the cAMP Universal Tag for imaging experiments (CUTie) sensor was developed (Figure 3.3) (Surdo, Berrera et al. 2017). Unlike the Epac1-camps sensors, in which YFP is fused N-terminally to the targeting domains, it was determined that fusion of YFP within the CNBD reduced the

interference of the targeting domain with the FRET molecule. CUTie sensors have a CNBD based on the structure of the regulatory subunit type IIß of PKA (PKA-RIIß). YFP is fused within the CNBD, meaning that the N-terminal targeting domain does not interfere with the conformation of the fluorophores. CFP was fused then C-terminally. CUTie probes were developed which targeted to a number of proteins, including TnI, HSP20, AKAP79, AKAP18δ and PDE4A1. It was shown that saturating these sensors by activation of AC with forskolin and global inhibition of PDEs with IBMX led to consistent maximal responses for each differentially targeted sensor (Surdo, Berrera et al. 2017).

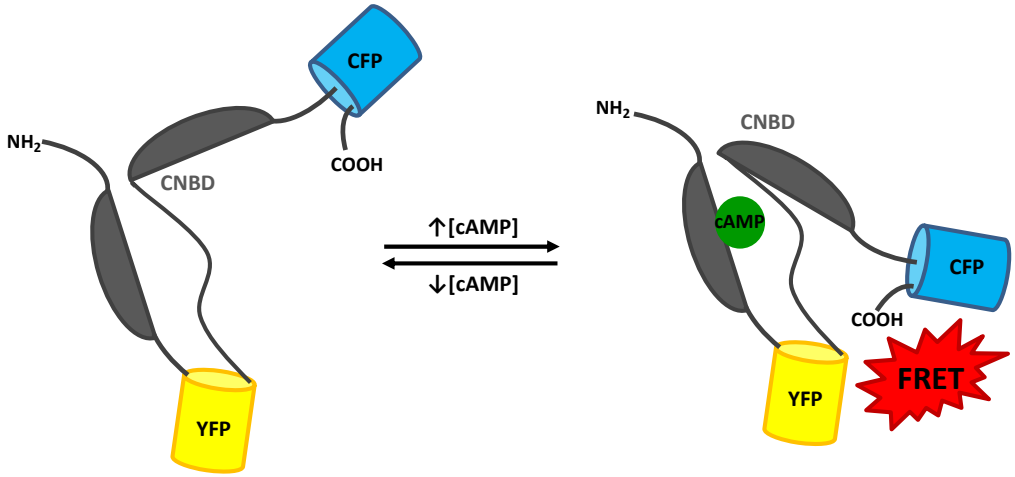

Figure 3.3: Schematic representation of CUTie FRET probes. In conditions of low [cAMP], the conformation of CUTie is such that the donor fluorophore, CFP, and the acceptor fluorophore, YFP, are far enough apart that FRET does not occur. When excited at a specific wavelength, only the donor's emission wavelength can be detected. When [cAMP] increases, the conformation of the CUTie molecule changes, bringing CFP and YFP into close proximity. Now, when the donor is excited at a specific wavelength, the transfer of energy, or FRET occurs, and the acceptor fluorophore's emission is detected. (CFP, cyan fluorescent protein; CNBD, cyclic nucleotide binding domain; YFP, yellow fluorescent protein). (Adapted from (Surdo, Berrera et al. 2017)).

FRET has been used previously to study cAMP signalling in specific subcellular locations, but now this can be done with unprecedented accuracy due to the improvements in targeted sensors.

3.2 Hypothesis and Aims

Although preliminary evidence has shown that PDE4D9 interacts with TnI to regulate cAMP dynamics at the myofilament and PKA phosphorylation of TnI, the verification of this interaction and the establishment of a functional role for the complex have not yet been determined. It was hypothesised that PDE4D9 directly interacts with TnI at the myofilament thereby regulating the cAMP dynamics in this cellular microdomain. Additionally, it was hypothesised that the disruption of this interaction would cause increased PKA phosphorylation of Ser 23/24 of TnI, which would improve cardiac function in the failing heart. The aims of the experimental work detailed in this chapter are as follows:

- To determine whether cAMP dynamics at the myofilament are significantly affected by PDE4D9 as measured by TnI-CUTie FRET sensors; this was studied under several conditions, including overexpression of dominant-negative, catalytically inactive PDE4D9 and pretreatment with peptides to disrupt the proposed interaction

- To determine whether the levels of phosphorylated TnI are significantly altered by unhinging the proposed interaction with disruptor peptide treatment

- To confirm the existence of the proposed interaction by immunoprecipitation, in combination with western blotting, proteomic analysis and PDE activity assays

- To confirm that phospho-Ser23/24 levels were altered between healthy and diseased myocardium in human cardiac samples

3.3 Methods

3.3.1 Localisation and Functionality of CUTie Probes in NRVM

Throughout the results displayed in this chapter, FRET imaging was used to observe the cAMP dynamics and how they changed as a result of pharmacological manipulation. As previously discussed, FRET probes can be tethered to various proteins to allow subcellular targeting of the probes to discrete locations or microdomains. To obtain measurements of cAMP dynamics at the myofilament, CUTie probes, described previously, which were tethered to TnI (CUTie TnI) were used. These were compared to untethered CUTie probes, which would uniformly distribute throughout the cell, allowing measurement of changes in bulk cytosolic cAMP concentration. While CUTie probes were observed to distribute uniformly, CUTie TnI transfected cells displayed a clear striated pattern, confirming the localisation of these probes to the myofilament (Figure 3.4).

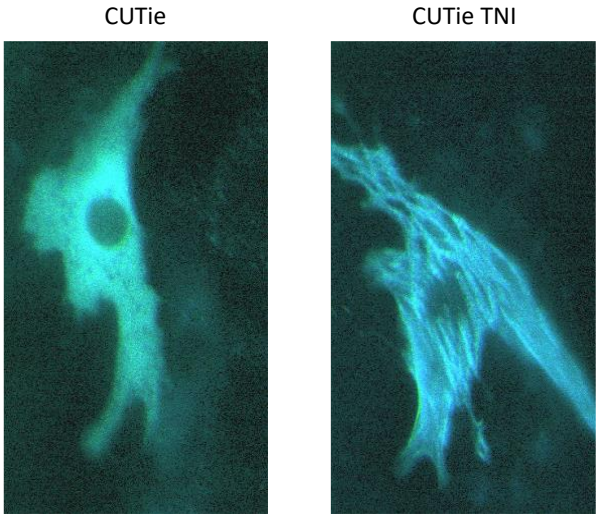

Figure 3.4: Localisation of FRET probes in NRVM. Representative microscopic images of NRVM transfected with CUTie or CUTie-TnI probes showed that the CUTie probe was uniformly distributed within the cytosol, while CUTie-TnI displayed a clear striated pattern, indicating localisation at the myofilament.

Throughout this chapter, FRET experiments using CUTie and CUTie-TnI were performed using a standard protocol with varied treatment or transfection conditions. After initial image acquisition, cells were allowed to reach a stable base line, with minimal detectable change in FRET ratio. A submaximal dose of

ß-adrenergic agonist, isoproterenol (5 nM), was then added to the cells, leading to a small increase in FRET. After this treatment, the FRET ratio was allowed to stabilise before the next stimulation. At this point, PDE family specific inhibitors were added. In most experiments, PDE4 inhibitor, rolipram (10 µM) was used, but in some, PDE3 was inhibited with cilostamide (10 µM). This led to a further increase in FRET. Finally, after a new stable baseline was reached, a saturating dose of AC activator (forskolin, 25 µM) and non-specific PDE inhibitor (IBMX, 100 µM) was added to establish the maximum response of the sensors. A representative example of a trace recorded from a single cell is shown in Figure 3.5.

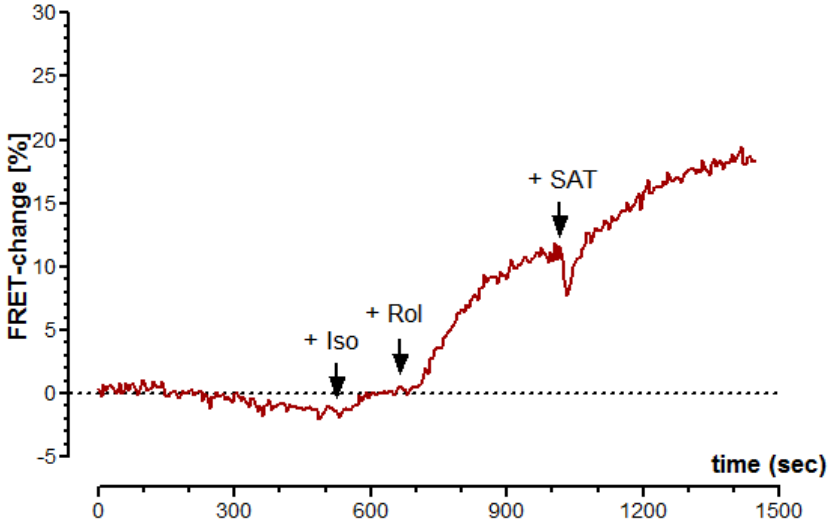

Figure 3.5: Changes in FRET recorded from a single cell. Increases in FRET represent increases in the cAMP concentration. When the cell was treated with various stimuli (indicated by the arrows), the FRET change, and therefore, the cAMP concentration in the vicinity of the probe increased. This trace is a representative example of all of the experiments described in this chapter.

3.4 Results

3.4.1 β-adrenergic stimulation and PDE inhibition cause greater FRET changes at the myofilament

Results from single cell traces were combined and compared to determine differences between the effects of pharmacological stimulations in different cellular microdomains. The FRET change resulting from submaximal ß-adrenergic stimulation was significantly greater in the vicinity of TnI than in the cytosol (Figure 3.6A) (1.8±0.2% vs. 2.9±1.5%, p=0.0395, unpaired *t*-test). This is consistent with the concept of compartmentalised cAMP signalling in NRVM such that cAMP increases in specific microdomains associated with PKA substrates following ß-adrenergic signalling.

The effects of PDE3 and PDE4 inhibition were also compared in both cellular compartments. Interestingly, PDE4 inhibition with rolipram resulted in a significantly larger FRET change compared to PDE3 inhibition with cilostamide as measured by both CUTie-TnI and CUTie, suggesting a more dominant role of PDE4 in the regulation of cAMP dynamics in both of these subcellular locations (Figure 3.6B). Furthermore, both PDE inhibitors had greater effects in the vicinity of TnI. Together, these results suggest that PDE4 has dominant activity, and PDE3 and PDE4 have greater regulatory roles at the myofilament than in the cytosol. These data are consistent with the previous data which employed the use of PDE activity assays to show that PDE4 inhibition with rolipram resulted in a dramatically greater reduction in PDE activity in NRVM lysates than the specific inhibition of any other PDE family (Edwards 2012).

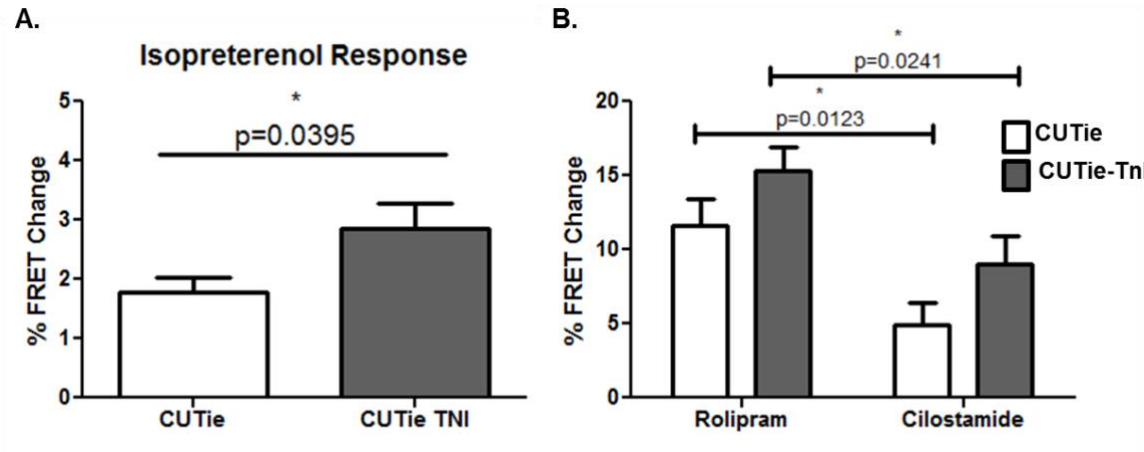

Figure 3.6: Comparison of the effects of various stimulations on cytosolic and myofilament cAMP dynamics. A. Average % FRET change of the cytosolic CUTie probe and the myofilament CUTie-cTnI probe. Submaximal treatment of NRVM with 0.5 nM isoproterenol resulted in a significantly larger FRET change as detected by CUTie-cTnI compared to CUTie. Results represented as mean ± SEM, n=32-38 cells, *=p<0.05, student's *t*-test. B. Inhibition of PDE4 (10 µM rolipram) caused a larger response detected by both probes compared to inhibition of PDE3 (10 µM cilostamide). Results represented as mean ± SEM, n=23-26 cells rolipram, n=9-12 cells cilostamide. *=p<0.05, student's *t*-test.

3.4.2 Overexpression of dominant-negative PDE isoforms

Pharmacological agents which globally inhibit PDE families are limited by their lack of specificity to interrogate the activity of PDE subfamilies or isoforms. One approach to achieve isoform-level specificity is through the overexpression of dominant-negative (D/N), catalytically inactive PDE isoforms in NRVM. In theory, the overexpressed, inactive protein would displace the endogenous, functional isoform, attenuating its endogenous function in the cell (McCahill, McSorley et al. 2005). FRET changes were recorded in single NRVMs with the protocol displayed in Figure 3.5, in the presence of PDE4D9 D/N-RFP or PDE4D5 D/N-RFP; transfection was confirmed by visualising RFP emission microscopically (Figure 3.7).

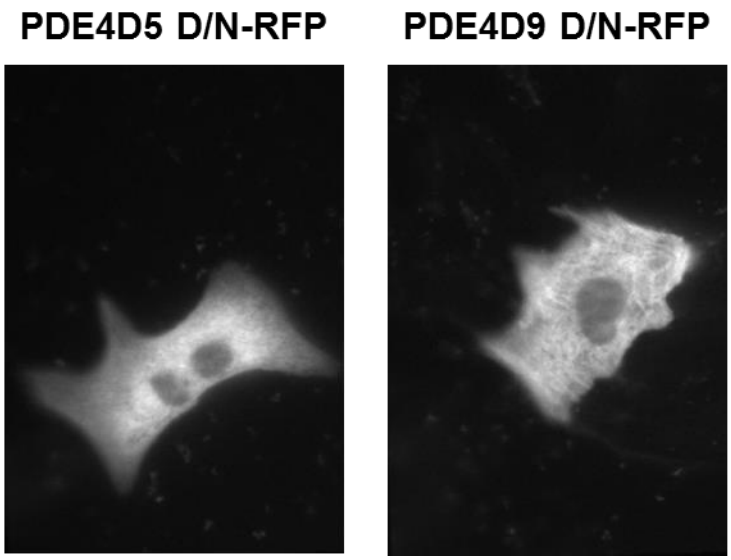

Figure 3.7: Confirmation of transfection of PDE4D5 D/N-RFP and PDE4D9 D/N-RFP. The successful transient transfection of PDE4D5 D/N-RFP and PDE4D9 D/N-RFP was confirmed in each cell for which a FRET change was recorded.

Interestingly, in the cytosol, overexpression of PDE4D9 D/N attenuated the FRET response to PDE4 inhibition with rolipram as well as saturating treatment with forskolin and IBMX, while overexpression of PDE4D5 D/N had no significant effects. Although unexpected, this suggests that PDE4D9 has a more dominant role than PDE4D5 in the cytosol of NRVM. Contrary to the hypothesis, overexpression of either PDE4D9 D/N or PDE4D5 D/N did not have any significant effects on the FRET change in response to ß-adrenergic stimulation or PDE4 inhibition at the myofilament; similarly to the cytosolic effects, the overexpression of the inactive form of PDE4D9 attenuated the saturated FRET response (Figure 3.8). Considering the previously published evidence for a direct interaction between PDE4D9 and TnI, these data did not support the hypothesis that this interaction exists in NRVM.

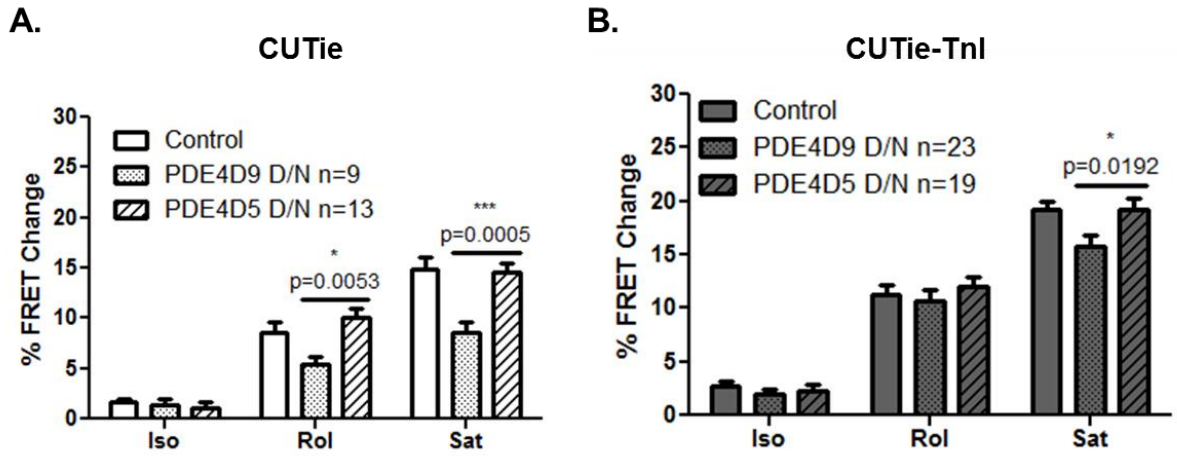

Figure 3.8: The effect of overexpression of dominant negative PDEs on FRET. A. FRET experiments were repeated as shown in Figure 3.5 in NRVM overexpressing dominant negative PDE4D9 or PDE4D5 as a control. A. FRET change measured by the cytosolic probe was significantly affected by the overexpression of PDE4D9 D/N but not PDE4D5 D/N. The FRET change in response to PDE4 inhibition and saturating concentrations of IBMX and forskolin were significantly dampened by the presence of PDE4D9 D/N. B. When measured with CUTie-cTnI, FRET change in response to isoproterenol and rolipram was unchanged, but the overexpression of PDE4D9 D/N significantly reduced the response to saturating doses of IBMX and forskolin. Results represented as mean ± SEM, n=9-23. *=p<0.05, PDE4D9 D/N vs PDE4D5 D/N, student's *t*-test.

3.4.3 Effect of disrupting PDE4D9/TnI interaction on FRET change

As previously described, peptide array technology allowed the 25-mer site of TnI to which PDE4D9 binds to be determined. This allowed the development of a disruptor peptide, which, in theory, would disrupt the interaction, thereby unhinging the TnI microdomain from the PDE's regulation. The use of a peptide disruptor adds a layer of specificity beyond the use of dominant negative isoform overexpression. The same PDE isoform may have multiple roles at different microdomains within the same cell. Therefore, the use of a peptide disruptor would only affect the specific pool of that isoform in the relevant part of the cell. The cell permeable disruptor peptide was based on the 25-mer sequence of TnI and had the sequence: St-GTRAKESLDLRAHLKQVKKEDIEKE. A scrambled peptide containing the same amino acids in a random order was included as a control; this had the sequence: St-KTELKAERGIKSDVAKERELHDLGK. To determine the effects of the disruptor peptide on cAMP dynamics, FRET experiments were performed as previously described on NRVM which had been incubated for 2 hours with 10 μM disruptor peptide or scrambled control. Neither the disruptor peptide nor the scrambled control had any significant effects on the cAMP dynamics in the cytosol (Figure 3.9A). This was consistent with the hypothesis as

the disruptor peptide would specifically displace the PDE bound to TnI. At the myofilament, treatment with disruptor peptide but not scrambled control resulted in a small but significant increase in the FRET change in response to submaximal ß-adrenergic stimulation (Figure 3.9B) (4.6±0.58% vs. 2.9±0.4%; paired *t*-test; p=0.0451). This was also consistent with the hypothesis such that the disruption of the PDE from TnI's cellular microdomain would allow cAMP to increase to a greater level, resulting in a larger FRET change detected by CUTie-TnI.

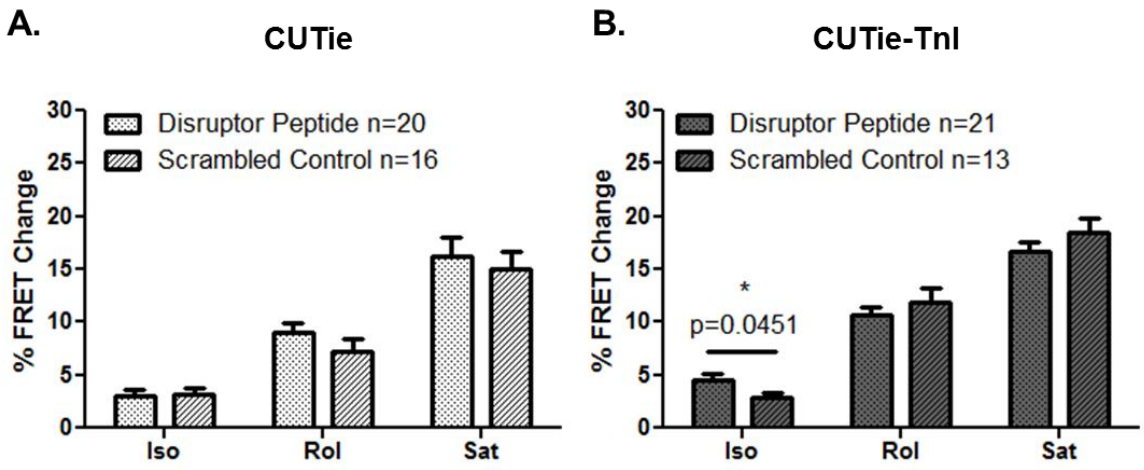

Figure 3.9: The effect of disruptor peptide treatment on FRET change in the cytosol and the myofilament. NRVM were pretreated for two hours with 10 µM disruptor peptide or scrambled control before live-cell FRET imaging as shown in Figure 3.5. A. Disruptor peptide treatment had no significant effects on FRET change in response to pharmacological stimulation in the cytosol. B. On the other hand, disruptor peptide treatment enhanced the FRET change in response to submaximal stimulation with isoproterenol in the vicinity of TnI. The FRET change in response to PDE4 inhibition with rolipram and saturation were not affected. Results represented as mean ± SEM, n=16-21. *=p<0.05, student's *t*-test.

3.4.4 Confirmation of β-adrenergic stimulation-induced increase in phosphorylation

It is well established that ß-adrenergic stimulation of NRVM results in the phosphorylation of a number of cardiac excitation-contraction proteins, including TnI. The first step in the biochemical analysis of the proposed interaction was to confirm that increased phospho-TnI levels could be detected following stimulation with various concentrations and times of isoproterenol treatment. NRVM were stimulated with 1 nM-10 µM (10 fold incremental increases) for 10 minutes. These experiments were only carried out twice due to the limited resource of primary cells isolated from animals. It was determined

that a 1 μM dose would be taken forward for time course evaluation (Figure 3.10). Additionally, similar experiments which had been completed using NRVM previously in the lab had used 1 μM treatments successfully (Edwards 2012).

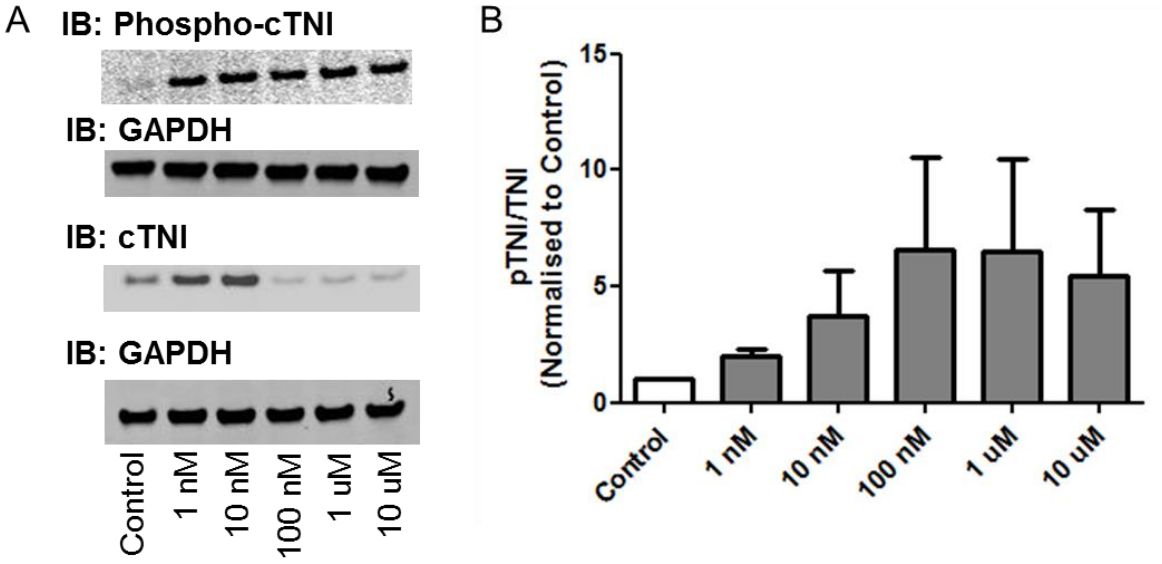

Figure 3.10: The effect of increasing doses of isoproterenol on phospho-TnI levels. NRVM were treated with 1 nM-10 μM isoproterenol for 10 minutes prior to production of cell lysates. Phospho-TnI and TnI signals were detected via immunoblotting and normalised to GAPDH before a ratio of phosphorylated:total TnI was determined. Results represented as mean ± SEM, n=2.

Having determined that a dose of 1 μM would be used in subsequent experiments, a time course was then carried out to confirm that optimal effects could be seen at 10 minutes after treatment; these were the conditions used in previous studies (Edwards 2012).

By 5 minutes, phospho-TnI appeared to reach maximal levels, which were sustained until the 20 minute time point (Figure 3.11). The levels of phospho-TnI displayed a trend toward decreasing by 60 minutes. It is important to note that these data are described as trends due to the fact that high variability between quantitation of replicates led to an absence of statistically significant differences between treatments. Nonetheless, visual observation of western blot images probed for phospho-TnI revealed consistent increases in band intensity following ß-adrenergic stimulation. These observations, coupled with previous lab protocols, resulted in the use of 1 μM 10 minute isoproterenol treatments in subsequent experiments.

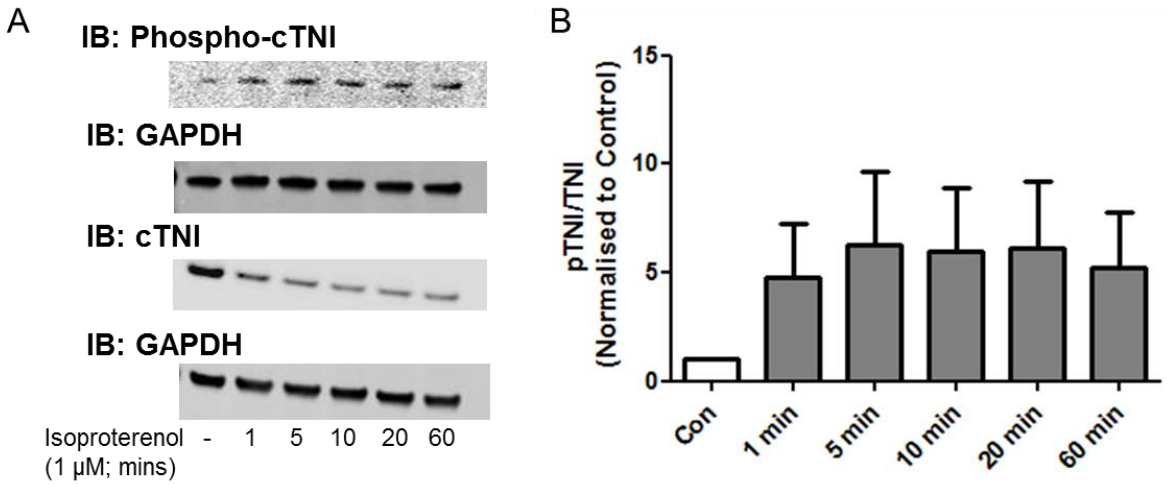

Figure 3.11: The effect of isoproterenol time course on phospho-TnI levels. NRVM were treated with 1 μM isoproterenol for 1-60 minutes prior to production of cell lysates. Phospho-TnI and TnI signals were detected via immunoblotting and normalised to GAPDH before a ratio of phosphorylated:total TnI was determined. Results represented as mean ± SEM, n=3.

3.4.5 Effects of disruptor peptide treatment on phospho-TnI levels

As previously described, FRET experiments showed that treatment with disruptor peptide, but not scrambled control, resulted in a small but significant increase in the FRET change associated with β-adrenergic stimulation at the myofilament (Figure 3.9). The next step was to determine whether this small enhancement in signalling resulted in increased phospho-TnI levels. It was hypothesised that treatment of NRVM with disruptor peptide but not scrambled control would increase phospho-TnI levels. However, contrary to this hypothesis, there were no significant increases in phosphorylation with disruptor peptide or scrambled control treatment (Figure 3.12). The lack of significance was likely due to high variability between the five experimental replicates. Although there were no significant differences, there was a trend towards increased phospho-TnI following treatment with 10 μM disruptor peptide, although the scrambled control yielded an increase of similar amplitude. Interestingly, this trend did not appear to increase with increased dose of disruptor peptide, as a ten-fold increase in dose led to a reduced phospho-TnI level compared to the lower dose.

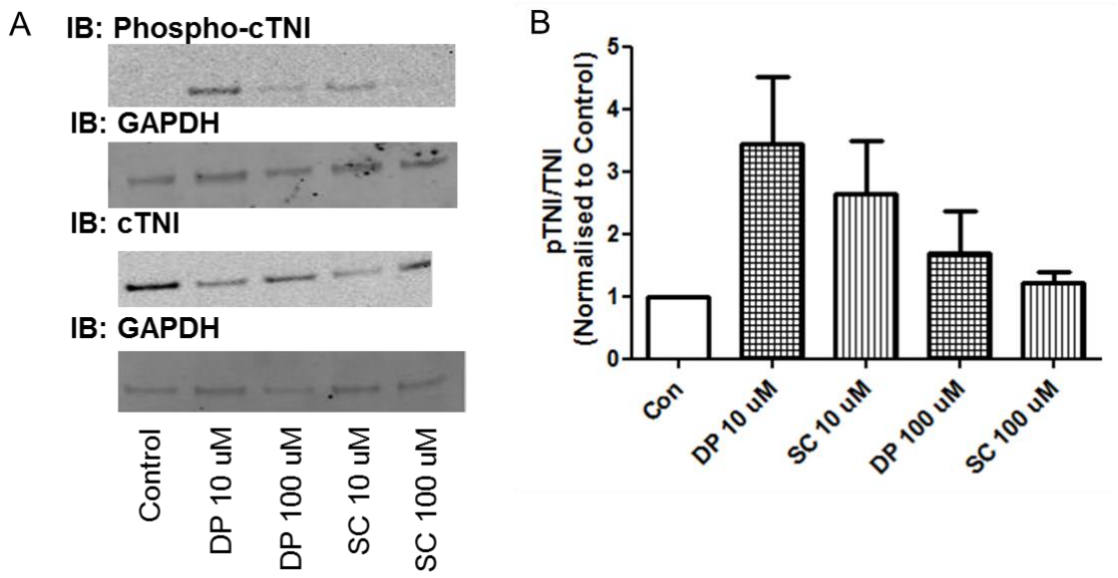

Figure 3.12: The effect disruptor peptide treatment on phosphorylation of TnI. NRVM were treated with 10 or 100 μM disruptor peptide (DP) or scrambled control (SC) for two hours prior to production of cell lysates. Phospho-TnI and TnI signals were detected via immunoblotting and normalised to GAPDH before a ratio of phosphorylated:total TnI was determined. Results represented as mean ± SEM, n=4-7.

As no significant effects of disruptor peptide treatment alone were observed, it was determined that the effects of disruptor peptide treatment would be studied in combination with ß-adrenergic stimulation. In these experiments, NRVM were pre-treated with disruptor peptide or scrambled control (10 μM, 2 hours) or PDE4 inhibitor, rolipram (10 μM, 10 min) prior to stimulation with ß-adrenergic agonist, isoproterenol (1 μM, 10 min). Similarly to other biochemical experiments reported in the present work, high variability between replicates meant that no significant differences in phosphorylation levels were observed (Figure 3.13). Additionally, there were no convincing trends that disruptor peptide treatment enhanced the ß-adrenergic induced increase in phospho-TnI. In this experiment, it is important to note that PDE4 inhibition did not significantly enhance the ß-adrenergic induced increase in phospho-TnI. This was contrary to both the hypothesis and previously reported data (Edwards 2012).

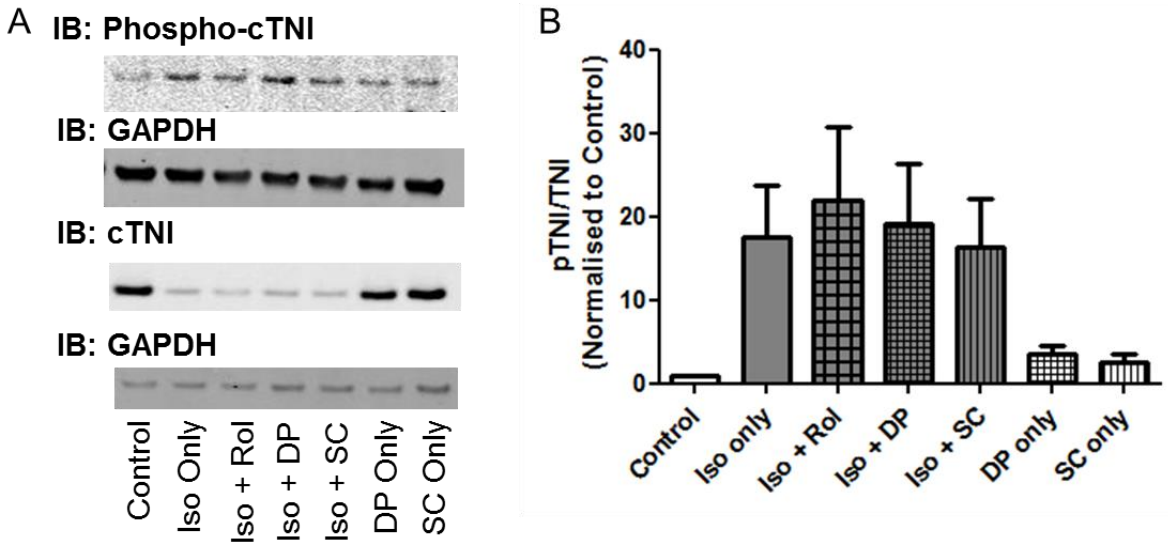

Figure 3.13: The effect disruptor peptide treatment on β-adrenergic induced phosphorylation of TnI. NRVM were pre-treated with disruptor peptide or scrambled control (10 μM, 2 hours) or PDE4 inhibitor, rolipram (10 μM, 10 min) prior to stimulation with β-adrenergic agonist, isoproterenol (1 μM, 10 min). Resulting cell lysates were immunoblotted for phospho-TnI and total TnI, which were normalised to GAPDH before a ratio of phosphorylated:total TnI was determined. Results represented as mean ± SEM, n=3.

3.4.6 PDE4D9 does not co-immunoprecipitate with TnI

Following these data that did not support the hypotheses, it was determined that the proposed interaction should be confirmed. The first step in this confirmation was to probe TnI immunoprecipitates for PDE4D9. The PDE4D9-specific antibody was developed in house. Although the majority of PDE4 sequences are conserved between isoforms, each isoform has a specific N-terminal region important for targeting to intracellular locations. These isoform-specific regions were utilised for the production of isoform-specific antibodies. Due to the availability of large quantities of cells for lysate production, HEK239 cells overexpressing TnI-Flag were used for the first immunoprecipitation experiments. These immunoprecipitations were performed in two ways: first, by immunoprecipitating TnI using an antibody and G-sepharose beads (Figure 1.14A) and second, by immunoprecipitating flag using anti-flag agarose beads (Figure 1.14B). Both protocols led to successful immunoprecipitation of TnI-Flag as shown by immunoblotting for TnI. However, when immunoprecipitates were immunoblotted using a PDE4D9 specific antibody, there was no band at the relevant weight (~94 kDa) despite clear bands in the input lysate (Figure 3.14).

Therefore, it was concluded that PDE4D9 did not co-immunoprecipitate with TnI in HEK239 cells.

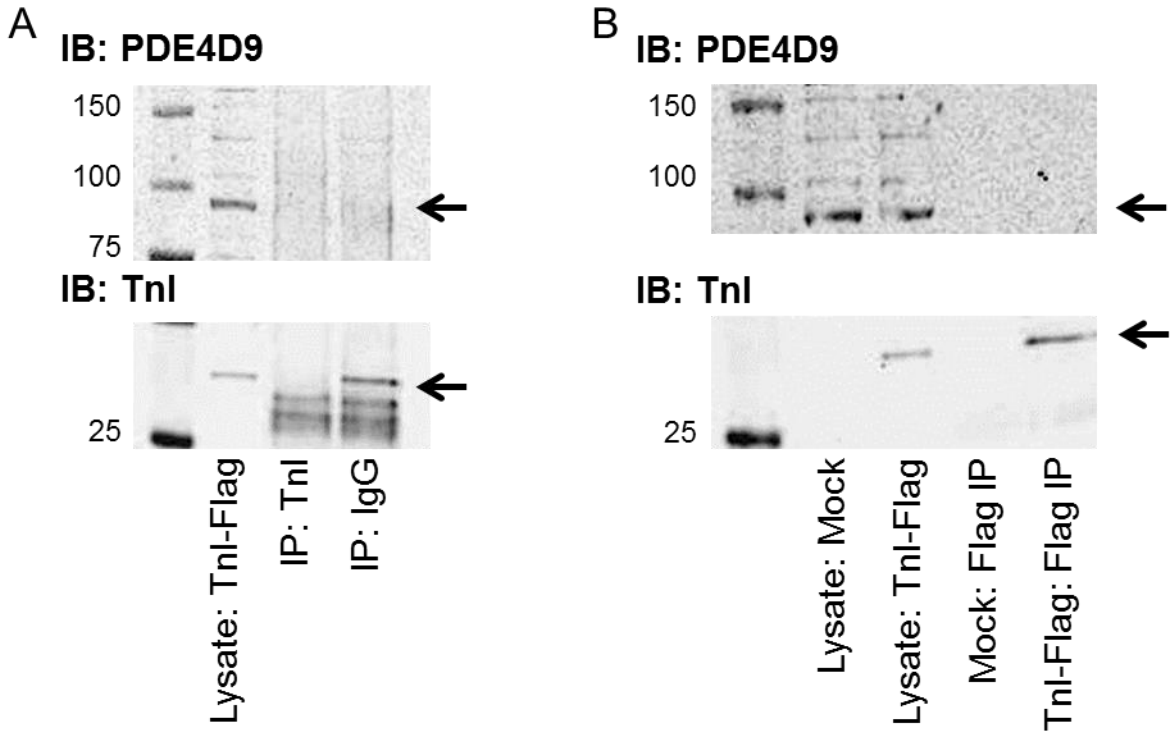

Figure 3.14: Endogenous PDE4D9 does not co-immunoprecipitate with overexpressed TnI-Flag in HEK-293 cells. HEK239 cells transiently transfected to overexpress TnI-Flag were used for immunoprecipitations. A. TnI was immunoprecipitated using G-sepharose beads and TnI specific antibody. Immunoprecipitates were probed for PDE4D9. Although TnI was clearly detected in immunoprecipitations, PDE4D9 did not co-immunoprecipitate. Representative of n=3 experiments. B. HEK-293 lysates were also subjected to immunoprecipitation with flag beads, using un-transfected lysate as a control. Again, although TnI-Flag was clearly pulled down by flag beads, PDE4D9 was not present in the immunoprecipitates. Representative of n=3 experiments.

Due to the fact that HEK239 cells are not representative of the complexity of ventricular myocytes, co-immunoprecipitation experiments were repeated using lysate from NRVM. In this case, TrueBlot® beads were used to ensure that successful immunoprecipitation of TnI could be visualised via immunoblotting. These beads were used combination with TrueBlot® mononclonal secondary antibodies for detection, which have the unique ability to recognise only native, non-reduced forms of IgG. Therefore, there is less interference of the heavy (55 kDa) and light (25 kDa) band on immunoblots. This was relevant for these experiments as TnI is often disguised by heavy staining of IgG light chains. The use of this technique allowed clear immunoprecipitation of TnI to be visualised. Despite clear success of TnI immunoprecipitation, there was no evidence of

PDE4D9 in immunoprecipitates (Figure 3.15). It is important to note that the PDE4D9 band at ~95 kDa was very faint and difficult to detect even in the lysate sample. This made it difficult to draw conclusions from the NRVM immunoprecipitations alone. Taken together with the immunoprecipitations performed using HEK-293 lysate overexpressing TnI-Flag, it was clear that PDE4D9 does not co-immunoprecipitate with TnI.

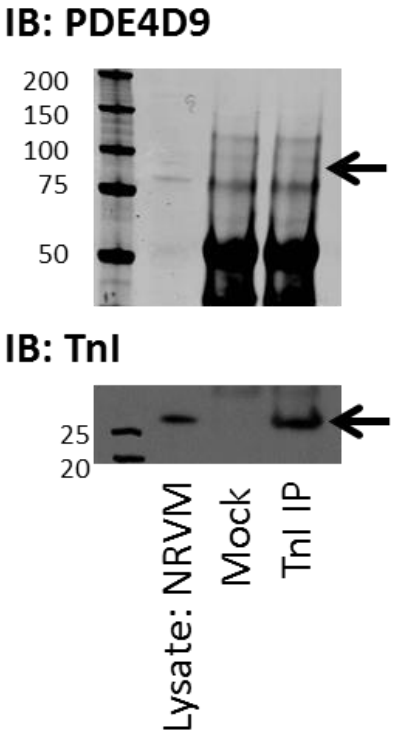

Figure 3.15: Endogenous PDE4D9 does not co-immunoprecipitate with endogenous TnI in NRVM. TrueBlot® beads were used to immunoprecipitate TnI from NRVM lysate. The immunoprecipitates were immunoblotted for PDE4D9. Despite clear immunoprecipitation of TnI, there was no evidence of PDE4D9 in immunoprecipitates. Representative of n=3 experiments.

3.4.7 Widening the search: Testing for interactions with other PDE isoforms

The data showing that PDE4D9 did not co-immunoprecipitate with TnI was in direct contrast to the original data set, which was what prompted initiation of the current research project. Therefore, it was determined that the next step would be to re-evaluate the proposed interaction and test for interactions with other PDE isoforms. As PDE3 and PDE4 are the most widely expressed cAMP-hydrolysing PDE isoforms in the heart, and other cardiac excitation-contraction

coupling proteins have been shown to interact with PDE3 or PDE4 isoforms, these PDE families were prioritised (Maurice, Ke et al. 2014).

First, TnI was immunoprecipitated from NRVM lysates. Immunoprecipitates were immunoblotted using PDE4 subfamily specific antibodies. Despite clear immunoprecipitation of TnI, neither PDE4A, 4B nor 4D family members co-immunoprecipitated (Figure 3.16).

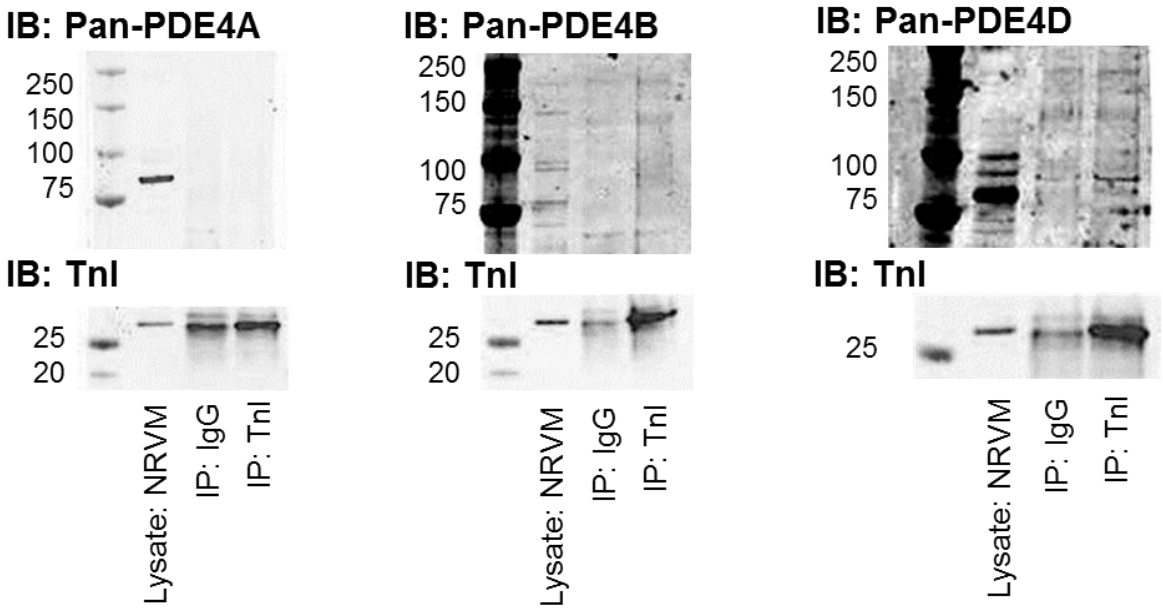

Figure 3.16: PDE4 subfamilies do not co-immunoprecipitate with TnI. G-sepharose beads were used to immunoprecipitate TnI from NRVM lysate. The immunoprecipitates were immunoblotted for the indicated PDE. Despite clear immunoprecipitation of TnI, there was no evidence of PDE4D9 in immunoprecipitates. Representative of n=3 experiments.

The next step was to widen the search to PDE families. NRVM were treated with PDE3 or PDE4 family-specific inhibitors, cilostamide and rolipram respectively, prior to challenge with ß-adrenergic stimulation (Figure 3.17). Similarly to previous analyses of phospho-TnI levels in NRVM, there was significant variation between experimental replicates, leading to a lack of specific differences between conditions. Therefore, minimal conclusions could be drawn based on the data compiled. There were trends in the data showing increased phosphorylation of TnI following PDE4 inhibition, which was enhanced when used in combination with ß-adrenergic stimulation. However, the inhibition of PDE3 and PDE4 together appeared to have an additive effect at baseline, but not in

conditions of ß-adrenergic stimulation. Again, these are reported as trends in the data only, as no significant differences were measured.

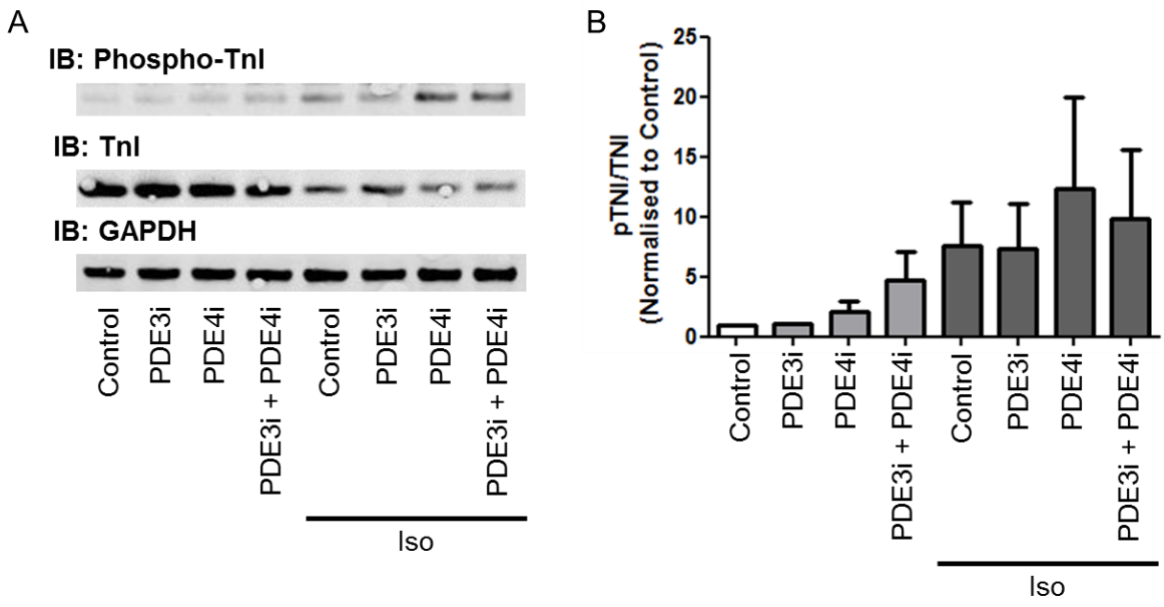

Figure 3.17: The effect PDE family-specific inhibitors on β-adrenergic induced phosphorylation of TnI. NRVM were pre-treated with PDE3 or PDE4 inhibitor, rolipram (10 μM, 10 min) prior to stimulation with β-adrenergic agonist, isoproterenol (1 μM, 10 min). Resulting cell lysates were immunoblotted for phospho-TnI and total TnI, which were normalised to GAPDH before a ratio of phosphorylated:total TnI was determined. Results represented as mean ± SEM, n=4.

Finally, TnI immunoprecipitations were subjected to analysis via PDE assay and by mass spectroscopy. PDE assays would determine whether any cAMP-hydrolysing PDE activity was associated with TnI, while mass spectrometry would determine whether any PDE isoforms could be detected in TnI immunoprecipitates regardless of PDE activity.

Immunoprecipitations were performed as previously described, pulling down endogenous TnI from NRVM lysates. IgG immunoprecipitations were included as a control. Immunoprecipitates were subjected to analysis by PDE assay as described in Section 2.13.1. The level of PDE activity detected in TnI immunoprecipitates was negligible (Figure 3.18). Although this was contrary to the hypothesis that a PDE interacts directly with TnI, it was consistent with data from immunoblots, showing that PDE4 isoforms could not be detected in TnI immunoprecipitates.

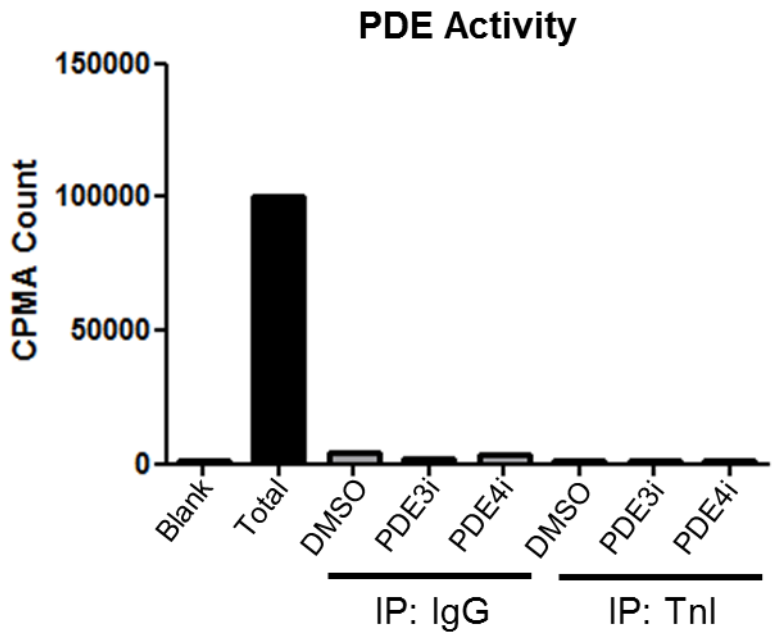

Figure 3.18: Radiolabelled PDE assay to determine PDE activity associated with TnI. The activity of PDEs in TnI immunoprecipitates was analysed by hydrolysis of an 8-[H_3]-labelled cAMP substrate as described in Section 1.13.1. Although PDE activity in pmol cAMP/min can be determined using this assay, raw CPMA counts are displayed here as they were determined to be the best representation of the data. The PDE activity in TnI immunoprecipitates is no different than mock immunoprecipitates or a blank sample control. Only one experimental replicate was carried out.

In preparation for proteomic analysis, immunopreciptates were run on gels, which were coomassie stained to visualise protein. By approximating protein weights according to the molecular weight markers, gel slices from ~50-150 kDa were excised and sent for analysis by Glasgow Polyomics. Most PDE isoforms lie within this size range. No PDE isoforms were detected by mass spectrometry in TnI immunoprecipitates. Unfortunately, because only gel slices encompassing specific weights were supplied for analysis, it was not possible to determine whether TnI was effectively immunoprecipitated in the samples sent for proteomic analysis. Inclusion of lower molecular weight gel slices to validate TnI immunoprecipitation was not deemed necessary due to consistent immunoprecipitation in experiments analysed via immunoblotting. However, unsuccessful immunoprecipitation of TnI or unsuccessful pulling down of interacting proteins cannot be ruled out in this experiment.

It is important to note that PDE assay and proteomic analysis of TnI immunoprecipitates were only carried out with one experimental replicate for each experiment. This was due to both the cost of carrying out the protocols and

the consistency with previous results showing a lack of PDE isoforms co-immunoprecipitating with TnI. It was at this point in the data collection that it was determined to take another direction and investigate other aspects of TnI post-translational modifications which will be described in the next two chapters.

3.4.8 Phospho-TnI was reduced in human diseased myocardium

To confirm that phospho-Ser 23/24 levels were altered in human disease, human samples from healthy and diseased patients were immunoblotted for phospho-TnI and total TnI. Confirmation of reduced phospho-TnI in disease would show consistency with published data showing this trend (Bodor, Oakeley et al. 1997). The human heart tissue samples were kindly gifted from Professor Kenneth Campbell (University of Kentucky Biobank, USA). Samples were taken from healthy hearts from organ donors or diseased hearts at the time of transplant (Blair, Haynes et al. 2016). Diseased hearts were from patients diagnosed with ischaemic heart failure, although the primary diagnosis was somewhat variable between ischaemic cardiomyopathy, ishchaemic heart failure and chronic systolic heart failure. The diseased group was considered together for comparisons. Tissue lysates were immunoblotted for phospho-TnI, TnI and GAPDH. This study was blinded until quantitative analysis was completed. Relevant characteristics of each sample are shown in Table 3.1. Consistent with the previous studies, there was a significantly reduced level of phospho-Ser23/24 TnI in diseased myocardium while the total levels of TnI were consistent between healthy and diseased samples (Figure 3.19).

Table 3.1 Characteristics of human heart samples.

Sample No.	Case Type	Heart Failure	Primary Diagnosis
1	Organ donor		
2	Organ donor		
3	Organ donor		
4	Organ donor		
5	Organ donor		
6	Organ donor		
7	Organ donor		
8	Heart transplant	Ischaemic	Ischaemic cardiomyopathy
9	Heart transplant	Ischaemic	Ischaemic cardiomyopathy
10	Organ donor		
11	Heart transplant	Ischaemic	Ischaemic cardiomyopathy
12	Heart transplant	Ischaemic	Ischaemic cardiomyopathy
13	Organ donor		
14	Heart transplant	Ischaemic	Ischaemic cardiomyopathy
15	Heart transplant	Ischaemic	Chronic systolic heart failure
16	Heart transplant	Ischaemic	Ischaemic cardiomyopathy
17	Organ donor		
18	Organ donor		
19	Heart transplant	Ischaemic	Ischaemic cardiomyopathy
20	Heart transplant	Ischaemic	Ischaemic cardiomyopathy
21	Organ donor		
22	Organ donor		
23	Heart transplant	Ischaemic	Ischaemic cardiomyopathy
24	Heart transplant	Ischaemic	Ischaemic heart failure and post-MI pericarditis
25	Heart transplant	Ischaemic	Ischaemic heart failure
26	Organ donor		
27	Heart transplant	Ischaemic	Ischaemic cardiomyopathy
28	Heart transplant	Ischaemic	Ischaemic cardiomyopathy
29	Organ donor		
30	Heart transplant	Ischaemic	Ischaemic cardiomyopathy
31	Heart transplant	Ischaemic	Ischaemic cardiomyopathy
32	Heart transplant	Ischaemic	Ischaemic cardiomyopathy
33	Organ donor		
34	Heart transplant	Ischaemic	Chronic systolic heart failure
35	Organ donor		
36	Heart transplant	Ischaemic	Ischaemic cardiomyopathy
37	Organ donor		
38	Heart transplant	Ischaemic	Ischaemic heart failure
39	Organ donor		
40	Heart transplant	Ischaemic	Ischaemic heart failure
41	Organ donor		

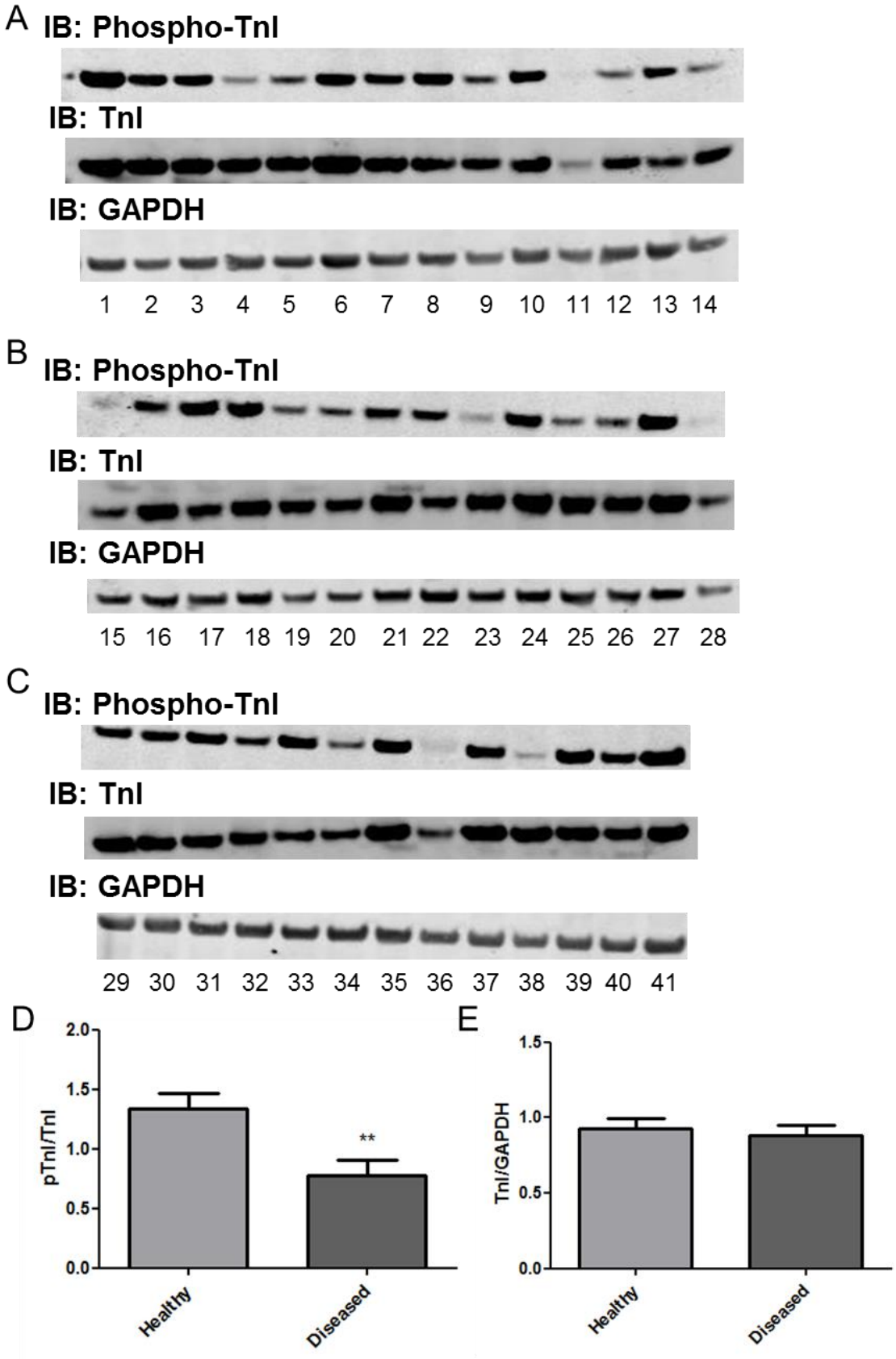

Figure 3.19: Phospho-TnI was reduced in human diseased myocardium. Human heart tissue samples were immunoblotted for phospho-Ser23/24 TnI, total TnI and GAPDH as a loading control. The blots for samples 1-14, samples 15-28 and samples 29-41 are shown in A, B and C respectively. Quantitative analysis revealed that phospho-TnI (as a ratio of total TnI) was significantly reduced in diseased myocardium while total TnI was unchanged. Data are displayed as mean ± SEM, n=20 healthy and n=21 diseased. **=p<0.01, student's *t*-test.

3.5 Discussion

3.5.1 PDE4D9 may not directly interact with TnI

The vast majority of proteins in cells exist within interactions with other proteins. The identification of a protein's 'interactome' can provide information necessary to determine the functional role of the protein within the cell. PDEs have been shown to interact with a number of cardiac excitation-contraction coupling proteins, regulating their PKA phosphorylation. Based on these findings, it is likely that a PDE interacts with TnI complex at the myofilament, thereby regulating the PKA-mediated phosphorylation of Ser23/24. This was the basis for the project undertaken by previous lab members, which identified PDE4D9 as a direct interactor of TnI (Edwards 2012).

Interestingly, the data displayed in the present work are not consistent with these previous findings. In fact, taken together, the data from the present work suggest that it is likely that PDE4D9 does not have a functional role in the regulation of cAMP dynamics at the myofilament or the phosphorylation state of TnI. Additionally, it does not support the hypothesis that there is a direct interaction between PDE4D9 and TnI.

Firstly, FRET microscopy was used to measure cAMP dynamics in the cytosol and at the myofilament under various conditions. In NRVM overexpressing dominant-negative, catalytically inactive PDE4D9, there was no change in cAMP dynamics at the myofilament. This was contrary to the hypothesis; if PDE4D9 were active in this compartment, the mutant PDE would displace the endogenous, functional enzyme, causing enhanced signalling in response to agents which raise cAMP in these cells (in this case, ß-adrenergic agonist, isoproterenol) (McCahill, McSorley et al. 2005). It was also hypothesised that the overexpression of this protein would reduce the effect of PDE4 inhibitors at the myofilament, but the response to PDE4 inhibition with rolipram was unchanged by the PDE4D9-D/N overexpression at that location. On the other hand, pre-treatment of NRVM with disruptor peptides, which was hypothesised to unhinge the interaction between PDE4D9 and TnI, caused a small but significant increase in the FRET response to isoproterenol, which was consistent with the hypothesis and previous findings. The pre-treatment had no significant effect on cytosolic cAMP dynamics,

suggesting that the disruptor peptide acted specifically at the myofilament. This data, standing alone, suggests that the interaction between PDE4D9 may exist and that the disruptor peptide unhinged PDE4D9 from the myofilament, thereby enhancing the cAMP response. This claim, however, is refuted by all other experimental data shown here. A closer look at the design of the disruptor peptide may explain this discrepancy. The disruptor peptide was designed based on data from peptide array alanine scan experiments which identified the amino acids of TnI essential for the binding of PDE4D9. These identified the dual lysine residues at positions 177 and 178 of TnI as being necessary for the interaction to occur. The disruptor peptide was then produced as the 25 amino acid sequence surrounding this proposed binding region. Therefore, it is possible that the disruptor peptide did in fact cause an enhancement of signalling by competitively interacting with a PDE isoform, thereby reducing its influence at the myofilament. Considering the other data displayed in this chapter, it seems likely that this effect was not specific to PDE4D9. However, this does provide some evidence that this site may still be relevant for the binding of a different PDE isoform.

The use of disruptor peptides to displace PDEs has been validated in numerous studies. The ubiquitous nature of the cAMP signalling pathway and the role of PDEs make it difficult to target whole protein families, due to the global effects of these drugs and the resulting “off-target” effects they cause. Therefore, the targeting of specific protein-protein interactions using disruptor peptides within the signalling paradigm results in more specific events related to protein targeting (Lee, Maurice et al. 2013). Generally speaking, if a PDE’s interaction with a PKA substrate protein is disrupted, the phosphorylation of the substrate protein is upregulated. For example, the peptide disruption of the HSP20-PDE4 complex was shown to increase phosphorylation of S16; thereby, the cardioprotective effects mediated by the phosphorylated form of HSP20 were unlocked (Sin, Edwards et al. 2011, Edwards, Scott et al. 2012). Similarly, the interaction between ß-arrestin and PDE4D5 has been disrupted using a peptide designed based on peptide array identification of the binding site (Smith, Baillie et al. 2007). Upon $ß_2$-adrenergic receptor activation, ß-arrestin-PDE4D5 is recruited to the receptor, initiating a dual desensitisation event whereby ß-arrestin inhibits the receptors interaction with the G-protein and PDE4D5

hydrolyses the cAMP produced as a result of activation (Perry, Baillie et al. 2002, Lynch, Baillie et al. 2007). PDE4D5 also functions to inhibit the PKA phosphorylation of the ß2-adrenoceptor, adding another layer to the complicated desensitisation paradigm. Disruption of the ß-arrestin-PDE4D5 complex resulted in the hyper-phosphorylation of the ß2-adrenoceptor (Smith, Baillie et al. 2007). Moving away from the cardiac signalling, this approach has also been used in the vascular endothelium. Here, cell-permeable peptides were used to disrupt the PDE4-EPAC interaction, resulting in increased EPAC activation, ultimately reducing permeability of the cells (Rampersad, Ovens et al. 2010). The use of disruptor peptides to unhinge PDEs from interacting proteins has also been used out with the cardiovascular disease area. For example, the disruption of the C-Raf-PDE8A complex in increases the phosphorylation of C-Raf, causing an inhibition of damaging phospho-ERK signalling in melanoma (Blair, Walsh et al. 2019).

Despite the enhancement of cAMP signalling at the myofilament, disruptor peptide treatment did not result in any significant enhancements in the phosphorylation of Ser23/24 of TnI. It is possible that the difference between disruptor peptide and scrambled control observed in FRET experiments was too small to be biologically significant despite its statistical significance. Otherwise, it is difficult to understand how an enhancement of cAMP dynamics in the vicinity of TnI would not translate to increased PKA phosphorylation. Investigating PKA phosphorylation of Ser23/24 in isolation is perhaps not representative of the biological situation, as both PKC and PKG have also been shown to phosphorylate TnI at this site (Noland, Raynor et al. 1989, Layland, Solaro et al. 2005). PKC in cardiac myocytes can be activated by a number of agonists including angiotensin II, endothelin-1 and phenylephrine, an α-angiotensin receptor agonist. Interestingly, PKC activation has been shown to have a number of opposing effects in cardiac myocytes due to a number of substrate proteins depending on the study conditions (Pi, Sreekumar et al. 1997, Takeishi, Chu et al. 1998, Montgomery, Wolska et al. 2002, Pi, Zhang et al. 2003, Westfall and Borton 2003). Even on TnI itself, PKC can phosphorylate three sites, Ser23/24, Ser 43/45 and Thr144, which all have different effects on myofilament dynamics (Layland, Solaro et al. 2005). PKC phosphorylation of Ser23/24 results in similar effects to PKA phosphorylation of the same site, such as reduced

myofilament Ca^{2+} sensitivity. However, phosphorylation of Ser43/45 has been shown to have opposing effects (Burkart, Sumandea et al. 2003). To complicate the understanding of functional effects of TnI phosphorylation, PKG can also phosphorylate TnI at Ser23/24, resulting in the same functional effects as other enzymatic phosphorylations at this site. PKG phosphorylation occurs 100x more slowly than PKA phosphorylation, but it is likely still physiologically relevant due to the tethering to PKC to the Tn complex by interacting with TnT (Blumenthal, Stull et al. 1978, Yuasa, Michibata et al. 1999). Therefore, as Ser23/24 phosphorylation is not solely modulated by PKA phosphorylation, it is possible that alternative signalling paradigms through other enzymes may have affected phosphorylation levels in the present study.

These observations cast doubt on the proposed PDE4D9/TnI interaction, and it was determined that the interaction should be directly interrogated using immunoprecipitations. In contrast to data from previous studies, using a variety of protocols and reagents, no PDE4D9, nor any members of the PDE4A, 4B or 4D families were present in TnI immunoprecipitates, despite clear enrichment for TnI in samples. Taking a further step away from specificity, NRVM were treated with PDE4 or PDE3 inhibitors before ß-adrenergic stimulation, and still, the roles of these enzymes in the regulation of phosphorylation levels of TnI were unclear. Finally, immunoprecipitations were subjected to analysis by mass spectrometry and PDE activity assays, and still there was no evidence for PDE isoforms in immunoprecipitates. In previous studies investigating the effects of family specific inhibition of PDEs on excitation-contraction coupling, it was shown that PDE2 and PDE3 inhibition enhanced cardiac contractility parameters under basal conditions, but that PDE4 inhibition was more effective under submaximal ß-adrenergic stimulation (Mika, Bobin et al. 2013). PDE4 inhibition had no effect on contractility parameters under basal conditions. Furthermore, PDE2 and PDE3 inhibition but not PDE4 caused small increases in TnI phosphorylation under basal conditions. Interestingly, the dual inhibition of these PDE families together caused additive effects on cardiac contractility dynamics, with the most potent effects caused by dual inhibition of PDE3 and PDE4. These studies were limited by the use of rat cardiac myocytes, and the paradigm of synergistic PDE3 and PDE4 activity was then investigated in a porcine model (Mika, Bobin et al. 2019). In humans and large mammals, PDE3 has been shown to be dominant, while PDE4

is thought to have a larger role in rodents (Osadchii 2007, Richter, Xie et al. 2011). In adult myocytes isolated from pigs, both PDE3 and PDE4 were shown to have similar effects on cAMP and contractile dynamics under basal conditions, but dual inhibition enhanced these effects, suggesting synergistic activity (Mika, Bobin et al. 2019). Under conditions of ß-adrenergic stimulation, both PDE3 and PDE4 inhibition enhanced cAMP dynamics and contractility. Unlike in rodents, in large mammals, both PDE3 and PDE4 activity is functionally relevant both at basal conditions and under ß-adrenergic stimulation (Mika, Bobin et al. 2019). This evidence may help explain the difficulty in identifying a specific PDE isoform which regulates TnI phosphorylation. If multiple PDE families have been shown to regulate phosphorylation under different biological conditions, it is possible that a number of PDE isoforms are tethered to the myofilament, regulating cAMP dynamics at this cellular compartment at different times.

It is also possible that the signalosome containing TnI and a PDE isoform is more complex than a single direct interaction between these two proteins. Signalosomes containing PDEs in cardiac myocytes often contain PKA and its substrate protein. The particulate PKA which is integrated into these complexes is often bound to specialised scaffold proteins called AKAPs (Kapiloff and Chandrasekhar 2011). In the case of some cardiac signalosomes, the specific AKAP isoform tethering PKA to its substrate has been determined. For example, the ryanodine receptor (RyR) signalosome has been shown to contain the muscle-specific AKAP (mAKAP), which allows the direct tethering of PKA to its substrate for a fine-tuned cAMP/PKA signalling response to stimuli (Ruehr, Russell et al. 2003). As previously described, PDE4D3 is another component of this signalosome. It has been shown that PDE4D3 directly associates with mAKAP, which adds further fine-tuning of signalling to the RyR microdomain (Dodge, Khouangsathiene et al. 2001). This creates a precedent in which AKAPs within cardiac excitation-contraction coupling protein signalosomes allow the tethering of not only PKA, but also PDEs to the relevant subcellular microdomain. Therefore, it is possible that a PDE isoform is integrated into a signalosome with TnI, but that the PDE may be integrated via an interaction with an AKAP protein, rather than a single, direct interaction with TnI itself. This would help to equate the very small effect in FRET experiments with the lack of effects on phospho-TnI levels. If a PDE were bound to the signalosome via multiple interactions with

different proteins, disruption of one binding site with a disruptor peptide may result in an observable effect as the PDE could remain bound via another interaction with an AKAP or other protein. Interestingly, TnT has been shown to act as a sarcomeric AKAP, anchoring PKA to the myofilament (Sumandea, Garcia-Cazarin et al. 2011). In previous studies, PKG has also been shown to be tethered to the myofilament by interacting with TnT (Yuasa, Michibata et al. 1999). Due to the tight interactions and close proximities of the three subunits of the Tn complex, it is conceivable that TnI phosphorylation is modulated by kinases and PDEs which are tethered to TnT acting as an AKAP rather than to TnI itself.

Considering the lack of PDE4D9 in TnI immunoprecipitates and the unclear effects of PDE4 inhibition on phospho-TnI levels, it is likely that PDE4D9 is not the isoform which integrates into this signalosome. Given the physiological importance of TnI phosphorylation by PKA and the prevalence of PDE isoforms which integrate into signalosomes with other PKA substrate proteins, it is likely that a PDE isoform is present in this microdomain to regulate Ser23/24 phosphorylation. The data presented here does not allow the specific isoform to be determined. For this reason, this investigation has not informed any specific directions for therapeutic intervention in this signalling cascade. However, the relevance of PKA phosphorylation of this site in human heart disease suggests that further investigation of the role of PDEs in this paradigm should be pursued. This pathophysiological relevance was confirmed in the present work, which showed that there was a reduction in phosphorylation in diseased myocardium, consistent with the majority of literature in the field (Bodor, Oakeley et al. 1997, Zakhary, Moravec et al. 1999).

3.5.2 Methodological Considerations and Future Directions

With the benefit of hindsight, it is clear that a number of technical issues limited the scope of conclusions from this project. Some of these technical issues help explain the discrepancies between data from previous projects and the present work.

In previous work, FRET was used to show that PDE4 has a predominant role in the regulation of cAMP dynamics around TnI (Edwards 2012). As previously described, this work went on to identify PDE4D9 as the isoform at work. In this

study, Epac1-camps FRET probes were employed. The tethered probe Epac1-camps-TnI was compared to a cytosolic untethered probe. The FRET ratios following treatment were then compared and statistically evaluated. The present work showed that both PDE3 and PDE4 had greater effects at the myofilament compared to the cytosol, and PDE4 had greater effects in both compartments, making it difficult to draw conclusions about the relative roles of the PDE families. In the present work, a newer generation of FRET probes was used. In 2017, Surdo and colleagues published evidence to show that utility of Epac1-camps sensors are limited by the fact that the tethering of these probes to proteins results in inconsistent maximal responses (Surdo, Berrera et al. 2017). The tethering of the probes altered their conformation in such a way that function was affected. Therefore, if the FRET changes recorded by tethered probes were to be compared to results recorded from untethered probes, the results must have been normalised to the saturated response. Interestingly, in the previous FRET data, the saturating response to IBMX (100 μM) was not different for the two sensors. Therefore, there was no normalisation of the FRET changes in response to other treatments. Still, the altered FRET sensor functionality due to the tethering of the probe could have been a confounding factor within this data. The present work, however, overcame this specific limitation by using CUTie FRET probes, which were tested extensively and shown to have similar maximal responses despite tethering to a number of proteins for intracellular targeting (Surdo, Berrera et al. 2017). Here, there was no need to normalise FRET responses to the saturating response as the saturation response was expected to be consistent regardless of the probe being used. The use of different FRET probes could provide a technical explanation for the differences between the FRET results from prior studies and the present work.

Experiments in which NRVM were treated with combinations of PDE inhibitors, disruptor peptides and ß-adrenergic agonist were also limited by a number of technical considerations. Firstly, the dose of isoproterenol used to stimulate ß-adrenergic signalling may have saturated the PKA phosphorylation sites, masking any effects of pre-treatment with disruptor peptides or PDE inhibitors. In future experiments, varied doses of isoproterenol in combination with pre-treatments should be compared. Despite trends in the data, no significant differences in the level of phospho-TnI were observed between different treatment groups. There

are a number of technical limitations that could have contributed to the large variability between experimental replicates. Unexpectedly, treatment with ß-adrenergic agonists caused a disappearance of the TnI band upon visualisation of immunoblots. This phenomenon, observed across all experiments in this study, was highly confounding, as the antibody used was consistent with previous projects in which the TnI band was consistent despite similar stimulations. One explanation for this was that the TnI antibody was detecting only unphosphorylated TnI, but not the phosphorylated protein. To take this explanation into consideration for the quantitative analysis of these results, immunoblot data was re-analysed as phospho-TnI/(phospho-TnI+TnI). The reanalysis did not affect the trends nor the absence of significant differences between treatments. It was determined that data would be displayed here with the original analyses (pTnI/TnI) to retain consistency with previous studies.

Another intrinsic reason for variability in all data shown here was the use of an outbred rat stain (Sprague-Dawley rats) for the primary cell isolation of NRVMs; previous studies, although in different fields, have reported differences between strains and substrains of these rats (Langer, Brandt et al. 2011, Brandt, Bankstahl et al. 2016). Although a single colony of eight female and two male rats were bred to produce litters for the isolations, the genetic variation intrinsic of outbred strains cannot be ignored.

The lack of PDE4 isoforms present in TnI immunoprecipitates provided the final evidence refuting the claims made from the previous study. In the previous study, immunoprecipitates were probed only for the proposed PDE binding partners, but the presence of TnI itself in the samples was not confirmed due to the similarity of its molecular weight with the IgG light chain (Edwards 2012). In the present work, despite clear confirmation of TnI immunoprecipitation, no PDE was detected in the sample by immunoblotting, PDE assay or proteomic analysis. Analysis by PDE assay and mass spectrometry were, of course, limited by the fact that the experiments were not completed more than once. However, taken together, the multiple analyses of immunoprecipitates provided convincing evidence against the existence of the proposed interaction. To increase the confidence in this finding, it would have been beneficial to test immunoprecipitates for the presence of known TnI binding partners, such as the other members of the troponin complex, TnC and TnT. This could have been

done simply by immunoblotting for these proteins or by subjecting gel slices with the relevant molecular weight areas included (TnC and TnT are 18 and 34 kDa respectively) to mass spectroscopy. This would have allowed the purity of the TnI immunoprecipitates to be determined. It is possible that immunoprecipitation resulted in purification of TnI, its interactions with binding partners having been denatured and washed away during the protocol.

3.5.3 Conclusion

In conclusion, the data displayed in this chapter suggest that PDE4D9 may not be the appropriate PDE isoform to target to alter cAMP dynamics at the myofilament or to affect PKA phosphorylation of TnI. This was inconsistent with the hypothesis, which was based on data showing that a direct interaction exists between TnI and PDE4D9 (Edwards 2012). Despite this evidence, the presence of PDE isoforms in signalosomes containing other PKA targets suggest that TnI's phosphorylation at Ser23/24 is also fine-tuned in this way. Future investigation into the components of the TnI signalosome is worthwhile, especially considering the disease relevance of this phosphorylation site. These studies should begin with a wider approach, considering any cAMP-hydrolysing PDE isoforms expressed in the relevant tissue for interaction. Synergistic effects between PDE families should be taken into account, and it should not be assumed that one PDE isoform is responsible for the regulation of this phosphorylation event under all biological conditions. Finally, it should not be assumed that only PDEs which interact directly with TnI could regulate its phosphorylation. TnT's role as a sarcomeric AKAP should be taken into account, as any PDE interacting with the Tn complex could regulate cAMP dynamics and phosphorylation events in this cellular compartment.

Chapter 4 SUMOylation of Troponin I

4.1 Introduction

Numerous human proteins have been shown to be substrates of the post-translational modification, SUMOylation. However, studies investigating SUMOylation of cardiac specific proteins are almost entirely limited to the study of the calcium handling protein, SERCA2a (Kho, Lee et al. 2011, Tilemann, Lee et al. 2013, Kho, Lee et al. 2015, Lee, Oh et al. 2016). Identification of SERCA2a as a target of SUMOylation shows, at the very least, that the necessary components of the SUMOylation cascade are present in the cytosol of cardiac myocytes. Therefore, the SUMOylation of other cardiac excitation-contraction coupling proteins is a possibility. The existence of SERCA2a SUMOylation and its role in maintaining protein stability also provides a precedent for the relevance of cardiac protein SUMOylation in cardiac pathophysiology (McMurray and Smith 2011). Upregulation of SUMOylation of SERCA2a following SUMO1 gene transfer was found to be protective against pressure overload-induced heart failure in both rodent and porcine models (Kho, Lee et al. 2011, Tilemann, Lee et al. 2013).

Post-translational modification of TnI has been shown to be important in cardiac physiology and pathophysiology. Most widely studied have been TnI's phosphorylation sites. For example, phosphorylation by PKA at Ser23/24 contributes to the inotropic and lusitropic response to ß-adrenergic stimulation. This modification has been shown to be downregulated in conditions of chronic heart disease, which may contribute to myofilament dysfunction (Bodor, Oakeley et al. 1997, Zakhary, Moravec et al. 1999, Layland, Solaro et al. 2005). Other post-translational modifications of TnI are not as well established as the phosphorylation systems. For example, TnI has been shown to be ubiquitinated in murine cardiac tissues (Witt, Granzier et al. 2005). Ubiquitinated TnI was detected in cardiac tissues via immunoblotting, and the ubiquitination was reduced in tissues from MURF-1 KO mice. MURF-1 is a RING finger protein which has ubiquitin ligase activity. This study suggested that MURF-1 and MURF-2 redundantly ubiquitinate TnI and other myofibrillar proteins but offered little information on the functional relevance of the system (Witt, Granzier et al. 2005).

4.1.1 UBC9 Fusion Directed SUMOylation

The identification of SUMOylation substrates is often hampered by the fact that SUMOylation is a transient modification that often occurs at low levels in cells (Jakobs, Koehnke et al. 2007). A significant advancement in the field was made when UBC9 fusion-directed SUMOylation (UFDS) allowed SUMOylation to be directed to a fused substrate protein. This method was first used to show the SUMOylation of overexpressed p53 and STAT1in HEK-293 cells and has since been used to identify a number of other SUMOylation targets (Jakobs, Himstedt et al. 2007, Jakobs, Koehnke et al. 2007). Prior to the use of this approach, SUMOylated p53 and STAT1 were difficult to detect, but the introduction of the UFDS approach allowed not only the detection of these modified proteins but also the identification of the functional relevance of their SUMOylation. When p53-UBC9 and STAT1-UBC9 fusion proteins were overexpressed alongside SUMO-GFP, immunoblotting for UBC9 revealed two molecular weight bands, one at the weight of the substrate-UBC9 fusion, and another, higher band which represented the susbtrate-UBC9 fusion which had been SUMOylated via binding of the overexpressed SUMO-GFP protein. The specificity of the UFDS approach was confirmed using fusion proteins in which the proposed SUMOylation motif's essential lysine residues were mutated in a site-specific manner. Mutation of the SUMOylation motif of either protein eliminated the detection of the higher molecular weight band. Finally, fusion proteins containing a mutation in the active site of UBC9, rendering the enzyme catalytically inactive, also eliminated the detection of the higher molecular weight band. Taken together, the use of these mutants confirmed that the higher molecular weight band represented substrate protein which had been SUMOylated specifically at the proposed motif by the fused UBC9, and not by endogenous UBC9. This powerful tool allows the detection of SUMOylated substrate proteins indirectly when detection is technically challenging. It is important to note that this system is not representative of the biological environment, as SUMOylation is "forced" by the UBC9 fusion. Therefore, the interpretation of data must be limited to the identification of motifs that can be SUMOylated. UFDS cannot inform whether a motif is SUMOylated *in vivo*. A schematic representation of how UFDS was used in the present study is shown in Figure 4.1.

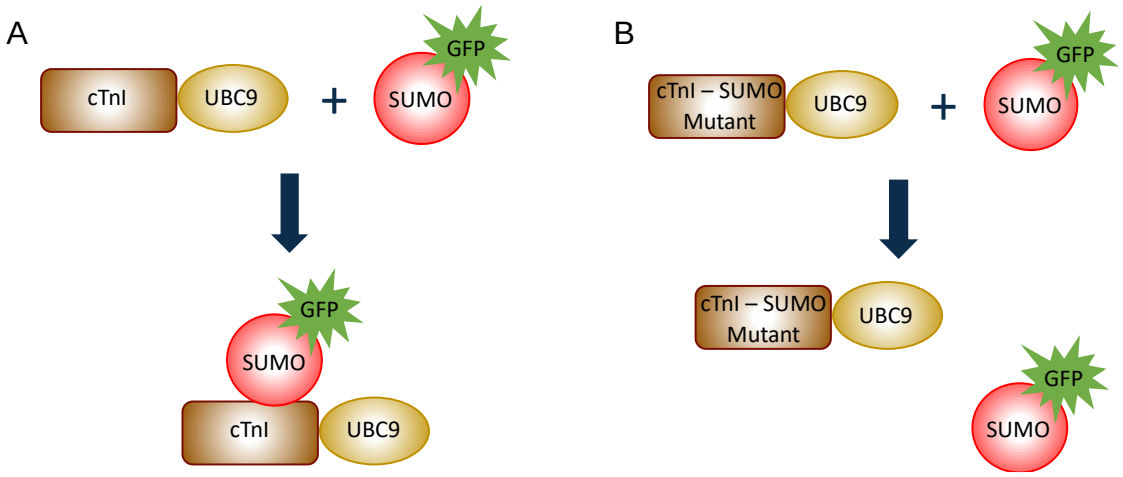

Figure 4.1: Schematic representation of UFDS of TnI. A. Co-transfection of TnI-UBC9 and SUMO-GFP into HEK-293 cells would theoretically allow the detection of SUMOylated TnI-UBC9 at the weight of the two fusion proteins added together. B. To confirm that the SUMOylation is specific to the putative SUMOylation motif, a mutation ablating the SUMO accepting lysine was introduced. In this case, the TnI-UBC9 fusion would not be SUMOylated, and the higher molecular weight band would not be detected in immunoblots. (Adapted from (Jakobs, Koehnke et al. 2007)).

4.2 Hypothesis and Aims

It has never been established whether TnI contains a SUMOylation motif to which a SUMO protein can be covalently linked. It is hypothesised that TnI can be SUMOylated at the putative SUMOylation motif, 175-178VKKE. The main aim of the experimental work in this chapter was to determine whether this motif in the TNI sequence can be SUMOylated *in vitro*. More specifically, the aims were as follows:

- To confirm that the proposed motif can be SUMOylated using peptide array
- To determine whether endogenous TnI in NRVM can be SUMOylated *in vitro* by including cell lysates in an *in vitro* SUMOylation assay
- To determine whether SUMOylated TnI can be detected by "forcing" SUMOylation using TnI-UBC9 fusion protein overexpression in HEK-293 cells
- To test a custom-made SUMO-TnI antibody's ability to selectively detect SUMOylated TnI in a variety of experimental protocols
- To establish whether the level of SUMOylated TnI is altered in cardiac disease using porcine MI samples and human heart failure samples

4.3 Results

4.3.1 Prediction of post-translational modification sites

SUMOylation of target proteins occurs via the conjugation of a SUMO protein to a lysine of a substrate within the consensus motif, ψKxD/E, where ψ is a large hydrophobic residue, K is a lysine, x is any amino acid and D/E is aspartic acid/glutamic acid (Hannoun, Greenhough et al. 2010).

To determine whether TnI contained any SUMOylation consensus motifs, the amino acid sequence of the protein was analysed for potential SUMOylation sites using SUMOplot™ software (Abgent). SUMOplot™ identifies possible SUMOylation sites and determines the probability that lysine residue within these sites might be SUMOylated based on the similarity to the classical consensus motif, ψKxE. The software allows prediction based on the identification of direct SUMO consensus motifs within the amino acid sequence as well as indirect identification of close consensus motif matches in cases where residues exhibit similar hydrophobicity patterns (Abgent, 2019).

Eight putative SUMOylation sites within the primary structure of TnI were identified by the software (Figure 4.2). One site in particular, K177, was determined to be the most likely site of SUMOylation due to the consistency of the surrounding amino acids (VKKE176-9) with the consensus motif.

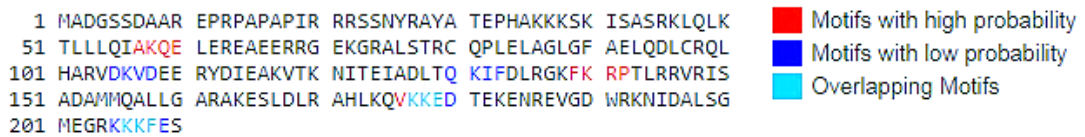

No.	Pos.	Group	Score	No.	Pos.	Group	Score
1	K177	AHLKQ **VKKE** DTEKE	0.93	5	K207	MEGRK **KKFE** S	0.48
2	K58	LLLQI **AKQE** LEREA	0.79	6	K178	HLKQV **KKED** TEKEN	0.48
3	K140	DLRGK **FKRP** TLRRV	0.74	7	K131	IADLT **QKIF** DLRGK	0.15
4	K106	LHARV **DKVD** EERYD	0.5	8	K206	GMEGR **KKKF** ES	0.13

Figure 4.2: Prediction of TnI SUMOylation sites. Human TnI primary structure (accession number P19429) was analysed using SUMOplot™ software (Abgent) to identify SUMOylation motifs. Lysine residues (K) with higher probability scores are more likely to be SUMOylated due to their location within a classical SUMOylation motif.

4.3.2 SUMO Consensus Motif required for TnI SUMOylation

The SUMOylation consensus motif with the highest probability determined by prediction software was then analysed for its ability to be SUMOylated *in vitro*. Peptide array technology in conjunction with *in vitro* SUMOylation assays (Enzo) was used to show that TnI's consensus motif (VKKE176-9) could be SUMOylated. Peptide arrays based around the 25-mer section of TnI's primary structure which included the SUMO motif were constructed. This 25-mer was progressively C-terminally truncated, N-terminally truncated, truncated from both ends and shifted by 5 amino acids. Finally, each amino acid in the SUMO motif was sequentially mutated to alanine. All of the truncations, shifts and mutated spots were subjected to *in vitro* SUMOylation using a SUMOylation Kit (Enzo). Briefly, this assay involves the incubation of a substrate protein (in this case, on a peptide array) with all of the components of the SUMOylation cascade, including E1 and E2 ligase, SUMO orthologues and Mg-ATP. An antibody only control was also performed to account for non-specific antibody binding.

Following SUMOylation of the array, positive spots detected using a primary antibody for SUMO1 were present in sequences containing the SUMO motif but were absent in any spots which did not contain the complete four amino acid SUMO motif (Figure 4.3). Such data indicates that this TNI site can be SUMOylated and that SUMOylation is specific to these amino acids. Interestingly, SUMOylation of this motif seems to depend on several of the surrounding amino acids N-terminally and C-terminally to the consensus motif. Some spots on the peptide array, which contains the SUMO consensus motif fail to be SUMOylated due to the truncation of the 25-mer close to this site.

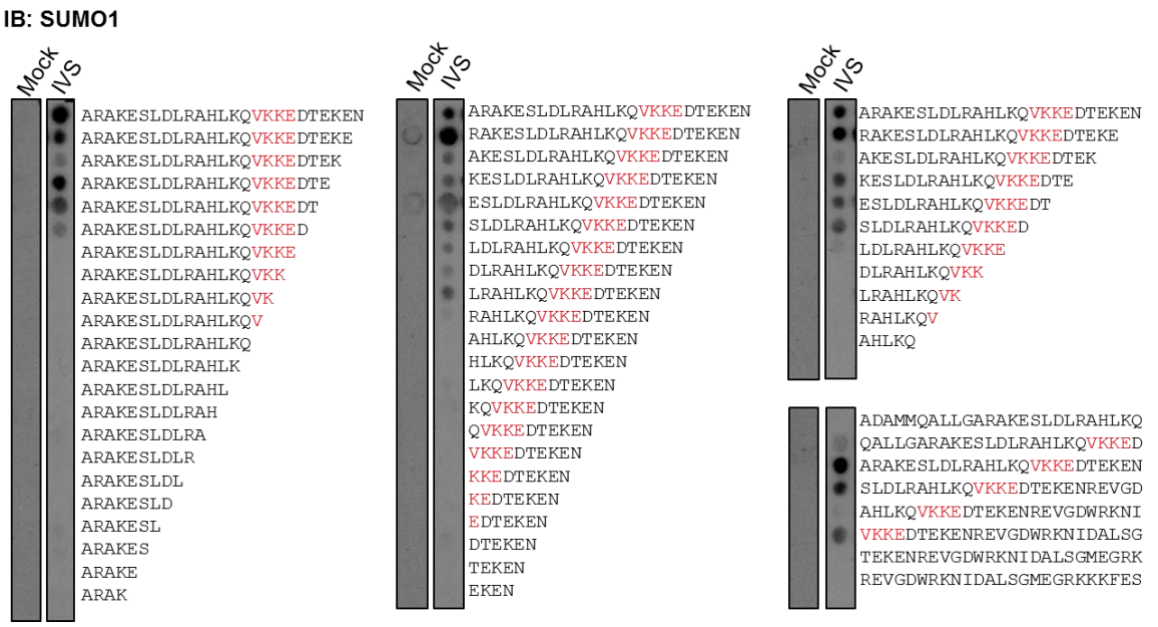

Figure 4.3: cTNI can be SUMOylated at 175-178VKKE. The 25-mer peptide sequence from which this peptide array was designed was based on the sequence of TnI containing the SUMO consensus motif. The 25-mer was sequentially N- and C-terminally truncated and shifted by 5 amino acids. The arrays were then subjected to incubation with either PBS alone (Mock) or *in vitro* SUMOylation (IVS). SUMOylation was then detected using SUMO1 primary antibody. Positive spots indicating that SUMOylation had occurred were only present for 25-mers which contained the complete 4 amino acid SUMO motif (175-8VKKE) (shown in red).

Next, an alanine scan was performed. In this peptide array experiment, each of the four amino acids in the SUMO motif was sequentially mutated to an alanine, which would allow the identification of residues essential for SUMO conjugation. The substitution of an alanine for any of the four amino acids in the motif resulted in the clear elimination of positive spots, indicating that all four amino acids were necessary for this post-translational modification to occur (Figure 4.4).

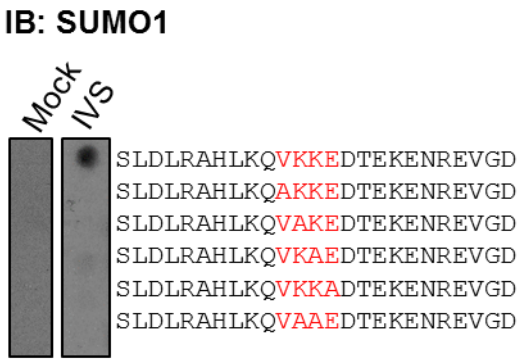

Figure 4.4: Alanine substitution of SUMO site residues eliminates SUMOylation. Peptide arrays were designed using a 25-mer sequence of TnI which included the SUMO site. Each of the four amino acids which make up the SUMO site was sequentially substituted with alanine. The arrays were subjected to *in vitro* SUMOylation (IVS) or PBS alone (Mock) and SUMOylation was detected by immunoblotting with a SUMO1 primary antibody. When the amino acids which comprise the SUMO site of TnI are serially mutated to alanine the positive spot as detected in the wild-type 25-mer is eliminated. This demonstrates that each of the amino acids in the SUMO consensus motif is necessary for SUMOylation to occur. SUMOylation site is displayed in red.

Taken together, the results from SUMOylated peptide array experiments highlight the specificity of the modification to proposed motif at 176-9VKKE. Each amino acid of the consensus motif as well as some surrounding residues must be present for the modification of the substrate protein.

4.3.3 *In vitro* SUMOylation of endogenous NRVM TnI

Although it was informative that SUMOylation could occur at the proposed motif on peptide arrays, this format is not always representative of the protein within cells because the synthetic 25-mer peptides do not have the same characteristics or secondary structure as cellular proteins. Therefore, NRVM lysates were subjected to *in vitro* SUMOylation assay (Enzo) according to manufacturer's instructions. The resulting assays were then immunoblotted for the target protein and bandshifts indicated positive results showing that the target protein had been SUMOylated. Negative control assays were also performed which excluded Mg-ATP from the reaction. Mg-ATP is essential for SUMOylation as it is a necessary cofactor for SUMO E1 ligase activity. A Rangap1 fragment (positive control) was also subjected to *in vitro* SUMOylation with and without Mg-ATP to ensure that all assay components were functional. When NRVM lysate was subjected to *in vitro* SUMOylation and immunoblotted for TnI, there was a clear bandshift, indicating SUMOylation of TnI (Figure 4.5). This

band was significantly stronger than the equivalent areas of the immunoblot image for the sample in which Mg-ATP was omitted from the reaction (p=0.0088; two sample *t*-test). To add confidence to this observation, the Rangap1 positive control assays indicated that the SUMOylation assay was working perfectly as almost all of Rangap1 existed in the modified form. Therefore, endogenous TnI from NRVM was successfully SUMOylated *in vitro*.

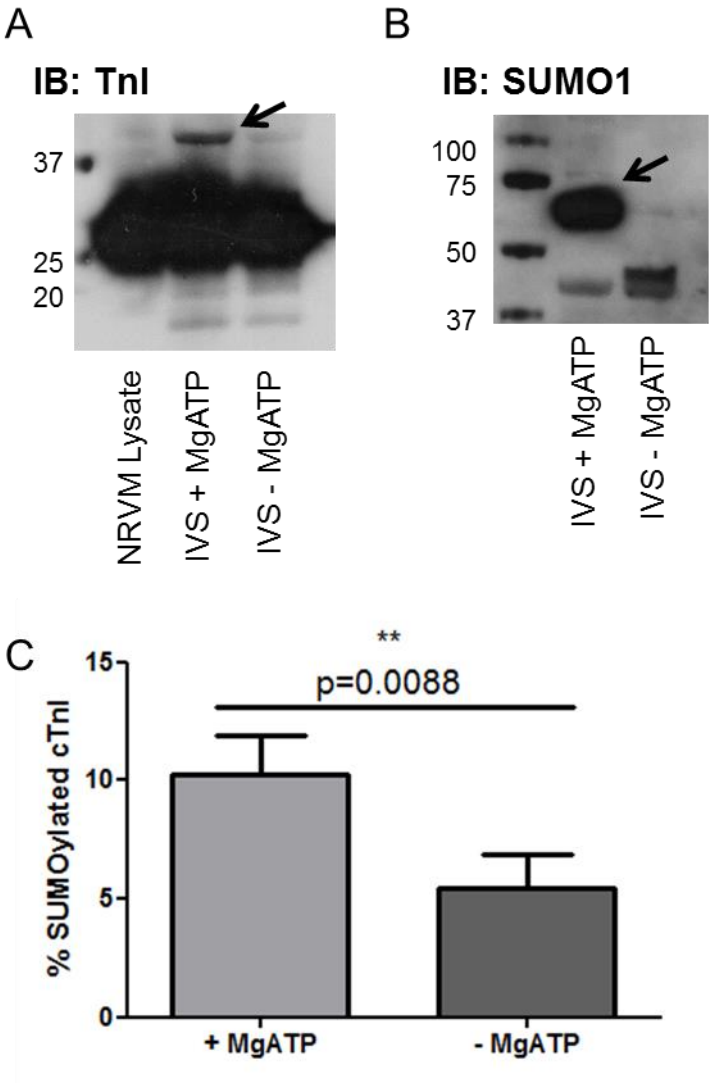

Figure 4.5: *In vitro* SUMOylation assay using NRVM lysates. A. NRVM lysate was subjected to *in vitro* SUMOylation (IVS), resulting in a clear bandshift of ~18 kDa in the sample containing all assay components, including MgATP, a cofactor of the SUMO E2 ligase which is necessary for SUMOylation to occur. When compared to the intensity of total TnI, it was determined that ~10% of total TnI was SUMOylated by this assay. This was significantly increased compared to the sample in which MgATP was omitted, although the bandshift was still visible, suggesting some basal SUMOyaltion or some residual MgATP within the sample due to the use of cell lysate instead of purified protein as per the manufacturer's instructions. B. Positive control SUMOylation assay showing SUMOylated RagGAP1, indicating that all assay components were active and functional. C. Quantitative analysis of TnI SUMOylation. Results represented as mean ± SEM, n=3. **=p<0.01, paired *t*-test.

4.3.4 UBC9 directly interacts with TnI

For a target protein to be SUMOylated, it must directly interact with UBC9, the only known SUMO E2 ligase. Therefore, peptide arrays were performed to confirm that TnI interacts with UBC9. Peptide arrays containing full length TnI were produced in which each spot represented a 25-mer segment sequentially shifted by 5 amino acid residues. These arrays were then overlaid with purified UBC9-GST or GST only as a control. The arrays were then immunoblotted for UBC9. Positive spots were detected only on arrays which were overlaid with UBC9-GST (Figure 4.6). The results from this experiment made it difficult to narrow down a specific binding site as a large portion of TnI's primary structure was observed to bind to UBC9. In fact, binding was detected on spots corresponding to residues 1-80, 125-160 and 185-210. Even though it was not possible to identify a cogent binding site using this approach, it was clear that UBC9 directly interacts with TnI, adding evidence to support the hypothesis that TnI is a SUMOylation substrate. As UBC9 binding typically occurs directly upstream or downstream of the acceptor lysine, so this data suggests that additional SUMOylation motifs, such as those identified by prediction software (Figure 4.2), may also be SUMOylated and should be investigated in future studies.

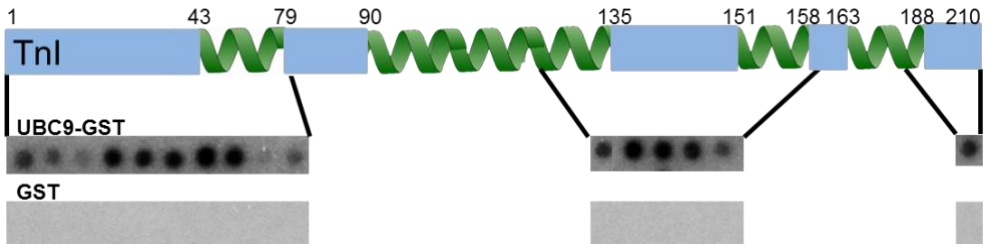

Figure 4.6: UBC9 directly interacts with TnI. Purified UBC9-GST was overlaid onto a full length TnI peptide array in which each spot contained a 25-mer peptide which was sequentially shifted by 5 amino acid residues. Positive spots were detected by immunoblotting for UBC9 on arrays incubated with UBC9-GST but not GST alone (0.2 μM), confirming a direct interaction between the two proteins. The areas of TnI in which UBC9 was shown to interact are displayed schematically here. Positive signal was detected on spots corresponding to residues 1-80, 125-160 and 185-210.

4.3.5 Co-transfection of TnI-UBC9 fusion with SUMO-GFP allows detection of SUMOylation

As previously described, the use of UBC9 fusion proteins has been used to direct SUMOylation to specific target proteins. The co-transfection of a TnI-UBC9 fusion

with SUMO-GFP in HEK-293 cells allowed the detection of a band at approximately 70 kDa (Figure 4.7). This was proposed to be a band comprised of the TnI-UBC9 fusion (predicted molecular weight: 48 kDa) and SUMO-GFP (predicted molecular weight: 36 kDa). The significantly increased presence of this band in lysates co-transfected with TnI-UBC9 and SUMO-GFP but not in lysates transfected with TnI-UBC9 or SUMO-GFP alone suggests that this band represents SUMOylated TnI (band intensity in co-transfection vs. TnI-UBC9 single transfection p=0.01; two sample *t*-test).

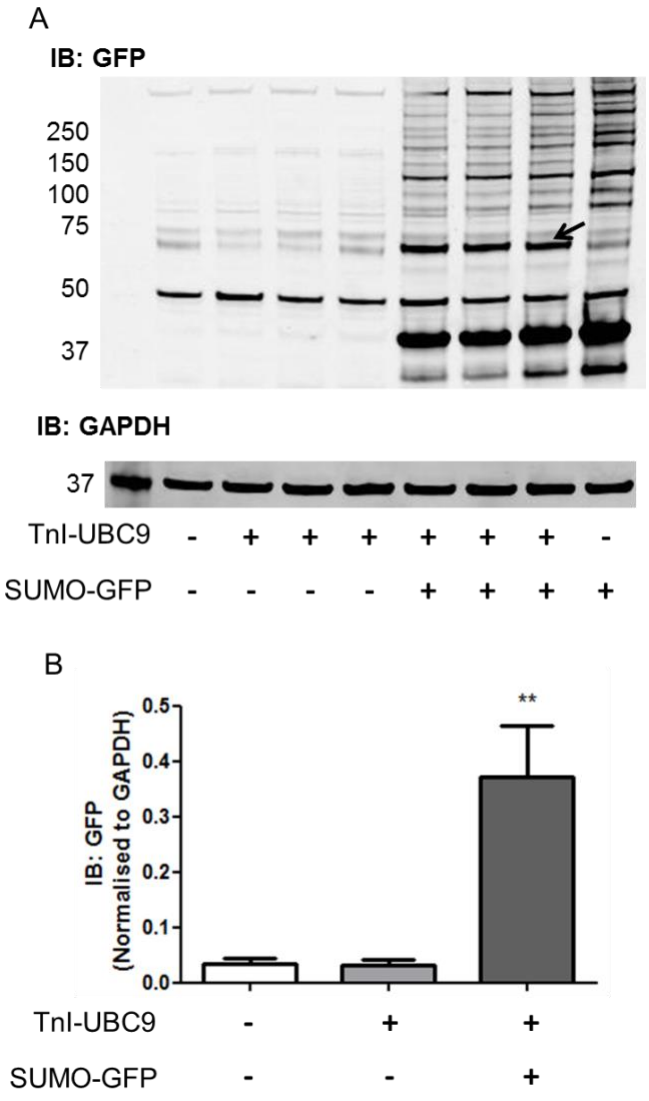

Figure 4.7: HEK-293 co-transfection with TnI-UBC9 and SUMO-GFP allows the detection of TnI SUMOylation. Single transfections and co-transfections of TnI-UBC9 and SUMO-GFP were performed in triplicate with three separate plasmid DNA preparations of TnI-UBC9. The presence of a ~70 kDa band in the co-transfection, which is absent in lysates that had been transfected with TnI-UBC9 or SUMO-GFP alone is presumed to be due to the SUMOylation of the TnI SUMO site. A quantitative comparison of the SUMOylated TnI band intensity of single transfections vs. co-transfections reveals that there is a significantly significant increase in the intensity of the band of interest in the co-transfected samples. Results represented as mean ± SEM, n=6. **=p<0.01, One-ANOVA with post hoc analysis: Tukey's multiple comparison test.

4.3.6 Mutation of the SUMOylation site eliminates detection of SUMOylation

In Figure 4.7, the band which was identified as the TnI-UBC9 fusion which had been SUMOylated by SUMO-GFP appeared at approximately 70 kDa. This was lighter than the predicted molecular weight (added together, TnI-UBC9 and SUMO-GFP should run at approximately 84 kDa). Therefore, it was necessary to include additional control experiments to ensure that this band was being identified correctly. As a negative control, a mutant TnI-UBC9 construct was produced which lacked the proposed SUMOylation site.

Using site directed mutagenesis, the SUMOylation site on TnI of the TnI-UBC9 fusion was mutated to VRRE176-9 (compared to the wildtype construct which had a sequence of VKKE176-9). It was decided that the dual lysine site would be modified to arginines to remove the potential of SUMOylation while preserving the basic charge characteristic of the amino acids. The site directed mutagenesis introduced a novel FspI restriction endonuclease site, which allowed screening of potential mutant construct containing bacterial colonies. Prediction of restriction fragments which would result from FspI digestion indicated that wildtype DNA would be broken into two fragments of 2.36 and 4.19 Kb while the mutant would results in three fragments of weights 2.02, 2.17 and 2.36. Figure 4.8 shows the presence of the expected fragments as bands on an agarose gel, showing that the site-directed mutagenesis had been successful. The successful introduction of the SUMO site mutation was confirmed by commercial sequence analysis by GATC Biotech.

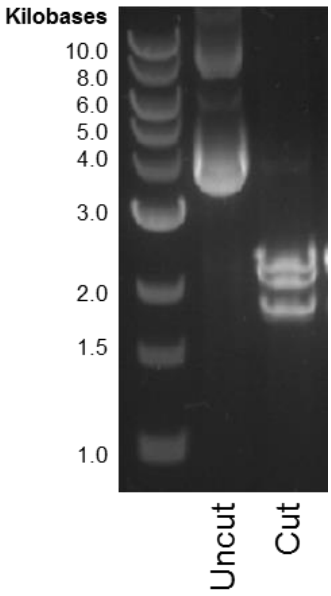

Figure 4.8: Screening of TnI-UBC9 KK176-7RR mutants using FspI restriction digest identified colony containing correct mutant. Following a restriction digest of purified plasmid DNA from bacterial colonies, uncut DNA and restricted DNA (cut) were run on a 1% agarose gel containing SYBR safe (1:10,000) for UV visualisation. The restricted sample in lane 3 resulted in the expected bands, indicating the presence of an extra FspI site which had been introduced by the mutation.

Co-transfection experiments in HEK-293 cells were then repeated using the TnI-UBC9 KK176-7RR construct. When the construct lacking the SUMOylation site was transfected with SUMO-GFP, there was a significant reduction in the intensity of this band as shown in Figure 4.9 (band intensity in WT co-transfection vs. KK176-7RR co-transfection p=0.009; two sample *t*-test). The elimination of the band of interest confirmed that the ~70 kDa band was specific to SUMOylated TnI and that the presence of the SUMOylation motif in TnI was necessary for the SUMOylation to occur.

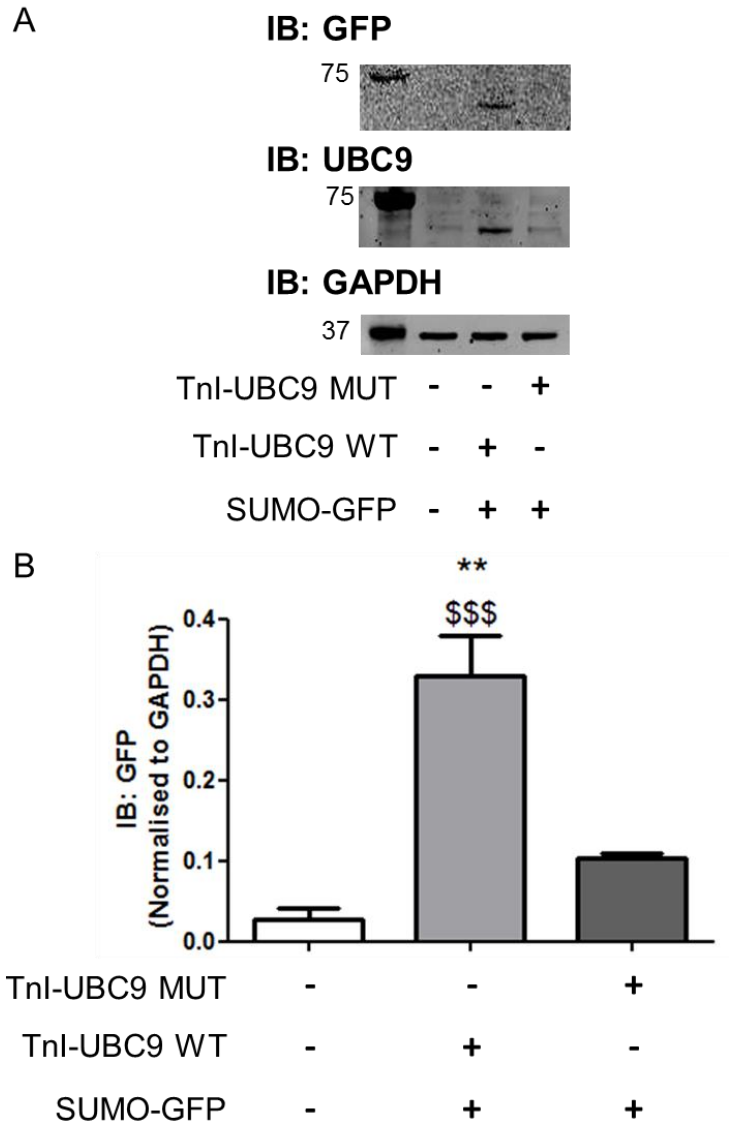

Figure 4.9: HEK-293 co-transfection with TnI-UBC9 KK176-7RR and SUMO-GFP eliminated SUMOylated TnI band. HEK-293 cells were co transfected with either TnI-UBC9 KK176-7RR (MUT) or TnI-UBC9 WT and SUMO-GFP. Mutation of the SUMOylation site resulted in the elimination of the ~70 kDa band in the co-transfected samples, which was present in the WT co-transfection via immunoblotting for GFP or UBC9. Results represented as mean ± SEM, n=4. **=p<0.01 vs. TnI-UBC9 Mut + SUMO-GFP, $$$=p<0.001 vs. Mock, One-ANOVA with post hoc analysis: Tukey's multiple comparison test.

Furthermore, as shown in Figure 4.9, the band representing SUMOylated TnI was detected by immunoblotting for both GFP and UBC9, which provided evidence that components of each of the fusion constructs were present in this band. TnI primary antibodies were also used for immunoblotting, but detection was unsuccessful. It is important to note that detection of the TnI-UBC9 construct in single transfected lysates produced only a very faint band at the expected weight, especially when compared to the very bright band detected in lysates

overexpressing TnI-Myc-DDK or simply in untransfected NRVM lysates (showing endogenous TnI). Therefore, it was determined that the inability to detect the 70 kDa band with TnI primary antibodies was probably due to the UBC9 fusion hindering the antibody binding to its antigen.

The clear detection of the TnI-UBC9/SUMO-GFP band by immunoblotting for both GFP and UBC9 and the elimination of the band when the SUMO site was mutated were compelling evidence to show that a viable SUMOylation consensus motif exists on TNI and that it can be SUMOylated in cells. This was highly consistent with peptide array data (Figure 4.3 and Figure 4.4), which identified the SUMOylation site and showed that all four amino acid residues are necessary for SUMOylation to occur.

4.3.7 SUMOylation of TnI is not cAMP-dependent

In an effort to determine whether the SUMOylation of TnI and the phosphorylation of TnI were related in any way, HEK-293 cells which were co-transfected with TnI-UBC9 and SUMO-GFP were treated with high doses of Fsk and IBMX (25 µM and 100 µM, respectively) to cause a large increase in cAMP in the cells. The level of SUMOylated TnI in these cells was unchanged by the treatment (Figure 4.10) (two sample *t*-test, p=0.79). The levels of phosphorylated TnI were unable to be determined in these samples due to technical difficulties in the detection of the TnI-UBC9 fusion using phospho-Ser23/24 TnI specific antibodies.

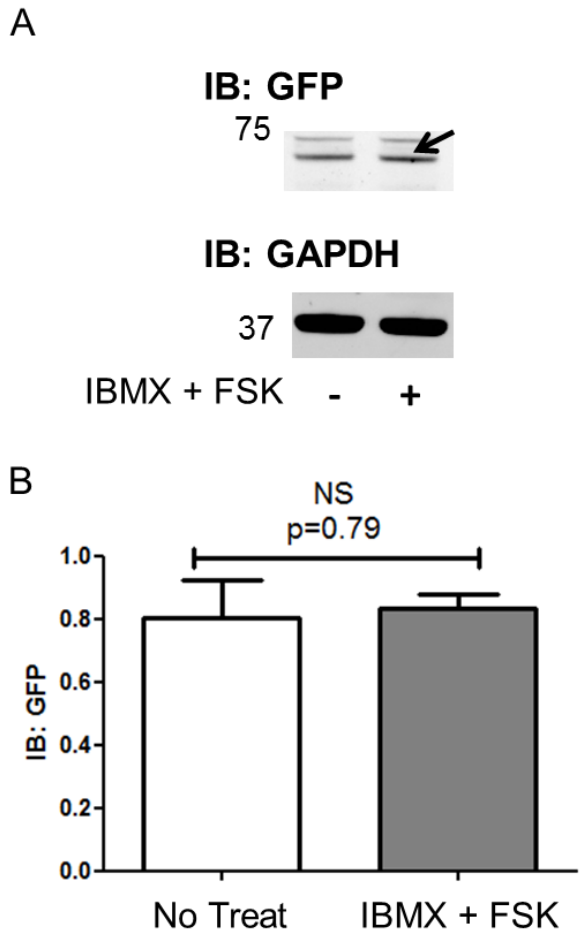

Figure 4.10: Increasing the concentration of cAMP in co-transfected cells did not affect SUMOylation of TnI. HEK-293 cells which were co-transfected with TnI-UBC9 and SUMO-GFP were treated with 25 µM Fsk and 100 µM IBMX to increase intracellular cAMP for 10 minutes prior to preparation of cell lysates. Increasing cAMP did not alter the levels of SUMOylated TnI as detected by immunoblotting for GFP. Results represented as mean ± SEM, n=4. NS=p>0.05, paired *t*-test.

4.3.8 SUMO-TnI Custom detects SUMOylated TnI

Previously in our lab, an antibody was designed to recognise an epitope representing SUMOylated TnI (Figure 4.11). This custom antibody was produced in rabbits by a commercial collaborator, Badrilla.

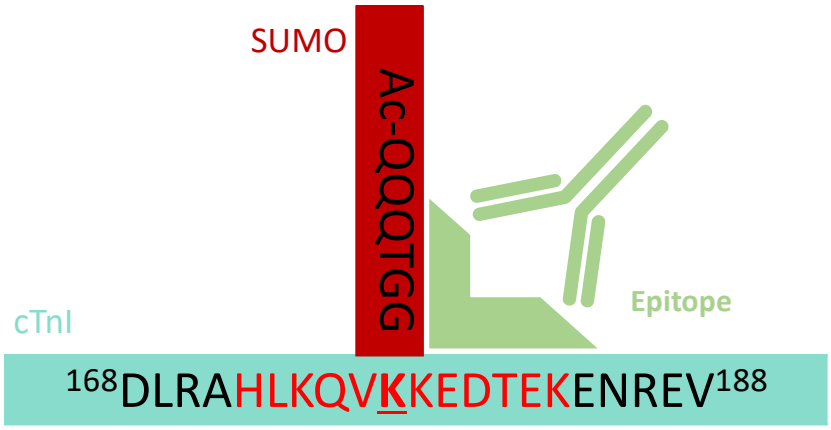

Figure 4.11: Schematic representation of SUMO-TnI antibody and its specificity. Custom SUMO-TnI antibodies were raised against the 12 amino acid segment of TnI highlighted in red combined with SUMO1. This design led to specific detection of SUMOylated TnI but not unmodified TnI or other SUMOylated targets.

Peptide arrays were used to determine whether the antibody was able to recognise the SUMOylated epitope without recognising the unSUMOylated epitope. Therefore, a peptide array was designed to include the antibody's epitope. The array was then subjected to *in vitro* SUMOylation and immunoblotted with the custom SUMO-TnI antibody. Prior to immunoblotting, SUMO-TnI antibody was incubated with a blocking peptide, which had the same sequence as the unSUMOylated epitope to reduce non-specific binding. Figure 4.12 shows that the antibody was successful in the detection of the SUMOylated epitope without recognising the SUMOylation motif on the unSUMOylated control peptide array. It is necessary to note that the sequences surrounding the epitopes are random amino acid sequences, due to the incorrect spotting of this array because of software issues. Nonetheless, when the epitope was present in spots which had been subjected to *in vitro* SUMOylation, there was successful detection by the SUMO-TnI antibody.

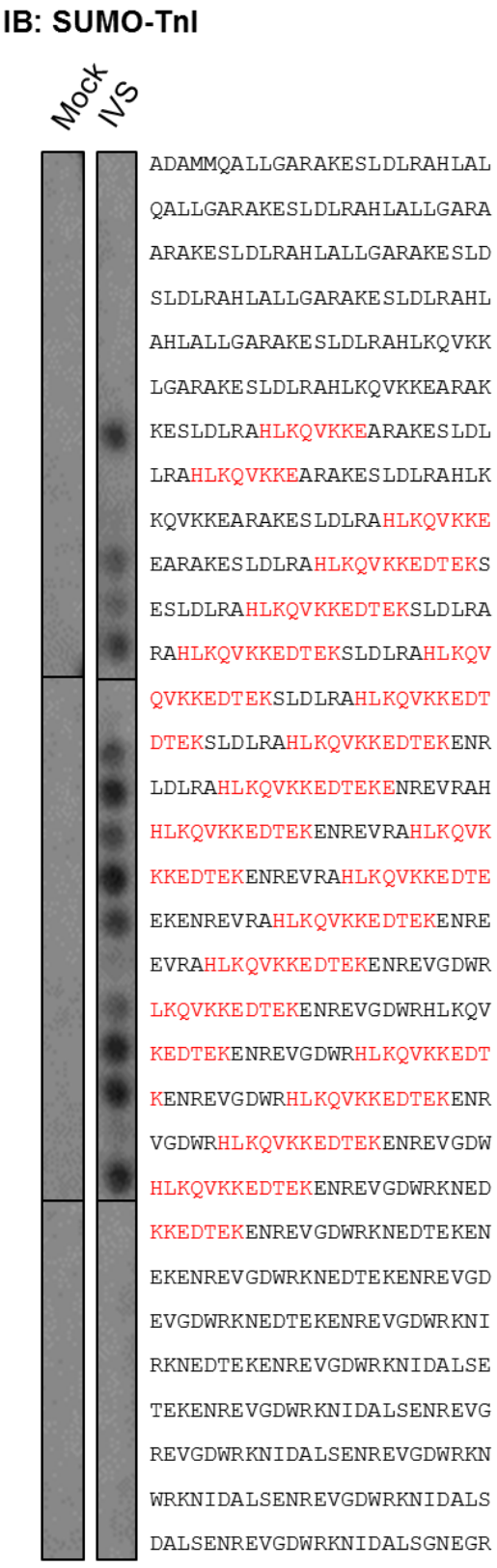

Figure 4.12: SUMO-TnI custom antibody recognises SUMOylated TnI but not un-SUMOylated epitope. 25-mer peptides containing the SUMO-TnI antibody epitope were spotted onto glass slides, subjected to *in vitro* SUMOylation (IVS) or PBS alone (Mock) and immunoblotted for SUMO-TnI. Dark spots, which are present only on the SUMOylated array, indicate antibody binding. Positive spots appear only when the epitope is present and the slide has been subjected to *in vitro* SUMOylation. The epitope recognised by the SUMO-TnI antibody is highlighted in red.

Although incorrect spotting of the previous peptide array led to limitations in the way the data could be interpreted, the results were consistent with previous experiments from former members of the lab. When an appropriately spotted peptide array with the same sequence pattern as the peptide array in Figure 4.3 was subjected to *in vitro* SUMOylation and immunoblotted for SUMO-TnI with the custom antibody, positive spots were present only when the epitope was present (Figure 4.13). Furthermore, there was no evidence of non-specific binding to the un-SUMOylated array (Mock), confirming that the epitope alone, without the attached SUMO protein, was not sufficient for antibody binding.

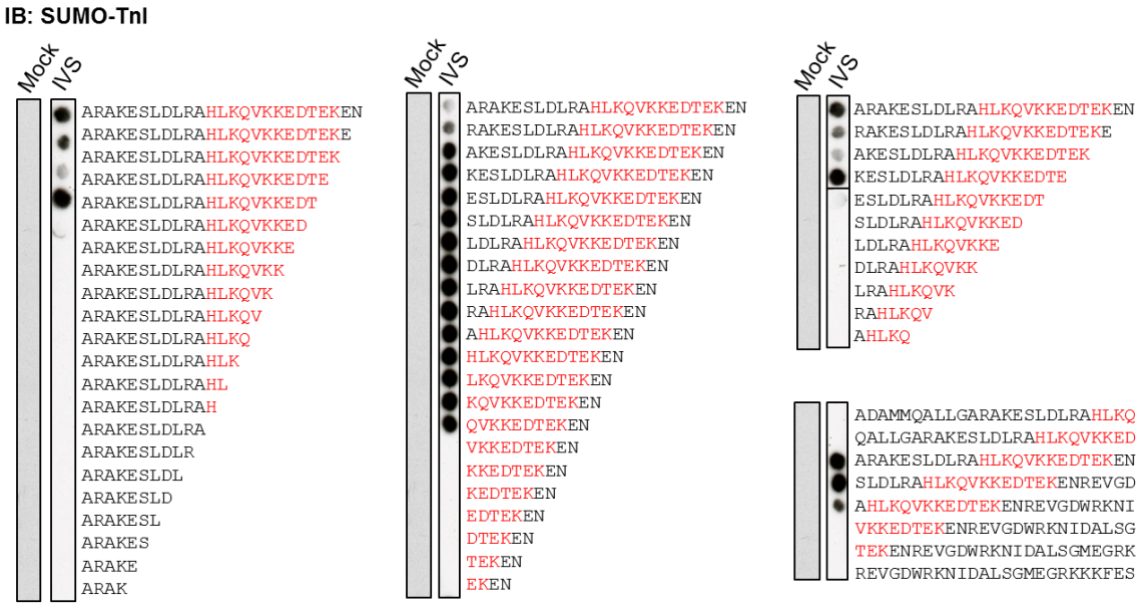

Figure 4.13: SUMO-TnI custom antibody recognises SUMOylated epitope within TnI sequence. Peptides containing the SUMO-TnI antibody epitope were spotted onto membranes, subjected to *in vitro* SUMOylation (IVS) or PBS alone (Mock) and immunoblotted for SUMO-TnI. Dark spots, which are present only on the SUMOylated array, indicate antibody binding. Positive spots appear only when the epitope is present and the slide has been SUMOylated. The epitope recognised by the SUMO-TnI antibody is highlighted in red. This work was performed by Dr. Kirsten Munro, University of Glasgow, UK.

Although peptide arrays confirmed that the SUMOylated epitope was specifically identified by the custom SUMO-TNI antibody, it was necessary to test the SUMO-TnI antibody in other applications. Peptide array experiments are limited by the fact that immobilised peptides do not replicate the biological secondary or tertiary structures of the protein. Therefore, the next step was to test the SUMO-TnI antibody's ability to detect SUMOylated TnI using another technique, western blotting.

To test the functional effect of TnI SUMOylation, an adenovirus for the overexpression of a TnI-HA mutant without the SUMO consensus motif (KK177-8RR) was produced. An un-mutated virus, TnI-HA WT, was used as a control. Functional utilising viral overexpression of mutant TnI is displayed in Chapter 5. However, the viruses were also used to validate then specificity of the SUMO-TnI antibody. Lysates from HEK-293 cells overexpressing TnI-HA MUT and TnI-HA WT were immunoblotted using the antibody, which had been pre-incubated with blocking peptide (1 μM). The resulting image revealed a band at ~75 kDa which was specific to the TnI-HA WT sample, suggesting that this band was representative of SUMOylated TnI (Figure 4.14). The larger shift from the unmodified weight of TnI (26 kDa) was likely due to poly-SUMOylation. Each SUMO2 and SUMO3 paralogue contains a SUMOylation motif, allowing polySUMOylation to occur (Kroetz 2005, Ulrich 2009). It is important to note that there were a number of nonspecific bands detected by the antibody. UnSUMOylated TnI-HA was still detected (~30 kDa) despite incubation with blocking peptide.

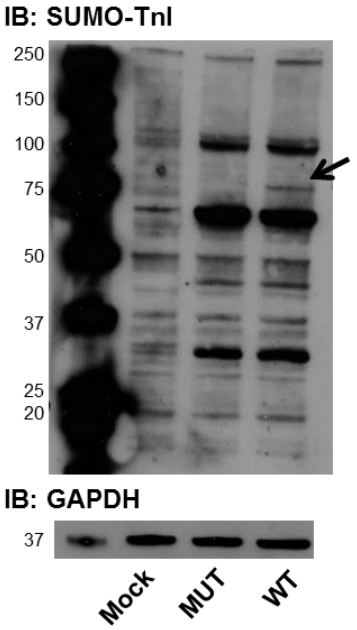

Figure 4.14: SUMO-TnI antiody detects SUMOylated TnI in cell lysate. HEK-293 lysates overexpressing viral TnI-HA MUT or WT were immunoblotted with SUMO-TnI. A band at ~75 kDa (indicated by the arrow) was present in only the TnI-HA WT lane but not in mock or MUT samples.

Taken together, these data show that the custom SUMO-TnI antibody could successfully detected SUMOylated TnI.

4.3.9 SUMOylated TnI is increased in porcine and human heart disease

Following the successful testing of the custom SUMO-TnI primary antibody and the identification of the correct band of interest, the antibody was used to measure levels of modified TnI in biologically relevant samples.

Firstly, levels of SUMOylated TnI were measured in porcine cardiac tissue samples which were kindly gifted from Dr. Roger Hajjar (New York, USA). Porcine hearts are often used as a model to study heart disease due to their anatomical similarities to human hearts, making them a better model in many ways than rodents (Lelovas, Kostomitsopoulos et al. 2014). Pigs were subjected to left anterior descending (LAD) artery balloon occlusion, which is an established model of MI. Briefly, this involves the insertion of a balloon into the LAD cardiac artery, stemming the flow of blood to a large portion of the left ventricle, resulting in a large infarction (Koudstaal, Jansen of Lorkeers et al. 2014). MI animals showed a trend towards increased SUMOylation compared to sham operated controls, although this difference only had borderline significance ($p=0.0671$; unpaired *t*-test). This trend was revealed with only n=3 animals per experimental group; with increased numbers, it is likely that a significant difference would be revealed.

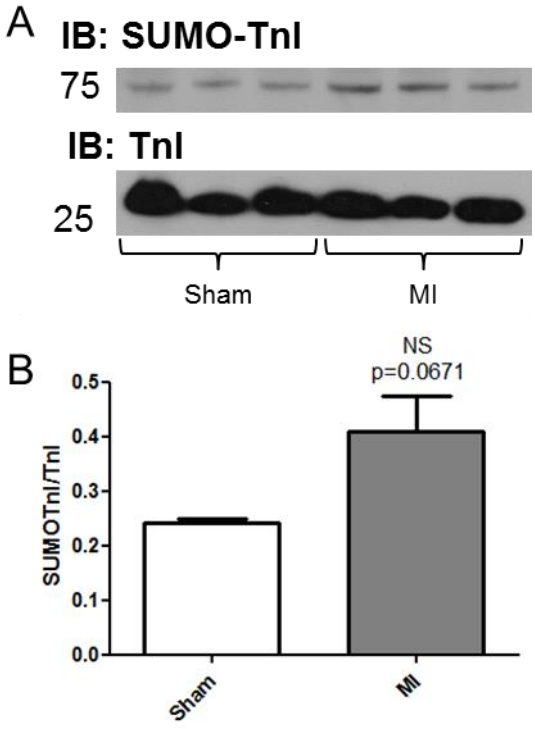

Figure 4.15: LAD artery balloon occlusion increased SUMOylated TnI. Pigs were subjected to LAD balloon artery occlusion to induce MI. Compared to sham operated controls, there was a trend towards increased SUMOylation of TnI in MI animals. Results represented as mean ± SEM, n=3. NS=p=0.0671, unpaired *t*-test.

Healthy and diseased human heart samples (Table 3.1) were immunoblotted for SUMO-TnI and the band at ~75 kDa was compared between groups. Interestingly, the ratio of SUMOylated TnI compared to total TnI was significantly increased in diseased myocardium (Figure 4.16), while the expression of SUMO E2 ligase, UBC9, and SUMO1 expression remained constant (Figure 4.17). The upregulation of SUMOylated TnI in disease was therefore, unlikely to be due to a global increase in SUMOylation within the cardiac muscle cells, but rather specifically enhanced by modified targeting of the SUMOylation cascade. This observation showed that SUMOylation of TnI is likely to be relevant to the pathophysiological function and remodelling of the myocardium.

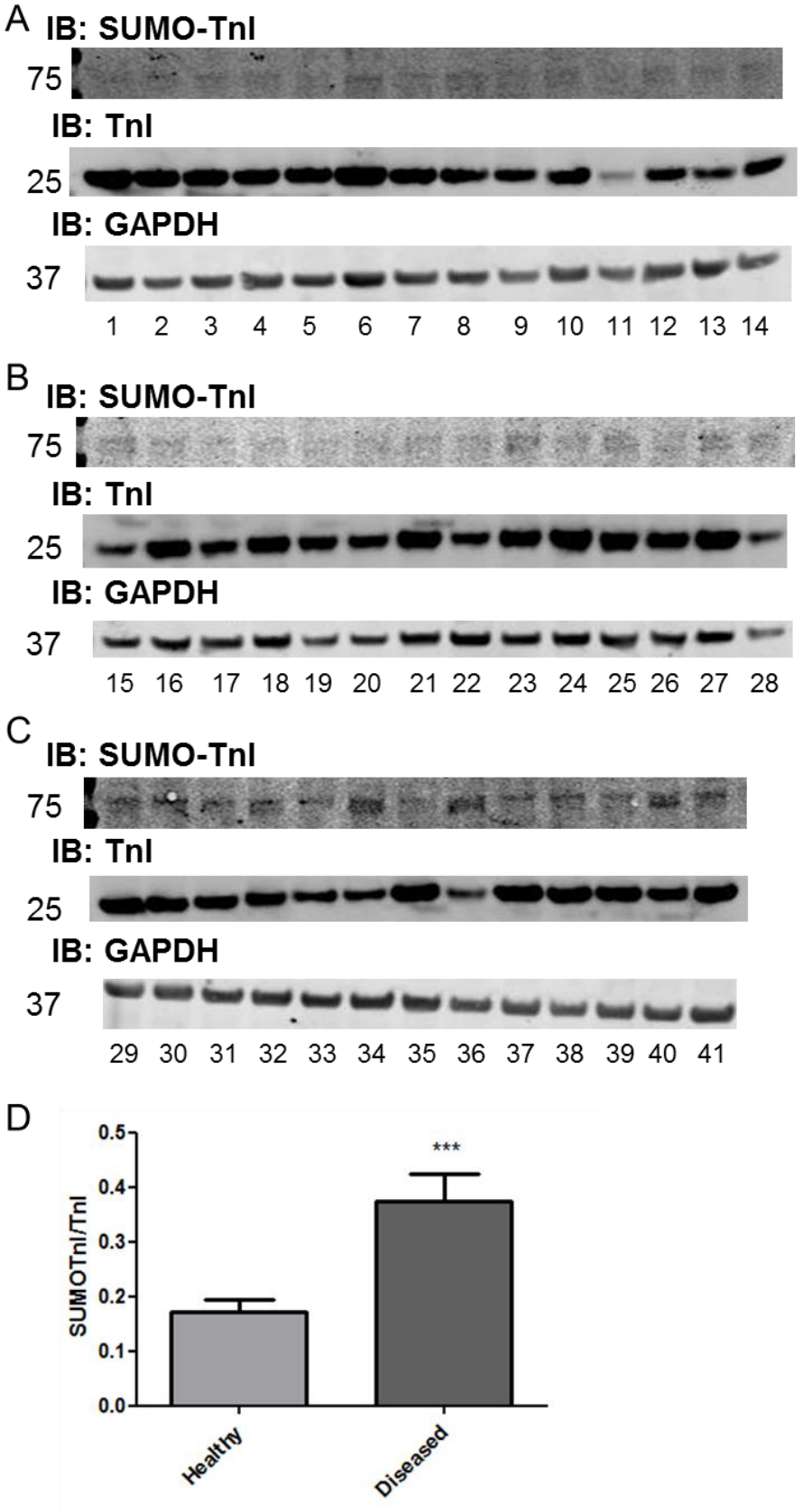

Figure 4.16: SUMO-TnI was increased in human diseased myocardium. Human heart tissue samples were immunoblotted for SUMO-TnI, total TnI and GAPDH as a loading control. The blots for samples 1-14, samples 15-28 and samples 29-41 are shown in A, B and C respectively. Quantitative analysis revealed that SUMO-TnI (as a ratio of total TnI) was significantly increased in diseased myocardium while total TnI was unchanged. Data are displayed as mean ± SEM, n=20 healthy and n=21 diseased. ***=p<0.001, student's *t*-test.

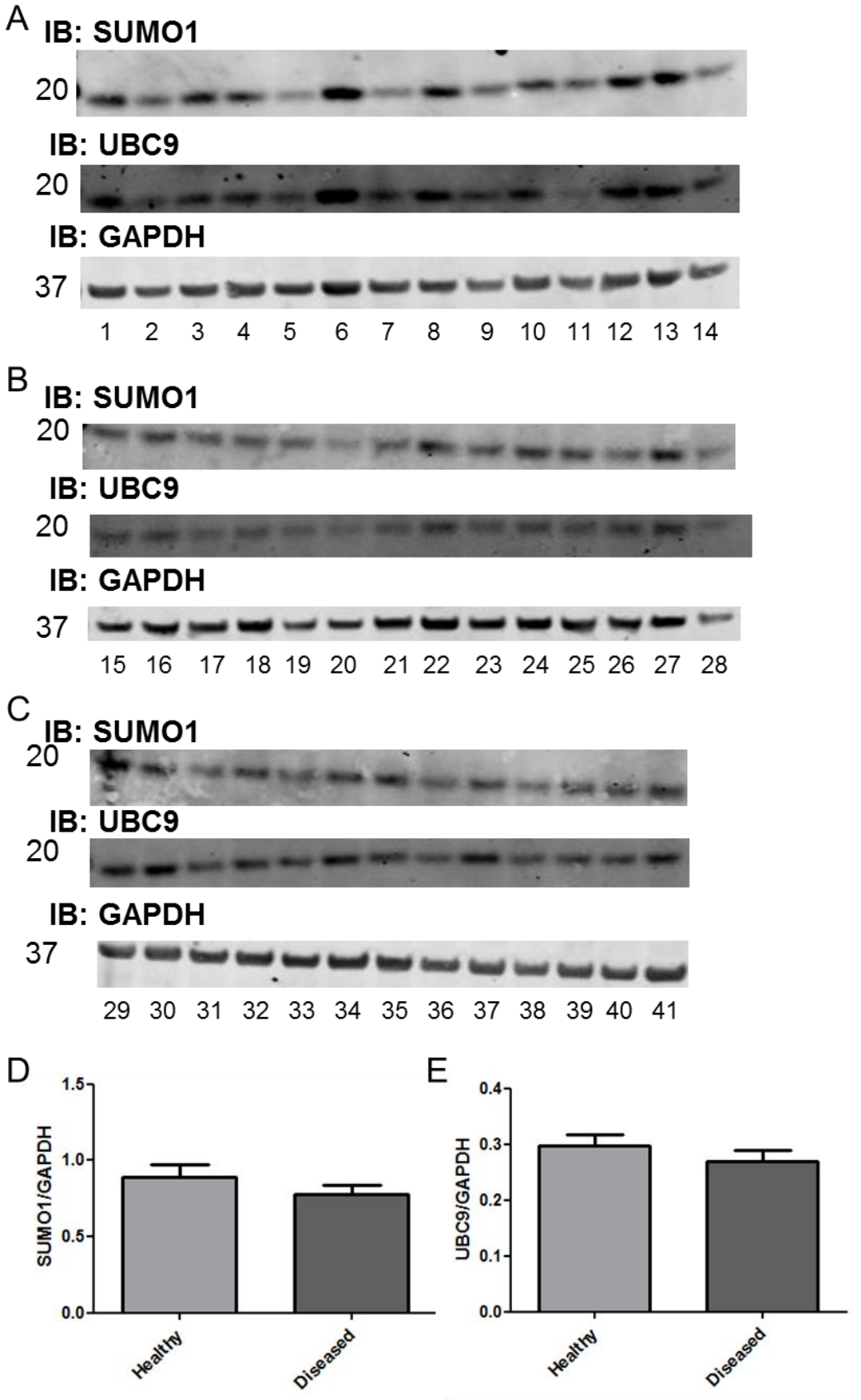

Figure 4.17: Expression of SUMO1 and UBC9 was not affected by human heart disease. Human heart tissue samples were immunoblotted for SUMO1, UBC9 and GAPDH as a loading control. The blots for samples 1-14, samples 15-28 and samples 29-41 are shown in A, B and C respectively. Quantitative analysis revealed that the expression of these proteins was not affected by the pathophysiological state of the myocardium. Data are displayed as mean ± SEM, n=20 healthy and n=21 diseased.

4.4 Discussion

4.4.1 TnI can be SUMOylated at K177

This study presents the first evidence that TnI can be SUMOylated at K177 within the consensus motif VKKE176-9. Initially, detection required SUMOylation to be 'forced' using an *in vitro* SUMOylation assay. This approach allowed the putative site to be identified using peptide arrays. Furthermore, it was clear from this data that all four amino acids within the SUMO consensus motif were necessary for the conjugation of SUMO to TNI. The assay was also used to force the SUMOylation of endogenous TnI in NRVM lysates, which was successfully detected. Although *in vitro* SUMOylation showed that TnI could be SUMOylated, the environment in which the reaction was taking place was not representative of the biological environment. In the assay, all enzymatic components as well as SUMO proteins were added in unrealistically high concentrations, to allow target protein SUMOylation to reach a detectable level. Therefore, it was necessary to determine whether TnI could be SUMOylated in cells. To this end, TnI-UBC9 and SUMO-GFP fusion proteins were co-transfected into HEK-293 cells, and the detection of a band shift at the weight of the proteins added together in the co-transfected samples, but not in single transfected samples, signified successful SUMOylated TnI. Direct interaction of UBC9 with the target protein is a key step in the SUMOylation cascade (Jakobs, Himstedt et al. 2007). By fusing UBC9 to TnI, the SUMOylation was greatly upregulated. Additionally, the labelling of SUMO with GFP allowed for straightforward detection of the SUMOylated protein compound. Therefore, it was concluded that TnI could be SUMOylated in cells. This data did not rule out the possibility that TnI was being SUMOylated at a different site; in fact, online SUMOylation motif prediction revealed the possibility of multiple SUMOylation sites within TnI's primary structure. Co-transfection of a mutant TnI-UBC9 (KK177-8RR) with SUMO-GFP eliminated the band shift present in the samples expressing WT TnI-UBC9, confirming that the SUMOylation was specific to K177. This was consistent with prediction software, which identified K177 as the highest probability residue, and *in vitro* SUMOylation assay peptide array experiments. Interestingly, K177 was also identified as a putative acceptor for ubiquitination using *in silico* prediction software (Appendix: Figure 7.2). The relationship between ubiquitination and

SUMOylation of this site and the effect of SUMOylation on protein stability is further investigated in Chapter 5.

Although K177 fits within the classical SUMOylation motif, there are additional elements to the motif that must be considered. In addition to the canonical ψKxD/E, several additional, longer sequences have been identified for certain SUMO substrates. The presence of additional motif elements can provide more information about the functional effects or the conditions in which SUMOylation occurs. Additional elements include the phosphorylation-dependent SUMOylation motif (PDSM), negatively charged amino-acid dependent SUMOylation motif (NDSM) and hydrophobic cluster-dependent SUMOylation motifs (HCSM). The PDSM was first identified in heat shock factors; in this motif, an adjacent phosphorylation site resulted in an increase in SUMOylation of the heat shock factor, but phosphorylation of adjacent sites can also negatively regulate SUMOylation as in ELK1 (Hietakangas, Ahlskog et al. 2003, Yang, Jaffray et al. 2003). In this case, TnI's SUMOylation motif does not fit into the PDSM motif, as TnI's phosphorylation sites are not adjacent to K177. Investigating the SUMOylation of ELK1 also identified another extended SUMOylation motif, NDSM, in which the third to sixth residues immediately downstream of the consensus motif are enriched for negatively charged amino acids, thereby upregulating SUMOylation (Yang, Galanis et al. 2006). Interestingly, TnI's SUMOylation site conforms to this extended motif: TnI contains negatively charged glutamic acid, E, residues at positions 182 and 184, which are 4 and 6 amino acids downstream from the consensus motif. Future investigation should determine the result of mutation of these residues on TnI SUMOylation. Finally, in a HCSM, at least three hydrophobic residues are positioned directly N-terminal to the SUMO-accepting lysine (Matic, Schimmel et al. 2010). TnI's SUMOylation motif does not conform to HCSM as the two residues (174-5KQ) directly N-terminal to the motif are not hydrophobic. All three of these extended motifs are thought to act through increasing interactions with UBC9, thereby upregulation SUMOylation by increasing enzymatic activity at the substrate (Hietakangas, Ahlskog et al. 2003, Yang, Galanis et al. 2006, Matic, Schimmel et al. 2010). Unusually, UBC9 was not shown to bind directly N-terminally or C-terminally to K177 of TnI (Figure 4.6), which contrasts to other substrate motifs which are within extended SUMO motifs facilitating nearby UBC9 binding.

Although it has been experimentally shown here that TnI can be SUMOylated *in vitro* it was yet to be determine whether, and to what extent, this modification occurs *in vivo*. In fact, contrary to the data shown here, large scale compilations of proteomics screens for SUMOylation targets have not identified TnI (Hendriks and Vertegaal 2016, Hendriks, Lyon et al. 2018). Interestingly, the β_2-adrenergic receptor is also absent from proteomic screening data, even though the receptor has been extensively studied as a SUMOylation target (Wills 2017). Proteomics screens, although informative, are predisposed to missing proteins which may be modified at very low levels or only during certain physiological conditions (Angel, Aryal et al. 2012). Therefore, the absence of TnI from proteomics screens does not disqualify it as a target of SUMOylation.

4.4.2 SUMO-TnI antibody successfully detects SUMOylated TnI

The present work provides one of the first examples of a primary antibody specific to a SUMOylated target protein. The SUMO-TnI custom antibody was created by commercial collaborator Badrilla to detect a SUMOylated epitope of TnI, which was shown to be successful for use in both peptide arrays and western blotting.

Previously, detection of SUMOylated substrate proteins relied upon searching for (sometimes faint) bandshifts on western blots, as directed in the SUMOylation assay protocol (Enzo) or for the UBC9 fusion-directed SUMOylation approach (Jakobs, Himstedt et al. 2007). Otherwise, substrate protein immunoprecipitates were immunoblotted for SUMO paralogues (Kho, Lee et al. 2015). None of these approaches allowed direct detection of SUMOylated TnI. Therefore, the comparison of the proportion of SUMOylated protein within a biological sample was technically challenging. The development of the SUMO-TnI primary antibody has allowed these challenges to be overcome, with direct detection allowing comparison between clinical samples as shown in the present work.

Although SUMOylated TnI was successfully detected, further optimisation of the antibody is necessary. Prior to use for immunoblotting, the antibody was incubated with 1 μM blocking peptide, which has the sequence of the un-SUMOylated TnI epitope. This, theoretically, should have blocked non-specific binding to the unSUMOylated TnI within the sample, making the antibody

specific for the SUMOylated species. However, the antibody continued to detect unSUMOylated TnI at its expected weight of ~26 kDa. Other non-specific bands, particularly at ~70 and ~100 kDa were also present, although further investigation is required to determine the identity of the proteins being detected at these weights.

Regardless of minor technical challenges, the successful identification of SUMO-TnI represents the first antibody to specifically recognise a SUMOylated substrate protein. Although a number of phospho-substrate specific antibodies are commercially available, production of antibodies against other post-translationally modified proteins has long challenged the scientific community for a number of reasons (Hattori and Koide 2018). Often post-translational modifications involve the addition of a very small chemical moiety to the protein substrate, which is difficult to detect. Additionally, for an antibody to specifically recognise a specific modified substrate, the epitope must encompass the modification and the surrounding area of the substrate protein beyond the generalised modification motif. A number of commercially available antibodies identify modified motifs for post-translational modification such as methylation or acetylation. These antibodies, however, are unable to distinguish between different substrates which have been modified in the same way. Recently, new structural biology approaches have been identified to aid in the effective generation of anti-post translational modification antibodies which allow for increased antigen binding surfaces (Hattori and Koide 2018). However, these recent advances focus mainly on phosphorylation, methylation and GlcNAcylation (Calarese, Scanlan et al. 2003, Hattori, Lai et al. 2016, Malia, Teplyakov et al. 2016). Post-translational modifications are integral to the function of many proteins and are highly relevant in the pathophysiology of disease; enhanced modes of detection using specific antibodies as shown in the current work will allow more accurate and efficient study of these signalling paradigms.

4.4.3 TnI SUMOylation is altered in human and porcine cardiac disease

Successful testing of the SUMO-TnI antibody allowed the detection and comparison of SUMOylated TnI in samples from healthy and diseased porcine and

human myocardium. It was found that SUMOylation of TnI was significantly upregulated in ischaemic heart failure, suggesting that the modification is relevant in the pathophysiology of disease. Consistent with human data, there was a trend towards increased SUMOylation in porcine MI. From this data, it was not possible to speculate on the functional role of SUMOylation of TnI in disease; although, the functional role was investigated, resulting in data displayed in Chapter 5 of the present work. Further suggesting a functional role of this modification, mutations of K177 have been observed in patients with hypertrophic cardiomyopathy (Ashrafian, Redwood et al. 2003, Willott, Gomes et al. 2010, Sheng and Jin 2016). The ablation of SUMOylation at this site due to the mutation may have resulted in functional changes that contributed to the pathophysiology of disease. At present, there has been no further elucidation of the functional role of the mutation of K177 and whether it contributes to pathophysiology. Now that it is known that TnI can be SUMOylated at this specific lysine residue, the relative SUMOylation states of the protein should be investigated. This is a perfect example of a study which would benefit greatly from the use of the SUMO-TnI antibody which has been tested here. Before the development of this antibody, it would have been technically challenging to determine the ratio of SUMOylated TnI:total TnI. Now, the SUMO-specific antibody means that this measurement is no more challenging than the measurement of phosphorylated protein, for which antibodies are readily available. An investigation of the protein's SUMO state, coupled with an understanding of functional changes due to SUMOylation at this site, is required to determine whether the TnI SUMOylation was relevant in the case of K177 mutation in hypertrophic cardiomyopathy.

The precedent for a functional role of SUMOylation of cardiac excitation-contraction coupling proteins exists in SERCA2a. In the case of SERCA2a, it was shown that SUMOylation was protective in disease due to its stabilisation of the protein's expression and function, both of which are diminished in disease (Kho, Lee et al. 2011). An investigation of the effect of TnI SUMOylation on protein stability and expression is shown in Chapter 5. The upregulation of SUMO1 by gene therapy enhanced SERCA2a SUMOylation and improved cardiac function. In the absence of SERCA2a, the beneficial effects of SUMO1 overexpression were ablated (Lee, Oh et al. 2016). This observation suggests that the functional

contribution of TnI SUMOylation may not be significant in the physiological improvements observed after SUMO1 overexpression. However, these studies focussed on SERCA2a specifically and did not take any other targets into account in the analyses, so it is difficult to rule out the functional effects of other SUMOylation targets. The evidence for increased TnI SUMOylation in disease coupled with the beneficial role of SERCA2a SUMOylation suggests that TnI SUMOylation may be protective in heart failure. It is possible that the upregulation of this modification at the myofilament is an adaptive, protective mechanism.

Furthermore, as SUMOylation has been shown to be altered in disease, it is important to look to the future and to determine whether the signalling paradigm would be an appropriate therapeutic target. It has previously been asserted that targeting specific SUMOylation substrates would be challenging therapeutically, due to the ubiquitous nature of the SUMOylation pathway (McMurray and Smith 2011, Wang 2011). Various proteomic screens identifying SUMOylation targets have listed thousands of target proteins, although not all of these have been confirmed or validated (Hendriks and Vertegaal 2016, Hendriks, Lyon et al. 2018). Nonetheless, the ubiquitous nature of SUMOylation is undeniable, and specificity of therapeutic intervention would be necessary for the successful targeting of TnI SUMOylation.

Beyond the targeting of TnI SUMOylation therapeutically, it is possible that the protein's SUMOylation state could be used as a biomarker. Currently, blood Tn levels are used as a biomarker for diagnostics, whereby elevated TnI or TnT is indicative of damaged myocardial tissue (Mahajan and Jarolim 2011). The damaged tissue releases Tn into the blood, where it can be detected with high sensitivity ((SIGN) 2016). It would be interesting to measure the SUMOylation state of TnI in the blood. If TnI SUMOylation were detected at a lower rate in blood TnI compared to TnI in the myocardium, this would indicate that SUMOylation has a role in the stabilisation of the protein, similar to its role in SERCA2a SUMOylation (Kho, Lee et al. 2011). Furthermore, if higher throughput studies confirmed the consistent upregulation of SUMO-TnI in heart failure or other cardiac diseases, and an efficient detection method were established, measurement of SUMO-TnI has potential to become a disease biomarker in its own right.

4.4.4 Methodological Considerations

UBC9 fusion-directed SUMOylation was used here to upregulate the SUMOylation of TnI in HEK-293 cells. Although this system allows the detection of SUMOylation, there were several complications in the detection of the SUMOylated band that limited these experiments. Although several antibodies against TnI were used in an attempt to detect the transfection of TnI-UBC9, none were able to detect the protein despite clear expression as detected by UBC9. Therefore, the SUMOylated TnI band (~75 kDa) was not detected by immunoblotting for TnI, but instead, by immunoblotting for UBC9 and GFP. Therefore, a member of each fusion protein was confirmed to be present in the band of interest, confirming the band's identity as SUMO-GFP+TnI-UBC9 as hypothesised. This was consistent with published data using this approach in which SUMOylated substrate bands were primarily detected using antibodies against UBC9 (Jakobs, Himstedt et al. 2007, Jakobs, Koehnke et al. 2007). The detection issue caused more of a problem when these samples were probed for phospho-TnI. Co-transfected samples were treated with forskolin and IBMX to raise intracellular cAMP and activate PKA phosphorylation of Ser23/24. These samples were then probed for GFP to determine whether phosphorylation affected SUMOylation; phosphorylation did not have an effect on the level of SUMOylated TnI detected. The counterpart to this observation was to determine whether SUMOylation affected the level of phosphorylation. This was not determined in the present work as the phospho-Ser23/24 antibody did not allow the detection of the TnI-UBC9 fusion protein. It is possible that the UBC9 fusion changed the conformation of TnI such that the antibody epitope was no longer available for binding. Initially, it was hypothesised that the SUMOylation at K177 could have interfered with antibody binding, but this was determined to be unlikely as the antibody which was used primarily to detect TnI in other experiments was raised against a synthetic peptide derived from residues 1-100 of human TnI.

Finally, an additional control could have been used in experiments in which TnI-UBC9 and SUMO-GFP were co-transfected. In these experiments, a ~70 kDa was detected, indicating the combination of the two constructs covalently linked by the addition of SUMO to the identified motif of TnI (Figure 4.7). This band was eliminated when TnI's SUMO site was ablated using site directed mutagenesis,

confirming the specificity of SUMOylation to this site (Figure 4.9). These experiments would have benefitted from the inclusion of an additional control in which TnI was fused to catalytically inactive UBC9. This would have provided additional confirmation of that the detection of the ~70 kDa band was specific to SUMOylation of TnI.

4.4.5 Conclusions

The data presented here shows, for the first time, that TnI can be SUMOylated at K177 and that this modification is upregulated in human cardiac disease. Research involving protein SUMOylation has long been hampered by difficulties in detecting SUMOylated proteins, with previous studies only detecting SUMOylated protein using proteomic approaches or enrichment via immunoprecipitation. Now, with the successful testing of a SUMO-substrate specific antibody, the detection of SUMOylated samples directly in tissue samples has been made possible. This provides an important precedent for the possibility of developing specific antibodies against proteins modified by post-translational modifications, and will greatly enhance future investigation of this signalling paradigm. Taken together, these findings suggest that it is critical to elucidate the functional role of SUMOylated TnI.

Chapter 5 Functional effects of Troponin I SUMOylation

5.1 Introduction

Having shown that K177 on TnI can be SUMOylated in cells, the next step was to determine the functional relevance of this modification. Investigation of the functional roles of SUMO modification for any target protein is complicated by the fact that SUMOylation can have a wide range of functional effects, from changes in target protein interactions with other proteins, to alterations in protein stability, to regulation of transcriptional activity (Ulrich 2009).

Knockout and overexpression studies in rodents have highlighted the functional importance of SUMOylation in the heart (Da Silva-Ferrada, Ribeiro-Rodrigues et al. 2016). SUMO1-KO resulted in congenital heart disease while SUMO2-KO and UBC9-KO were embryonic lethal (Nacerddine, Lehembre et al. 2005, Wang, Chen et al. 2011, Wang, Wansleeben et al. 2014). Various SENP-KO animals displayed embryonic lethality or congenital heart defects (Gu, Fan et al. 2014). Taken together, it is clear that this system has important developmental and functional effects in the heart. Despite clear functional roles for the SUMOylation system globally within the heart, it is difficult to determine the role of SUMOylation of specific substrate proteins. However, the role of SERCA2a SUMOylation has been characterised, whereby SUMOylation has been shown to maintain the function and stability of SERCA2a, making the modification protective in heart failure (Kho, Lee et al. 2011, Tilemann, Lee et al. 2013).

5.1.1 TnI degradation and proteolysis

A number of studies have documented the cleavage of the C-terminal region of TnI (192-210) following various cardiac pathophysiological states (Sheng and Jin 2016). First observed in rats following I/R injury, truncated TnI was also observed in humans following myocardial stunning in coronary bypass grafting (McDonough, Arrell et al. 1999, McDonough, Labugger et al. 2001). Studies in which full length TnI was replaced with C-terminally truncated TnI showed that this proteolytic cleavage was likely to affect contractile dynamics, particularly diastolic function (Murphy, Kogler et al. 2000, Narolska, Piroddi et al. 2006). The C-terminal truncation of TnI is catalysed by proteases called calpains, with m-calpain and μ-calpain both acting on the protein (Di Lisa, De Tullio et al. 1995). Calpains are cysteine proteases which have calcium-dependent activity; two

calpain isoforms are expressed in muscle, m-calpain and μ-calpain, which are activated by high (uM) Ca^{2+} concentration and low (mM) Ca^{2+} concentrations respectively (Cong, Goll et al. 1989, Portbury, Willis et al. 2011). Interestingly, TnI cleavage by μ-calpain has been shown to be regulated by phosphorylation at S199 whereby increased PKC phosphorylation increased susceptibility to proteolysis (Wijnker, Li et al. 2015).

TnI has also been shown to be modified by ubiquitination in murine cardiac tissues. The ubiquitinated form of TnI was reduced in MURF-1 KO mice, which led to the conclusion that MURF-1 and MURF-2 redundantly ubiquitinate TnI (Witt, Granzier et al. 2005). The study offered little information on the functional relevance of this modification, but the classical role of ubiquitination is the directing of the substrate to the proteasome for degradation, suggesting that TnI might be degraded in this way (Hershko, Heller et al. 1983).

There is evidence to show that both ubiquitin and calpain mediated proteolysis can be modulated by SUMOylation, although the relationships are not well understood (Rodriguez, Li et al. 2016). Increasing the expression of UBC9 has been shown to decrease protein aggregation and maintain normal proteasome function (Gupta, McLendon et al. 2016). Furthermore, several other factors suggest extensive crosstalk between ubiquitination and SUMOylation. For example, SUMO or ubiquitin sometimes modify the same lysine residues on target proteins and hybrid chains made of both ubiquitin and SUMO proteins have been observed (Ulrich 2005, Liebelt and Vertegaal 2016). In fact, several proteins have been identified in which SUMOylation stabilises the protein via inhibition of ubiquitination at the same lysine. These proteins include MDM2, a ubiquitin E3 ligase (Meek and Knippschild 2003); NEMO, inhibitor of nuclear factor kappa B (Huang, Wuerzberger-Davis et al. 2003); axin (a component of the Wnt pathway) (Kim, Chia et al. 2008); and RNA helicases p68 and p72 (Mooney, Grande et al. 2010). Interactions between SUMOylation and the calpain system, on the other hand, involve the identification of calpains as SUMOylation targets as well as the identification of SUMO E3 ligase, PIAS3 as a calpain substrate (Kramerova, Kudryashova et al. 2005, Wang, Huang et al. 2009, Da Silva-Ferrada, Ribeiro-Rodrigues et al. 2016). It is conceivable that SUMOylation of target proteins in the heart could affect their proteolytic degradation by the calpain system; although direct evidence of this has not yet been found.

5.1.2 Evaluating TnI function

SUMOylation of TnI may also affect its function as the inhibitory subunit of the Tn complex of the myofilament. Previous studies which have investigated the role of phosphorylation at specific phospho-sites have employed the use phospho-mimic or phospho-null mutants to replace endogenous TnI before functional analysis (Kentish, McCloskey et al. 2001, Pi, Kemnitz et al. 2002, Pi, Zhang et al. 2003). Myofilament properties, such as Ca^{2+} sensitivity, rate of Ca^{2+} dissociation, cross-bridge cycling rate and unloaded shortening velocity, could then be measured using skinned muscle fibres from cardiac myocytes. There are several things to note when using data generated from skinned muscle fibres. When using skinned muscle fibres to analyse myofilament dynamics, the myofilaments are observed in isolation, without the interference of Ca^{2+} handling processes in intact cells. Although this allows more specific myofilament-related parameters to be observed, it is necessary to note that its biological relevance is limited due to the absence of Ca^{2+} handling proteins. For this reason, two techniques were used in the present work to evaluate the function of TnI SUMOylation. Firstly, monolayers of NRVM overexpressing SUMO-null mutant TnI were paced and contractility was analysed. Second, ARVM overexpressing SUMO-null mutant TnI were skinned and myofilament dynamics were analysed.

5.1.3 Upregulation of SUMOylation with N106

It has previously been shown that upregulation of SERCA2a SUMOylation is protective in heart failure (Kho, Lee et al. 2011, Tilemann, Lee et al. 2013). Therefore, a small molecule activator of SUMOylation, N106 (*N*-(4-methoxybenzo[d[thiazol-2yl0-5-94-methoxyphenyl0-1,3,4-oxadiazol-2-amine) (Tocris Bioscience), was developed to enhance the modification (Kho, Lee et al. 2015).

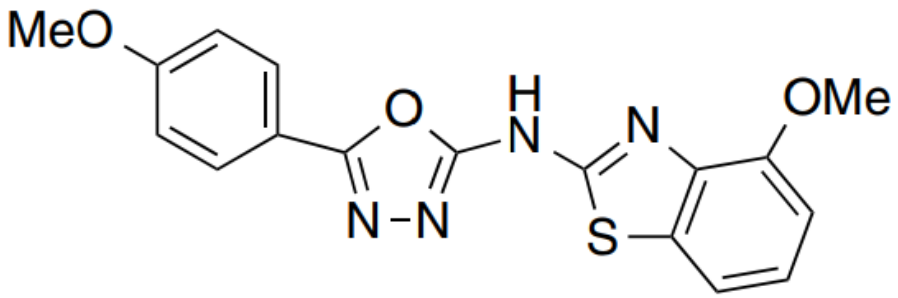

Figure 5.1: Chemical structure of N106, a small molecule activator of SUMO-activating enzyme, E1 ligase. Adapted from (Kho, Lee et al. 2015).

N106 directly activates SUMO-activating enzyme, E1, which thereby enhances the activation of the rest of the SUMOylation cascade, causing upregulation of SERCA2a SUMOylation. Treatment with N106 caused increased contractility in isolated adult rat cardiac myocytes as well as the improvement of ventricular function in surgically induced heart failure in mice (Kho, Lee et al. 2015). Although the functional effects have been ascribed to an increase in the SUMOylation of SERCA2a specifically, the activation of the SUMO E1 ligase increased global SUMOylation of multiple – if not all – cellular targets.

5.2 Hypothesis and Aims

The functional effects of TnI SUMOylation have not yet been determined. Adenoviral overexpression of mutant TnI protein lacking the SUMOylation site (TnI-HA MUT) or wildtype TnI (TnI-HA WT) was used to determine whether the ablation of SUMOylation resulted in any physiological effects. It was hypothesised that SUMOylated forms of TnI would function differently within the myofilament of cardiac myocytes when compared with unSUMOylated TnI. The aims of the experimental work in this chapter were as follows:

- To confirm the expression of viral proteins in NRVM and ARVM using western blotting and immunofluorescence

- To determine whether ablation of TnI's SUMO site resulted in any functional effects on NRVM and ARVM contractility using live cell contractility imaging

- To determine whether ablation of TnI's SUMO site and/or upregulation of SUMOylation with N106 resulted in any functional effects in isolated skinned muscle fibres

5.3 Methods

The methods described in this section were used to collect the data displayed within this chapter. Experiments were also completed using cell culture and biochemical methods which were described in Chapter 2 of this thesis.

5.3.1 Contractility Imaging with CellOPTIQ®

5.3.1.1 NRVM Preparation for CellOPTIQ®

For adequate contractile activity, NRVM were seeded in monolayers for the recording of contraction videos. Following isolation, cells were counted and seeded in 2 well culture-inserts (Ibidi®) on glass bottom 35 mm dishes (MatTek®) at a density of $5x10_4$ cells per well in a final volume of 100 µl of medium. One day after seeding, NRVM were virally transfected to overexpress TnI-HA proteins (WT and SUMO site mutant). Following a 24 hour incubation with virus, and directly prior to the acquisition of videos, the medium was aspirated and the culture-inserts were carefully removed. The 35 mm dishes were then filled with 2 mls of M199 for imaging, which took place at room temperature.

5.3.1.2 Contractility measurements

CellOPTIQ® (Clyde Biosciences Ltd; Glasgow, UK) was used for the collection of high speed images of contracting cell monolayers. This *in vitro* system allows simultaneous measurement of contractility, voltage and calcium in live cells, but for the purposes of the present project, only contractility was analysed. Cells were paced using electrodes at 40V with 20 ms duration at a frequency of 1.2 Hz. For each field, an eight second recording at 100 frames per second was acquired using a 60x objective lens and Contractility Tool software. Between six and ten fields of each monolayer were recorded over five experimental days using five separate NRVM isolations.

5.3.1.3 Analysis

Contractility recordings were analysed using an ImageJ Macro called MUSCLEMOTION (Sala, van Meer et al. 2018). Briefly, this software converts changes in pixel intensity between image frames to a measure of movement during contraction and relaxation. Representative examples of a raw acquired

image and an analysed image displaying moving pixels are shown in Figure 5.2. The measure of movement was displayed as a trace of contraction (a.u.) over time. For each contraction, a variety of parameters could be determined and compared between conditions (Figure 5.3).

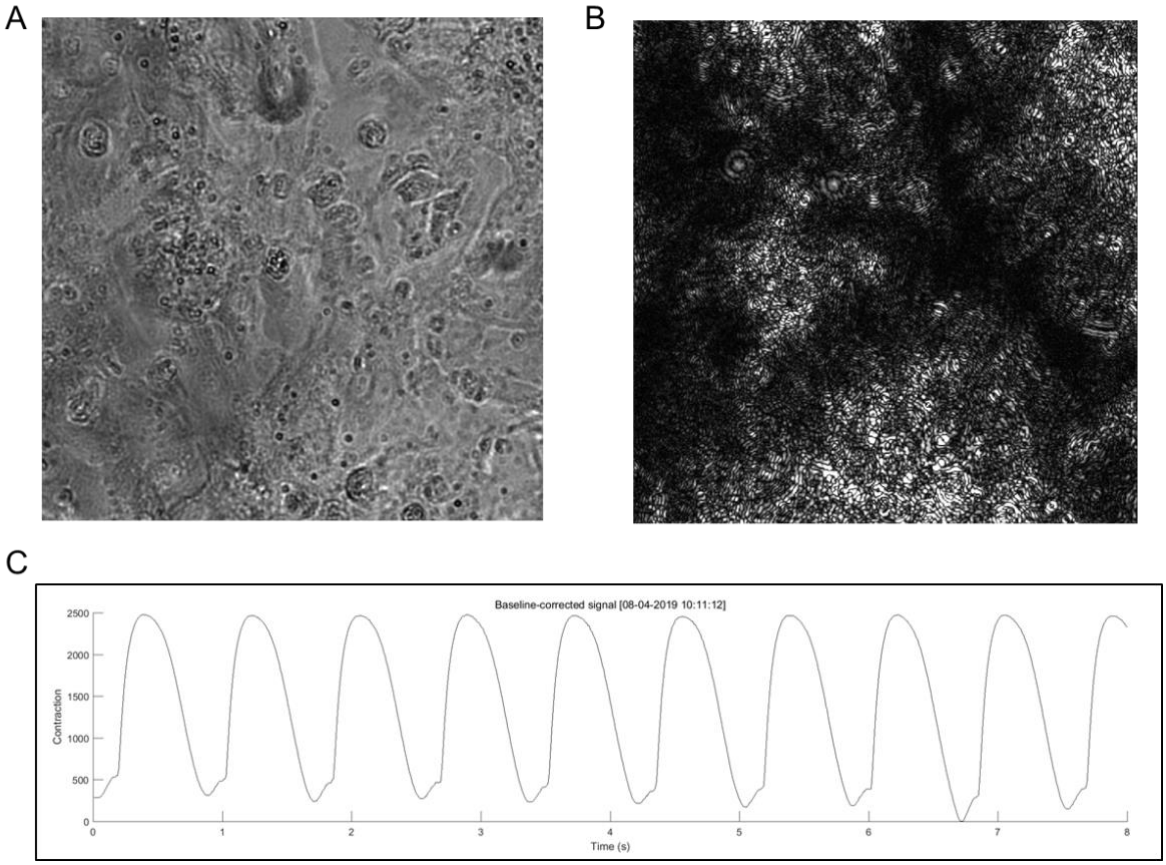

Figure 5.2: Representative example of images acquired by CellOPTIQ® and contraction traces produced from one image stack. A. Single image taken of a NRVM monolayer in brightfield at 60x magnification. B. As the monolayer contracts, the moving pixels were converted to white on a black background. C. The amount of white pixels was then converted into a contraction trace from which measurements could be taken.

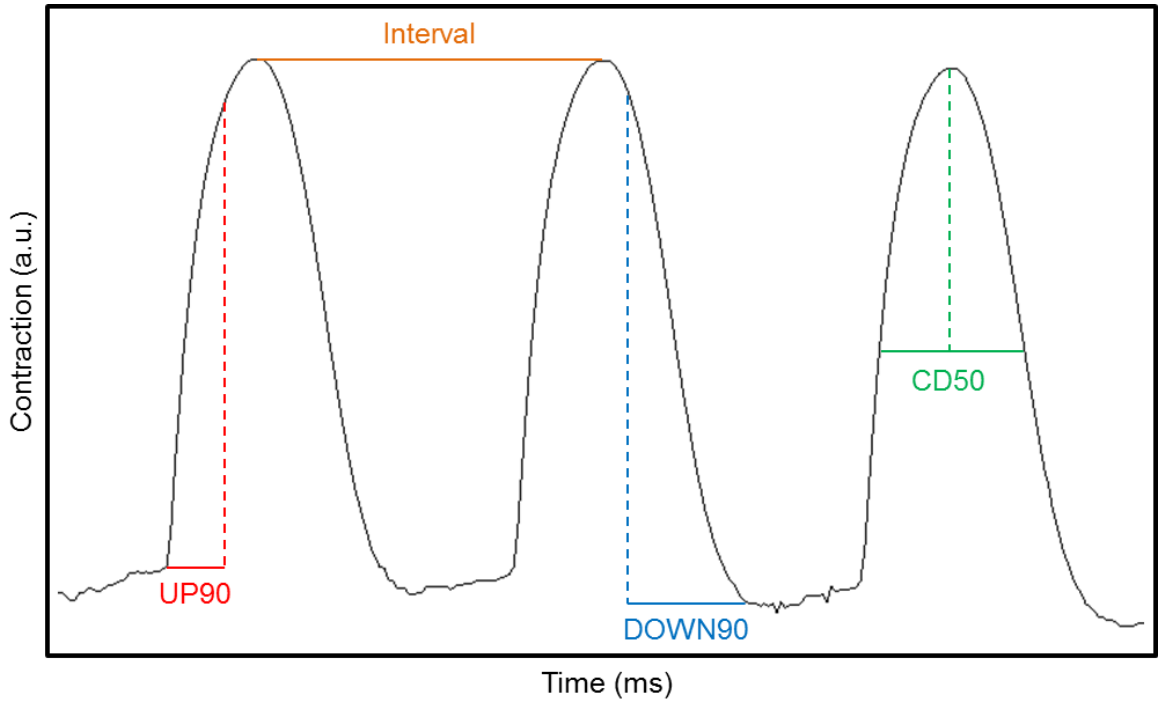

Figure 5.3: Schematic representation of contraction and relaxation parameters. Contraction traces generated by MUSCLEMOTION software can be used to measure numerous parameters. Several of these, used in the present work, are explained here. Interval, or the time between contractions, was used to monitor how well NRVM monolayers were adhering to pacing. UP90, a measure of the time to contract, was calculated as the time from baseline to 90% of the peak. Similarly, DOWN90 is a measure of the time to relax, and was calculated as the time from 90% peak to baseline. Finally, contraction duration at 50% was measured as the time between 50% of the upstroke to 50% of the downstroke.

5.3.2 Skinned fibre experiments

5.3.2.1 Preparation of skinned ARVM

All steps were performed on ice using pre-chilled buffers. Medium was removed from cultured ARVM. An appropriate volume of relaxing buffer (5.95 mM Na_2ATP, 6.04 mM $MgCl_2$, 2.0 mM EGTA, 139.6 mM KCl, 10 mM imidazole, pH 7.0) with 0.5% triton was added. Cells were incubated for 5 minutes with gentle agitation on an orbital shaker. Cell samples were scraped and collected in 1.5 ml Eppendorf tubes. Samples were centrifuged at 1200 rpm to pellet and supernatant was removed. Cell pellets were washed at least three times with relaxing buffer to remove residual triton. After the final wash, cells were resuspended in 50% glycerol in relaxing solution for storage at -20˚C.

5.3.2.2 Force measurements

Force measurements were recorded in collaboration with Professor Jolanda van der Velden at VU Medical Centre Department of Physiology in Amsterdam, Netherlands as previously described (van der Velden, Klein et al. 1998). Cell suspensions were diluted in relaxing solution and added to a glass slide which was placed on a temperature-controlled stage for visualisation on a Zeiss Axiovert S100 microscope. Images were recorded using a Balser scA640 camera and Image Grabber software (VUmc). The temperature of the stage was maintained by the flow of cold water from a 4°C water bath (Julabo F10) through the metal stage using a pump (Julabo C). Single cells were selected on the basis of size (100-150 µm length by 15-30 µm width) and clear visibility of sarcomere striations. Once a single cell had been selected, two small stainless steel needles with 10 µm diameters were dipped into shellac adhesive (Sigma, dissolved in 70% EtOH 0.12 g/ml) to cover the needle tips and then directed to the left and right edges of the cell using joystick-controlled micromanipulators. The left needle was attached to a force transducer and the right needle was attached to a piezoelectric motor. Carefully, the needles were lowered and attached to the left and right edges of the cell and left to cure for 60 seconds. The attached cell was then raised from the surface of the glass slide, suspending the cell in relaxing solution. The suspended cell was then stretched to a sarcomere length of 2.2 µm by adjusting the position of the needles in small increments. The sarcomere length was measured in real time by Image Grabber software which employed a spatial Fourier Transform algorithm (van der Velden, Klein et al. 1999). The width and length (distance between the needle edges) of the cell were measured and recorded. The cell was then transferred from the mounting area to fresh relaxing solution contained within a small glass bottomed well (volume 80 µl). A schematic view of the experimental setup is shown in Figure 5.4.

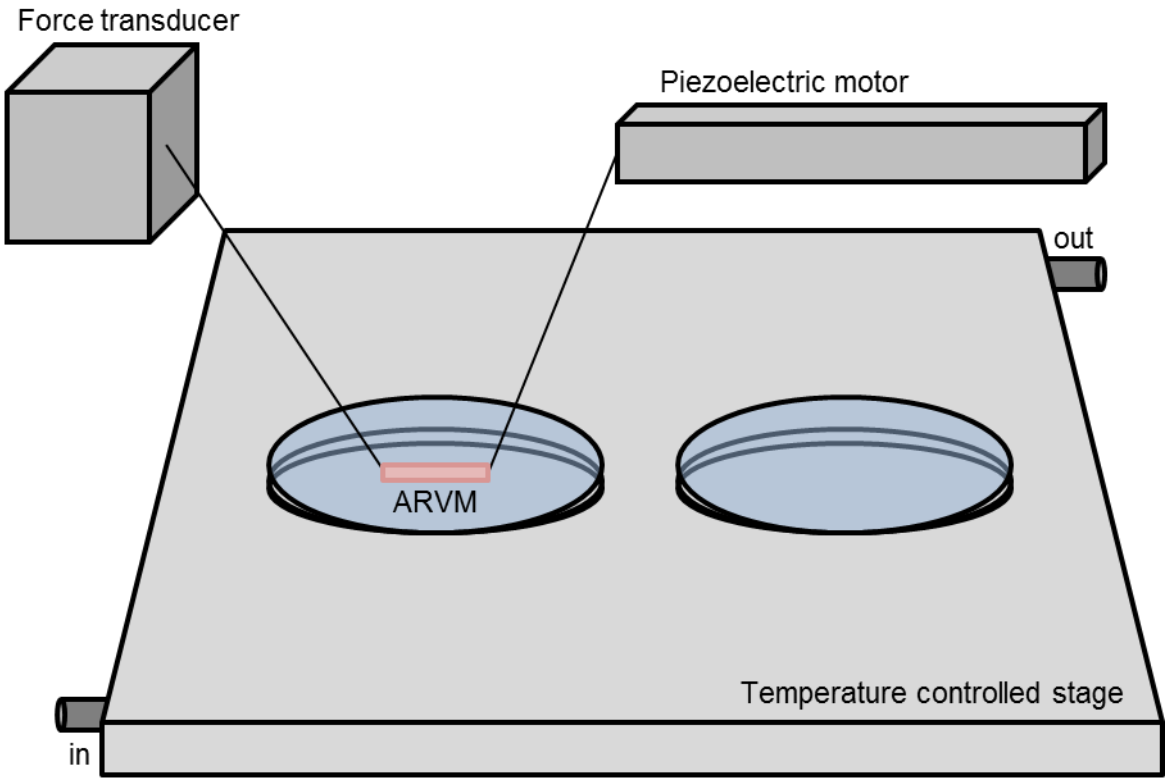

Figure 5.4: Schematic representation of the experimental setup for the measurement of force produced by single skinned cardiac myocytes. Two small needles were attached to the left and right edges of a single cell. The left needle was attached to a force transducer while the right was attached to a piezoelectric motor. The cell was then moved by adjusting the stage position, into the left hand droplet, which contained relaxing solution. For each activation/relaxation cycle, the cell was moved between the left hand relaxing solution droplet to a right hand droplet containing activating solution with pCa_{2+} ranging from 5.0-6.8. The solutions in each droplet were temperature controlled by the flow of cold water through the metal stage. (Adapted from (van der Velden, Klein et al. 1998).

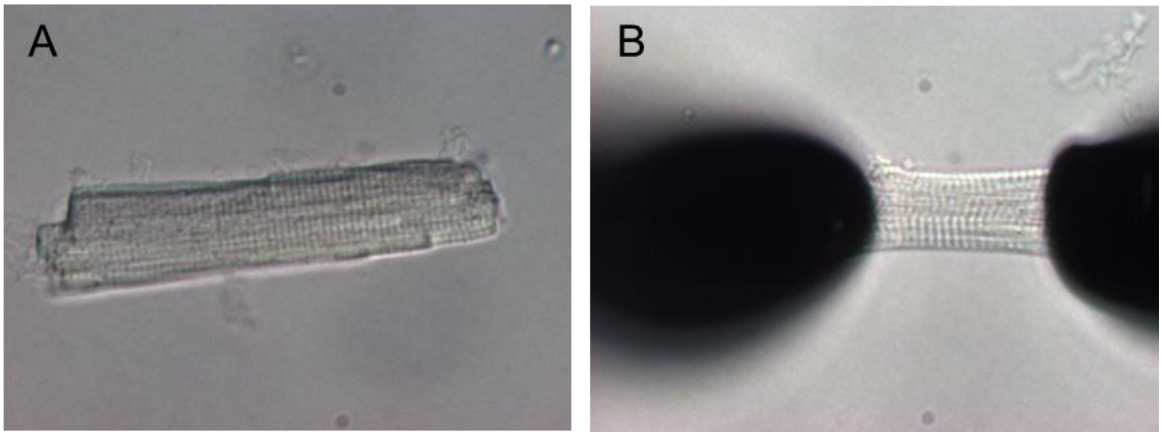

Figure 5.5: Representative example of a single ARVM before (A) and after (B) gluing. In both images, sarcomeres are clearly visible in a striated pattern. After gluing to needles, cells were stretched to sarcomere length 2.2 µm as shown by increased distance between sarcomeres in (B).

At this point in the protocol, the activation/relaxation cycles were commenced. Force was monitored and recorded in real time using Chart software (VUmc). Cells were exposed to seven activating solutions which had pCa^{2+} ranging from 5.0-6.8 so that dose-response curves could be generated. A representative example of a trace from one activation/relaxation cycle is shown in Figure 5.6. For each activation cycle, activating solutions were first added to an adjacent glass bottomed well. By adjusting the position of the stage, the cell was moved into the activating solution quickly to minimise exposure to air. In response to the increased pCa^{2+}, the force increased. When the force reached a plateau, the cell was slacked by 30% of its length. To slack the cell, the piezoelectric motor was controlled by a function generator, which moved the right needle closer to the left needle by a distance determined by the cell length, thereby eliminating tension generated by the sarcomere. Following this initial, short slack, the needle was returned to its original position, causing the force to increase. This time, when a plateau was reached, the cell was returned to the relaxing solution. Again, under the control of the function generator, the cell was slacked for 10 seconds to determine the passive force of the sarcomere at the stretched length of 2.2 μm. This completed one activation cycle and the next could be commenced immediately.

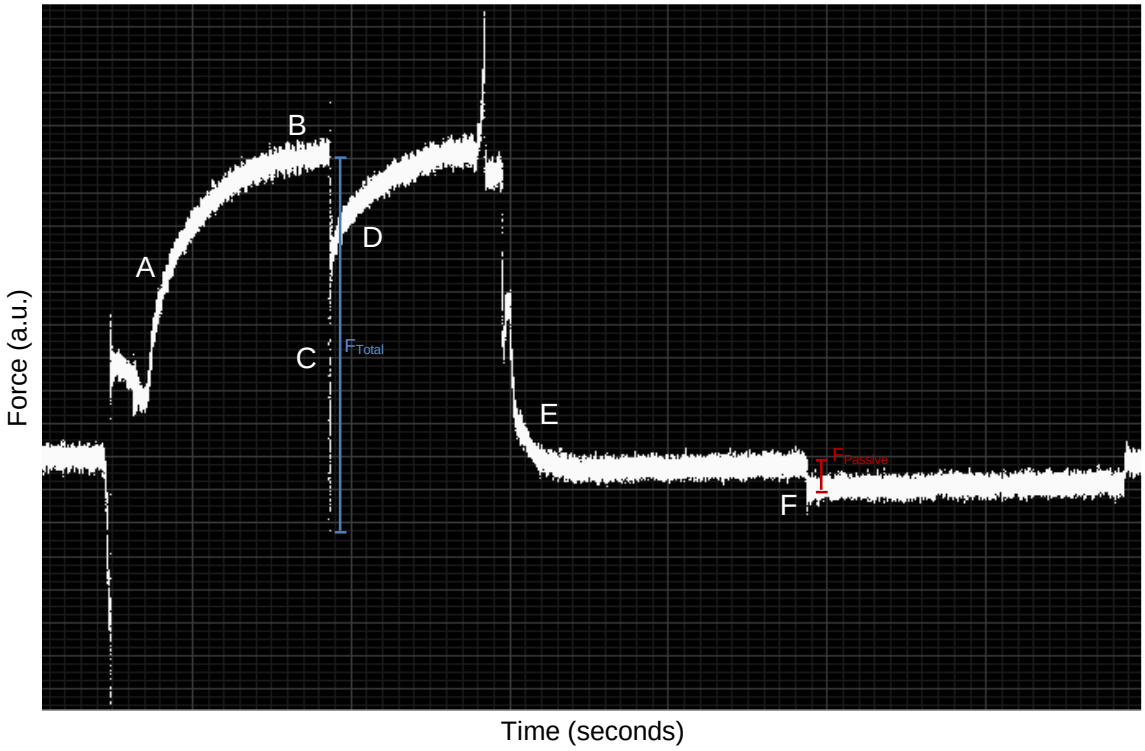

Figure 5.6: Representative example trace from a single activation/relaxation cycle. Each activation/relaxation cycle began with the movement of the cell into activating solution. Due to the increase in pCa_{2+}, the force increased (A). When a plateau was reached (B), the cell was slacked to 30% of the original length, which reduced the force momentarily (C). The amplitude between B and C was used to calculate F_{Total}. When the cell was restored to a sarcomere length of 2.2 µm, the force increased again (D). This time, when a plateau was reached, the cell was moved back into relaxing solution, and the force decreased (E). Finally, the cell was slacked for 15 seconds, causing the force to decrease (F). The amplitude between E and F was used to calculate $F_{passive}$.

Upon completion of the activation/relaxation protocol, cell width was measured using a small mirror to visualise the z axis of the cell. Therefore, the force could be normalised to the volume of the cell for calculation of accurate EC_{50} values.

5.3.2.3 Calcium sensitivity analysis

Activation/relaxation traces were analysed using Myo software (VUmc). Analyses of force-Ca_{2+} relationships were performed as previously described (Sequeira, Wijnker et al. 2013). First, F_{max} was calculated by subtracting $F_{passive}$ from F_{total} (Figure 5.6). This value was then used to calculate the maximal tension (kN/m_2) by normalising F_{max} to the cross-sectional area of the cardiac myocyte. This analysis was then performed for each activation/relaxation cycle for a single cell. The force-Ca_{2+} relationships were then fit to a modified Hill equation using GraphPad Prism®, which was used to determine myofilament Ca_{2+} sensitivity, which was denoted as EC_{50}, or the [Ca_{2+}] at which half of F_{max} was produced. A

representative example of a force-Ca^{2+} relationship for a single cell is shown in Figure 5.7.

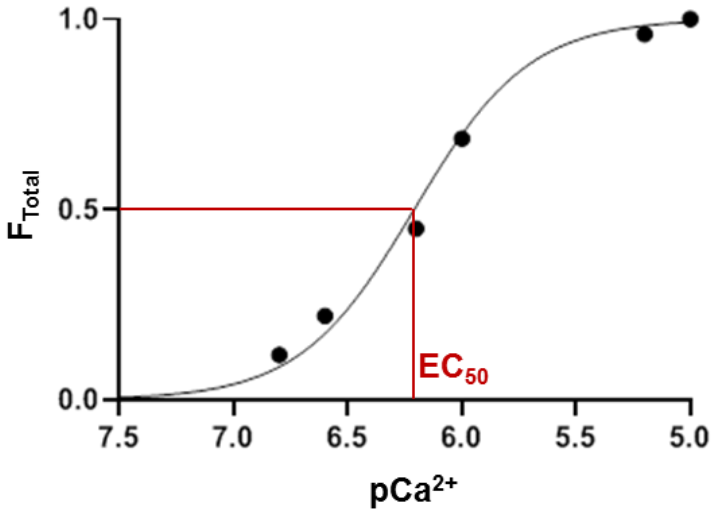

Figure 5.7: Representative force-Ca^{2+} curve for a single cardiac myocyte. The F_{Total} values for each pCa^{2+} solution were compiled into force-Ca^{2+} curves, which could then be used to determine the EC_{50}.

5.4 Results

5.4.1 Confirmation of viral overexpression of TnI-HA proteins

Adenoviruses containing TnI-HA WT and TnI-HA SUMO site mutant (KK177-8RR) for mammalian overexpression were obtained commercially from Welgen, Inc. Before any functional experiments could proceed, it was necessary to confirm that the viruses produced successful overexpression of the TnI-HA proteins in relevant cells. TnI-HA proteins were successfully detected with robust expression levels in HEK-293 cells following incubation with 10^3-10^4 MOI of virus for 24 hours (Figure 5.8). Importantly, there was no significant difference between the expression of TnI-HA between the MUT and WT proteins at the same dose, suggesting that cells treated with the same doses of the two viruses would be comparable.

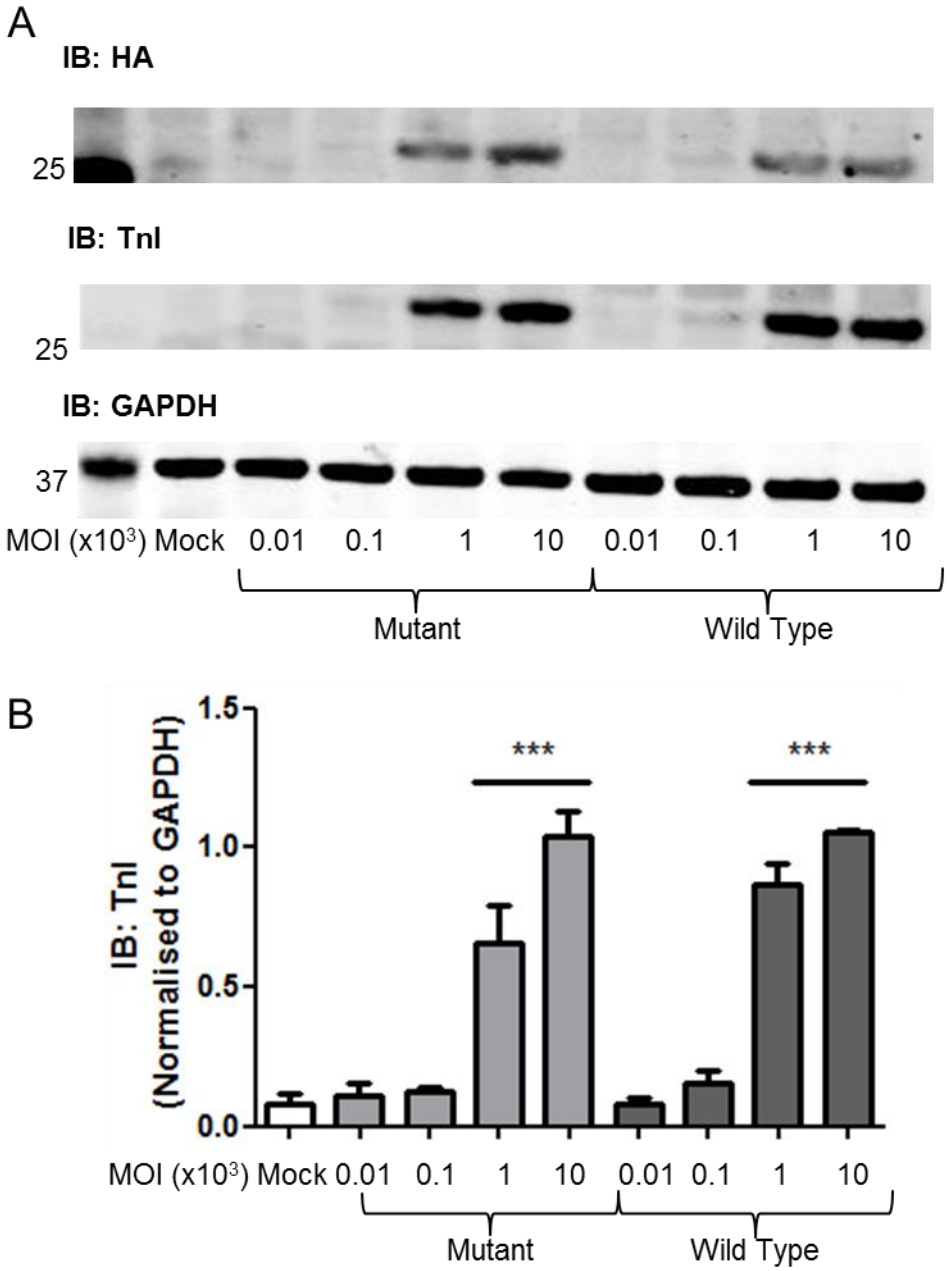

Figure 5.8: Confirmation of viral overexpression of TnI-HA in HEK-293. HEK-293 cells were infected with viruses increasing from 10_1-10_4 MOI for 24 hours prior to harvesting of cell lysates and analysis via immunoblotting. A. Representative example. B. Results represented as mean ± SEM, n=4. ***=p<0.001 vs. Mock, One-way-ANOVA with post hoc analysis: Tukey's multiple comparison test.

Similarly, robust viral overexpression of TnI-HA MUT and WT was detected in NRVM following 24 hour incubation of 10_4 MOI (Figure 5.9). The appropriate targeting of TnI-HA was shown using immunocytochemistry (Figure 5.10). The striated pattern of HA staining confirms targeting of the viral proteins to the myofilament.

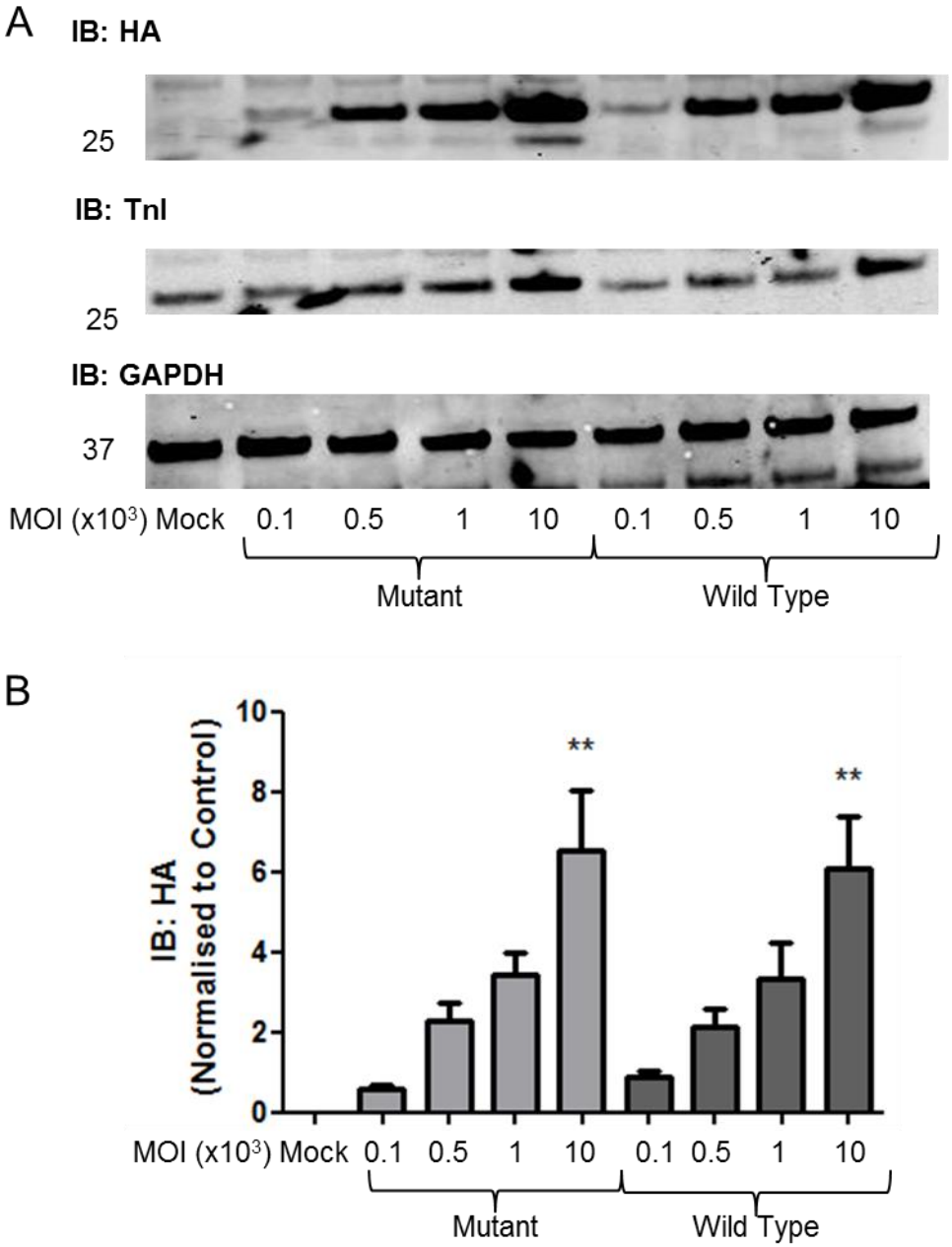

Figure 5.9: Confirmation of viral overexpression of TnI-HA in NRVM. NRVM were infected with viruses in doses increasing from 10^2-10^4 MOI for 24 hours prior to harvesting of cell lysates and analysis via immunoblotting. A. Representative example. B. Results represented as mean ± SEM, n=4. **=p<0.001 vs. Mock, One-way-ANOVA with post hoc analysis: Tukey's multiple comparison test.

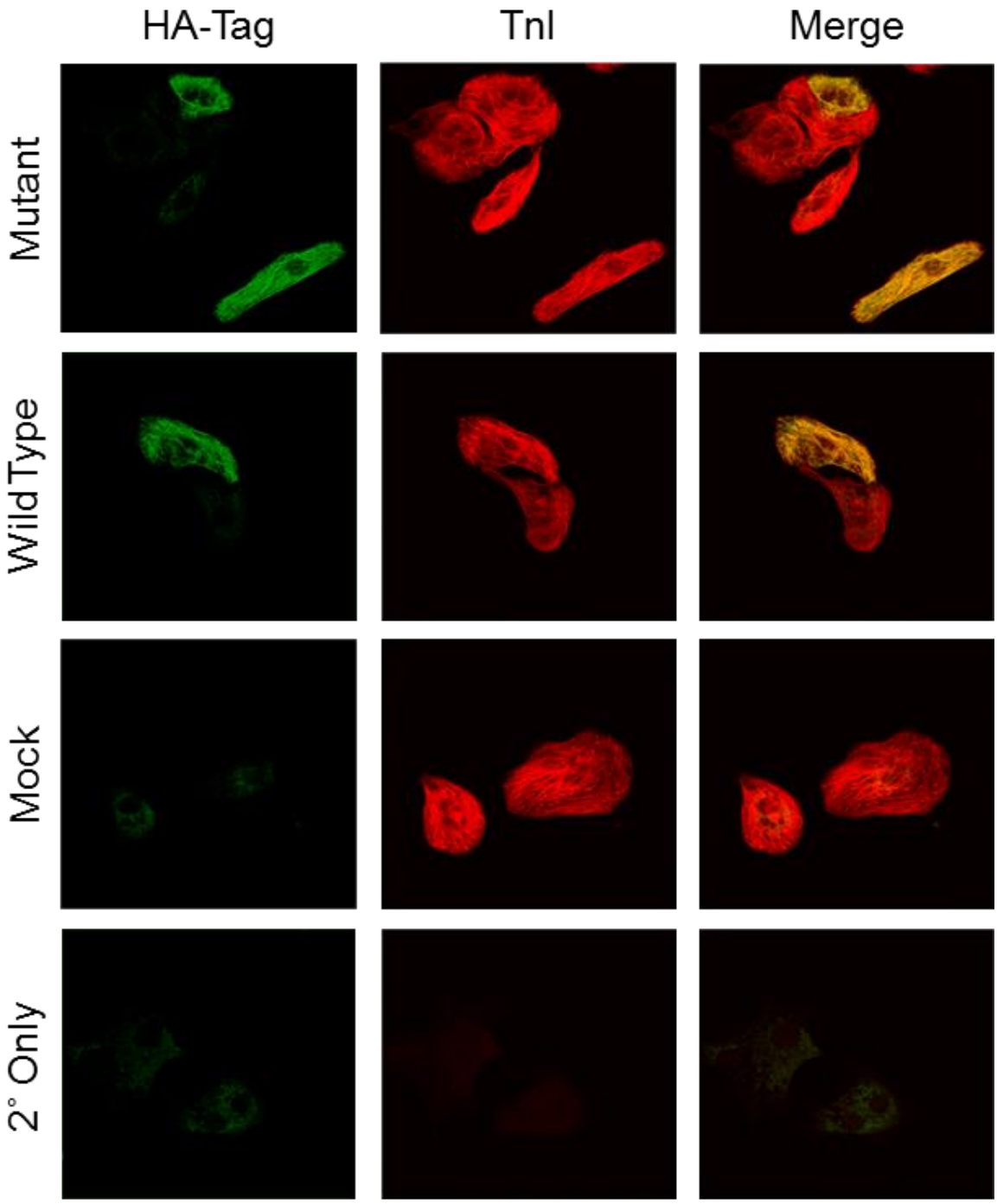

Figure 5.10: Immunocytochemical analysis of TnI-HA protein localisation. NRVM were infected with TnI-HA MUT or TnI-HA WT viruses for 24 hours at MOI 10^2. The cells were then fixed, permeabilised and labelled with antibodies against TnI and HA, which were then fluorescently labelled with goat anti-rabbit AlexaFluor® 633 and goat anti-mouse AlexaFluor® 488 respectively.

Finally, viral overexpression of TnI-HA proteins was confirmed in ARVM via immunoblotting (Figure 5.11). Adequate expression in ARVM required 10-fold higher doses of virus than HEK-293 cells or NRVM, with detection by immunoblotting for HA present at doses of 10^4-10^5 MOI for 24 hours.

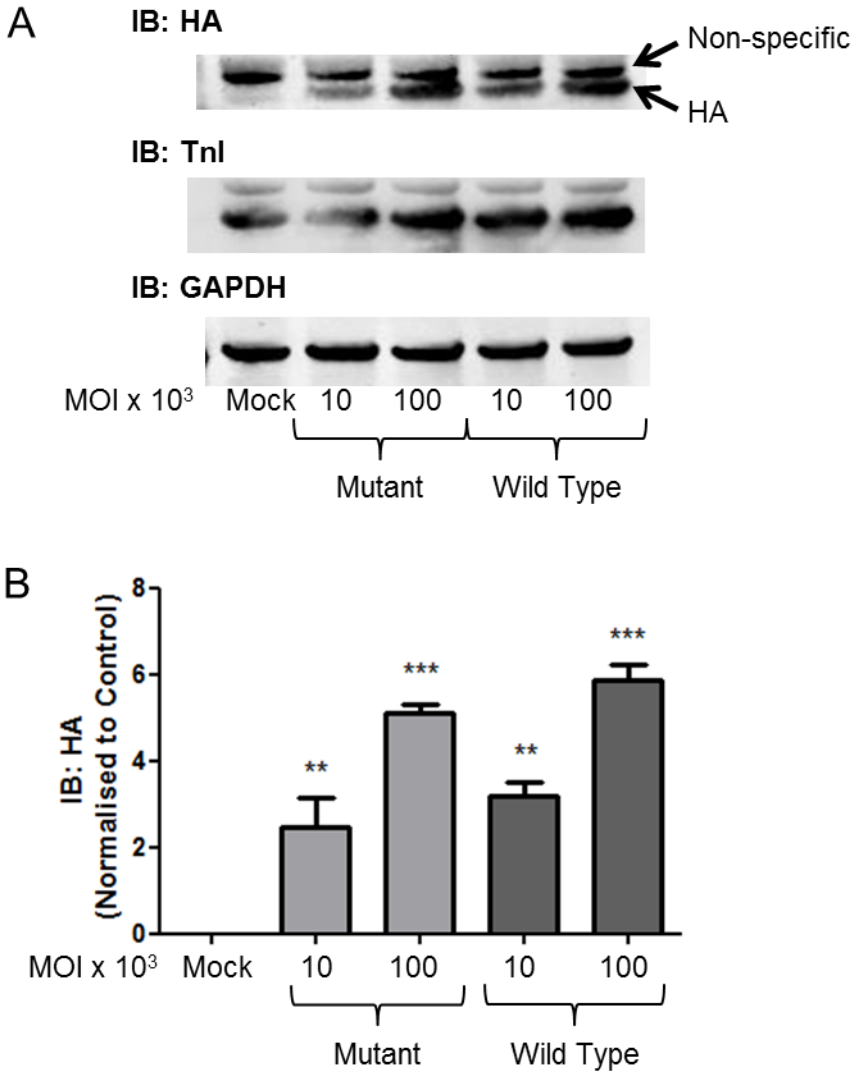

Figure 5.11: Confirmation of viral overexpression of TnI-HA in ARVM. ARVM were infected with viruses in doses increasing from 10^4-10^5 MOI for 24 hours prior to harvesting of cell lysates and analysis via immunoblotting. A. Representative example. B. Results represented as mean ± SEM, n=4. **=p<0.001, ***=p<0.001 vs. Mock, One-way-ANOVA with post hoc analysis: Tukey's multiple comparison test.

5.4.2 Analysis of half-life of TnI-HA proteins

To determine whether the ablation of TnI's SUMOylation motif resulted in changes in protein turnover, TnI-HA proteins were virally overexpressed in HEK-293 cells which were then treated with the protein synthesis inhibitor,

cyclohexamide (CHX) over an eight-hour time course. Cells were then harvested, and the level of TnI-HA protein expression was analysed by immunoblotting. Both TnI-HA MUT and TnI-HA WT had relatively short half-lives in HEK-293 cells; expression declined to ~40% of baseline expression following two hours of incubation with CHX. However, there were no significant differences between the turnover of TnI-HA MUT and TnI-HA WT (Figure 5.12). The levels of both proteins declined at comparable rates over the course of the eight-hour time course treatments.

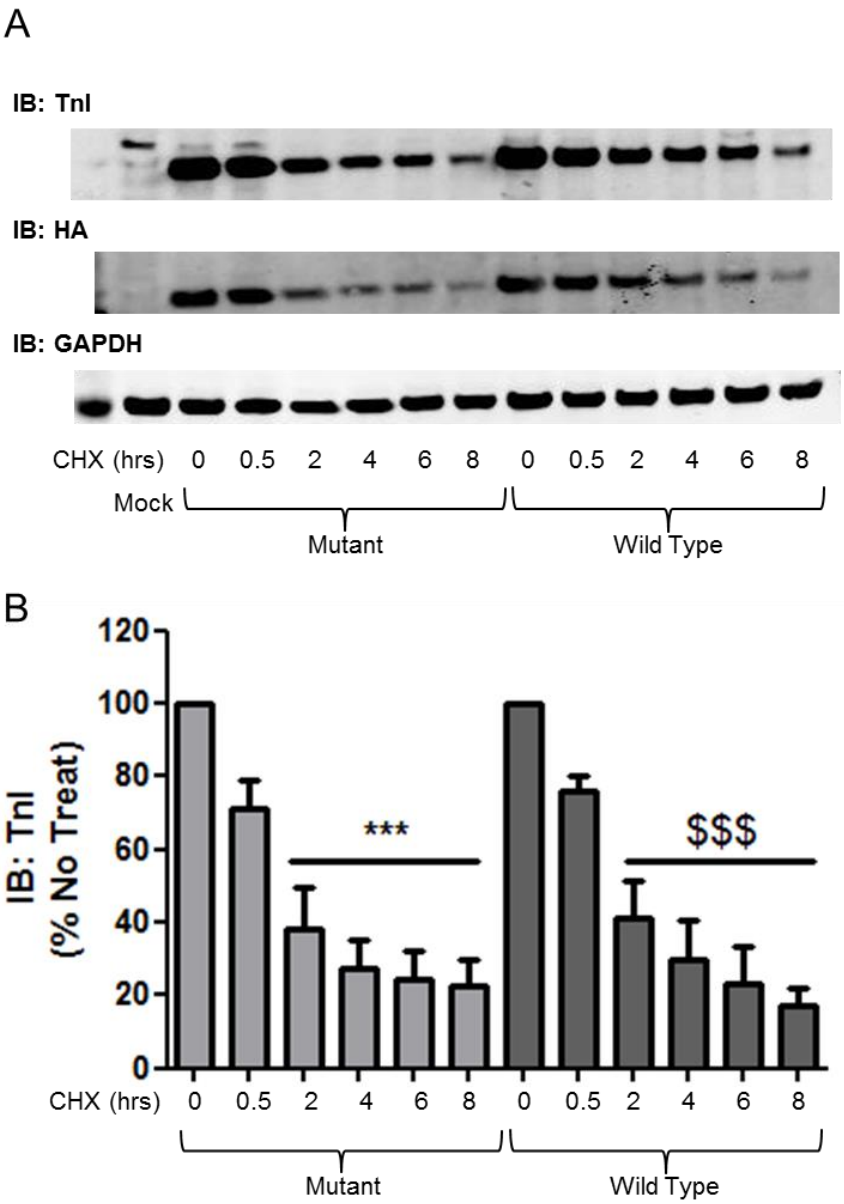

Figure 5.12: TnI-HA half-life is not affected by SUMOylation in HEK-293. HEK-293 cells overexpressing TnI-HA MUT or WT were treated with 50 µg/ml CHX to inhibit protein synthesis. Expression levels following treatments were determined by immunoblotting lysates for TnI and HA. A. Representative example. B. Results represented as mean ± SEM, n=4. ***=p<0.001 vs. Mutant 0 and ***=p<0.001 vs. WT 0, One-ANOVA with post hoc analysis: Tukey's multiple comparison test.

Although ablation of the SUMO motif did not affect protein turnover, HEK-293 cells overexpressing TnI-HA proteins were also treated with proteasome inhibitor, MG-132, to determine whether SUMOylation affects proteasomal degradation. Inhibition of the proteasome did not significantly affect the expression of TnI-HA proteins in HEK-293 cells (Figure 5.13). However, the inhibition did result in trend towards the accumulation of these proteins, suggesting that they had been spared from degradation. There were neither significant differences nor trends in the level of expression between TnI-HA MUT and TnI-HA WT following treatment, suggesting that SUMOylation at K177 does not interact functionally with the directing of TnI for proteasomal degradation.

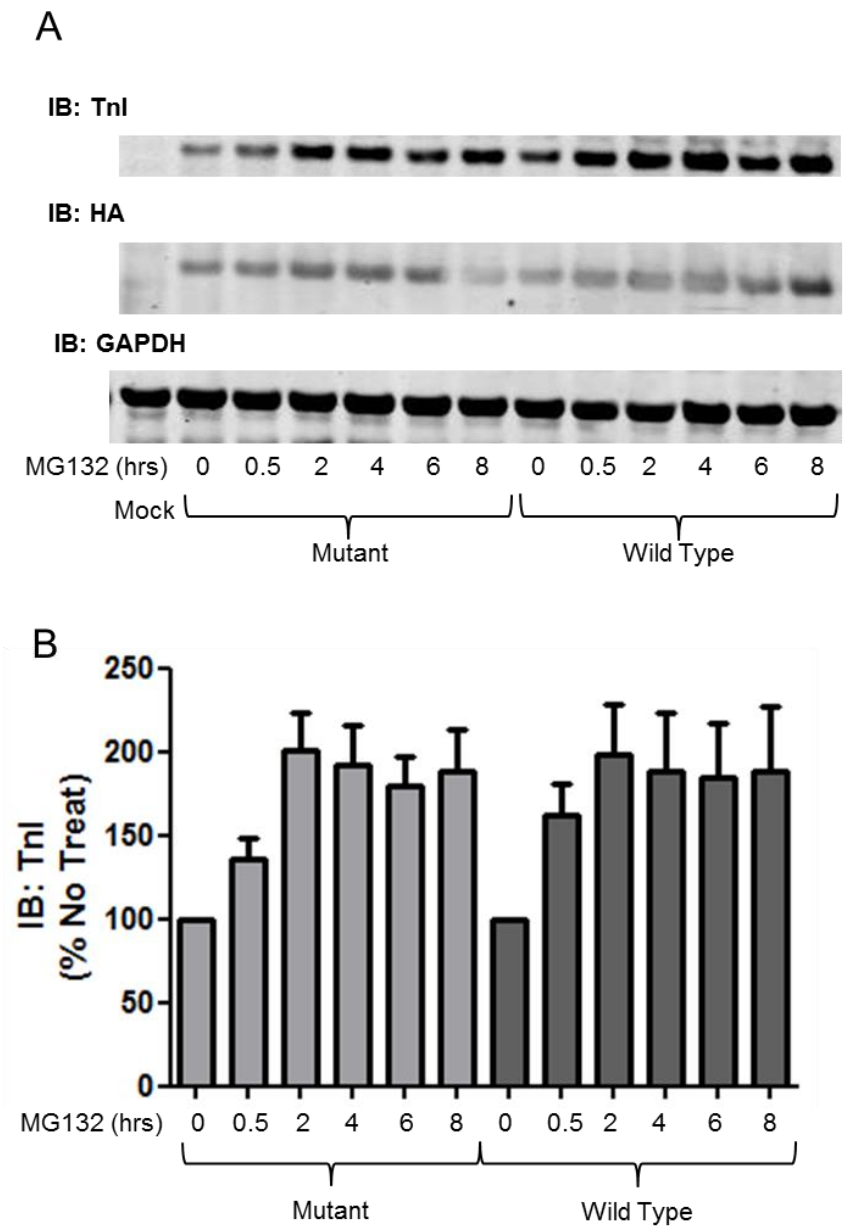

Figure 5.13: TnI-HA proteasomal degradation is not affected by SUMOylation in HEK-293. HEK-293 cells overexpressing TnI-HA MUT or WT were treated with 20 μM MG-132 to inhibit the proteasome. Expression levels following treatments were determined by immunoblotting lysates for TnI and HA. A. Representative example. B. Results represented as mean ± SEM, n=4. One-way-ANOVA with post hoc analysis: Tukey's multiple comparison test.

CHX and MG-132 time course treatment experiments were then repeated using NRVM overexpressing TnI-HA proteins as it was a much more representative biological system than the relatively simple environment of the HEK-293 cell. Inhibition of protein synthesis with CHX over an eight-hour time course did not result in a significant reduction of TnI expression compared to non-treated control samples (Figure 5.14). However, there was a trend towards decreased expression over the course of the treatments. This data suggests that the half-life of TnI-HA proteins in NRVM was longer than in HEK-293 cells. Perhaps the

localisation of the TnI-HA proteins to the myofilament resulted in increased stability. This observation highlighted the importance of using biologically relevant cells.

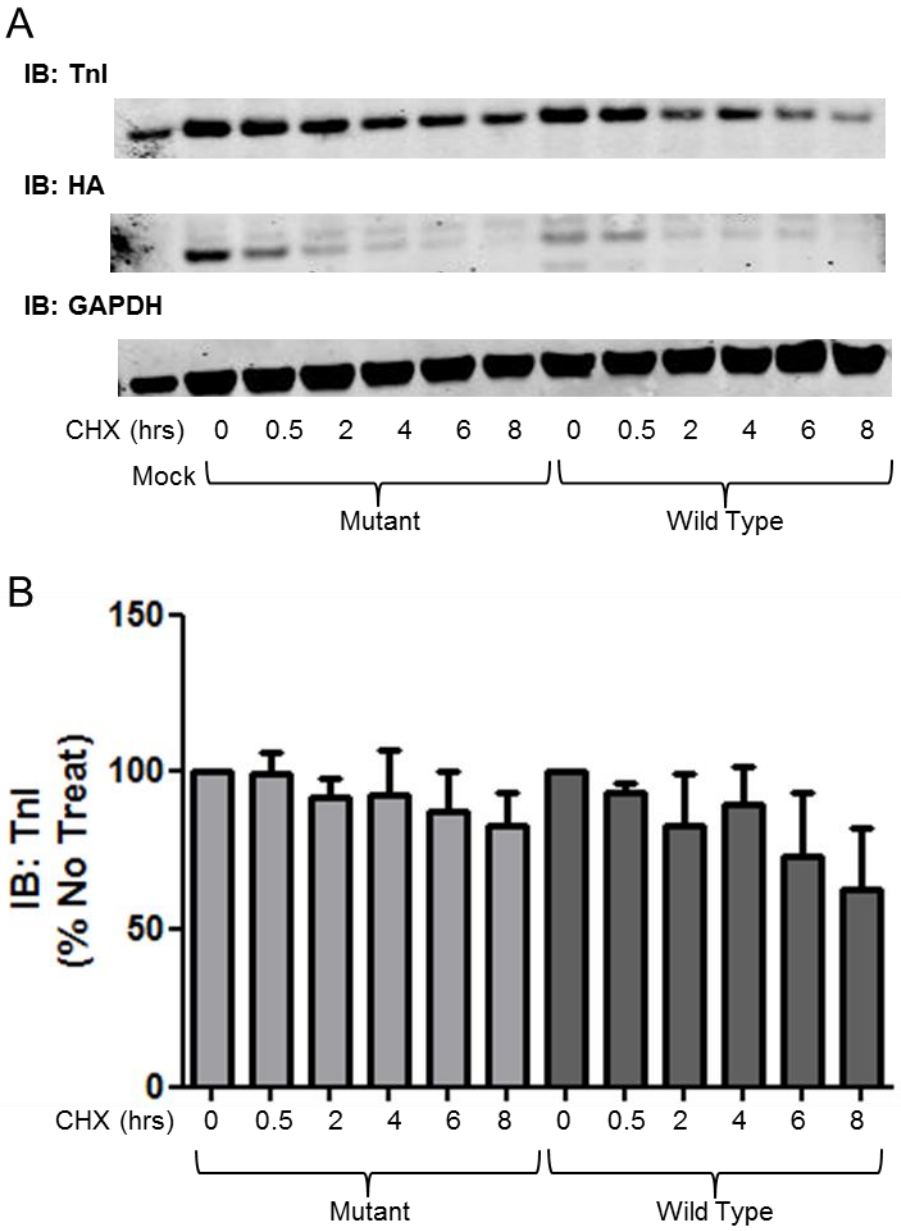

Figure 5.14: TnI half-life was not affected by SUMOylation in NRVM. NRVM overexpressing TnI-HA MUT or WT were treated with 50 µg/ml CHX to inhibit protein synthesis. Expression levels following treatments were determined by immunoblotting lysates for TnI and HA. A. Results represented as mean ± SEM, n=4. One-way-ANOVA with post hoc analysis: Tukey's multiple comparison test.

Inhibition of the proteasome using MG-132 did not cause any significant increases in TnI-HA expression in NRVM (Figure 5.15). However, there was trend towards increasing expression with increased time of MG-132 treatment for both TnI-HA

MUT and TnI-HA WT. The trend was for increased expression was similar between experimental groups, suggesting that SUMOylation state did not have any effect on proteasomal degradation.

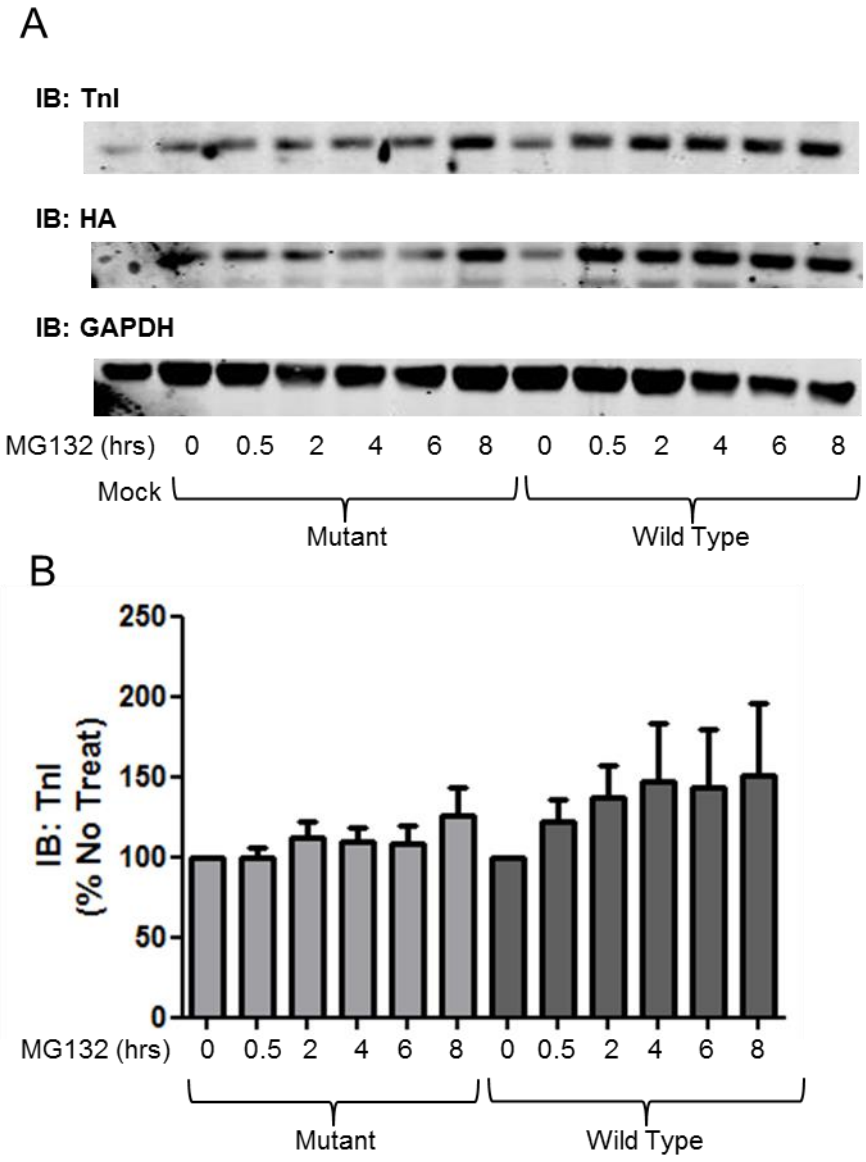

Figure 5.15: TnI-HA proteasomal degradation is not affected by SUMOylation in NRVM. NRVM overexpressing TnI-HA MUT or WT were treated with 20 μM MG-132 to inhibit the proteasome. Expression levels following treatments were determined by immunoblotting lysates for TnI and HA. A. Representative example. B. Results represented as mean ± SEM, n=4. One-way-ANOVA with post hoc analysis: Tukey's multiple comparison test.

5.4.3 SUMOylation of TnI does not affect cardiac myocyte contractility

To determine whether SUMOylation of TnI affected the contraction dynamics of cardiac myocytes, NRVM monolayers were infected with adenoviruses to

overexpress TnI-HA MUT and TnI-HA WT. Replacement of endogenous TnI with TnI-HA MUT, with the SUMOylation site ablated, and subsequent evaluation of contractile parameters would allow the functional effects of SUMOylation to be evaluated. Furthermore, these experiments were undertaken in cells which were paced at 1.2 Hz at baseline conditions as well as under conditions of β-adrenergic stimulation with 100 μM isoproterenol. As described in Section 5.3.1, image stacks of contracting NRVM monolayers were converted into contraction traces using MUSCLEMOTION software (Sala, van Meer et al. 2018). These traces were used to obtain measurements of several time-dependent contractile parameters which were used for comparisons, including interval, UP90, DOWN90 and CD50 (Figure 5.3).

Firstly, the interval, or the time between contractions, provides information on the rate of contraction. Of course, in these experiments, the monolayers were paced at 1.2 Hz, which resulted in consistent intervals between the different conditions. Nonetheless, it was important to include this measurement because NRVM monolayers were observed to have endogenous contractile activity. Therefore, it was necessary to ensure that the cells were conforming to the exogenous pacing so that meaningful comparisons could be made. The data revealed that the cells were paced successfully, with the intervals remaining highly consistent between groups (Figure 5.16A).

The second parameter that was analysed was UP90, which is the time from baseline to 90% of the peak contraction. This is often used as a measure of the time to contract. Interestingly, overexpression of TnI-HA, regardless of MUT or WT, caused a significant reduction in the time taken to reach 90% contraction (Figure 5.16B). This difference was only significantly different from mock for MUT MOI 10^3 and WT MOI 10^4; however, the trend towards a reduction in UP90 was present in all untreated, virally infected experimental groups. This was contrary to the hypothesis that TnI-HA overexpression would not have any effects on contraction, but rather on relaxation parameters. Isoproterenol treatment also caused a significant reduction in the UP90 in mock infected cells, which was consistent with the hypothesis that β-adrenergic stimulation would increase the speed of contraction. Again, there was a trend towards reduced UP90 in all experimental groups which were treated with isoproterenol.

Contrary to the hypothesis that TnI SUMOylation would result in lusitropic effects, there were no significant differences in the parameter measuring the time for relaxation (DOWN90) when cells were overexpressing TnI-HA proteins (Figure 5.16C). NRVM monolayers overexpressing TnI-HA MUT or WT took the same time to relax as mock samples, suggesting that SUMOylation at this site did not have any effect on relaxation at baseline or under conditions of ß-adrenergic stimulation. On the other hand, when cells were treated with isoproterenol, there was a trend towards a positive lusitropic effect in all experimental groups, which was consistent with the hypothesis that ß-adrenergic stimulation would enhance the speed of relaxation of the cells.

The final parameter, contraction duration 50 (CD50) measured the time from 50% upstroke to 50% downstroke, taking both contraction and relaxation into account. Viral overexpression of TnI-HA proteins did not significantly affect the CD50, despite a trend towards a reduced duration (Figure 5.16D). This most likely reflected the increased speed of contraction as displayed by UP90 data. Finally, consistent with data from other parameters, ß-adrenergic stimulation with isoproterenol caused a decrease in the contraction duration in mock cells. Increased speed of both contraction and relaxation likely contributed to this observation.

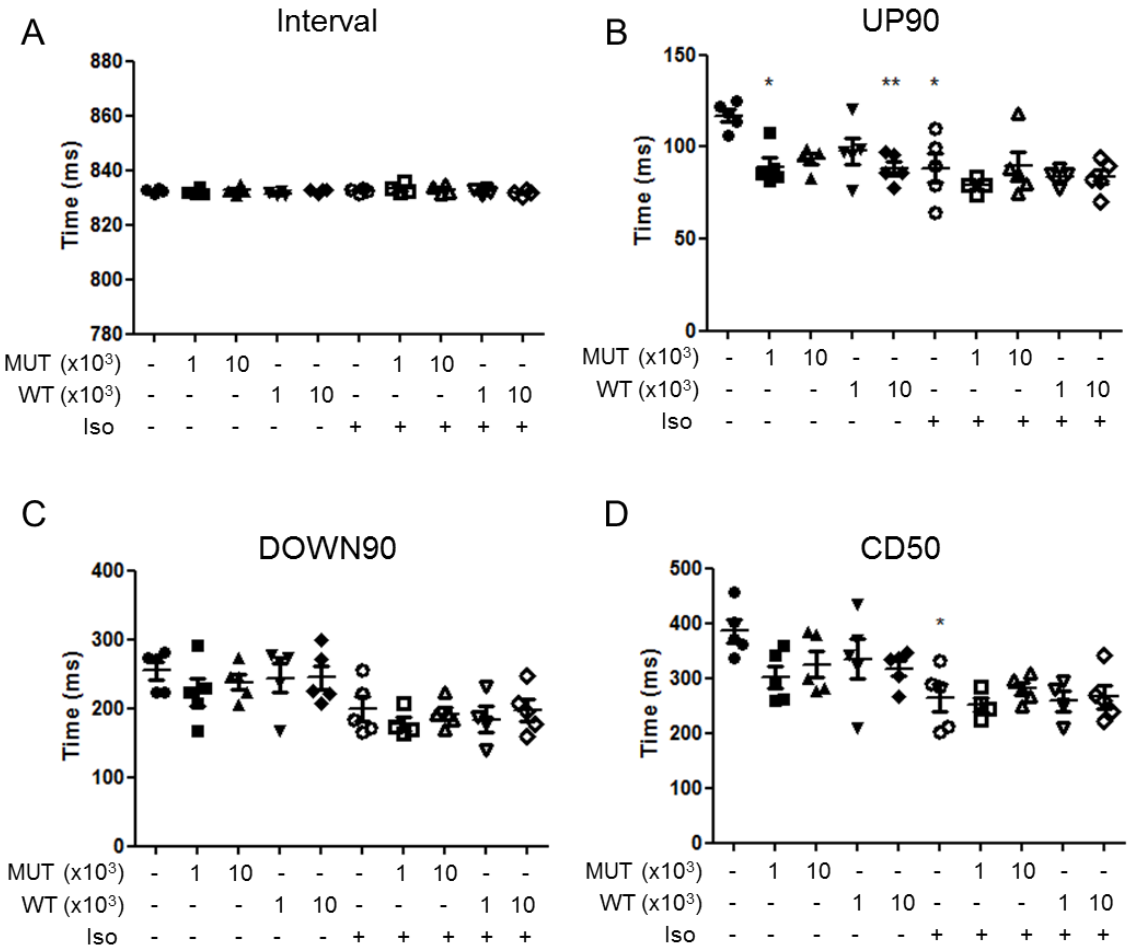

Figure 5.16: Ablation of TnI SUMOylation does not affect NRVM contractility. Using CellOPTIQ®, NRVM monolayers were subjected to pacing at 1.2 Hz and images were captured at a rate of 100 frames per second for eight seconds. The image stacks were analysed using the ImageJ plug-in, MUSCLEMOTION, to create contractility traces. Traces were then analysed for several time-dependent contractility parameters. Each sample was measured at baseline and following 10 minutes of 100 nM isoproterenol stimulation. A. Interval, or the time between contractions, confirms that the NRVM monolayers conformed to exogenous pacing. B. UP90, the time from baseline to 90% of peak upstroke, is a measure of the time to contract. C. DOWN90, the time from 90% contraction after the peak back down to baseline, is a measure of the time to relax. D. CD50, the time from 50% upstroke to 50% downstroke, takes both contraction and relaxation into account. Each data point is representative of the mean value from one experimental day, n=5 experimental days. Each mean value was calculated from 6-10 recordings of 8-10 contractions per condition. *=p<0.05 vs. Mock and **=p<0.01 vs. Mock, One-way-ANOVA with post hoc analysis: Tukey's multiple comparison test.

5.4.4 SUMOylation of TnI affects myofilament calcium sensitivity

Although contractility analysis did not show any significant differences associated with SUMOylation, it was necessary to pursue other functional studies due to technical limitations associated with the analysis of contractile dynamics of intact NRVM. Analysis of the calcium sensitivity and force of contraction of skinned muscle fibres would eliminate the confounding variables of Ca^{2+}

signalling in intact myocytes which could have masked differences caused by changes in myofilament properties. In many studies investigating the role of TnI phosphorylation, skinned muscle fibres have been analysed in this way (van der Velden, Boontje et al. 2002, van der Velden, Merkus et al. 2004).

Contrary to the hypothesis, there were no significant differences between the Ca^{2+} sensitivity of the myofilament in ARVM virally overexpressing TnI-HA MUT (Figure 5.17). This data suggested that at baseline, SUMOylation had no effect on Ca^{2+} sensitivity of the myofilament. These experiments were also completed in samples which had been incubated with N106 (10 μm; 24 hours) to globally upregulate SUMOylation. It was hypothesised that the upregulation of SUMOylation would affect the Ca^{2+} sensitivity of the myofilament in cells containing TnI-HA WT, but not cells overexpressing TnI-HA MUT. Paradoxically, Ca^{2+} sensitivity was significantly increased in ARVM expressing mutant unSUMOylatable TnI in which SUMOylation had been upregulated.

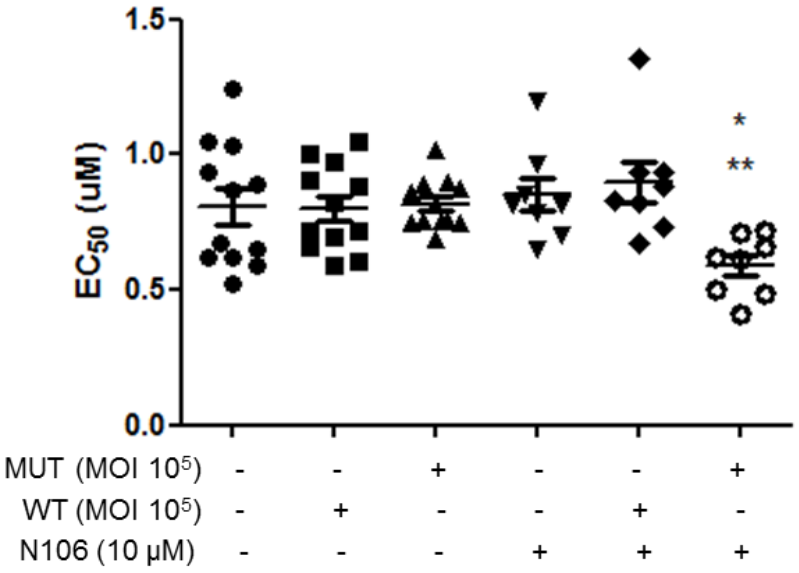

Figure 5.17: Ca^{2+} sensitivity of myofilaments affected by expression of mutant TnI and upregulation of SUMOylation with N106. ARVM virally overexpressing TnI-HA WT or MUT were incubated with N106 for 24 hours and skinned. Single cell force measurements were taken and analysed to determine Ca^{2+} sensitivity, expressed as EC_{50}, or the $[Ca^{2+}]$ resulting in half maximal force. Overexpression of mutant or wildtype TnI did not affect Ca^{2+} sensitivity in skinned ARVM. N106 treatment significantly decreased the EC50 in cells overexpressing mutant unSUMOylatable TnI. Results represented as mean ± SEM, n=12 cells from 3 isolations for untreated samples; n=8 cells from 2 isolations for N106 treated samples. *=p<0.05 vs. Mock + N106 and **=p<0.01 vs. WT + N106, One-way-ANOVA with post hoc analysis: Tukey's multiple comparison test.

When the maximum force (F_{max}) was compared between conditions, no significant differences were observed, suggesting that SUMOylation did not

affect the development of force in response to Ca^{2+} in the skinned cells (Figure 5.18A). The passive force ($F_{Passive}$) of the cells was also measured at a sarcomere length of 2.2 µm. When cells were stretched, they exerted tension against the force transducer. Therefore, a comparison of the tension at the stretched sarcomere length of 2.2 µm to the tension when the myocyte had been slacked allowed a measurement of $F_{Passive}$. There were no significant differences in $F_{Passive}$ due to expression of TnI-HA proteins or upregulation of SUMOylation (Figure 5.18B).

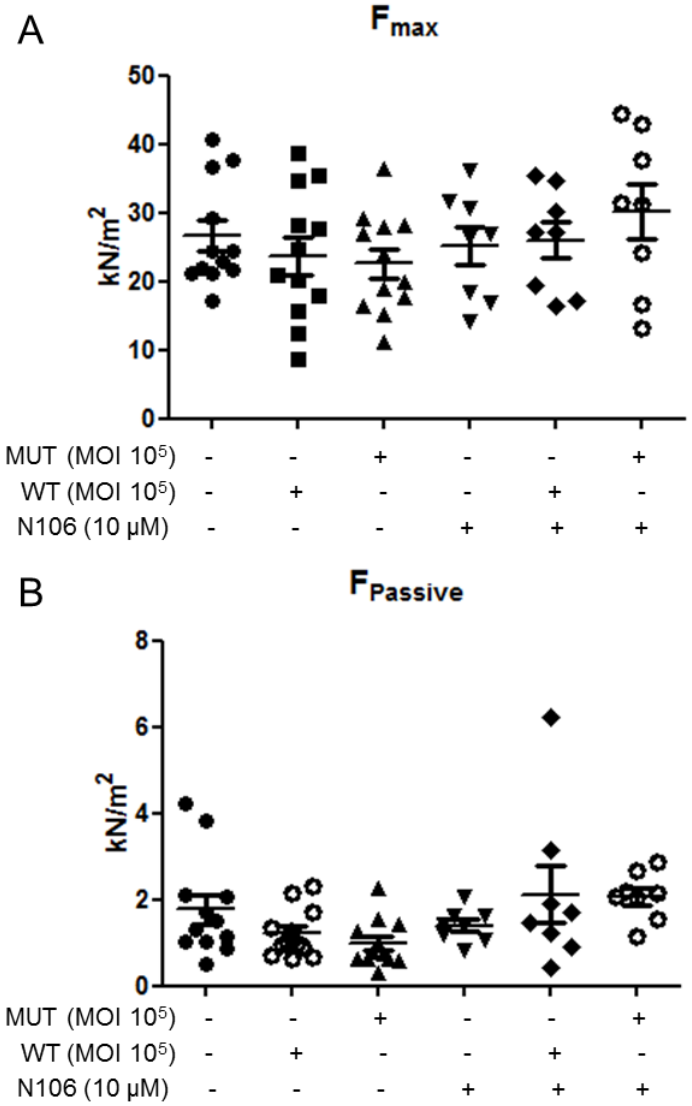

Figure 5.18: SUMOylation does not alter passive or maximum force in skinned ARVM. Neither overexpression of TnI-HA proteins nor upregulation of SUMOylation with N106 altered the maximum or passive force. Results represented as mean ± SEM, n=12 cells from 3 isolations for untreated samples; n=8 cells from 2 isolations for N106 treated samples. One-way-ANOVA with post hoc analysis: Tukey's multiple comparison test.

The final parameter collected from skinned ARVM experiments was the Hill Slope (Figure 5.19). The hill slope is a measure of the steepness of the dose response curve for Ca^{2+} and force. Biologically, this translates to a measure of the cooperativity of binding. In the context of TnI, a reduced hill slope is indicative of reduced cooperativity of interacting TnI units and the recruitment of the next cross-bridging activity of the myofilament. Interestingly, upregulation of SUMOylation with N106 caused a significant reduction in the hill slope in mock, endogenously expressing cells and in cells overexpressing TnI-HA MUT. In these groups, there would be reduced cooperativity of crossbridging. This was contrary to the hypothesis that upregulation of SUMOylation would significantly alter the functional dynamics of myofilaments containing endogenously expressed TnI and TnI-HA WT, but not of myofilaments expressing TnI-HA MUT.

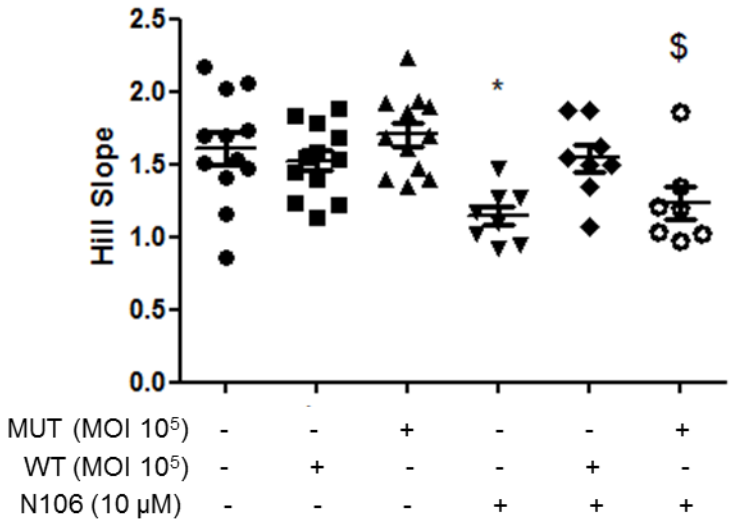

Figure 5.19: Upregulation of SUMOylation with N106 reduces the cooperativity of Ca^{2+} binding in mock cells and cells overexpressing TnI-HA MUT. Results represented as mean ± SEM, n=12 cells from 3 isolations for untreated samples; n=8 cells from 2 isolations for N106 treated samples. *=p<0.05 vs. Mock and $=p<0.05 vs. MUT, One-way-ANOVA with post hoc analysis: Tukey's multiple comparison test.

5.5 Discussion

5.5.1 Ablation of TnI SUMOylation site does not affect TnI stability or myocyte contraction

Mutation of the SUMOylation site of TnI did not have any significant effects on the stability of TnI-HA proteins in HEK-293 cells or NRVM. In both cell types, TnI-HA expression decreased at similar rates following inhibition of protein synthesis with CHX regardless of the presence of the SUMO site mutation. Interestingly, TnI-HA was much more stable in NRVM than in HEK-293 cells. HEK-293 cells lack a myofilament, meaning that overexpressed TnI-HA proteins were likely cytosolic. In NRVM, however, TnI-HA localised to the myofilament (Figure 5.10). It is possible that the localisation within the myofilament and the interactions with other parts of the Tn complex and the rest of the thin filament stabilised TnI-HA.

Similarly, the mutation caused no difference in the effect of proteasome inhibition with MG-132. In fact, there were no significant effects of MG-132 treatment on TnI-HA expression. These findings suggested that TnI is not degraded by the proteasome. Although it has been observed that TnI can be ubiquitinated, which usually targets a protein for proteasomal degradation, it has not yet been shown that TnI is degraded through the ubiquitin proteasome system (Witt, Granzier et al. 2005). This biological explanation for the lack of MG-132 activity on TnI expression is consistent with the observed activity of calpains in the proteolytic cleavage and degradation of TnI (Di Lisa, De Tullio et al. 1995, Wijnker, Li et al. 2015). It would be interesting to determine the effects of calpain inhibition on the expression of TnI-HA proteins which cannot be SUMOylated. Additionally, treatments with cyclohexamide, MG-132 and calpain inhibitors should be done in combination with N106 to globally upregulate SUMOylation in cells expressing TnI-HA proteins. It is possible that TnI can be SUMOylated, but that the cellular conditions for this modification to occur are not being replicated experimentally. For example, SUMOylation of the ß-adrenergic receptor occurs in response to stimulation with the agonist, isoproterenol (Wills 2017). The cellular conditions in which TnI SUMOylation is upregulated is not yet established; therefore, global upregulation of the SUMOylation cascade with N106 would allow any differences in protein stability to be determined.

As little is currently known about the ways in which TnI is degraded, it would be useful to determine the routes by which degradation occurs. This study suggests that ubiquitin proteasomes may not have a role, but did not determine whether lysosomal degradation is relevant for TnI. Treatment with lysosome inhibitor, chloroquine, and subsequent analysis of protein expression would show whether TnI is degraded in this way.

The ablation of SUMOylation also did not have an effect on the contraction of NRVM monolayers. Interestingly, overexpression of TnI-HA, regardless of the mutation, significantly decreased the time for contraction (UP90). This was contrary to the hypothesis that overexpression of TnI would exert an inhibitory effect on contraction due to its function as the inhibitory subunit of the Tn complex. It is possible that the fusion of the HA tag onto the C-terminal end of TnI impaired its function, leading to an enhanced speed of contraction by the removal of an inhibitory influence. However, the lack of effect of TnI overexpression on relaxation suggests that the overexpressed protein functioned as normal within the cell monolayers. ß-adrenergic stimulation caused a trend for quicker contraction and relaxation, suggesting a positive inotropic and lusitropic effect of the treatment. This was consistent with the established effects of ß-adrenergic stimulation in the literature and the known physiological effects of increased sympathetic stimulation of the heart (Bers 2002).

The observed trends in response to isoproterenol added a layer of confidence to the ability of the imaging and analysis protocols to detect differences in the contractility parameters included here; however, the lack of significant effects suggest that the experimental numbers could have been increased to enhance detection of significant differences between groups. Only limited experimental conditions were included in the present work. Cells were analysed either at baseline or after ß-adrenergic stimulation. SUMOylation has been known to occur at very low levels in cells (Jakobs, Koehnke et al. 2007), and certain stimulations, conditions or cellular stresses may be necessary to cause levels of SUMOylation sufficient for functional effects to be observed. Similarly to protein expression experiments, it would be useful to repeat these experiments in the presence of N106 in case experimental conditions are not optimally replicating the *in vivo* situation in which SUMOylation occurs.

It is also a possibility that the SUMOylation of TnI functions separately from myofilament function. A study in drosophila has shown that TnI has an important function in non-muscle cells, as a regulator of chromosomal stability and cell polarity in the context of early embryogenesis (Sahota, Grau et al. 2009). TnI was identified in the nucleus of S2 cells (drosophila embryonic stable cell line) and the mechanism of nuclear transport was investigated. It was determined that K262 was SUMOylated due to the presence of SUMO in TnI immunoprecipitates. Mutation of the putative SUMOylation site eliminated TnI translocation to the nucleus, confirming the role of SUMOylation in this process. The scope of this study to explain the role of TnI SUMOylation in mammals is limited by the low sequence similarities between drosophila and human TnI. In fact, drosophila have only one TnI isoform from a single gene while mammals express three isoforms from three separate genes (*TNNI1* or slow skeletal, *TNNI2* or fast skeletal and *TNNI3* or cardiac). Comparison between mammalian cardiac TnI and drosophila TnI using UniProt's Alignment tool revealed only a 22% sequence identity. For full alignment results see the appendix of this thesis (Appendix 7.1). Furthermore, the putative mammalian TnI SUMO site identified in the present work (K177) is conserved within a similar motif in drosophila, but this was not the site that was functionally relevant in the drosophila study. Experiments investigating the role of TnI SUMOylation in mammalian embryogenesis and chromosomal stability were beyond the scope of the current project, which focussed entirely on the myofilament function of TnI and employed the use of mammalian cells and tissues.

5.5.2 Upregulation of SUMOylation affects myofilament function

The force development in response to Ca^{2+} was measured in skinned ARVM to observe myofilament function in the absence of Ca^{2+} signalling. The results from these experiments were not consistent with the hypotheses and therefore, it was difficult to explain some of the trends in the data. Myofilament force was not affected by TnI-HA overexpression or upregulation of SUMOylation with N106. Paradoxically, the calcium sensitivity of the myofilaments overexpressing unSUMOylatable TnI was increased when SUMOylation was upregulated. Assuming that this was not an experimental artefact, this data suggests that upregulation of SUMOylation was having a functional effect that did not involve SUMOylation of K177 of TnI. Somewhat consistent with this data, the cooperativity of TnI's

activity was decreased in response to N106 in cells with endogenous TnI and unSUMOylatable TnI (Figure 5.19).

It is important to note that across all groups, the skinned myocytes were unusually sensitive to Ca^{2+}. In fact, the range of pCa^{2+} used for measurements was slightly altered to include activating solutions with lower [Ca^{2+}] than is typically used this protocol. In the experiments performed for the present work, activating solutions with pCa^{2+} values between 5.0 and 6.8 were used to produce complete dose-response curves. These had a lower range of Ca^{2+} concentrations compared to a range of 4.5 to 6.4 in normal experimental protocols used mainly to analyse skinned myofilaments derived from human cardiac samples (van der Velden, Klein et al. 1998, van der Velden, Boontje et al. 2002). Furthermore, the mean EC_{50} values measured for all experimental groups were substantially lower than the established value of approximately 1 uM Ca^{2+} (pCa^{2+} 6) (Chung, Biesiadecki et al. 2016). It is likely the unusually high Ca^{2+} sensitivity was due to low baseline phosphorylation of TnI; TnI phosphorylation at Ser22/23 causes reduced Ca^{2+} sensitivity (Zhang, Zhao et al. 1995). The depletion of baseline phosphorylation could have been caused by extended period of time (48 hrs) in culture following isolation, which would have made these cells unrepresentative of the biological situation.

It is possible that SUMOylation of TnI at K177 sequesters SUMO away from other sites which may be more functionally relevant at the myofilament. If K177 of TnI had a large propensity for SUMO conjugation, but not a significant functional effect on its own, it could sequester SUMO proteins away from other functionally relevant SUMO targets of the myofilament. Therefore, when TnI's SUMO site was ablated by overexpression of TnI-HA MUT, this sequestering effect was removed, increasing SUMOylation of other unknown myofilament targets and affecting functional dynamics. In the case of the Hill Slope data, overexpression of TnI-HA WT eliminated the functional effect of N106 treatment. This could be explained by increased sequestering of SUMO due to more K177 sites, thereby reducing the functional effect caused by the SUMOylation of other myofilament targets. Of course, further experiments would be necessary to understand the mechanism underlying these observations; if experimentally confirmed, this would be the first indication of a sequestering action of a SUMOylation target.

5.5.3 Methodological considerations

There are several methodological considerations which limit the conclusions which can be made from the presently described data.

Firstly, TnI-HA proteins appear to have different half-lives if analysed in HEK-293 cells compared to NRVM. It is possible that the localisation of TnI to the myofilament stabilised TnI; in HEK-293 cells, with no myofilament, TnI was cytosolic and perhaps more readily available for degradation. Particularly in experiments using NRVM, the treatment times may have been too short to elicit significant results of the treatments. The data were contrary to the hypothesis that inhibition of protein synthesis would have no significant effects on TnI-HA expression, and this could be explained by a limited efficacy of the drug in NRVM and/or a necessity for longer incubation times to reveal reduced expression levels.

CellOPTIQ® is a powerful tool for the analysis of contraction dynamics in live cells. Combined with the analysis program, MUSCLEMOTION, the high-speed image stacks acquired using the CellOPTIQ® systems could be analysed into contractility traces from which a number of parameters were analysed. This analysis method has been used previously for a wide range of contracting biological samples, from isolated single adult cardiac myocytes, to monolayers of human pluripotent stem cell-derived cardiac myocytes (hPSC-CMs), to three-dimensional contractile tissues such as engineered heart tissues, or cardiac “organoids” (Sala, van Meer et al. 2018). The systems had never before been used for monolayers of NRVM as in the present study. There were several potential issues which were expected before undertaking this part of the project. Firstly, unlike isolated adult ventricular myocytes, NRVM, especially when arranged in monolayers, have intrinsic contractile activity. This was expected to interfere with the pacing of the monolayers. However, when the intervals between contractions were measured and analysed, it was determined that the pacing was highly successful and consistent between experimental conditions and different experimental days. The exogenous electrical pacing was able to overcome the intrinsic contractile activity of the NRVM monolayers. Secondly, the sarcomeres of NRVM are much less organised than the sarcomeres of isolated adult cardiac myocytes, which are arranged along a single axis. However, the

analysis software's optimisation for contraction of hPSC-CM monolayers probably aided its ability to analyse the contraction of NRVM monolayers. Despite initial concerns about compatibility, there were no issues encountered with the analysis of contractility traces. Furthermore, the significant effects of ß-adrenergic stimulation on the speed of contraction and relaxation and the reduction of contraction duration were consistent with the hypothesis. This added confidence to the use of this technique to detect differences in contractile dynamics in NRVM monolayers.

To investigate the properties of the myofilament alone, without the confounding effects of Ca^{2+} signalling, skinned ARVM were analysed in collaboration with the van der Velden Lab at VUmc Amsterdam. The force developed in response to exposure to various Ca^{2+} concentrations was measured and analysed to determine Ca^{2+} sensitivity of the myofilament. There were several limitations associated with the use of this approach that must be taken into account when interpreting the resulting data. Firstly, this approach involved the analysis of single cells, which were selected for analysis on the basis of size and clear visualisation of striations. There was no way to confirm that the chosen cell had taken up the adenovirus and was adequately overexpressing the TnI-HA protein. Although western blot analysis revealed that the virally expressed proteins were present in the cell samples as a whole, this could not be confirmed at the single cell level. Therefore, if viral infection rate was not 100%, there is a chance that some cells analysed in TnI-HA overexpressing groups may not have overexpressed the viral proteins. Secondly, due to time constraints, the N106 treated groups contain only eight cells from two isolations. For an adequately powered study, it would be necessary to cells from at least three separate isolations. With increased numbers, each cell could be considered as a separate data point, or alternatively, single data points could be produced by calculating the mean of all cells from a single isolation. Finally, it is possible that the functional effects observed could have been due to overexpression of TnI-HA regardless of the mutation or due to an interference of the HA tag with TnI's normal function. In some of the data, for example the trends in $F_{Passive}$ data (Figure 5.18) suggested that TnI overexpression itself results in functional changes in the passive force, rather than the introduction of the mutated SUMOylation site. However, this claim was not supported by statistical significance. Similarly, these observed

trends could be explained by the addition of the HA tag to the protein. The possibility that a tag would alter the protein's functional properties was reduced by the use of the HA-tag, which is only 4.3 kDa, compared to a larger tag, such as GFP, which is 26.9 kDa. However, this had some implications for the design of the study, as GFP tagging would have allowed the confirmation of overexpressed proteins in individual cells.

5.5.4 Conclusions

In conclusion, TnI SUMOylation at K177 was not determined to have consistent functional effects at the myofilament or on TnI stability. However, it may have a sequestering effect, out-competing SUMOylation of other myofilament targets. Additional work is required to characterise the molecular routes which underpin the physiology to explain these findings.

Chapter 6 Discussion

6.1 Background

TnI is the inhibitory subunit of the troponin complex of the myofilament (Bers 2002). The study of post-translational modifications of TnI has been ongoing for several decades, but has focussed mainly on the protein's various phosphorylation sites (Layland, Solaro et al. 2005). Specifically, phosphorylation of the dual serine site Ser23/24 has been shown to contribute to the ß-adrenergic stimulation induced positive lusitropy and inotropy, enhancing cardiac contractility (Zhang, Zhao et al. 1995, Fentzke, Buck et al. 1999, Pi, Kemnitz et al. 2002, Pi, Zhang et al. 2003). Phosphorylation of this site has been shown to be reduced in chronic heart disease, prompting investigation of the functional role of this modification (Bodor, Oakeley et al. 1997, Zakhary, Moravec et al. 1999). Many PKA mediated phosphorylation events of cardiac excitation-contraction coupling proteins have been shown to be regulated by PDE isoforms which are tethered to specific signalosomes (Maurice, Ke et al. 2014). Previous work identified PDE4D9 as a regulator of Ser23/24 phosphorylation via direct interaction with TnI (Edwards 2012).

Very little is known about other post-translational modifications of TnI. In the available literature, there are some indications that TnI can be ubiquitinated (Witt, Granzier et al. 2005, Sahota, Grau et al. 2009). It has not been established whether mammalian TnI can be SUMOylated, and whether this has any functionally relevant effects in cardiac myocytes. Previously, it has been shown that drosophila TnI can be SUMOylated, but low sequence conservation limits the translatability of this research to mammals (Sahota, Grau et al. 2009). SUMOylation has been shown to induce a variety of functional effects depending on the target protein, including changes in protein stability or cellular location and modulation of other post-translational modifications (Ulrich 2009).

6.2 PDEs and the myofilament

The first aims of the present work involved investigation of the proposed TnI-PDE4D9 interaction and its disruption using a custom-designed cell permeable peptide.

Interestingly, the data directly contradict previous evidence that PDE4D9 interacts with TnI thereby regulating PKA phosphorylation of Ser23/24. In fact, none of the data supported the hypothesis that PDE4 regulates this phosphorylation event despite convincing evidence in previously published work (Edwards 2012). The reason for the discrepancies between previously published data and the data displayed here is unknown. It is possible that technical challenges prevented previous findings from being replicated. Numerous signalosomes containing cardiac excitation-contraction coupling proteins, which can be phosphorylated by PKA have been shown to contain specific PDE isoforms (Maurice, Ke et al. 2014). In these signalosomes, PDE isoforms regulate the phosphorylation of the targets in a specific, non-redundant manner. For example, PDE4D3 has been shown to be present within the RyR signalosome, regulating its phosphorylation and activity (Lehnart, Wehrens et al. 2005). PDE4D deficient mice had marked signalling and pathophysiological changes despite normal global cAMP signalling; this highlights the essential, non-compensated role of PDE4D at this cellular compartment. Similarly, in the LTCC signalosome, both PDE4B and PDE4D were detected, but only PDE4B was shown to functionally regulate Ca^{2+} current and channel activity (Leroy, Richter et al. 2011).

It is possible that this paradigm of specific isoform regulation via integration into a signalosome is not relevant in the context of TnI. Insight into PDE family roles at the myofilament may be gained from studies employing the use of family-specific inhibitors. Under basal conditions, PDE2 and PDE3 appear to be the functionally relevant isoforms governing Ca^{2+}, contractility and TnI phosphorylation in adult rat ventricular cardiac myocytes (Mika, Bobin et al. 2013). However, under submaximal ß-adrenergic stimulation, PDE4 had dominant functional effects on global excitation-contraction coupling. These observations suggest that different PDEs may have differential effects on signalling and even on the regulation of specific phosphorylation events depending on the physiological environment of the cell. If multiple, different PDE families or isoforms were involved in the regulation of TnI phosphorylation, this would help explain this work's inability to pinpoint a specific isoform.

Species differences in PDE isoform activity and expression levels are an important factor. In most of the published studies identifying PDE isoforms within cardiac signalosomes, rodent cells and tissues were used (Bolger, McCahill

et al. 2003, Lehnart, Wehrens et al. 2005, Terrenoire, Houslay et al. 2009, Beca, Helli et al. 2011, Leroy, Richter et al. 2011, Sin, Edwards et al. 2011). However, PDE family activity and expression is different in rodents than in large mammals and humans (Osadchii 2007, Richter, Xie et al. 2011). Although PDE4 expression is similar between humans and rodents, PDE4 affects global cAMP signalling only in rodents (Richter, Xie et al. 2011). Human PDE4 comprises a much smaller portion of the total cardiac PDE activity than it does in rodents. Taken together, this suggests that while PDE4 expression remains the same between species, its activity is reduced, representing a smaller proportion of total PDE activity in these cells. Clinical trial data supports the notion that PDE4 activity is less functionally relevant in the human heart. Treatment of psoriatic arthritis with non-specific PDE4 inhibitor, apremilast, caused no cardiac-specific off-target effects, despite global PDE4 inhibition (Perez-Aso, Montesinos et al. 2015, Schafer, Chen et al. 2015, Baillie, Tejeda et al. 2019). The presence of specific PDE4 isoforms in cardiac signalosomes has been shown predominantly using rodent models (Lehnart, Wehrens et al. 2005, Beca, Helli et al. 2011, Leroy, Richter et al. 2011, Sin, Edwards et al. 2011). For the most part, these interactions have not been confirmed using human cells or tissues due to tissue availability and technical challenges. One of the purposes of identifying PDE isoforms in signalosomes is to inform development of more specific therapeutic interventions in comparison to the readily available family-specific PDE inhibitors which can result in off-target effects. However, the species differences in PDE4 activity limit the translational and therapeutic potential of these studies. A recently published study using cardiac myocytes isolated from pigs represents a new direction in PDE research, whereby the model used is likely more representative of human cardiac physiology and protein biochemistry (Mika, Bobin et al. 2019).

6.3 Is SUMOylation of TnI protective?

The next set of aims were to characterise the SUMOylation of TnI. More specifically, thee aims were to determine whether TnI could be SUMOylated, whether this could be detected using a custom-designed SUMO-TnI antibody and whether the SUMOylation of TnI has a functional role at the myofilament.

The data displayed here is highly novel as it represents the first evidence that mammalian TnI can be SUMOylated. Although it is informative to determine whether a target protein can be SUMOylated using different biochemical methods to “force” the SUMOylation, it is then necessary to determine whether the target actually is SUMOylated *in vivo*. It is at this point that studies involving SUMOylation become technically challenging, as the modification often occurs in very small amounts, making it difficult to compare levels of SUMOylated and unSUMOylated proteins in different biological samples or under different biological conditions (Jakobs, Koehnke et al. 2007). The successful development and testing of a SUMO-TnI antibody recorded here is also highly novel as it represents the first antibody to detect a SUMOylated target protein at a specific and well-defined site. The development of this antibody represents a solution to a key technical challenge in the detection and measurement of SUMOylated substrate proteins. This approach could transform SUMOylation research in the same way that phospho-antibodies transformed for kinase research (Czernik, Girault et al. 1991). The SUMO-site antibody for TNI facilitated the measurement of SUMOylation in healthy and diseased human samples, showing the significant upregulation of modified TnI in chronic cardiac disease.

The functional relevance of TnI SUMOylation was then investigated using viral overexpression of TnI-HA proteins, which were mutated to eliminate the SUMOylated lysine (K177). These studies suggested that SUMOylation of TnI had limited effects on the myofilament, perhaps exerting a sequestering effect, out-competing other myofilament SUMOylation targets. Data collected from intact cells suggested that ablation of TnI SUMOylation did not have any effect on contractility of the cells. It is important to note that these studies were undertaken using NRVM, which do not have the same physiological or morphological characteristics as adult cardiac myocytes. Therefore, it is possible that changes in contractility were not observed due to the immature phenotype. The lack of functional effect of TnI SUMOylation in intact cells was consistent with conclusions drawn in previous studies highlighting the functional importance of SERCA2a SUMOylation. In small and large animal models of heart failure, the upregulation of SUMOylation using SUMO1 gene transfer or small molecule (N106) resulted in improved contractile function and attenuation of pathophysiological remodelling of the left ventricle (Tilemann, Lee et al. 2013,

Kho, Lee et al. 2015). However, these beneficial effects were eliminated in the absence of SERCA2a protein, suggesting that these effects were mediated largely through the SUMOylation of SERCA2a (Lee, Oh et al. 2016). Therefore, the data from the present work supports the dominant role of SERCA2a SUMOylation in the mechanism underlying the therapeutic effects of upregulation of SUMOylation. Although functional effects at the myofilament were observed when they were analysed in isolation, it is likely that these effects would not be problematic for the therapeutic strategy of upregulation of SUMOylation of SERCA2a.

In contrast to intact cell contractility data, experiments analysing myofilament dynamics in isolation showed that TnI SUMOylation had an effect on myofilament function and its response to Ca^{2+}. The observations from this study led to the hypothesis that TnI SUMOylation at K177 had a scavenging effect, whereby SUMO proteins were sequestered at this site. Therefore, when the SUMOylation site was ablated, alternative SUMOylation targets of the myofilament would be SUMOylated, resulting in the observed functional changes in Ca^{2+} sensitivity or cooperativity.

Little is known about other SUMOylation targets at the myofilament. Systematic review of proteomics screens which identified SUMOylation target proteins and target lysine residues compiled 3,617 proteins at 7,327 sites (Hendriks and Vertegaal 2016, Hendriks, Lyon et al. 2018). The vast majority of the proteins identified were nuclear, and therefore, had functions involving mRNA and DNA processing and replication (Hendriks and Vertegaal 2016). The database compiled within this study was then compared to a comprehensive list of cardiac myofilament protein isoforms identified using mass spectrometry (Kooij, Venkatraman et al. 2014). Surprisingly, the only myofilament protein identified as a SUMOylation target in the systematic review of proteomics studies was titin (Hendriks and Vertegaal 2016). Titin is a giant protein which connects the Z line to the M line of the sarcomere, providing elasticity and passive force to the myofilament. It was a rather confounding observation that TnI did not appear in the database of SUMOylation targets discovered by other researchers. However, this does not necessarily undermine the data displayed here, as another known SUMOylation target, $ß_2$-adrenergic receptor, was also not present in the proteomics screens, despite extensive evidence of its SUMOylation (Wills 2017).

Current evidence from ongoing investigations has also identified MyBP-C as a SUMOylation target (Main & Baillie, unpublished). It is conceivable that other myofilament proteins also could be SUMOylated, just in low levels that were not detected in proteomics studies. Furthermore, it is possible that SUMOylation of certain targets only occurs under specific physiological conditions (for example, β_2-adrenergic receptors have been shown to be SUMOylated following receptor stimulation with isoproterenol (Wills 2017)) which were not met in the samples screened for proteomics.

6.4 Interplay between PDE interaction and SUMOylation

The disruptor peptide which was hypothesised to 'unhinge' the interaction between TnI and PDE4D9 was designed based on the region of TnI to which the PDE was shown to bind in peptide array (Edwards 2012). The previous study identified a single amino acid of TnI, K177, as being essential for PDE binding. Of course, K177 is also the acceptor lysine for SUMOylation. Although the present work did not confirm that K177 is, in fact, necessary for PDE binding, some of the data in the present work indicated that the disruptor peptide effectively altered the cAMP dynamics at the myofilament. This suggested that the 25-amino acid segment of TnI surrounding K177, if not K177 itself, was functionally important for PDE binding. Therefore, it is possible that SUMOylation regulates the binding of PDEs to TnI. There is abundant precedent for SUMOylation to functionally affect a substrate protein by regulating its interactions with other proteins. Interestingly, SUMOylation has been shown to both positively and negatively modulate protein-protein interactions, by providing additional binding sites for the recruitment of the interactor or by blocking interaction sites respectively (Ulrich 2009). Recruitment of interacting proteins to a SUMOylated protein typically occurs via a SIM, which interacts non-covalently with the protein, tethering it to the substrate (Hannich, Lewis et al. 2005). For example, SIMs have been identified on some of the E3 ligases of the SUMOylation cascade; in fact, the presence of these motifs at the C-terminal end of the PIAS family proteins is necessary for their role in the SUMOylation cascade (Song, Durrin et al. 2004, Rytinki, Kaikkonen et al. 2009, Kaur, Park et al. 2017). In contrast, SUMOylation has been shown to inhibit substrate protein interactions. For example, SUMOylation of human thymine-DNA glycosylase (TDG) results in its dissociation from DNA by inducing a conformational change in the enzyme

(Steinacher and Schar 2005). Although this is an example of a protein-DNA interaction, it illustrates the mechanism by which SUMOylation affects the conformational change of a protein, thereby altering its interaction with other molecules. Further investigation is necessary to determine whether SUMOylation and PDE binding functionally interact due to the hypothesised sharing of a binding site. The present work did not confirm that PDE binding occurs at this site, but the possibility of the interaction should be considered in future study of the functional role of TnI SUMOylation.

6.5 Final Conclusions

Post-translational modifications of key cardiac signalling proteins are essential to their functional responses to cellular stimuli. Although the PKA phosphorylation of numerous cardiac signalling proteins have been shown to be regulated by localised PDE isoforms, the mechanism by which TnI's phosphorylation is regulated has not been established by this study. The data presented here suggest that the situation at the myofilament may be more complex than for other cardiac proteins. This has led to the development of a number of further hypotheses that should be tested in future studies, including they hypothesis that PDE regulation of TnI phosphorylation may involve different PDE families depending on cellular conditions. Furthermore, if technically feasible, studies involving PDEs would ideally take place using cells and tissues from large animal models, such as pigs, which have PDE activity profiles more similar to humans.

The work presented represents a major contribution of the field as it is the first to show that TnI can be modified by SUMOylation at K177. SUMOylated TnI was specifically detected using a custom antibody, which is one of the first to detect a SUMOylated substrate. The SUMO-specific antibody represents a major advance in the field, which has previously been marked by difficulties in detection of proteins which are SUMOylated in low levels. Interestingly, the SUMOylation of TnI did not have any functional effects on protein turnover nor on myofilament dynamics. Significant changes in TnI SUMOylation were also observed in diseased human samples. Although explanations have been provided for the pattern of effects observed, further investigation is required to determine the molecular mechanisms underlying these physiological observations.

Chapter 7 Appendix

7.1 Sequence alignment of human cardiac TnI and drosophila TnI

```
P19429 TNNI3_HUMAN          1   ------------------------------------MADGSSDAAREPRPAP--------        16
P36188 TNNI_DROME           1   MADDEKKAAAPAAAPAAAAKPAAPAAAPAANGKAAPAANGKAAPAAAAAPAGPPKDPNDP        60
                                                                    *:*.:  *    **

P19429 TNNI3_HUMAN         17   ------------APIRRRSSNYRAYAT---EPHAKKKSKISASRKLQLKTLLLQIAKQEL        61
P36188 TNNI_DROME          61   KVKAEEAKKAKQAEIERKRAEVRKRMEEASKAKKAKKGFMTPERKKKLRLLLLRKKAAEEL       120
                                     * *.*: :: *       : :  **. :: .** :*: ** : * :**

P19429 TNNI3_HUMAN         62   EREAEERRGEKGRALSTRCQ-PLELAGLGFAELQDLCRQLHARVDKVDEERYDIEAKVTK       120
P36188 TNNI_DROME         121   KKEQERKAAERRRIIEERCGSPRNLSDASEGELQEICEEYYERMYICEGQKWDLEYEVRK       180
                                ::* *.: .*: * :. **  * :*:. . .***::*.: : *:   : :::*:* :* *

P19429 TNNI3_HUMAN        121   NITEIADLTQKIFDLRGKFKRPTLRRVRISADAMMQALLGARAKESLDLRAHLKQVKKED       180
P36188 TNNI_DROME         181   KDWEINDLNAQVNDLRGKFVKPALKKVSKYENKFAKLQK---KAAEFNFRNQLKVVKKKE       237
                                :  ** **. :: ****** :*:*::*    : : :         .:::* :** ***::

P19429 TNNI3_HUMAN        181   TE---KENREVGDWRKNIDALSGMEGRKKKFES--                           210
P36188 TNNI_DROME         238   FTLEEEEKEKKPDWSKGKPGDAKV---KEEVEAEA                           269
                                    :*:.:  ** *.  . : :   *::.*:
```

Figure 7.1: Alignment of human cardiac TnI and drosophila TnI using UniProt Align Tool. Alignment revealed 22% sequence identity between the two proteins. * denotes a fully conserved amino acid; : denotes a different amino acid with strongly conserved properties; . denotes a different amino acid with weakly conserved properties.

7.2 *In silico* prediction of ubiquitination of TnI

>
MADGSSDAAREPRPAPAPIRRRSSNYRAYATEPHAKKKSKISASRKLQLKTLLLQIAKQELEREAEERRGEKGRALSTRC
QPLELAGLGFAELQDLCRQLHARVDKVDEERYDIEAKVTKNITEIADLTQKIFDLRGKFKRPTLRRVRISADAMMQALLG
ARAKESLDLRAHLKQVKKEDTEKENREVGDWRKNIDALSGMEGRKKKFES

Output:

Residue	Score	Ubiquitinated
36	0.13	No
37	0.13	No
38	0.13	No
40	0.11	No
46	0.15	No
50	0.21	No
58	0.72	Yes Medium confidence
72	0.73	Yes Medium confidence
106	0.53	No
117	0.42	No
120	0.35	No
131	0.28	No
138	0.05	No
140	0.03	No
164	0.61	No
174	0.56	No
177	0.63	Yes Low confidence
178	0.76	Yes Medium confidence
183	0.58	No
193	0.68	Yes Low confidence
205	0.54	No
206	0.52	No
207	0.08	No

Legend:

Label	Score range	Sensitivity	Specificity
Low confidence	0.62 ≤ s ≤ 0.69	0.464	0.903
Medium confidence	0.69 ≤ s ≤ 0.84	0.346	0.950
High confidence	0.84 ≤ s ≤ 1.00	0.197	0.989

Figure 7.2: Prediction of ubiquitination sites of TnI. Putative ubiquitination sites on TnI were predicted *in silico* using UbPred® as described in ((Radivojac, Vacic et al. 2010)

List of References

(SIGN), S. I. G. N. (2016). Management of chronic heart failure (SIGN publication no. 147). Edinburgh, SIGN.

Alcalay, Y., E. Hochhauser, V. Kliminski, J. Dick, M. A. Zahalka, D. Parnes, H. Schlesinger, Z. Abassi, A. Shainberg, R. F. Schindler, T. Brand and G. Kessler-Icekson (2013). "Popeye domain containing 1 (Popdc1/Bves) is a caveolae-associated protein involved in ischemia tolerance." PLoS One **8**(9): e71100.

Aldrich, S. (2019). "Solid Phase Synthesis." Retrieved 10 October, 2019.

Angel, T. E., U. K. Aryal, S. M. Hengel, E. S. Baker, R. T. Kelly, E. W. Robinson and R. D. Smith (2012). "Mass spectrometry-based proteomics: existing capabilities and future directions." Chem Soc Rev **41**(10): 3912-3928.

Anyanwu, A. C., C. A. Rogers, A. J. Murday and G. Steering (2002). "Intrathoracic organ transplantation in the United Kingdom 1995-99: results from the UK cardiothoracic transplant audit." Heart **87**(5): 449-454.

Ashrafian, H., C. Redwood, E. Blair and H. Watkins (2003). "Hypertrophic cardiomyopathy:a paradigm for myocardial energy depletion." Trends Genet **19**(5): 263-268.

Baillie, G. S. (2009). "Compartmentalized signalling: spatial regulation of cAMP by the action of compartmentalized phosphodiesterases." FEBS J **276**(7): 1790-1799.

Baillie, G. S., G. S. Tejeda and M. P. Kelly (2019). "Therapeutic targeting of 3',5'-cyclic nucleotide phosphodiesterases: inhibition and beyond." Nat Rev Drug Discov.

Barany, M. (1967). "ATPase activity of myosin correlated with speed of muscle shortening." J Gen Physiol **50**(6): Suppl:197-218.

Barefield, D. and S. Sadayappan (2010). "Phosphorylation and function of cardiac myosin binding protein-C in health and disease." J Mol Cell Cardiol **48**(5): 866-875.

Baryshnikova, O. K., M. X. Li and B. D. Sykes (2008). "Modulation of cardiac troponin C function by the cardiac-specific N-terminus of troponin I: influence of PKA phosphorylation and involvement in cardiomyopathies." J Mol Biol **375**(3): 735-751.

Bavishi, C., S. Chatterjee, S. Ather, D. Patel and F. H. Messerli (2015). "Beta-blockers in heart failure with preserved ejection fraction: a meta-analysis." Heart Fail Rev **20**(2): 193-201.

Beca, S., P. B. Helli, J. A. Simpson, D. Zhao, G. P. Farman, P. Jones, X. Tian, L. S. Wilson, F. Ahmad, S. R. W. Chen, M. A. Movsesian, V. Manganiello, D. H. Maurice, M. Conti and P. H. Backx (2011). "Phosphodiesterase 4D regulates baseline sarcoplasmic reticulum Ca2+ release and cardiac contractility, independently of L-type Ca2+ current." Circ Res **109**(9): 1024-1030.

Benarroch, E. E. (2013). "HCN channels: function and clinical implications." Neurology **80**(3): 304-310.

Bender, A. T. and J. A. Beavo (2006). "Cyclic nucleotide phosphodiesterases: molecular regulation to clinical use." Pharmacol Rev **58**(3): 488-520.

Berridge, M. J. (1984). "Inositol trisphosphate and diacylglycerol as second messengers." Biochem J **220**(2): 345-360.

Bers, D. M. (2002). "Cardiac excitation-contraction coupling." Nature **415**(6868): 198-205.

Blair, C. A., P. Haynes, S. G. Campbell, C. Chung, M. I. Mitov, D. Dennis, M. R. Bonnell, C. W. Hoopes, M. Guglin and K. S. Campbell (2016). "A Protocol for Collecting Human Cardiac Tissue for Research." VAD J **2**(1).

Blair, C. M., N. M. Walsh, B. H. Littman, F. W. Marcoux and G. S. Baillie (2019). "Targeting B-Raf inhibitor resistant melanoma with novel cell penetrating peptide disrupters of PDE8A - C-Raf." BMC Cancer **19**(1): 266.

Blumenthal, D. K., J. T. Stull and G. N. Gill (1978). "Phosphorylation of cardiac troponin by guanosine 3':5'-monophosphate-dependent protein kinase." J Biol Chem **253**(2): 324-326.

Bobin, P., M. Belacel-Ouari, I. Bedioune, L. Zhang, J. Leroy, V. Leblais, R. Fischmeister and G. Vandecasteele (2016). "Cyclic nucleotide phosphodiesterases in heart and vessels: A therapeutic perspective." Arch Cardiovasc Dis **109**(6-7): 431-443.

Bodor, G. S., A. E. Oakeley, P. D. Allen, D. L. Crimmins, J. H. Ladenson and P. A. Anderson (1997). "Troponin I phosphorylation in the normal and failing adult human heart." Circulation **96**(5): 1495-1500.

Bolger, G. B., A. McCahill, E. Huston, Y. F. Cheung, T. McSorley, G. S. Baillie and M. D. Houslay (2003). "The unique amino-terminal region of the PDE4D5 cAMP phosphodiesterase isoform confers preferential interaction with beta-arrestins." J Biol Chem **278**(49): 49230-49238.

Bos, J. L. (2006). "Epac proteins: multi-purpose cAMP targets." Trends Biochem Sci **31**(12): 680-686.

Bradford, M. M. (1976). "A rapid and sensitive method for the quantitation of microgram quantities of protein utilizing the principle of protein-dye binding." Anal Biochem **72**: 248-254.

Brand, T. and R. Schindler (2017). "New kids on the block: The Popeye domain containing (POPDC) protein family acting as a novel class of cAMP effector proteins in striated muscle." Cell Signal **40**: 156-165.

Brandt, C., M. Bankstahl, K. Tollner, R. Klee and W. Loscher (2016). "The pilocarpine model of temporal lobe epilepsy: Marked intrastrain differences in female Sprague-Dawley rats and the effect of estrous cycle." Epilepsy Behav **61**: 141-152.

Bristow, M. R., R. Ginsburg, V. Umans, M. Fowler, W. Minobe, R. Rasmussen, P. Zera, R. Menlove, P. Shah, S. Jamieson and et al. (1986). "Beta 1- and beta 2-adrenergic-receptor subpopulations in nonfailing and failing human ventricular myocardium: coupling of both receptor subtypes to muscle contraction and selective beta 1-receptor down-regulation in heart failure." Circ Res **59**(3): 297-309.

Brown, N. J. and D. E. Vaughan (1998). "Angiotensin-converting enzyme inhibitors." Circulation **97**(14): 1411-1420.

Brunton, L. L., J. S. Hayes and S. E. Mayer (1981). "Functional compartmentation of cyclic AMP and protein kinase in heart." Adv Cyclic Nucleotide Res **14**: 391-397.

Burkart, E. M., M. P. Sumandea, T. Kobayashi, M. Nili, A. F. Martin, E. Homsher and R. J. Solaro (2003). "Phosphorylation or glutamic acid substitution at protein kinase C sites on cardiac troponin I differentially depress myofilament tension and shortening velocity." J Biol Chem **278**(13): 11265-11272.

Calarese, D. A., C. N. Scanlan, M. B. Zwick, S. Deechongkit, Y. Mimura, R. Kunert, P. Zhu, M. R. Wormald, R. L. Stanfield, K. H. Roux, J. W. Kelly, P. M. Rudd, R. A. Dwek, H. Katinger, D. R. Burton and I. A. Wilson (2003). "Antibody domain exchange is an immunological solution to carbohydrate cluster recognition." Science **300**(5628): 2065-2071.

Campbell, T. J. and P. S. MacDonald (2003). "Digoxin in heart failure and cardiac arrhythmias." Med J Aust **179**(2): 98-102.

Carrier, L., G. Mearini, K. Stathopoulou and F. Cuello (2015). "Cardiac myosin-binding protein C (MYBPC3) in cardiac pathophysiology." Gene **573**(2): 188-197.

Chapman, A. R., K. K. Lee, D. A. McAllister, L. Cullen, J. H. Greenslade, W. Parsonage, A. Worster, P. A. Kavsak, S. Blankenberg, J. Neumann, N. A. Sorensen, D. Westermann, M. M. Buijs, G. J. E. Verdel, J. W. Pickering, M. P. Than, R. Twerenbold, P. Badertscher, Z. Sabti, C. Mueller, A. Anand, P. Adamson, F. E. Strachan, A. Ferry, D. Sandeman, A. Gray, R. Body, B. Keevil, E. Carlton, K. Greaves, F. K. Korley, T. S. Metkus, Y. Sandoval, F. S. Apple, D. E. Newby, A. S. V. Shah and N. L. Mills (2017). "Association of High-Sensitivity Cardiac Troponin I Concentration With Cardiac Outcomes in Patients With Suspected Acute Coronary Syndrome." JAMA **318**(19): 1913-1924.

Chen, T. Y. and K. W. Yau (1994). "Direct modulation by Ca(2+)-calmodulin of cyclic nucleotide-activated channel of rat olfactory receptor neurons." Nature **368**(6471): 545-548.

Cheng, X., Z. Ji, T. Tsalkova and F. Mei (2008). "Epac and PKA: a tale of two intracellular cAMP receptors." Acta Biochim Biophys Sin (Shanghai) **40**(7): 651-662.

Cherezov, V., D. M. Rosenbaum, M. A. Hanson, S. G. Rasmussen, F. S. Thian, T. S. Kobilka, H. J. Choi, P. Kuhn, W. I. Weis, B. K. Kobilka and R. C. Stevens (2007). "High-resolution crystal structure of an engineered human beta2-adrenergic G protein-coupled receptor." Science **318**(5854): 1258-1265.

Christopher, B., G. O. Pizarro, B. Nicholson, S. Yuen, B. D. Hoit and O. Ogut (2009). "Reduced force production during low blood flow to the heart correlates with altered troponin I phosphorylation." J Muscle Res Cell Motil **30**(3-4): 111-123.

Chung, J. H., B. J. Biesiadecki, M. T. Ziolo, J. P. Davis and P. M. Janssen (2016). "Myofilament Calcium Sensitivity: Role in Regulation of In vivo Cardiac Contraction and Relaxation." Front Physiol **7**: 562.

Cong, J., D. E. Goll, A. M. Peterson and H. P. Kapprell (1989). "The role of autolysis in activity of the Ca2+-dependent proteinases (mu-calpain and m-calpain)." J Biol Chem **264**(17): 10096-10103.

Conrad, N., A. Judge, J. Tran, H. Mohseni, D. Hedgecott, A. P. Crespillo, M. Allison, H. Hemingway, J. G. Cleland, J. J. V. McMurray and K. Rahimi (2018).

"Temporal trends and patterns in heart failure incidence: a population-based study of 4 million individuals." Lancet **391**(10120): 572-580.

Czernik, A. J., J. A. Girault, A. C. Nairn, J. Chen, G. Snyder, J. Kebabian and P. Greengard (1991). "Production of phosphorylation state-specific antibodies." Methods Enzymol **201**: 264-283.

Da Silva-Ferrada, E., T. M. Ribeiro-Rodrigues, M. S. Rodriguez and H. Girao (2016). "Proteostasis and SUMO in the heart." Int J Biochem Cell Biol **79**: 443-450.

de Rooij, J., F. J. Zwartkruis, M. H. Verheijen, R. H. Cool, S. M. Nijman, A. Wittinghofer and J. L. Bos (1998). "Epac is a Rap1 guanine-nucleotide-exchange factor directly activated by cyclic AMP." Nature **396**(6710): 474-477.

de Tombe, P. P. (2003). "Cardiac myofilaments: mechanics and regulation." J Biomech **36**(5): 721-730.

DeBerg, H. A., P. S. Brzovic, G. E. Flynn, W. N. Zagotta and S. Stoll (2016). "Structure and Energetics of Allosteric Regulation of HCN2 Ion Channels by Cyclic Nucleotides." J Biol Chem **291**(1): 371-381.

Desterro, J. M., M. S. Rodriguez and R. T. Hay (1998). "SUMO-1 modification of IkappaBalpha inhibits NF-kappaB activation." Mol Cell **2**(2): 233-239.

Di Lisa, F., R. De Tullio, F. Salamino, R. Barbato, E. Melloni, N. Siliprandi, S. Schiaffino and S. Pontremoli (1995). "Specific degradation of troponin T and I by mu-calpain and its modulation by substrate phosphorylation." Biochem J **308 (Pt 1)**: 57-61.

Dodge, K. and J. D. Scott (2000). "AKAP79 and the evolution of the AKAP model." FEBS Lett **476**(1-2): 58-61.

Dodge, K. L., S. Khouangsathiene, M. S. Kapiloff, R. Mouton, E. V. Hill, M. D. Houslay, L. K. Langeberg and J. D. Scott (2001). "mAKAP assembles a protein kinase A/PDE4 phosphodiesterase cAMP signaling module." EMBO J **20**(8): 1921-1930.

Donahue, J. K., K. Kikkawa, D. C. Johns, E. Marban and J. H. Lawrence (1997). "Ultrarapid, highly efficient viral gene transfer to the heart." Proc Natl Acad Sci U S A **94**(9): 4664-4668.

Edwards, H. V. (2012). Mechanisms regulating PKA phosphorylation of the key cardiac proteins Troponin I and Hsp20, University of Glasgow.

Edwards, H. V., J. D. Scott and G. S. Baillie (2012). "The A-kinase-anchoring protein AKAP-Lbc facilitates cardioprotective PKA phosphorylation of Hsp20 on Ser(16)." Biochem J **446**(3): 437-443.

El-Armouche, A., L. Pohlmann, S. Schlossarek, J. Starbatty, Y. H. Yeh, S. Nattel, D. Dobrev, T. Eschenhagen and L. Carrier (2007). "Decreased phosphorylation levels of cardiac myosin-binding protein-C in human and experimental heart failure." J Mol Cell Cardiol **43**(2): 223-229.

Fentzke, R. C., S. H. Buck, J. R. Patel, H. Lin, B. M. Wolska, M. O. Stojanovic, A. F. Martin, R. J. Solaro, R. L. Moss and J. M. Leiden (1999). "Impaired cardiomyocyte relaxation and diastolic function in transgenic mice expressing slow skeletal troponin I in the heart." J Physiol **517 (Pt 1)**: 143-157.

Fertig, B. A. and G. S. Baillie (2018). "PDE4-Mediated cAMP Signalling." J Cardiovasc Dev Dis **5**(1).

Fredriksson, R., M. C. Lagerstrom, L. G. Lundin and H. B. Schioth (2003). "The G-protein-coupled receptors in the human genome form five main families. Phylogenetic analysis, paralogon groups, and fingerprints." Mol Pharmacol **63**(6): 1256-1272.

Froese, A., S. S. Breher, C. Waldeyer, R. F. Schindler, V. O. Nikolaev, S. Rinne, E. Wischmeyer, J. Schlueter, J. Becher, S. Simrick, F. Vauti, J. Kuhtz, P. Meister, S. Kreissl, A. Torlopp, S. K. Liebig, S. Laakmann, T. D. Muller, J. Neumann, J. Stieber, A. Ludwig, S. K. Maier, N. Decher, H. H. Arnold, P. Kirchhof, L. Fabritz and T. Brand (2012). "Popeye domain containing proteins are essential for stress-mediated modulation of cardiac pacemaking in mice." J Clin Invest **122**(3): 1119-1130.

Gautel, M., O. Zuffardi, A. Freiburg and S. Labeit (1995). "Phosphorylation switches specific for the cardiac isoform of myosin binding protein-C: a modulator of cardiac contraction?" EMBO J **14**(9): 1952-1960.

Gesellchen, F., A. Stangherlin, N. Surdo, A. Terrin, A. Zoccarato and M. Zaccolo (2011). "Measuring spatiotemporal dynamics of cyclic AMP signaling in real-time using FRET-based biosensors." Methods Mol Biol **746**: 297-316.

Glish, G. L. and R. W. Vachet (2003). "The basics of mass spectrometry in the twenty-first century." Nat Rev Drug Discov **2**(2): 140-150.

Gordon, A. M., E. Homsher and M. Regnier (2000). "Regulation of contraction in striated muscle." Physiol Rev **80**(2): 853-924.

Greenberg, B., J. Butler, G. M. Felker, P. Ponikowski, A. A. Voors, A. S. Desai, D. Barnard, A. Bouchard, B. Jaski, A. R. Lyon, J. M. Pogoda, J. J. Rudy and K. M. Zsebo (2016). "Calcium upregulation by percutaneous administration of gene therapy in patients with cardiac disease (CUPID 2): a randomised, multinational, double-blind, placebo-controlled, phase 2b trial." Lancet **387**(10024): 1178-1186.

Gu, J., Y. Fan, X. Liu, L. Zhou, J. Cheng, R. Cai and S. Xue (2014). "SENP1 protects against myocardial ischaemia/reperfusion injury via a HIF1alpha-dependent pathway." Cardiovasc Res **104**(1): 83-92.

Gupta, M. K., P. M. McLendon, J. Gulick, J. James, K. Khalili and J. Robbins (2016). "UBC9-Mediated Sumoylation Favorably Impacts Cardiac Function in Compromised Hearts." Circ Res **118**(12): 1894-1905.

Hamdani, N., V. Kooij, S. van Dijk, D. Merkus, W. J. Paulus, C. D. Remedios, D. J. Duncker, G. J. Stienen and J. van der Velden (2008). "Sarcomeric dysfunction in heart failure." Cardiovasc Res **77**(4): 649-658.

Hannich, J. T., A. Lewis, M. B. Kroetz, S. J. Li, H. Heide, A. Emili and M. Hochstrasser (2005). "Defining the SUMO-modified proteome by multiple approaches in Saccharomyces cerevisiae." J Biol Chem **280**(6): 4102-4110.

Hannoun, Z., S. Greenhough, E. Jaffray, R. T. Hay and D. C. Hay (2010). "Post-translational modification by SUMO." Toxicology **278**(3): 288-293.

Hattori, T. and S. Koide (2018). "Next-generation antibodies for post-translational modifications." Curr Opin Struct Biol **51**: 141-148.

Hattori, T., D. Lai, I. S. Dementieva, S. P. Montano, K. Kurosawa, Y. Zheng, L. R. Akin, K. M. Swist-Rosowska, A. T. Grzybowski, A. Koide, K. Krajewski, B. D. Strahl, N. L. Kelleher, A. J. Ruthenburg and S. Koide (2016). "Antigen clasping by two antigen-binding sites of an exceptionally specific antibody for histone methylation." Proc Natl Acad Sci U S A **113**(8): 2092-2097.

Hayes, J. S. and L. L. Brunton (1982). "Functional compartments in cyclic nucleotide action." J Cyclic Nucleotide Res **8**(1): 1-16.

Hayes, J. S., L. L. Brunton and S. E. Mayer (1980). "Selective activation of particulate cAMP-dependent protein kinase by isoproterenol and prostaglandin E1." J Biol Chem **255**(11): 5113-5119.

Hendriks, I. A., D. Lyon, D. Su, N. H. Skotte, J. A. Daniel, L. J. Jensen and M. L. Nielsen (2018). "Site-specific characterization of endogenous SUMOylation across species and organs." Nat Commun **9**(1): 2456.

Hendriks, I. A. and A. C. Vertegaal (2016). "A comprehensive compilation of SUMO proteomics." Nat Rev Mol Cell Biol **17**(9): 581-595.

Herrmann, S., S. Schnorr and A. Ludwig (2015). "HCN channels--modulators of cardiac and neuronal excitability." Int J Mol Sci **16**(1): 1429-1447.

Hershko, A., H. Heller, S. Elias and A. Ciechanover (1983). "Components of ubiquitin-protein ligase system. Resolution, affinity purification, and role in protein breakdown." J Biol Chem **258**(13): 8206-8214.

Herzberg, O. and M. N. James (1985). "Structure of the calcium regulatory muscle protein troponin-C at 2.8 A resolution." Nature **313**(6004): 653-659.

Hietakangas, V., J. K. Ahlskog, A. M. Jakobsson, M. Hellesuo, N. M. Sahlberg, C. I. Holmberg, A. Mikhailov, J. J. Palvimo, L. Pirkkala and L. Sistonen (2003). "Phosphorylation of serine 303 is a prerequisite for the stress-inducible SUMO modification of heat shock factor 1." Mol Cell Biol **23**(8): 2953-2968.

Hietakangas, V., J. Anckar, H. A. Blomster, M. Fujimoto, J. J. Palvimo, A. Nakai and L. Sistonen (2006). "PDSM, a motif for phosphorylation-dependent SUMO modification." Proc Natl Acad Sci U S A **103**(1): 45-50.

Hochstrasser, M. (2001). "SP-RING for SUMO: new functions bloom for a ubiquitin-like protein." Cell **107**(1): 5-8.

Hoffmann, R., G. S. Baillie, S. J. MacKenzie, S. J. Yarwood and M. D. Houslay (1999). "The MAP kinase ERK2 inhibits the cyclic AMP-specific phosphodiesterase HSPDE4D3 by phosphorylating it at Ser579." EMBO J **18**(4): 893-903.

Holroyde, M. J., S. P. Robertson, J. D. Johnson, R. J. Solaro and J. D. Potter (1980). "The calcium and magnesium binding sites on cardiac troponin and their role in the regulation of myofibrillar adenosine triphosphatase." J Biol Chem **255**(24): 11688-11693.

Houslay, K. F., F. Christian, R. MacLeod, D. R. Adams, M. D. Houslay and G. S. Baillie (2017). "Identification of a multifunctional docking site on the catalytic unit of phosphodiesterase-4 (PDE4) that is utilised by multiple interaction partners." Biochem J **474**(4): 597-609.

Houslay, M. D., G. S. Baillie and D. H. Maurice (2007). "cAMP-Specific phosphodiesterase-4 enzymes in the cardiovascular system: a molecular toolbox for generating compartmentalized cAMP signaling." Circ Res **100**(7): 950-966.

Huang, T. T., S. M. Wuerzberger-Davis, Z. H. Wu and S. Miyamoto (2003). "Sequential modification of NEMO/IKKgamma by SUMO-1 and ubiquitin mediates NF-kappaB activation by genotoxic stress." Cell **115**(5): 565-576.

Jakobs, A., F. Himstedt, M. Funk, B. Korn, M. Gaestel and R. Niedenthal (2007). "Ubc9 fusion-directed SUMOylation identifies constitutive and inducible SUMOylation." Nucleic Acids Res **35**(17): e109.

Jakobs, A., J. Koehnke, F. Himstedt, M. Funk, B. Korn, M. Gaestel and R. Niedenthal (2007). "Ubc9 fusion-directed SUMOylation (UFDS): a method to analyze function of protein SUMOylation." Nat Methods **4**(3): 245-250.

Janssen, P. M. and P. P. de Tombe (1997). "Protein kinase A does not alter unloaded velocity of sarcomere shortening in skinned rat cardiac trabeculae." Am J Physiol **273**(5 Pt 2): H2415-2422.

Johns, E. C., S. J. Simnett, I. P. Mulligan and C. C. Ashley (1997). "Troponin I phosphorylation does not increase the rate of relaxation following laser flash photolysis of diazo-2 in guinea-pig skinned trabeculae." Pflugers Arch **433**(6): 842-844.

Jones, P. P., X. Meng, B. Xiao, S. Cai, J. Bolstad, T. Wagenknecht, Z. Liu and S. R. Chen (2008). "Localization of PKA phosphorylation site, Ser(2030), in the three-dimensional structure of cardiac ryanodine receptor." Biochem J **410**(2): 261-270.

Kapiloff, M. S. and K. D. Chandrasekhar (2011). "A-kinase anchoring proteins: temporal and spatial regulation of intracellular signal transduction in the cardiovascular system." J Cardiovasc Pharmacol **58**(4): 337-338.

Karin, M. and Y. Ben-Neriah (2000). "Phosphorylation meets ubiquitination: the control of NF-[kappa]B activity." Annu Rev Immunol **18**: 621-663.

Kaur, K., H. Park, N. Pandey, Y. Azuma and R. N. De Guzman (2017). "Identification of a new small ubiquitin-like modifier (SUMO)-interacting motif in the E3 ligase PIASy." J Biol Chem **292**(24): 10230-10238.

Kawasaki, H., G. M. Springett, N. Mochizuki, S. Toki, M. Nakaya, M. Matsuda, D. E. Housman and A. M. Graybiel (1998). "A family of cAMP-binding proteins that directly activate Rap1." Science **282**(5397): 2275-2279.

Ke, H. and H. Wang (2007). "Crystal structures of phosphodiesterases and implications on substrate specificity and inhibitor selectivity." Curr Top Med Chem **7**(4): 391-403.

Kemp, B. E., D. B. Bylund, T. S. Huang and E. G. Krebs (1975). "Substrate specificity of the cyclic AMP-dependent protein kinase." Proc Natl Acad Sci U S A **72**(9): 3448-3452.

Kensler, R. W., R. Craig and R. L. Moss (2017). "Phosphorylation of cardiac myosin binding protein C releases myosin heads from the surface of cardiac thick filaments." Proc Natl Acad Sci U S A **114**(8): E1355-E1364.

Kentish, J. C., D. T. McCloskey, J. Layland, S. Palmer, J. M. Leiden, A. F. Martin and R. J. Solaro (2001). "Phosphorylation of troponin I by protein kinase A accelerates relaxation and crossbridge cycle kinetics in mouse ventricular muscle." Circ Res **88**(10): 1059-1065.

Kerscher, O. (2007). "SUMO junction-what's your function? New insights through SUMO-interacting motifs." EMBO Rep **8**(6): 550-555.

Kho, C., A. Lee, D. Jeong, J. G. Oh, A. H. Chaanine, E. Kizana, W. J. Park and R. J. Hajjar (2011). "SUMO1-dependent modulation of SERCA2a in heart failure." Nature **477**(7366): 601-605.

Kho, C., A. Lee, D. Jeong, J. G. Oh, P. A. Gorski, K. Fish, R. Sanchez, R. J. DeVita, G. Christensen, R. Dahl and R. J. Hajjar (2015). "Small-molecule activation of SERCA2a SUMOylation for the treatment of heart failure." Nat Commun **6**: 7229.

Kim, E. Y., L. Chen, Y. Ma, W. Yu, J. Chang, I. P. Moskowitz and J. Wang (2012). "Enhanced desumoylation in murine hearts by overexpressed SENP2 leads to congenital heart defects and cardiac dysfunction." J Mol Cell Cardiol **52**(3): 638-649.

Kim, E. Y., Y. Zhang, I. Beketaev, A. M. Segura, W. Yu, Y. Xi, J. Chang and J. Wang (2015). "SENP5, a SUMO isopeptidase, induces apoptosis and cardiomyopathy." J Mol Cell Cardiol **78**: 154-164.

Kim, E. Y., Y. Zhang, B. Ye, A. M. Segura, I. Beketaev, Y. Xi, W. Yu, J. Chang, F. Li and J. Wang (2015). "Involvement of activated SUMO-2 conjugation in cardiomyopathy." Biochim Biophys Acta **1852**(7): 1388-1399.

Kim, M. J., I. V. Chia and F. Costantini (2008). "SUMOylation target sites at the C terminus protect Axin from ubiquitination and confer protein stability." FASEB J **22**(11): 3785-3794.

Kliminski, V., O. Uziel and G. Kessler-Icekson (2017). "Popdc1/Bves Functions in the Preservation of Cardiomyocyte Viability While Affecting Rac1 Activity and Bnip3 Expression." J Cell Biochem **118**(6): 1505-1517.

Kooij, V., R. J. Holewinski, A. M. Murphy and J. E. Van Eyk (2013). "Characterization of the cardiac myosin binding protein-C phosphoproteome in healthy and failing human hearts." J Mol Cell Cardiol **60**: 116-120.

Kooij, V., M. Saes, K. Jaquet, R. Zaremba, D. B. Foster, A. M. Murphy, C. Dos Remedios, J. van der Velden and G. J. Stienen (2010). "Effect of troponin I Ser23/24 phosphorylation on Ca2+-sensitivity in human myocardium depends on the phosphorylation background." J Mol Cell Cardiol **48**(5): 954-963.

Kooij, V., V. Venkatraman, J. A. Kirk, C. Ubaida-Mohien, D. R. Graham, M. J. Faber and J. E. Van Eyk (2014). "Identification of cardiac myofilament protein isoforms using multiple mass spectrometry based approaches." Proteomics Clin Appl **8**(7-8): 578-589.

Koruth, J. S., A. Lala, S. Pinney, V. Y. Reddy and S. R. Dukkipati (2017). "The Clinical Use of Ivabradine." J Am Coll Cardiol **70**(14): 1777-1784.

Koudstaal, S., S. Jansen of Lorkeers, J. M. Gho, G. P. van Hout, M. S. Jansen, P. F. Grundeman, G. Pasterkamp, P. A. Doevendans, I. E. Hoefer and S. A. Chamuleau (2014). "Myocardial infarction and functional outcome assessment in pigs." J Vis Exp(86).

Kramerova, I., E. Kudryashova, G. Venkatraman and M. J. Spencer (2005). "Calpain 3 participates in sarcomere remodeling by acting upstream of the ubiquitin-proteasome pathway." Hum Mol Genet **14**(15): 2125-2134.

Kroetz, M. B. (2005). "SUMO: a ubiquitin-like protein modifier." Yale J Biol Med **78**(4): 197-201.

Krupinski, J., F. Coussen, H. A. Bakalyar, W. J. Tang, P. G. Feinstein, K. Orth, C. Slaughter, R. R. Reed and A. G. Gilman (1989). "Adenylyl cyclase amino acid sequence: possible channel- or transporter-like structure." Science **244**(4912): 1558-1564.

Krupinski, J., T. C. Lehman, C. D. Frankenfield, J. C. Zwaagstra and P. A. Watson (1992). "Molecular diversity in the adenylylcyclase family. Evidence for eight forms of the enzyme and cloning of type VI." J Biol Chem **267**(34): 24858-24862.

Lang, S. E., J. Schwank, T. K. Stevenson, M. A. Jensen and M. V. Westfall (2015). "Independent modulation of contractile performance by cardiac troponin I Ser43 and Ser45 in the dynamic sarcomere." J Mol Cell Cardiol **79**: 264-274.

Langer, M., C. Brandt and W. Loscher (2011). "Marked strain and substrain differences in induction of status epilepticus and subsequent development of

neurodegeneration, epilepsy, and behavioral alterations in rats. [corrected]." Epilepsy Res **96**(3): 207-224.

Layland, J., R. J. Solaro and A. M. Shah (2005). "Regulation of cardiac contractile function by troponin I phosphorylation." Cardiovasc Res **66**(1): 12-21.

Lee, A., J. G. Oh, P. A. Gorski, R. J. Hajjar and C. Kho (2016). "Post-translational Modifications in Heart Failure: Small Changes, Big Impact." Heart Lung Circ **25**(4): 319-324.

Lee, L. C., D. H. Maurice and G. S. Baillie (2013). "Targeting protein-protein interactions within the cyclic AMP signaling system as a therapeutic strategy for cardiovascular disease." Future Med Chem **5**(4): 451-464.

Lehman, W., R. Craig and P. Vibert (1994). "Ca(2+)-induced tropomyosin movement in Limulus thin filaments revealed by three-dimensional reconstruction." Nature **368**(6466): 65-67.

Lehnart, S. E., X. H. Wehrens, S. Reiken, S. Warrier, A. E. Belevych, R. D. Harvey, W. Richter, S. L. Jin, M. Conti and A. R. Marks (2005). "Phosphodiesterase 4D deficiency in the ryanodine-receptor complex promotes heart failure and arrhythmias." Cell **123**(1): 25-35.

Lelovas, P. P., N. G. Kostomitsopoulos and T. T. Xanthos (2014). "A comparative anatomic and physiologic overview of the porcine heart." J Am Assoc Lab Anim Sci **53**(5): 432-438.

Leroy, J., W. Richter, D. Mika, L. R. Castro, A. Abi-Gerges, M. Xie, C. Scheitrum, F. Lefebvre, J. Schittl, P. Mateo, R. Westenbroek, W. A. Catterall, F. Charpentier, M. Conti, R. Fischmeister and G. Vandecasteele (2011). "Phosphodiesterase 4B in the cardiac L-type Ca(2)(+) channel complex regulates Ca(2)(+) current and protects against ventricular arrhythmias in mice." J Clin Invest **121**(7): 2651-2661.

Li, M. X., L. Spyracopoulos and B. D. Sykes (1999). "Binding of cardiac troponin-I147-163 induces a structural opening in human cardiac troponin-C." Biochemistry **38**(26): 8289-8298.

Li, X., S. Vadrevu, A. Dunlop, J. Day, N. Advant, J. Troeger, E. Klussmann, E. Jaffrey, R. T. Hay, D. R. Adams, M. D. Houslay and G. S. Baillie (2010). "Selective SUMO modification of cAMP-specific phosphodiesterase-4D5 (PDE4D5) regulates the functional consequences of phosphorylation by PKA and ERK." Biochem J **428**(1): 55-65.

Liebelt, F. and A. C. Vertegaal (2016). "Ubiquitin-dependent and independent roles of SUMO in proteostasis." Am J Physiol Cell Physiol **311**(2): C284-296.

Liu, B., J. J. Lopez, B. J. Biesiadecki and J. P. Davis (2014). "Protein kinase C phosphomimetics alter thin filament Ca2+ binding properties." PLoS One **9**(1): e86279.

Liu, M., T. Y. Chen, B. Ahamed, J. Li and K. W. Yau (1994). "Calcium-calmodulin modulation of the olfactory cyclic nucleotide-gated cation channel." Science **266**(5189): 1348-1354.

Lompre, A. M., J. J. Mercadier, C. Wisnewsky, P. Bouveret, C. Pantaloni, A. D'Albis and K. Schwartz (1981). "Species- and age-dependent changes in the relative amounts of cardiac myosin isoenzymes in mammals." Dev Biol **84**(2): 286-290.

Lompre, A. M., K. Schwartz, A. d'Albis, G. Lacombe, N. Van Thiem and B. Swynghedauw (1979). "Myosin isoenzyme redistribution in chronic heart overload." Nature **282**(5734): 105-107.

Lu, Q. W., A. C. Hinken, S. E. Patrick, R. J. Solaro and T. Kobayashi (2010). "Phosphorylation of cardiac troponin I at protein kinase C site threonine 144 depresses cooperative activation of thin filaments." J Biol Chem **285**(16): 11810-11817.

Lynch, M. J., G. S. Baillie and M. D. Houslay (2007). "cAMP-specific phosphodiesterase-4D5 (PDE4D5) provides a paradigm for understanding the unique non-redundant roles that PDE4 isoforms play in shaping compartmentalized cAMP cell signalling." Biochem Soc Trans **35**(Pt 5): 938-941.

MacKenzie, S. J., G. S. Baillie, I. McPhee, C. MacKenzie, R. Seamons, T. McSorley, J. Millen, M. B. Beard, G. van Heeke and M. D. Houslay (2002). "Long PDE4 cAMP specific phosphodiesterases are activated by protein kinase A-mediated phosphorylation of a single serine residue in Upstream Conserved Region 1 (UCR1)." Br J Pharmacol **136**(3): 421-433.

Mahajan, V. S. and P. Jarolim (2011). "How to interpret elevated cardiac troponin levels." Circulation **124**(21): 2350-2354.

Malia, T. J., A. Teplyakov, R. Ernst, S. J. Wu, E. R. Lacy, X. Liu, M. Vandermeeren, M. Mercken, J. Luo, R. W. Sweet and G. L. Gilliland (2016). "Epitope mapping and structural basis for the recognition of phosphorylated tau by the anti-tau antibody AT8." Proteins **84**(4): 427-434.

Marchmont, R. J. and M. D. Houslay (1980). "Insulin trigger, cyclic AMP-dependent activation and phosphorylation of a plasma membrane cyclic AMP phosphodiesterase." Nature **286**(5776): 904-906.

Matic, I., J. Schimmel, I. A. Hendriks, M. A. van Santen, F. van de Rijke, H. van Dam, F. Gnad, M. Mann and A. C. Vertegaal (2010). "Site-specific identification of SUMO-2 targets in cells reveals an inverted SUMOylation motif and a hydrophobic cluster SUMOylation motif." Mol Cell **39**(4): 641-652.

Matulef, K. and W. N. Zagotta (2003). "Cyclic nucleotide-gated ion channels." Annu Rev Cell Dev Biol **19**: 23-44.

Maurice, D. H., H. Ke, F. Ahmad, Y. Wang, J. Chung and V. C. Manganiello (2014). "Advances in targeting cyclic nucleotide phosphodiesterases." Nat Rev Drug Discov **13**(4): 290-314.

McCahill, A., T. McSorley, E. Huston, E. V. Hill, M. J. Lynch, I. Gall, G. Keryer, B. Lygren, K. Tasken, G. van Heeke and M. D. Houslay (2005). "In resting COS1 cells a dominant negative approach shows that specific, anchored PDE4 cAMP phosphodiesterase isoforms gate the activation, by basal cyclic AMP production, of AKAP-tethered protein kinase A type II located in the centrosomal region." Cell Signal **17**(9): 1158-1173.

McConnell, B. K., C. S. Moravec and M. Bond (1998). "Troponin I phosphorylation and myofilament calcium sensitivity during decompensated cardiac hypertrophy." Am J Physiol **274**(2 Pt 2): H385-396.

McDonough, J. L., D. K. Arrell and J. E. Van Eyk (1999). "Troponin I degradation and covalent complex formation accompanies myocardial ischemia/reperfusion injury." Circ Res **84**(1): 9-20.

McDonough, J. L., R. Labugger, W. Pickett, M. Y. Tse, S. MacKenzie, S. C. Pang, D. Atar, G. Ropchan and J. E. Van Eyk (2001). "Cardiac troponin I is modified in the myocardium of bypass patients." Circulation **103**(1): 58-64.

McMurray, J. J. and G. L. Smith (2011). "Calcium handling in the failing heart and SUMO--weighing the evidence." N Engl J Med **365**(18): 1738-1739.

Meek, D. W. and U. Knippschild (2003). "Posttranslational modification of MDM2." Mol Cancer Res **1**(14): 1017-1026.

Mercadier, J. J., P. Bouveret, L. Gorza, S. Schiaffino, W. A. Clark, R. Zak, B. Swynghedauw and K. Schwartz (1983). "Myosin isoenzymes in normal and hypertrophied human ventricular myocardium." Circ Res **53**(1): 52-62.

Mesnard-Rouiller, L., J. J. Mercadier, G. Butler-Browne, M. Heimburger, D. Logeart, P. D. Allen and F. Samson (1997). "Troponin T mRNA and protein isoforms in the human left ventricle: pattern of expression in failing and control hearts." J Mol Cell Cardiol **29**(11): 3043-3055.

Messer, A. E., A. M. Jacques and S. B. Marston (2007). "Troponin phosphorylation and regulatory function in human heart muscle: dephosphorylation of Ser23/24 on troponin I could account for the contractile defect in end-stage heart failure." J Mol Cell Cardiol **42**(1): 247-259.

Metzger, J. M. and M. V. Westfall (2004). "Covalent and noncovalent modification of thin filament action: the essential role of troponin in cardiac muscle regulation." Circ Res **94**(2): 146-158.

Mika, D., P. Bobin, M. Lindner, A. Boet, A. Hodzic, F. Lefebvre, P. Lechene, M. Sadoune, J. L. Samuel, V. Algalarrondo, C. Rucker-Martin, V. Lambert, R. Fischmeister, G. Vandecasteele and J. Leroy (2019). "Synergic PDE3 and PDE4 control intracellular cAMP and cardiac excitation-contraction coupling in a porcine model." J Mol Cell Cardiol **133**: 57-66.

Mika, D., P. Bobin, M. Pomerance, P. Lechene, R. E. Westenbroek, W. A. Catterall, G. Vandecasteele, J. Leroy and R. Fischmeister (2013). "Differential regulation of cardiac excitation-contraction coupling by cAMP phosphodiesterase subtypes." Cardiovasc Res **100**(2): 336-346.

Minty, A., X. Dumont, M. Kaghad and D. Caput (2000). "Covalent modification of p73alpha by SUMO-1. Two-hybrid screening with p73 identifies novel SUMO-1-interacting proteins and a SUMO-1 interaction motif." J Biol Chem **275**(46): 36316-36323.

Miyata, S., W. Minobe, M. R. Bristow and L. A. Leinwand (2000). "Myosin heavy chain isoform expression in the failing and nonfailing human heart." Circ Res **86**(4): 386-390.

Montgomery, D. E., B. M. Wolska, W. G. Pyle, B. B. Roman, J. C. Dowell, P. M. Buttrick, A. P. Koretsky, P. Del Nido and R. J. Solaro (2002). "alpha-Adrenergic response and myofilament activity in mouse hearts lacking PKC phosphorylation sites on cardiac TnI." Am J Physiol Heart Circ Physiol **282**(6): H2397-2405.

Mooney, S. M., J. P. Grande, J. L. Salisbury and R. Janknecht (2010). "Sumoylation of p68 and p72 RNA helicases affects protein stability and transactivation potential." Biochemistry **49**(1): 1-10.

Moss, R. L., D. P. Fitzsimons and J. C. Ralphe (2015). "Cardiac MyBP-C regulates the rate and force of contraction in mammalian myocardium." Circ Res **116**(1): 183-192.

Mukhopadhyay, D. and M. Dasso (2007). "Modification in reverse: the SUMO proteases." Trends Biochem Sci **32**(6): 286-295.

Muller, S., C. Hoege, G. Pyrowolakis and S. Jentsch (2001). "SUMO, ubiquitin's mysterious cousin." Nat Rev Mol Cell Biol **2**(3): 202-210.

Murphy, A. M., H. Kogler and E. Marban (2000). "A mouse model of myocardial stunning." Mol Med Today **6**(8): 330-331.

Nacerddine, K., F. Lehembre, M. Bhaumik, J. Artus, M. Cohen-Tannoudji, C. Babinet, P. P. Pandolfi and A. Dejean (2005). "The SUMO pathway is essential for nuclear integrity and chromosome segregation in mice." Dev Cell **9**(6): 769-779.

Narolska, N. A., N. Piroddi, A. Belus, N. M. Boontje, B. Scellini, S. Deppermann, R. Zaremba, R. J. Musters, C. dos Remedios, K. Jaquet, D. B. Foster, A. M. Murphy, J. E. van Eyk, C. Tesi, C. Poggesi, J. van der Velden and G. J. Stienen (2006). "Impaired diastolic function after exchange of endogenous troponin I with C-terminal truncated troponin I in human cardiac muscle." Circ Res **99**(9): 1012-1020.

Narolska, N. A., R. B. van Loon, N. M. Boontje, R. Zaremba, S. E. Penas, J. Russell, S. R. Spiegelenberg, M. A. Huybregts, F. C. Visser, J. W. de Jong, J. van der Velden and G. J. Stienen (2005). "Myocardial contraction is 5-fold more economical in ventricular than in atrial human tissue." Cardiovasc Res **65**(1): 221-229.

NICE (2014). "Myocardial infarction (acute): Early rule out using high-sensitivity troponin tests (Elecsys Troponin T high-sensitive, ARCHITECT STAT High Sensitive Troponin-I and AccuTnI+3 assays). Diagnostics guidance DG15.".

Nikolaev, V. O., M. Bunemann, L. Hein, A. Hannawacker and M. J. Lohse (2004). "Novel single chain cAMP sensors for receptor-induced signal propagation." J Biol Chem **279**(36): 37215-37218.

Nikolaev, V. O., S. Gambaryan and M. J. Lohse (2006). "Fluorescent sensors for rapid monitoring of intracellular cGMP." Nat Methods **3**(1): 23-25.

Nikolaev, V. O. and M. J. Lohse (2006). "Monitoring of cAMP synthesis and degradation in living cells." Physiology (Bethesda) **21**: 86-92.

Noland, T. A., Jr., R. L. Raynor, N. M. Jideama, X. Guo, M. G. Kazanietz, P. M. Blumberg, R. J. Solaro and J. F. Kuo (1996). "Differential regulation of cardiac actomyosin S-1 MgATPase by protein kinase C isozyme-specific phosphorylation of specific sites in cardiac troponin I and its phosphorylation site mutants." Biochemistry **35**(47): 14923-14931.

Noland, T. A., Jr., R. L. Raynor and J. F. Kuo (1989). "Identification of sites phosphorylated in bovine cardiac troponin I and troponin T by protein kinase C and comparative substrate activity of synthetic peptides containing the phosphorylation sites." J Biol Chem **264**(34): 20778-20785.

Omori, K. and J. Kotera (2007). "Overview of PDEs and their regulation." Circ Res **100**(3): 309-327.

Osadchii, O. E. (2007). "Myocardial phosphodiesterases and regulation of cardiac contractility in health and cardiac disease." Cardiovasc Drugs Ther **21**(3): 171-194.

Packer, M., J. R. Carver, R. J. Rodeheffer, R. J. Ivanhoe, R. DiBianco, S. M. Zeldis, G. H. Hendrix, W. J. Bommer, U. Elkayam and M. L. Kukin (1991). "Effect of oral milrinone on mortality in severe chronic heart failure. The PROMISE Study Research Group." N Engl J Med **325**(21): 1468-1475.

Palvimo, J. J. (2007). "PIAS proteins as regulators of small ubiquitin-related modifier (SUMO) modifications and transcription." Biochem Soc Trans **35**(Pt 6): 1405-1408.

Perez-Aso, M., M. C. Montesinos, A. Mediero, T. Wilder, P. H. Schafer and B. Cronstein (2015). "Apremilast, a novel phosphodiesterase 4 (PDE4) inhibitor, regulates inflammation through multiple cAMP downstream effectors." Arthritis Res Ther **17**: 249.

Perry, S. J., G. S. Baillie, T. A. Kohout, I. McPhee, M. M. Magiera, K. L. Ang, W. E. Miller, A. J. McLean, M. Conti, M. D. Houslay and R. J. Lefkowitz (2002). "Targeting of cyclic AMP degradation to beta 2-adrenergic receptors by beta-arrestins." Science **298**(5594): 834-836.

Pi, Y., K. R. Kemnitz, D. Zhang, E. G. Kranias and J. W. Walker (2002). "Phosphorylation of troponin I controls cardiac twitch dynamics: evidence from phosphorylation site mutants expressed on a troponin I-null background in mice." Circ Res **90**(6): 649-656.

Pi, Y., R. Sreekumar, X. Huang and J. W. Walker (1997). "Positive inotropy mediated by diacylglycerol in rat ventricular myocytes." Circ Res **81**(1): 92-100.

Pi, Y., D. Zhang, K. R. Kemnitz, H. Wang and J. W. Walker (2003). "Protein kinase C and A sites on troponin I regulate myofilament Ca2+ sensitivity and ATPase activity in the mouse myocardium." J Physiol **552**(Pt 3): 845-857.

Pierce, K. L., R. T. Premont and R. J. Lefkowitz (2002). "Seven-transmembrane receptors." Nat Rev Mol Cell Biol **3**(9): 639-650.

Portbury, A. L., M. S. Willis and C. Patterson (2011). "Tearin' up my heart: proteolysis in the cardiac sarcomere." J Biol Chem **286**(12): 9929-9934.

Radivojac, P., V. Vacic, C. Haynes, R. R. Cocklin, A. Mohan, J. W. Heyen, M. G. Goebl and L. M. Iakoucheva (2010). "Identification, analysis, and prediction of protein ubiquitination sites." Proteins **78**(2): 365-380.

Rall, T. W. and E. W. Sutherland (1958). "Formation of a cyclic adenine ribonucleotide by tissue particles." J Biol Chem **232**(2): 1065-1076.

Rall, T. W. and T. C. West (1963). "The potentiation of cardiac inotropic responses to norepinephrine by theophylline." J Pharmacol Exp Ther **139**: 269-274.

Rampersad, S. N., J. D. Ovens, E. Huston, M. B. Umana, L. S. Wilson, S. J. Netherton, M. J. Lynch, G. S. Baillie, M. D. Houslay and D. H. Maurice (2010). "Cyclic AMP phosphodiesterase 4D (PDE4D) Tethers EPAC1 in a vascular endothelial cadherin (VE-Cad)-based signaling complex and controls cAMP-mediated vascular permeability." J Biol Chem **285**(44): 33614-33622.

Richter, W., M. Xie, C. Scheitrum, J. Krall, M. A. Movsesian and M. Conti (2011). "Conserved expression and functions of PDE4 in rodent and human heart." Basic Res Cardiol **106**(2): 249-262.

Ritter, O., H. P. Luther, H. Haase, L. G. Baltas, G. Baumann, H. D. Schulte and I. Morano (1999). "Expression of atrial myosin light chains but not alpha-myosin heavy chains is correlated in vivo with increased ventricular function in patients with hypertrophic obstructive cardiomyopathy." J Mol Med (Berl) **77**(9): 677-685.

Rodriguez, K. A., K. Li, E. Nevo and R. Buffenstein (2016). "Mechanisms regulating proteostasis are involved in sympatric speciation of the blind mole rat, Spalax galili." Autophagy **12**(4): 703-704.

Rose, A. S., A. R. Bradley, Y. Valasatava, J. M. Duarte, A. Prlic and P. W. Rose (2018). "NGL viewer: web-based molecular graphics for large complexes." Bioinformatics **34**(21): 3755-3758.

Ruehr, M. L., M. A. Russell, D. G. Ferguson, M. Bhat, J. Ma, D. S. Damron, J. D. Scott and M. Bond (2003). "Targeting of protein kinase A by muscle A kinase-anchoring protein (mAKAP) regulates phosphorylation and function of the skeletal muscle ryanodine receptor." J Biol Chem **278**(27): 24831-24836.

Rytinki, M. M., S. Kaikkonen, P. Pehkonen, T. Jaaskelainen and J. J. Palvimo (2009). "PIAS proteins: pleiotropic interactors associated with SUMO." Cell Mol Life Sci **66**(18): 3029-3041.

Sahota, V. K., B. F. Grau, A. Mansilla and A. Ferrus (2009). "Troponin I and Tropomyosin regulate chromosomal stability and cell polarity." J Cell Sci **122**(Pt 15): 2623-2631.

Sala, L., B. J. van Meer, L. G. J. Tertoolen, J. Bakkers, M. Bellin, R. P. Davis, C. Denning, M. A. E. Dieben, T. Eschenhagen, E. Giacomelli, C. Grandela, A. Hansen, E. R. Holman, M. R. M. Jongbloed, S. M. Kamel, C. D. Koopman, Q. Lachaud, I. Mannhardt, M. P. H. Mol, D. Mosqueira, V. V. Orlova, R. Passier, M. C. Ribeiro, U. Saleem, G. L. Smith, F. L. Burton and C. L. Mummery (2018). "MUSCLEMOTION: A Versatile Open Software Tool to Quantify Cardiomyocyte and Cardiac Muscle Contraction In Vitro and In Vivo." Circ Res **122**(3): e5-e16.

Schafer, P. H., P. Chen, L. Fang, A. Wang and R. Chopra (2015). "The pharmacodynamic impact of apremilast, an oral phosphodiesterase 4 inhibitor, on circulating levels of inflammatory biomarkers in patients with psoriatic arthritis: substudy results from a phase III, randomized, placebo-controlled trial (PALACE 1)." J Immunol Res **2015**: 906349.

Schmidt, D. and S. Muller (2002). "Members of the PIAS family act as SUMO ligases for c-Jun and p53 and repress p53 activity." Proc Natl Acad Sci U S A **99**(5): 2872-2877.

Seeler, J. S. and A. Dejean (2003). "Nuclear and unclear functions of SUMO." Nat Rev Mol Cell Biol **4**(9): 690-699.

Sequeira, V., P. J. Wijnker, L. L. Nijenkamp, D. W. Kuster, A. Najafi, E. R. Witjas-Paalberends, J. A. Regan, N. Boontje, F. J. Ten Cate, T. Germans, L. Carrier, S. Sadayappan, M. A. van Slegtenhorst, R. Zaremba, D. B. Foster, A. M. Murphy, C. Poggesi, C. Dos Remedios, G. J. Stienen, C. Y. Ho, M. Michels and J. van der Velden (2013). "Perturbed length-dependent activation in human hypertrophic cardiomyopathy with missense sarcomeric gene mutations." Circ Res **112**(11): 1491-1505.

Shaffer, J. F., R. W. Kensler and S. P. Harris (2009). "The myosin-binding protein C motif binds to F-actin in a phosphorylation-sensitive manner." J Biol Chem **284**(18): 12318-12327.

Shah, A. S. V., A. V. Ferry and N. L. Mills (2017). "Cardiac Biomarkers and the Diagnosis of Myocardial Infarction in Women." Curr Cardiol Rep **19**(5): 40.

Sheng, J. J. and J. P. Jin (2016). "TNNI1, TNNI2 and TNNI3: Evolution, regulation, and protein structure-function relationships." Gene **576**(1 Pt 3): 385-394.

Sin, Y. Y., H. V. Edwards, X. Li, J. P. Day, F. Christian, A. J. Dunlop, D. R. Adams, M. Zaccolo, M. D. Houslay and G. S. Baillie (2011). "Disruption of the cyclic AMP phosphodiesterase-4 (PDE4)-HSP20 complex attenuates the beta-agonist induced hypertrophic response in cardiac myocytes." J Mol Cell Cardiol **50**(5): 872-883.

Skalhegg, B. S. and K. Tasken (2000). "Specificity in the cAMP/PKA signaling pathway. Differential expression,regulation, and subcellular localization of subunits of PKA." Front Biosci **5**: D678-693.

Smith, F. D., J. L. Esseltine, P. J. Nygren, D. Veesler, D. P. Byrne, M. Vonderach, I. Strashnov, C. E. Eyers, P. A. Eyers, L. K. Langeberg and J. D. Scott (2017). "Local protein kinase A action proceeds through intact holoenzymes." Science **356**(6344): 1288-1293.

Smith, K. J., G. S. Baillie, E. I. Hyde, X. Li, T. M. Houslay, A. McCahill, A. J. Dunlop, G. B. Bolger, E. Klussmann, D. R. Adams and M. D. Houslay (2007). "1H NMR structural and functional characterisation of a cAMP-specific phosphodiesterase-4D5 (PDE4D5) N-terminal region peptide that disrupts PDE4D5 interaction with the signalling scaffold proteins, beta-arrestin and RACK1." Cell Signal **19**(12): 2612-2624.

Solaro, R. J. and H. M. Rarick (1998). "Troponin and tropomyosin: proteins that switch on and tune in the activity of cardiac myofilaments." Circ Res **83**(5): 471-480.

Song, J., L. K. Durrin, T. A. Wilkinson, T. G. Krontiris and Y. Chen (2004). "Identification of a SUMO-binding motif that recognizes SUMO-modified proteins." Proc Natl Acad Sci U S A **101**(40): 14373-14378.

Steen, H. and M. Mann (2004). "The ABC's (and XYZ's) of peptide sequencing." Nat Rev Mol Cell Biol **5**(9): 699-711.

Steinacher, R. and P. Schar (2005). "Functionality of human thymine DNA glycosylase requires SUMO-regulated changes in protein conformation." Curr Biol **15**(7): 616-623.

Steiner, A. L., T. H. Whitely, S. H. Ong and N. W. Stowe (1975). "Cyclic AMP and cyclic GMP: studies utilizing immunohistochemical techniques for the localization of the nucleotides in tissue." Metabolism **24**(3): 419-428.

Sumandea, C. A., M. L. Garcia-Cazarin, C. H. Bozio, G. A. Sievert, C. W. Balke and M. P. Sumandea (2011). "Cardiac troponin T, a sarcomeric AKAP, tethers protein kinase A at the myofilaments." J Biol Chem **286**(1): 530-541.

Sundaralingam, M., R. Bergstrom, G. Strasburg, S. T. Rao, P. Roychowdhury, M. Greaser and B. C. Wang (1985). "Molecular structure of troponin C from chicken skeletal muscle at 3-angstrom resolution." Science **227**(4689): 945-948.

Surdo, N. C., M. Berrera, A. Koschinski, M. Brescia, M. R. Machado, C. Carr, P. Wright, J. Gorelik, S. Morotti, E. Grandi, D. M. Bers, S. Pantano and M. Zaccolo (2017). "FRET biosensor uncovers cAMP nano-domains at beta-adrenergic targets that dictate precise tuning of cardiac contractility." Nat Commun **8**: 15031.

Sutherland, E. W. (1972). "Studies on the mechanism of hormone action." Science **177**(4047): 401-408.

Sutherland, E. W. and T. W. Rall (1958). "Fractionation and characterization of a cyclic adenine ribonucleotide formed by tissue particles." J Biol Chem **232**(2): 1077-1091.

Takahashi, Y., A. Toh-e and Y. Kikuchi (2001). "A novel factor required for the SUMO1/Smt3 conjugation of yeast septins." Gene **275**(2): 223-231.

Takeda, S. (2005). "Crystal structure of troponin and the molecular mechanism of muscle regulation." J Electron Microsc (Tokyo) **54 Suppl 1**: i35-41.

Takeda, S., A. Yamashita, K. Maeda and Y. Maeda (2003). "Structure of the core domain of human cardiac troponin in the Ca(2+)-saturated form." Nature **424**(6944): 35-41.

Takeishi, Y., G. Chu, D. M. Kirkpatrick, Z. Li, H. Wakasaki, E. G. Kranias, G. L. King and R. A. Walsh (1998). "In vivo phosphorylation of cardiac troponin I by protein kinase Cbeta2 decreases cardiomyocyte calcium responsiveness and contractility in transgenic mouse hearts." J Clin Invest **102**(1): 72-78.

Takimoto, E., D. G. Soergel, P. M. Janssen, L. B. Stull, D. A. Kass and A. M. Murphy (2004). "Frequency- and afterload-dependent cardiac modulation in vivo by troponin I with constitutively active protein kinase A phosphorylation sites." Circ Res **94**(4): 496-504.

Terrenoire, C., M. D. Houslay, G. S. Baillie and R. S. Kass (2009). "The cardiac IKs potassium channel macromolecular complex includes the phosphodiesterase PDE4D3." J Biol Chem **284**(14): 9140-9146.

Tesmer, J. J., R. K. Sunahara, A. G. Gilman and S. R. Sprang (1997). "Crystal structure of the catalytic domains of adenylyl cyclase in a complex with Gsalpha.GTPgammaS." Science **278**(5345): 1907-1916.

Tham, Y. K., B. C. Bernardo, J. Y. Y. Ooi, K. L. Weeks and J. R. McMullen (2015). "Pathophysiology of cardiac hypertrophy and heart failure: signaling pathways and novel therapeutic targets." Archives of Toxicology **89**(9): 1401-1438.

Tilemann, L., A. Lee, K. Ishikawa, J. Aguero, K. Rapti, C. Santos-Gallego, E. Kohlbrenner, K. M. Fish, C. Kho and R. J. Hajjar (2013). "SUMO-1 gene transfer improves cardiac function in a large-animal model of heart failure." Sci Transl Med **5**(211): 211ra159.

Ulrich, H. D. (2005). "Mutual interactions between the SUMO and ubiquitin systems: a plea of no contest." Trends Cell Biol **15**(10): 525-532.

Ulrich, H. D. (2005). "The RAD6 pathway: control of DNA damage bypass and mutagenesis by ubiquitin and SUMO." Chembiochem **6**(10): 1735-1743.

Ulrich, H. D. (2009). "SUMO Protocols. Preface." Methods Mol Biol **497**: v-vi.

Ulrich, H. D. (2009). "The SUMO system: an overview." Methods Mol Biol **497**: 3-16.

van der Velden, J., N. M. Boontje, Z. Papp, L. J. Klein, F. C. Visser, J. W. de Jong, V. J. Owen, P. B. Burton and G. J. Stienen (2002). "Calcium sensitivity of force in human ventricular cardiomyocytes from donor and failing hearts." Basic Res Cardiol **97 Suppl 1**: I118-126.

van der Velden, J., L. J. Klein, M. van der Bijl, M. A. Huybregts, W. Stooker, J. Witkop, L. Eijsman, C. A. Visser, F. C. Visser and G. J. Stienen (1998). "Force production in mechanically isolated cardiac myocytes from human ventricular muscle tissue." Cardiovasc Res **38**(2): 414-423.

van der Velden, J., L. J. Klein, M. van der Bijl, M. A. Huybregts, W. Stooker, J. Witkop, L. Eijsman, C. A. Visser, F. C. Visser and G. J. Stienen (1999). "Isometric tension development and its calcium sensitivity in skinned myocyte-sized preparations from different regions of the human heart." Cardiovasc Res **42**(3): 706-719.

van der Velden, J., D. Merkus, B. R. Klarenbeek, A. T. James, N. M. Boontje, D. H. Dekkers, G. J. Stienen, J. M. Lamers and D. J. Duncker (2004). "Alterations in myofilament function contribute to left ventricular dysfunction in pigs early after myocardial infarction." Circ Res **95**(11): e85-95.

van der Velden, J., Z. Papp, R. Zaremba, N. M. Boontje, J. W. de Jong, V. J. Owen, P. B. Burton, P. Goldmann, K. Jaquet and G. J. Stienen (2003). "Increased Ca2+-sensitivity of the contractile apparatus in end-stage human heart failure results from altered phosphorylation of contractile proteins." Cardiovasc Res **57**(1): 37-47.

Verger, A., J. Perdomo and M. Crossley (2003). "Modification with SUMO. A role in transcriptional regulation." EMBO Rep **4**(2): 137-142.

Walker, L. A., D. A. Fullerton and P. M. Buttrick (2013). "Contractile protein phosphorylation predicts human heart disease phenotypes." Am J Physiol Heart Circ Physiol **304**(12): H1644-1650.

Walker, L. A., J. S. Walker, S. K. Ambler and P. M. Buttrick (2010). "Stage-specific changes in myofilament protein phosphorylation following myocardial infarction in mice." J Mol Cell Cardiol **48**(6): 1180-1186.

Wang, H. C., Y. S. Huang, C. C. Ho, J. C. Jeng and H. M. Shih (2009). "SUMO modification modulates the activity of calpain-2." Biochem Biophys Res Commun **384**(4): 444-449.

Wang, J. (2011). "Cardiac function and disease: emerging role of small ubiquitin-related modifier." Wiley Interdiscip Rev Syst Biol Med **3**(4): 446-457.

Wang, J., L. Chen, S. Wen, H. Zhu, W. Yu, I. P. Moskowitz, G. M. Shaw, R. H. Finnell and R. J. Schwartz (2011). "Defective sumoylation pathway directs congenital heart disease." Birth Defects Res A Clin Mol Teratol **91**(6): 468-476.

Wang, L., C. Wansleeben, S. Zhao, P. Miao, W. Paschen and W. Yang (2014). "SUMO2 is essential while SUMO3 is dispensable for mouse embryonic development." EMBO Rep **15**(8): 878-885.

Westfall, M. V. and A. R. Borton (2003). "Role of troponin I phosphorylation in protein kinase C-mediated enhanced contractile performance of rat myocytes." J Biol Chem **278**(36): 33694-33700.

Wijnker, P. J., D. B. Foster, A. L. Tsao, A. H. Frazier, C. G. dos Remedios, A. M. Murphy, G. J. Stienen and J. van der Velden (2013). "Impact of site-specific phosphorylation of protein kinase A sites Ser23 and Ser24 of cardiac troponin I in human cardiomyocytes." Am J Physiol Heart Circ Physiol **304**(2): H260-268.

Wijnker, P. J., Y. Li, P. Zhang, D. B. Foster, C. dos Remedios, J. E. Van Eyk, G. J. Stienen, A. M. Murphy and J. van der Velden (2015). "A novel phosphorylation site, Serine 199, in the C-terminus of cardiac troponin I regulates calcium

sensitivity and susceptibility to calpain-induced proteolysis." J Mol Cell Cardiol **82**: 93-103.

Willott, R. H., A. V. Gomes, A. N. Chang, M. S. Parvatiyar, J. R. Pinto and J. D. Potter (2010). "Mutations in Troponin that cause HCM, DCM AND RCM: what can we learn about thin filament function?" J Mol Cell Cardiol **48**(5): 882-892.

Willoughby, D. and D. M. Cooper (2007). "Organization and Ca2+ regulation of adenylyl cyclases in cAMP microdomains." Physiol Rev **87**(3): 965-1010.

Wills, L. (2017). SUMOylation of the beta-2 AR influences receptor internalisation, desensitisation and downstream signalling. PhD, University of Glasgow.

Witt, S. H., H. Granzier, C. C. Witt and S. Labeit (2005). "MURF-1 and MURF-2 target a specific subset of myofibrillar proteins redundantly: towards understanding MURF-dependent muscle ubiquitination." J Mol Biol **350**(4): 713-722.

Wolff, M. R., S. H. Buck, S. W. Stoker, M. L. Greaser and R. M. Mentzer (1996). "Myofibrillar calcium sensitivity of isometric tension is increased in human dilated cardiomyopathies: role of altered beta-adrenergically mediated protein phosphorylation." J Clin Invest **98**(1): 167-176.

Yang, J., J. A. Drazba, D. G. Ferguson and M. Bond (1998). "A-kinase anchoring protein 100 (AKAP100) is localized in multiple subcellular compartments in the adult rat heart." J Cell Biol **142**(2): 511-522.

Yang, S. H., A. Galanis, J. Witty and A. D. Sharrocks (2006). "An extended consensus motif enhances the specificity of substrate modification by SUMO." EMBO J **25**(21): 5083-5093.

Yang, S. H., E. Jaffray, R. T. Hay and A. D. Sharrocks (2003). "Dynamic interplay of the SUMO and ERK pathways in regulating Elk-1 transcriptional activity." Mol Cell **12**(1): 63-74.

Yuasa, K., H. Michibata, K. Omori and N. Yanaka (1999). "A novel interaction of cGMP-dependent protein kinase I with troponin T." J Biol Chem **274**(52): 37429-37434.

Zaccolo, M., F. De Giorgi, C. Y. Cho, L. Feng, T. Knapp, P. A. Negulescu, S. S. Taylor, R. Y. Tsien and T. Pozzan (2000). "A genetically encoded, fluorescent indicator for cyclic AMP in living cells." Nat Cell Biol **2**(1): 25-29.

Zaccolo, M. and T. Pozzan (2002). "Discrete microdomains with high concentration of cAMP in stimulated rat neonatal cardiac myocytes." Science **295**(5560): 1711-1715.

Zakhary, D. R., C. S. Moravec, R. W. Stewart and M. Bond (1999). "Protein kinase A (PKA)-dependent troponin-I phosphorylation and PKA regulatory subunits are decreased in human dilated cardiomyopathy." Circulation **99**(4): 505-510.

Zhang, G., Y. Liu, A. E. Ruoho and J. H. Hurley (1997). "Structure of the adenylyl cyclase catalytic core." Nature **386**(6622): 247-253.

Zhang, R., J. Zhao, A. Mandveno and J. D. Potter (1995). "Cardiac troponin I phosphorylation increases the rate of cardiac muscle relaxation." Circ Res **76**(6): 1028-1035.